Diss. ETH No. 13599

Fault Tolerant Control Concepts Applied to Anesthesia

A dissertation submitted to the
Swiss Federal Institute of Technology (ETH)
Zurich

for the degree of
Doctor of Technical Sciences

presented by
Christian Walter Frei
MSEE Northwestern University, Dipl. NDS ETHZ
born July 17 1967
citizen of Rietheim, AG

accepted on the recommendation of

Prof. Dr. A.H. Glattfelder, examiner
Prof. Dr. P. Niederer,   co-examiner
Prof. Dr. A.M. Zbinden,   co-examiner
Prof. Dr. M. Blanke,   co-examiner

April, 2000

Seite Leer /
Blank leaf

Acknowledgments

The presented work covers a broad range of different aspects of automatic control. They range from software engineering to modeling of physiological processes to theoretical contributions on system recoverability. To deal with all these aspects would not have been possible without the support of various other people whom I would like to acknowledge here.

I first would like to thank my advisors Proff. A.H. Glattfelder and A.M. Zbinden. Without their initiative this interdisciplinary and extraordinarily interesting project would not exist. I am very thankful that I was allowed a large degree of freedom to chose my research directions within the boundaries of the NSF project and that they were both always available for discussions and advice despite their busy schedules. And I would like to thank Prof. P. Niederer for serving on the committee despite his sabbatical.

Important parts of the thesis have been influenced by my participation in the Theme 2 group of the ESF sponsored COSY network. This participation was initiated by Prof. W. Schaufelberger. A very special thank goes to Prof. M. Blanke who managed Theme 2. The recoverability concept would not exist without his encouragement. Several other Theme 2 members contributed to this concept in various discussions, in particular Dr. F. Kraus. Also Roozbeh Izadi-Zamanabadi and Tako Lootsma must not remain unmentioned. They introduced me to Jomfru Ane Gade during my stay at Aalborg.

Many thanks also go to the team of the research section at the department of anesthesiology and intensive care of the university hospital in Bern (Dr. R. Lauber, P. Feigenwinter, K. Schaad) and in particular to Dr. Th. Sieber, Dr. Ch. Pfister, and D. Leibundgut. Daniel Leibundgut significantly contributed to the research platform during evaluation, design, implementation as well as in maintenance. Christoph Pfister was conducting the stress response study which provided important information for the identification of the pain model. And Thomas Sieber supervised endtidal as well as blood pressure controller study. Of course special thanks also goes to all the (anonymous) patients who volunteered to have part of their anesthesia conducted automatically.

At the automatic control lab my thanks go to Prof. M. Morari who encourage me to elaborate on the use of disturbance predictions for blood pressure control, the members of the reading group (E. Bullinger, P. Menold, R. Findeisen, F. Kraus), the members of the anesthesia group (M. Derighetti, A. Gentilini, K. Stadler), and of course to all the staff members.

I would further like to thank all the students who contributed in one or the other way with their semester and diploma projects. They are M. Buob [68], A. Branca [60], A. Schmid [417], B.

Summary

The first application of automatic control to a physiological variable during general anesthesia was reported in 1949. Since then a lot of research has been devoted to this topic. Still, today there is no commercial anesthesia system available with the patient in a feedback loop. One reason for this is that research has mainly been focused on controller design. Important aspects of clinical practice such as the treatment of measurement artifacts and faults have only marginally been addressed. In this thesis exactly such problems which are usually tacitly neglected but which are of great relevance are addressed. We are referring to these aspects as supervisory functions.

Before addressing these supervisor functions some foundations are established. This involves in the first place a hard- and software research platform that allows to implement and test control algorithms as well as the supervisory functions in the operating theater. It is our view that fault handling must start with the design of a system. Special attention is therefore paid to the selection of the platform components and the software design. The software structure is built with special emphasis on extendibility. A second foundational building block is a mathematical model which describes the dynamic relationship between vaporizer concentrations and surgical stimulations on the input side and the inspiratory and endtidal Isoflurane concentration as well as mean arterial pressure (MAP) on the output side. A thorough review of the physiological background is followed by a step by step development of the model equations. Modeling is finalized with the identification of the system parameters and validation experiments.

Since the design of control algorithms is not the main focus, controllers are taken form a thesis by Marco Derighetti. They are refined for broader applicability where necessary. The result of extensive clinical validations of an observer based state feedback (OBSF) controller for the endtidal Isoflurane concentration and an OBSF with endtidal overrides for MAP are presented. In view of the limited ability of this MAP controller to compensate heavy disturbances a control scheme based on disturbance anticipation is suggested.

For the supervisor functions first a structure is suggested which allows to allocate all functions postulated in literature. A selection of these is developed in more detail. First, an elegant strategy to handle measurement artifacts in the framework of OBSF controller is proposed. It is based on a nonlinear modification of the output injection gain. The stability of this algorithm is proved and recordings of several successfully suppressed artifacts are shown. A large part of the thesis is then dedicated to fault tolerant control (FTC). Following a sequential design procedure developed by Prof. M. Blanke a strategy for handling the most critical faults in the system is obtained. In this context the concept of recoverability for linear time invariant (LTI) systems is developed.

This concept is utilized to analyze to what degree the functionality of a faulty system may be recovered in case of a fault. Finally, a man machine interface (MMI) is designed. Aspects of MMI are important in this context since a well designed MMI increases operational safety.

The main contribution of this thesis is to show that mathematical process models are a useful tool in dealing with faults also in a biomedical environment.

Zusammenfassung

Seit der ersten automatischen Regelung einer physiologischen Messgrösse während einer Generalanästhesie im Jahre 1949 wurde eine Vielzahl von wissenschaftlichen Arbeiten in diesem Gebiet publiziert. Trotzdem existiert bis heute kein kommerzielles Anästhesiesystem bei dem sich der Patient in einem geschlossenen Regelkreis befindet. Ein Grund dafür liegt darin, dass in den publizierten Arbeiten Aspekte des klinischen Alltages wie Fehler und Messartefakte, die eine Regelung arg beeinträchtigen können, oft ausgeblendet werden. In der vorgelegten Arbeit befassen wir uns mit gerade diesen Problemen. Wir subsummieren diese Fragestellungen unter dem Begriff Supervisorfunktionen.

Bevor allerdings diese Supervisorfunktionen behandelt werden, werden zwei Grundvoraussetzungen diskutiert. Dabei handelt es sich einerseits um eine Hard- und Softwareplattform, die es erlaubt, Regelalgorithmen und die Supervisorfunktionen zu implementieren und im Operationssaal einzusetzen. Nach unserer Auffassung muss die Fehlerbehandlung beim Systementwurf beginnen. Deshalb wird spezielles Gewicht auf die Auswahl der Plattformkomponenten und den Softwareentwurf gelegt. Die Softwarestruktur orientiert sich stark an der spätern Erweiterbarkeit des Systems. Als zweite Grundvoraussetzung wird ein mathematisches Systemmodell entworfen, das die dynamischen Zusammenhänge zwischen den Eingangsgrössen Anästhesiegas im Frischgas und chirurgischer Reiz und den Ausgangsgrössen inspiratorische und exspiratorische Anästhesiegaskonzentration sowie dem mittleren arteriellen Blutdruck beschreibt. Dazu wird zuerst eine detaillierte Zusammenfassung der benötigten physiologischen Grundlagen geliefert und darauf werden die Modellgleichungen schrittweise entwickelt. Die Modellierung wird durch die Bestimmung der Modellparameter und einige Validierungsexperimente abgeschlossen.

Der Entwurf von Regelalgorithmen selbst ist kein eigentlicher Schwerpunkt dieser Arbeit. Es werden deshalb Regelalgorithmen übernommen, die von Marco Derighetti in seiner Dissertation entworfen wurden und für die klinische Validierung angepasst. Für einen beobachterbasierten Zustandsregler für die endtidale Anästhesiegaskonzentration und für einen Blutdruckregler mit endtidalen Override-Reglern werden Resultate einer umfangreichen klinischen Validierung vorgestellt. Motiviert durch die begrenzte Fähigkeit der Blutdruckregelung grössere Störungen zu kompensieren wird ein Regler basierend auf einer Störgrössenantizipation vorgeschlagen.

Für die Supervisorfunktionen wird zuerst eine Struktur entworfen, die alle in der Literatur postulierten Funktionen beinhaltet. Einzelne dieser Funktionen werden dann eingehender behandelt. Zuerst wird eine elegante Möglichkeit aufgezeigt, wie die beobachterbasierten Zustandsregler insensitiv gegen Messartefakte gemacht werden können. Sie basiert auf einer nichtlinearen Gewich-

tung der Ausgangsrückführung im Beobachter. Die Stabilität dieses Verfahrens wird analysiert und mehrere Beispiele erfolgreich unterdrückter Artefakte werden gezeigt. Ein grosser Teil der Arbeit befasst sich dann mit der fehlertoleranten Regelung. Wir folgen einem Entwurfsverfahren, das von Prof. M. Blanke in Aalborg entwickelt wurde und gelangen dadurch zu einer Realisierung, die die schwerwiegendsten Systemfehler handhaben kann. In diesem Zusammenhang wird das Konzept "recoverability" entwickelt, welches es erlaubt zu beurteilen, wie weit ein fehlerhaftes System seiner ursprünglichen Funktion gerecht werden kann. Zum Schluss wird für die Bedienung des Systems eine Benutzerschnittstelle entworfen. Benutzerschnittstellenfragen sind in diesem Zusammenhang wichtig, weil eine klare Benutzerschnittstelle die Sicherheit eines Systems erhöht.

Neben verschiedenen originären Beiträgen besteht der Hauptbeitrag dieser Arbeit darin zu zeigen, dass mathematische Prozessmodelle auch in einem medizintechnischen Umfeld zur Behandlung von Fehlern herangezogen werden können.

Contents

Chapter 1

Introduction

1.1 Purpose and history of anesthesia

The history of surgery dates back into the prehistoric ages. From bones found it is presumed that very early even cranial surgery was performed. It is reasonable to assume that in parallel to the progress of surgery adequate pain relief was sought. For example reports of the application of opium may be found in the antique. In the middle ages as diverse methods as compression of nerve trunks, loud music, and alcohol were tried [216, 364, 332, 241] - with little success. The "quick knife" of the surgeon was basically the only relief. It took until 1846 for the first scientific publication [39] reporting the application of general anesthesia during surgery performed by William Morten and John Warren. An over-dramatized illustration of this event is given in the painting by Robert Hinckley (figure 1.1). The term "anesthesia" was suggested by Oliver Holmes to express the absence of sensation. But since reports about the narcotic effects of ether and nitrous oxide (N_2O) may be found earlier there is a certain debate on who the inventor of anesthesia really is.

The early anesthesia systems only consisted of a glass bulb with two attached glass cylinders and a sponge inside [364]. Through one cylinder the patient was inhaling the ether evaporating form the sponge tinctured with ether. The other cylinder was used to replenish ether. Since then clinical anesthesiology has changed considerably in terms of equipment, drugs, and procedure [332]. Today, the selection of procedures and drugs is tailored to the special requirements of the surgical procedure. This is important since the different objectives of anesthesia which are

O-1 provide hypnosis (unconsciousness, amnesia)

O-2 ensure analgesia (relief from pain)

O-3 relax muscles

O-4 maintain vital functions

Figure 1.1: An over-dramatized illustration of the first general anesthesia during surgery - also know as ether day.

are not always equally important. For example for removing small skin anomalities it is not required to make the patient completely unconscious. It is rather sufficient to insensitize him/her locally. This leads to a classification of anesthesia into local, regional and general anesthesia [332]. For local anesthesia anesthetics like Lidocaine are injected into the tissue surrounding the site where the surgical procedure shall be performed. It normally covers an area of several cm^2. A typical application is dental surgery. With regional anesthesia a whole body region like a limb is insensitized. This is done by injecting local anesthetics onto or immediately adjacent to nerve trunks. An example is the blocking of spinal nerves during a hip joint replacement. During regional and local anesthesia the patient is (more or less) conscious. In contrast, general anesthesia affects the whole body. The patient is completely unconscious. Usually the muscles are relaxed and artificial ventilation is required.

1.2 Drugs and measures

To achieve the different objectives of anesthesia (O-1 to O-4) various drugs are at disposition. While some drugs support several objectives other drugs only support a single objective.

Hypnosis is achieved with volatile anesthetics like N_2O, Xenon, and halogenated Ether anesthetics or with intravenously applied anesthetics like Thiopental, Propofol, and others. Analgesia is achieved mainly with opiods like Alfentanil, Remifentanil, and others. For muscle relaxation intravenously applied agents like Vecuronium, Atracurium are used.

The maintenance of the vital functions is a more disperse problem. An important element is the artificial ventilation. On one hand the ventilation delivers oxygen and removes carbon dioxide form the patient. On the other hand it also delivers the volatile anesthetics to the patient. Another important element in this context is the oxygen fraction of the fresh gas stream. A further important aspect is the hemodynamic stability. To some extent this is achieved with hemodynamically active hypnotics and with analgesics. In case of large blood loss the lost blood volume needs to be replaced. This is either done through infusions of physiological $NaCl$ solution or conserved blood.

And in some rare cases it is necessary to utilize strong hemodynamically active substances like ephedrine or others.

The formulation of objectives also immediately asks for measurements for these objectives. Of the four objectives the vital functions are most easily measurable. Standard patient monitors provide numerous measurements like inspired oxygen concentration, expired carbon dioxide concentration, blood pressure, heart rate, and many more. Fairy well established measures also exist for muscle relaxation. Relaxation might be assessed by electrically stimulating a nerve (e.g. ulnar nerve) and by measuring the response of the enervated muscle. This response is generally assessed by the anesthetist in physical contact with the patient. That is standard patient monitors do not provide measurements of relaxation. Less established measures exist for the remaining two objectives. Several measures of unconsciousness were proposed based on the EEG signal. The motivation for this seems obvious since unconsciousness is expected to be correlated with brain activity. A short
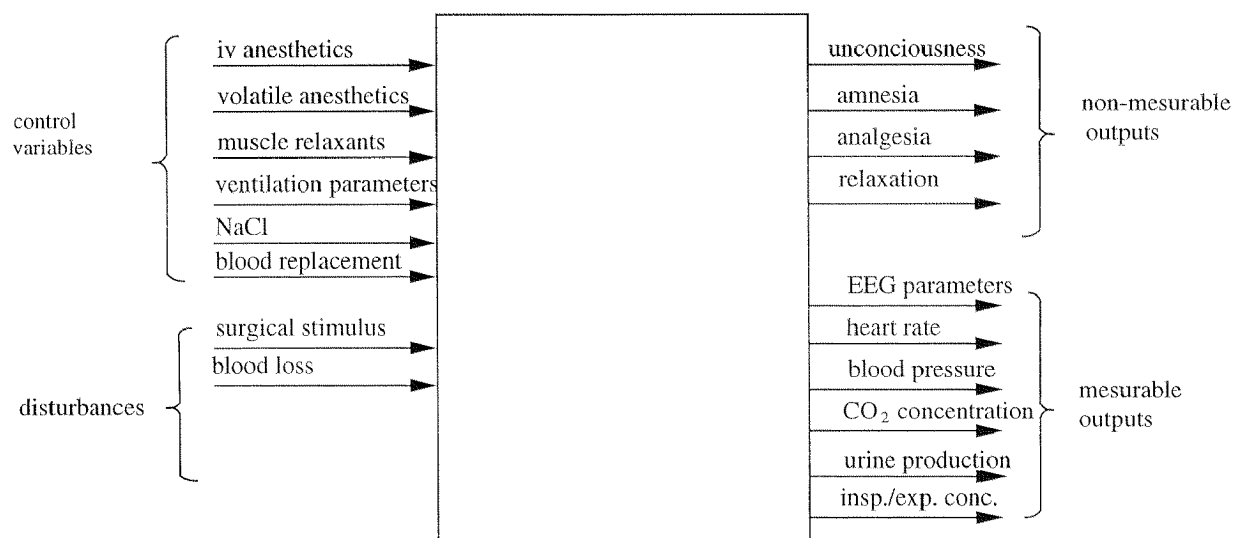
Figure 1.2: Viewing drugs and instrument settings as inputs and objectives as outputs anesthesia may be represented as a multi-input-multi-output (MIMO) system.

review of the use of EEG parameters in anesthesia may be found in [313] or [386]. Alternatively to spontaneous EEG, activity of the EEG evoked by external stimulations might be used. Most common is the EEG potential evoked by auditory stimuli as used in [277] for control purposes. No general measure is established for analgesia. The goal of analgesia is the absence of pain. But pain requires pain perception. Pain perception, however, is subjective and unconsciousness also disables pain perception. Studies conducted with almost pure hypnotic agents [519] revealed that the stress response of the body to noxious stimuli was basically undamped. The stimuli must have been received by the body without explicit pain perception. Measures for analgesia have thus been proposed based on body response to artificial stimuli. But until today no adequate quasi continuous measure is available.

Viewing drugs and instrument settings as inputs and objectives as outputs of a multi-input-multi-output (MIMO) system anesthesia may be represented as shown in figure 1.2.

surgeon's area   anesthetist's area
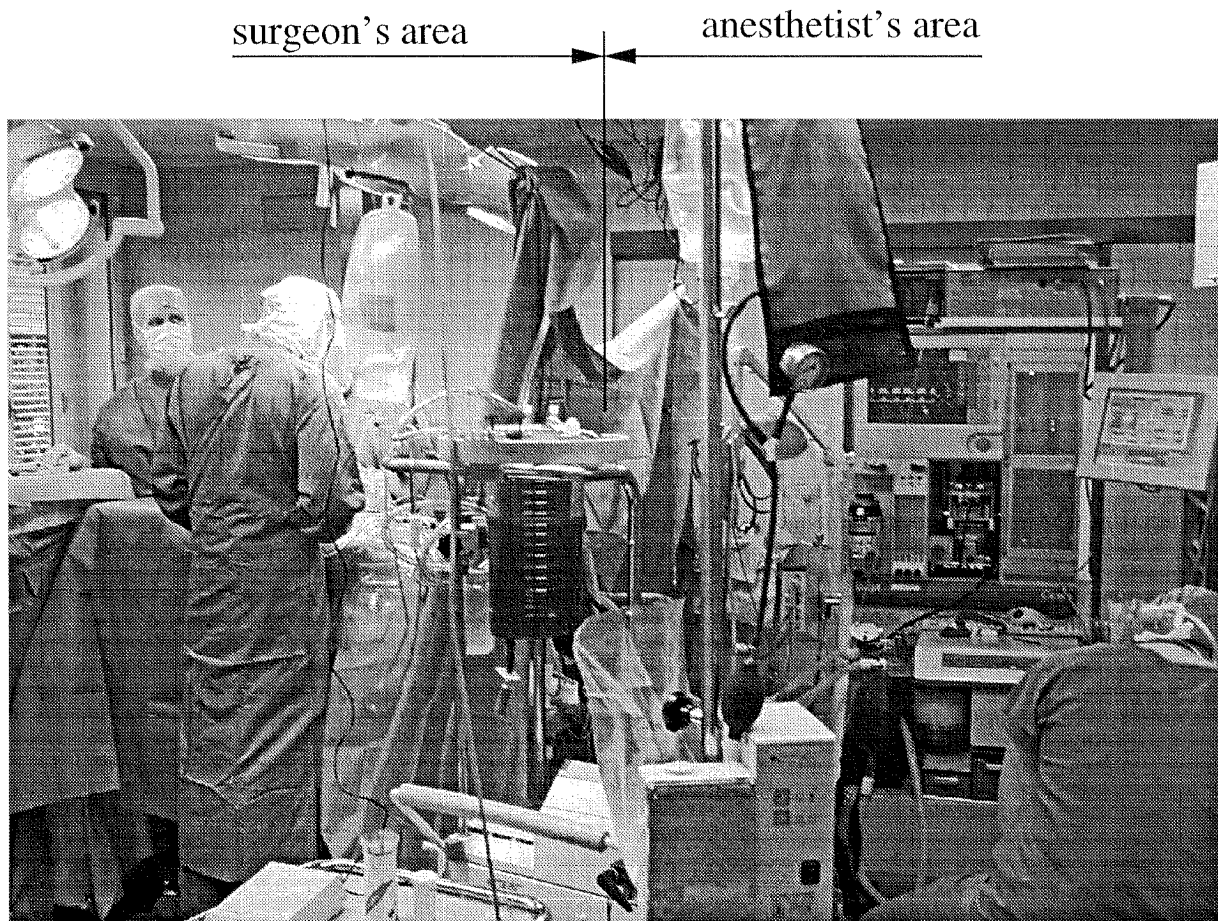
Figure 1.3: Usually the workplace of an anesthetist is clearly separated from the surgeon's area.

1.3   The anesthetist's workplace

A typical setup of a workplace of an anesthetist is shown in figure 1.3. A first thing we note is that there is a blanket that separates surgeons and anesthetists[1]. This leaves limited view for an anesthetist onto the site of surgery. The anesthetist also has limited access to be patient. Often this is a forearm which carries catheters and oximeter. And sometimes there is access to the patient's head (see figure 1.4). The state of the patient must thus mainly inferred from the measurements provided by the patient monitor. Based on these measurements and the objectives the anesthetist regularly adjusts drug application and device settings. The idea to support the anesthetist through automatic feedback controllers in his/her task is thus straight forward.

---

[1]Note at this point that we will distinguish between anesthetists and anesthesiologists. Anesthetist denotes the person conducting the anesthesia. In Switzerland this may be a doctor or a nurse with special training. Anesthesiologist denotes a person that had studied medicine and is specialized in anesthesiology.
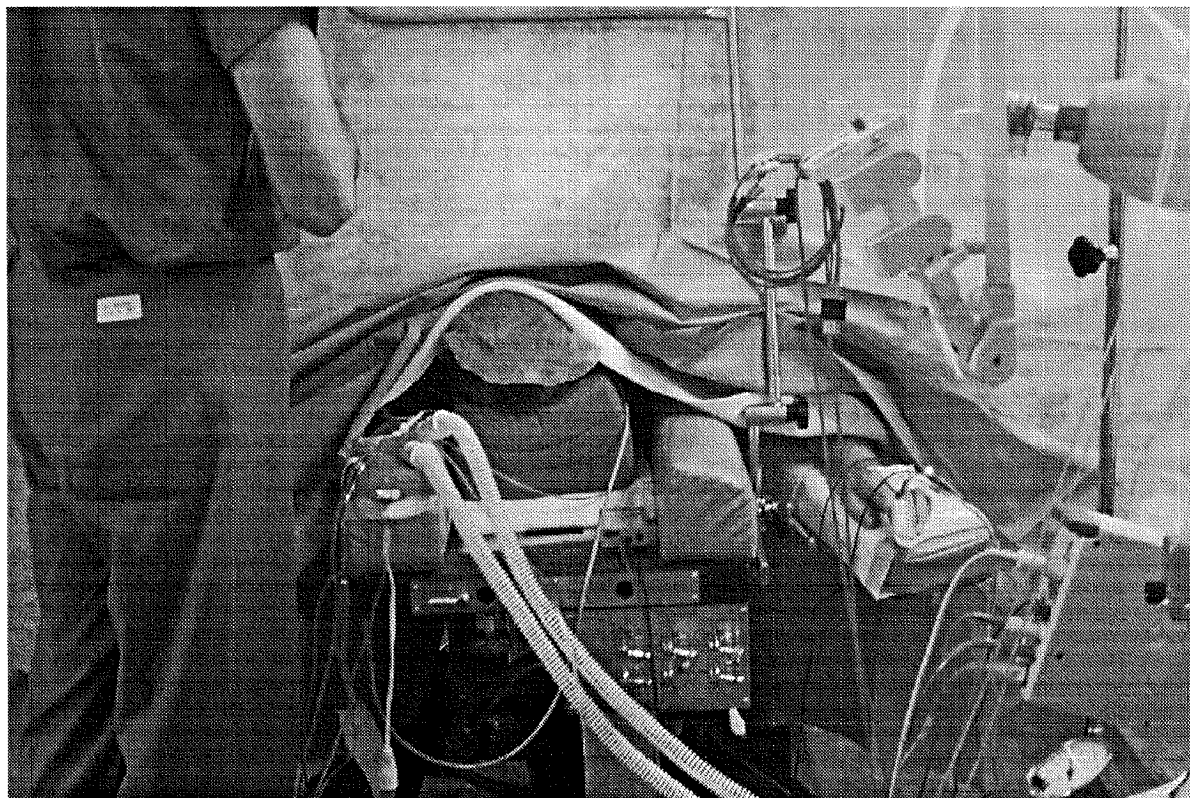
Figure 1.4: Often there is little access to the patient.

Roughly five different phases of anesthesia may be distinguished (compare figure 1.5). These are: Induction, Waiting, Begin, Operation, and Emergence.

During the induction the patient is prepared for surgery. From the anesthetist's side this involves

- inserting venous and arterial catheters

- set up monitoring through application of sensors like ECG electrodes, EEG electrodes, pulse oximeter, gas sampling line, etc.

- start the application of hypnotics, analgesics, and relaxants

- intubation.

In parallel all other preparations not related to anesthesia are made. This phase lasts normally from half an hour to an hour.

Following the induction there is a short waiting phase where the patient is moved into the OR and where last preparations of the surgeons are made. This phase lasts approximately 10 to 30 minutes.

The beginning of surgery is usually characterized by the opening of the skin. This event provokes a heavy response of the body in terms of blood pressure and heart rate increase. It is a phase

Phase	1	2	3	4	5
	Induction	Waiting	Begin	Operation	Emergence
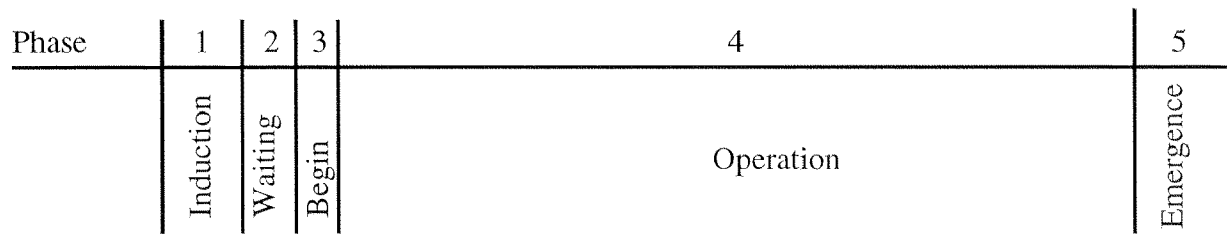
Figure 1.5: The different phases of anesthesia.

where the anesthetist pays much attention to damping this stress response. He/she is normally increasing drug application shortly before skin incision occurs. This phase typically has a duration of several minutes.

During the operation (phase 4) there are mainly the objectives 1 to 4 to be achieved. Most surgical procedures and most patients require less attention by the anesthetist in this phase than in phases 1 and 3. Depending on the type of surgery this phase lasts from half an hour to eight or more hours.

In the emergence phase at the end drug application has been stopped and the patient is slowly waking up. Monitoring and tracheal tube are removed as soon as the patient is awake. This phase depends on the duration of the operation as well as the amounts and the types of drugs that were used. It lasts from approximately 10 to 30 minutes.

Concerning the application of automatic control, phase 4 is certainly most suited, in particular for operations with long durations. However, also in the phases 2 and 3 the application of automatic control would be feasible.

1.4 Feedback control in anesthesia

Since the first reported application of automatic feedback control of a physiological variable during general anesthesia [38] numerous researchers have applied various control techniques to various physiological variables. Among the controlled variables are mean arterial pressure (MAP), EEG parameters, muscle relaxation, as well as inspired and endtidal gas concentrations. The control techniques applied include PID control, Fuzzy logic and neural network control, model based controllers, as well as adaptive controllers. For several physiological variables models for simulation have been built independently of control applications.

An exhaustive overview over feedback application during anesthesia lies outside the scope of this introduction. Nevertheless, applications known to the authors are summarized in the overview table 1.1. More detailed overviews are provided by the review publications [82, 106, 272, 355, 220, 303, 422].

The pro arguments for automatic control are several. First, there is the relief from routine tasks.

	Fuzzy and neural networks	PID family	OBSF	model based predictive	adaptive control	simulation models and open loop control
MAP control with volatile anesthetics	[273][274] [280][515] [318][345] [114][459] [293][111]	[416]	[111]	[281][273] [274][279] [280][293] [296][111]	[327][329]	[157][158] [524]
Control of exspiratory concentrations	[111]	[333][516] [397][489]	[463][111]	[111]	[450]	[267][268] [406][267] [268][299] [504][502] [407]
Control of inspired concentrations	[104][111]		[111]	[111]	[226][399] [477]	[267][268]
MAP control with intravenous drugs	[377][400] [507]	[77][320] [403][391] [426][436]	[388]	[159][387] [255]	[32][306] [326][510] [307][382] [304][305] [256]	[175][126] [498]
Intravenous hypnotics and analgesics						[40][478] [282][295]
Control of EEG parameter or brain concentration	[390]	[416]				[84]
Control of evoked potentials	[276][277]					
Control of muscle relaxation	[465][278] [280][273] [274][293] [294][309] [310][345] [346][398]	[321][357] [356]		[281][279] [280][273] [274][293] [292][294] [297][296] [298][432]		
Control of ventilation	[473][111]	[76]			[260]	[81][131]
Other applications	[381][275]	[520]				[227][257] [275][350]

Table 1.1: Classification of a selection of publications on feedback control in anesthesia.

This is expected to leave the anesthetist more capacity for patient supervision. Automatic control of one physiological variable might be viewed like automatic cruise control in a car. A drawback is that the anesthetist could loose some of the ability to conduct the anesthesia manually. An aspect that will have to be dealt with should automation make its way into clinical practice.

A second argument concerns the reduction of drug consumption. It is argued [518] that anesthetists tend to overdose and that feedback systems will only apply the dose necessary to achieve the desired objective.

A further motivation is a bit futuristic. Satava [408] gives a vision about the possible appearance of the future battlefield. He postulates a trauma pod that provides a life supporting environment for wounded while awaiting or during transport to a rear echelon. This trauma pod is envisioned to be an *"enclosed, modular stretcher, with a miniaturized portable ventilator, cardiopulmonary support, monitoring devices, remotely actuated therapeutic devices and a closed cycle environmental control unit"*. Such a pod best has automatic control loops for certain physiological variables or is completely autonomous.

Although automatic feedback control potentially reduces drug consumption the savings on gas will hardly justify the costs of developing a feedback loop. If, however, the introduction of feedback loops is able to reduce personnel the savings are of a different order. It might be envisioned that at some point in the future instead of one anesthetist per patient there will be two anesthetist supervising five patients. For such a vision to come true it is not sufficient to introduce a single feedback controller it would rather require an autonomous or semi-autonomous anesthesia system which is able to handle the complete MIMO control problem and which is equipped with supervisory and diagnostic functionality.

Despite the good arguments for feedback control or for anesthesia systems that are even autonomous to some degree and despite the large amount of research no commercial anesthesia workplace is available with feedback from a physiological variable. Why this might be so will be discussed in the next section.

1.5   Automated anesthesia systems and complexity

To discuss the various aspects that add to the complexity of the problem we will follow the general design process for control systems. That is

- problem formulation

- plant modeling

- controller design and implementation

- testing

- routine use .

1.5.1 Aspects of the problem formulation

There are three factors of difficulty. First, it is the MIMO nature of the control problem. Second, there is the large variety of drugs available. And third, there are the difficulties of defining and measuring adequate anesthesia.

It is important to note that a lot of research has not addressed the MIMO problem yet. Very often an isolated SISO aspect is treated, for example control of endtidal CO_2 concentration through adjustment of the minute volume or the control of mean arterial pressure with sodium nitroprusside infusion. Simply integrating such SISO control loops into an automated anesthesia system will in general not work because of interdependencies. For example a ventilation controller will affect a controller for volatile anesthetics since changes in the minute volume alter the uptake characteristics. That is controllers intended to work simultaneously can not be designed independently.

Some MIMO control problems have been considered though. For example control of CO and MAP through sodium nitroprusside and dopamine or as in this and in Derighetti's thesis control of MAP through Isoflurane with guaranteed endtidal concentration limits. But even these applications treat a small portion of the whole problem. Only, as long as a considerable part of the control loops is closed manually the value added by automatic control loops will be relatively small.

Similar reasoning applies to the drug variety. Only if feedback controllers in an anesthesia machine are able to handle the majority of available drugs will it be possible to sell them. However, since research often addresses only one drug in a particular setup considerable effort will still be necessary to make a specific control strategy applicable to other drugs.

One reason for the observed "theory practice gap' is the fact that from a feasible control loop for a single drug in a SISO setup to a salable product a lot of effort is required.

In addition, the adequate state of anesthesia for a patient is inferred by an anesthetist from monitor readings, the history of drug application, as well as the medical history of the patient. Although attempts have been made to formalize this inference process [401, 213] no "gold standard" has been established yet. Thus, an anesthetist has to pay more or less constant attention to the progress of anesthesia anyway even with selected feedback loops.

1.5.2 Aspects of modeling

Dynamic models are not just needed for controller design but also for the simulation validation prior to clinical tests. Building models for physiological processes is more difficult than model building for physical processes. The reasons are that there are no first principles, limitations in applicability of modular modeling, the inter-patient variability, and difficulties in parameter estimation and model validation.

First principles are applicable to some extent when modeling drug transport. The drug effects, however, are modeled rather phenomenologically.

The modular modeling paradigm suggest to build models from subblocks that are easier to describe. For physiological systems models may be obtained in this manner but subblocks are not necessarily easier to model. In particular when it comes to parameter identification. That is it is often easier to perform an experiment that involves the whole body than just a single organ.

The inter-patient variability plays an important role especially with respect to drug effects. This makes it difficult to build individualized models as they would be needed for individualized drug administration.

Finally, the limitations in performing in vivo experiments makes parameter estimation and model validation difficult. If for example one decided to build a black box model to avoid the troubles with physiology based models then the model parameters need to be determined experimentally. This requires an experiment that excites the system sufficiently rich. And for processes with time constants ranging from minutes to hours such an experiment will have considerable duration.

The difficulties in model building explains why researchers usually develop algorithms for one particular drug only. Extending an algorithm to other drugs will require considerable modeling effort but would bring little "academic credit" for a control engineer. The effort consequently will need to be made by a potential manufacturer.

1.5.3 Aspects of controller design

The main challenge for controller design is the inter-patient variability. Since this variability is less pronounced for drug distribution variability is e.g. less of a problem for control of endtidal concentrations. It is more pronounced for MAP or relaxation controllers where drug effects are controlled. Possible solutions to the problem are: robust control and adaptive control. The problem with robust control is that if the variability is broad potentially very conservative controllers result. And for adaptive control there is hardly enough time and excitation to guarantee a proper adaptation. What is required is some kind of pre-adjustment which must be possible based on a simple pre-operation experiment. Few work has been done in this direction.

1.5.4 Aspects of testing

One difficulty for testing is inherited from variations in drugs and procedures as well as patient variability. Another issue are ethical aspects.

Variations and variabilities require a large number of clinical validations until the applicability is "statistically proved". For example to obtain statistically significant answers for the validation of the controllers to presented in chapter 4, 22 patients were required. However, the validation was done for a limited class of patients under low flow conditions and constant ventilation. As soon as such restrictions are removed a larger number of trials will be necessary.

Ethical considerations require that first extensive simulations are performed, then "hardware in the loop" tests follow, and finally several pilot studies under the close supervision of the control

engineer in the OR are performed before a clinical study can start. The time required for these "preparations" can take up to a year. During the study every patient participating has to give written consent. And there are many people who are afraid of surgery already and who are not willing to take further "risk". Such a study easily also extends over a whole year.

Some research groups go through a test phase with animal experiments. Only, due to the potential parameter differences between humans and animals a successful animal experiment is no guarantee at all for successful tests on humans. This is the reason why our group does not perform animal experiments.

1.5.5 Aspects of clinical use

So far mainly control engineering aspects have been discussed. With the clinical routine use further problems arise. These aspects may be characterized as supervisor aspects. Some of these are handling of measurement artifacts, faults, and man machine interaction.

Artifacts are - as will be discussed in chapter 6 - unavoidable temporary invalidations of the measurements which - if not treated - deteriorate controller performance or endanger the patient. While for clinical studies artifacts can be avoided to some extent this is not possible during clinical routine use.

Faults are "out of spec" functioning system components. These can be hard- as well as software components. One might argue that this is also the case for manually conducted anesthesia. However, on one hand feedback algorithms potentially amplify the effects of faults. On the other hand the anesthetist - consciously or not - continuously checks the plausibility of measurements based on his/her expectations. This will likely be less the case when applying automated feedback systems. That is plausibility checks must also be performed by the feedback system.

Human machine interaction in this context includes not just the problem of designing a graphical user interface (GUI). It also concerns the separation of responsibilities. What decisions should the automated system be allowed to make and what not? Should the system be enabled to autonomously switch from one control mode to another in case of a fault? Similar questions have of course to be answered in any automated system - the answers to the questions, however, are likely to be application specific. Another topic concerns the update of the anesthetist in case of a problem. Suppose the automated system has been running autonomously for some time and a fault occurs that forces the system to ask for human assistance. What is the information that the anesthetist needs to be able to take over? This is a question which has not been addressed so far.

1.5.6 Conclusions about the complexity discussion

First, a large effort is necessary to bring a feasible controller to clinical practice. Second, a large effort is also required to transfer a feasible control strategy from one drug to other drugs.

On the other side the additional cost for an automated system must pay off. We conjecture that this is only possible if reductions of the cost on personnel are possible. This in turn seems only possible if a system has a reasonable degree of autonomy.

That is the requirements towards a salable automated anesthesia system are high and the gap between these requirements and published research results is still enormous. We view this fact to be the main reason why no commercial feedback systems are available.

1.6   Scope of this thesis

The previous discussion reveals two main directions in which research can evolve. A "horizontal" direction would more broadly address the actual control problem. That is extend the patient domain, address larger portions of the MIMO problem, or transfer existing solutions to new drugs. A "vertical" direction addresses the questions arising when intending to bring a feasible controller to clinical practice. That is the supervisor aspects. This is what will be done in this thesis.

The individual aspects addressed by the thesis are best discussed with figure 1.6. The "foundations" of the whole system are a solid hard- and software platform as well as good mathematical models. Both also build the foundations for the control algorithms. However, they need to be more "solid" for the vertical extension. Just like a tall building requires better foundations than a small building. Details on the hard- and software platform are discussed in chapter 2. The model is discussed in chapter 3. The control algorithms for which the clinical validation experiments will be provided are discussed in chapter 4. The main part of the thesis is devoted to the vertical extension of the system with supervisor functions. In chapter 5 the structure of the supervisor is outlined in more detail. Chapters 6, 7, and 8 discuss artifact tolerant control, fault tolerant control (FTC), and the human machine interface (HMI), respectively.

Anesthetist

HMI

Supervisor

Measurements   Control Variables

Controllers

Models
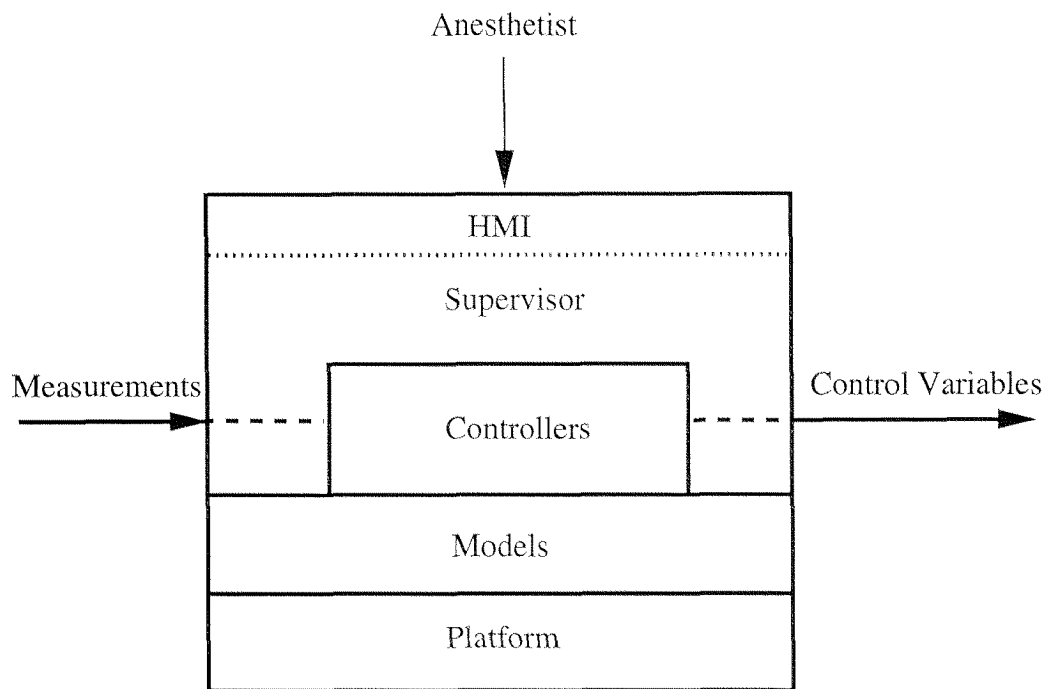
Platform

Figure 1.6: Schematic representation of the scope of this thesis.

Chapter 2

The research platform

2.1 Introduction

In chapter 1 we have pointed out that several research groups are active in the field of applying automatic control to anesthesia. The developed control algorithms are normally implemented on prototype hard- and software platforms (as for example described in [311] or [308]) designed to provide minimum functionality for demonstrating the feasibility of automatic control for a certain physiological variable. Moving from feasibility studies to a more routine use of automatic control in the OR increases the requirements to such a platform. A routine application of a (still experimental) feedback system is for example to apply a well defined level of anesthesia for clinical studies. While during feasibility studies control and software engineers are usually present in the OR to guarantee safe operation of the system, a single anesthetist not involved in the development process might be using the feedback system routinely. For such applications requirements in particular towards safety and user interaction grow. While it is sufficient for the control engineer to operate the feedback system via arrow and number keys on the keyboard this is generally not accepted by an anesthetist using the system routinely. Further, prototype systems implementations tend to be "quick and dirty", meaning that almost no attention is being paid to later extensions or modifications of the system.

Such a prototype system had been used for the first clinical trials in our project. It was implemented on a PC operating under MSDos using the programming language Modula II [48]. Although a number of clinical studies could successfully be completed [318, 515, 412, 104] the system suffered from considerable limitations. In particular

L-1 The PC hardware provided poor extendibility. Only two serial ports (RS232) were available which limited the number of devices to be connected simultaneously to the system.

L-2 The 64k-Byte block size restrictions under MSDos made it necessary to break up modules that in principle would have formed a entity. The logical coherence of the software structure
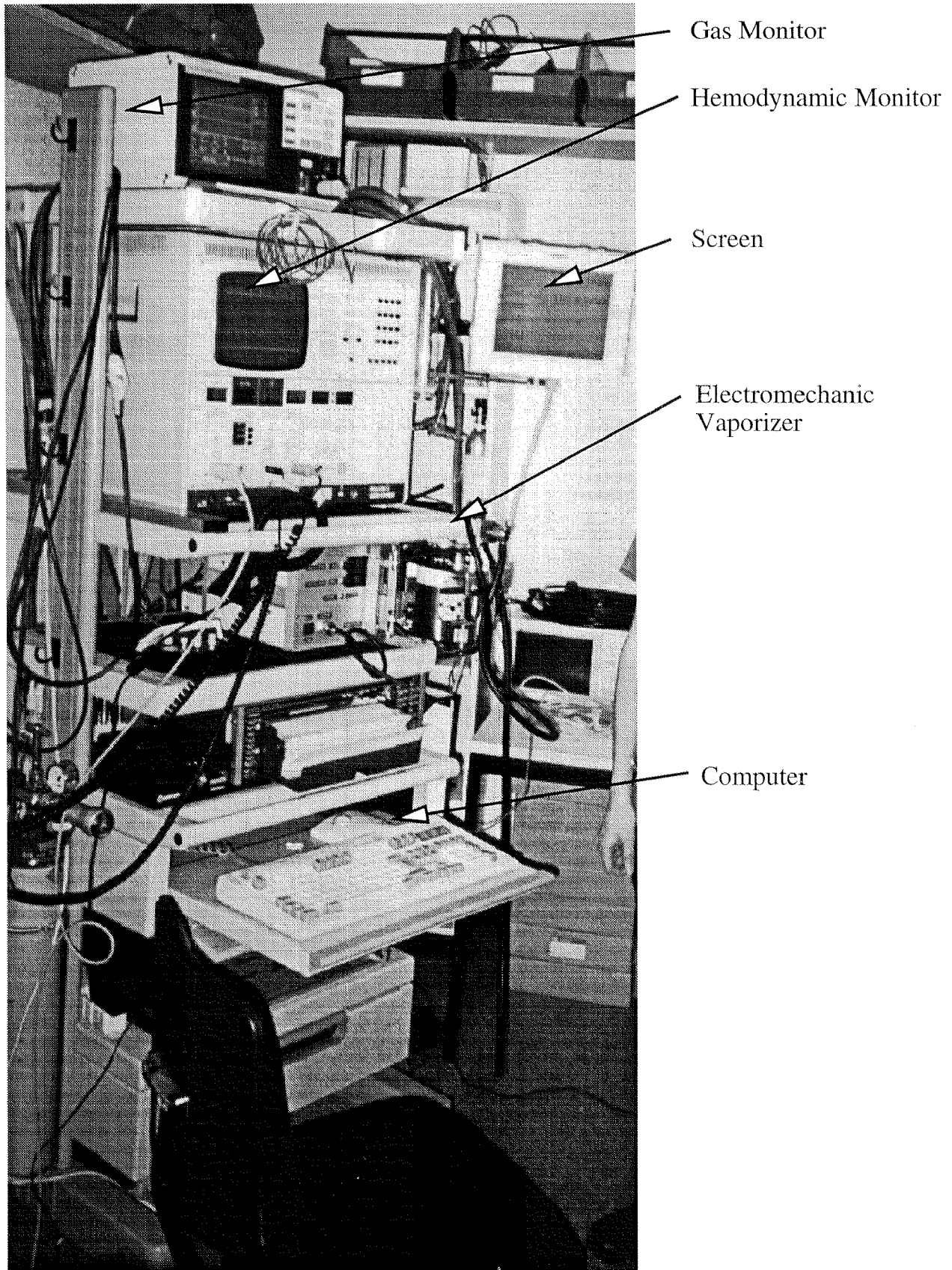
Figure 2.1: "Hardware tower" hosting the first prototype system.

```
00:00:11        SET VALUES                    MEASURED VALUES

          MAP set      75.00   mmHg        MAP meas    73.00   mmHg
                                           FE AA meas   0.36   vol%
          FIAA set      0.00   vol%        FIAA meas    0.44   vol%
                                           FE CO2 me    4.40   vol%
          FIO2 set     40.00   vol%        FI O2 meas  42.00   vol%


          FFAA set      0.00   vol%        FFAA meas    0.03   vol%
          FF set        5.00   l/min       fP meas      0.00   1/min
          FFO2 set      1.98   l/min
          FFN2O set     3.02   l/min

                          INPUT WINDOW

MAP Mode of the Program:

1) Change a set value
A) Show Alarmlimits
S) Change the Sound Modus
C) Change the Run Modus
U) Utilities

Q) Quit the program

                  ALARM AND INFORMATION WINDOW

MAP controller, INVASIV map measuring
fP me_Low    O2Opt_High
```

Figure 2.2: Screen for the Human Machine Interaction used to operate the first prototype system. Number and arrow keys on the keyboard were used to browse through the menus and to input data.

suffered enormously from this limitation.

L-3 Modula II did not provide graphical components that could have been used to conveniently compose graphical user interfaces (GUI). Although data was displayed quite structured (see figure 2.2) doctors found it not very convenient to work with.

L-4 The software grew during different project phases. The first implementations were made during a thesis by Steck [443]. From there it was extended during the theses of Meier and Nieuwland [316, 317] as well as Loppacher and Lüthi [286]. Finally, major extensions were made by Derighetti during his PhD thesis [111]. This evolutionary software design lacked a clear design philosophy which made it difficult to extend and maintain it.

L-5 All the devices needed to implement the control algorithms (computer, hemodynamic monitor, gas monitor, mass flow controller, etc.) were mounted on a separate cart (see figure 2.1) which had several disadvantages. First this heavy and spacious piece of equipment constituted an obstacle in the OR. Second, all devices required at least one connection to the anesthesia workplace used clinically. Due to this cabling a laboratory engineer was required to install the system in the OR.

Faced with promising results that triggered further research projects [518, 418, 517] and the limitations of this ad hoc system it seems natural to turn the experience gained into a more solid founded system design. Desired were a more compact integration on a standard anesthesia workplace and a new hard- and software platform for implementing the control algorithms.

The different steps in the design of this new hard- and software platform are discussed in the following sections. The first step represents the selection of suitable platform components. The requirements fro the individual components are discussed in section 2.2. The actually selected components are discussed in sections 2.3 to 2.6. Section 2.7 provides details about the software design. Section 2.8 discusses the hardware safety concept. And finally, concluding remarks about current state of the research platform are given in section 2.9.

2.2   System requirements

A list of requirements was collected from the group of potential users at the beginning of the redesign phase [155]. This group of users included the project supervisors (professors), senior anesthesiologists, laboratory engineers, as well as PhD students of the automatic control laboratory. These requirements may be condensed into the following four main requirements:

R-1   A high level of safety

R-2   Acceptable reliability and availability

R-3   Extendibility and easy to maintain

R-4   User friendliness

The potential users of the system may be grouped into three different classes (see also the context picture in figure 2.6). They are: the software engineer, the control engineer and the anesthetist. The requirements do not have the same weight for the different classes of users. Requirements R-1, R-2 and R-4 are of main interest for the anesthetist. For the control engineer who occasionally needs to change, alter or add a control algorithm, requirements R-3 and R-4 are of main interest. For the system and software engineer it is mainly requirement R-3 that counts.

The specifications R-1 to R-4 influence both, the selection of the platform components discussed in section 2.3 as well as the systems design, and in particular the software design discussed in section 2.7.

2.2.1 Comments on safety

Safety is of increased importance as the system moves from the designer to the user. According to [219] or [121] a system is deemed safe if the risk lies below a certain threshold (see also [187, 283, 202]). Where risk is defined as

$$Risk = Harm \times Probability\ of\ Occurrence \tag{2.1}$$

that is the product of damage which an incidence may cause and the probability with which that incidence might occur. The quantities harm and probability of occurrence are not always easy to quantify. [264] gives some guidelines on how to deal with these quantities for medical applications. According to equation (2.1) risk can be decreased in two ways. First constructive measures may be taken to reduce the probability that a fault occurs, i.e. by reducing the potential sources of errors. For software applications for example one might use a programming language which restricts the use of pointers or performs a strong type checking at compile time to reduce the probability of run time errors. However, fail safe behavior may not always be achieved by constructive measures. For these cases the harm may to be reduced by detecting the fault and by taking counter measures. Exception handling as provided by some programming languages is of this nature. Malfunctions may either be detected by a human supervisor or an algorithmic supervisor.

For a prototype system risk is considerably reduced by the presence of a person from the design team. Knowing about the structure of the system this person is able to detect a lot of malfunctions early. A fall back concept on the hardware level as will be discussed in section 2.8 allows to bring the system back into a safe state any time. The routine user may of course also rely on that fall back concept in case of a critical situation. Algorithmic supervisor functionality as will be described in chapters 5, 6, and 7 must support the human operator. However, for reasons discussed below it is first aimed at trying to select components and design methods such that the probability of occurrence of a malfunction is decreased so that fewer malfunctions need to be detected.

2.2.2   Comments on reliability and availability

Reliability and availability are both important properties if the feedback system is to be a relief. Both are linked to safety. Reliability (Zuverlässigkeit) characterizes how well a system is able to fulfill its purpose over a given interval of time. According to [219] it is defined as

$$Reliability \sim Mean\ time\ between\ failures. \tag{2.2}$$

Availability (Verfügbarkeit) is according to [219] defined as

$$Availability = \frac{Mean\ time\ between\ failures}{Mean\ time\ between\ failures + Mean\ downtime} \tag{2.3}$$

Clearly, both quantities are influenced by the rate at which faults occur. Thus any means that helps to reduce the probability of occurrence of malfunctions increases both reliability and availability.

2.2.3   Comments on extendibility

The current feedback system incorporates feedback loops for blood pressure, endtidal and inspiratory concentrations of anesthetics. However, it is planned to add feedback control for ventilation and intra venous drugs in the future. Further, it must be expected that different actuators for gas dosage or monitors will be introduced. These extensions and modifications must be possible without major changes to the design of the system. This requirement induces requirements on the software structure and any programming language which enforces a modular or object oriented design adds in this respect. Extendibility is also required concerning the hardware. Adding new devices might require additional I/O-ports at a later stage of the project. It might further be desirable to host supervisor functionality on a separate processor, as is often done for safety critical systems.

2.2.4   Comments on user friendliness

Finally the acceptance by the end user (anesthetist) will heavily depend on the user interface. Thus any programming language for which there exists a class library providing elements for the design of a state of the art user interface will be in favor.

2.3   Platform component selection

The hard- and software platform represents a core element of the whole experimental system. And the selection of its components should thus be done carefully with respect to the overall system specification listed in section 2.2.
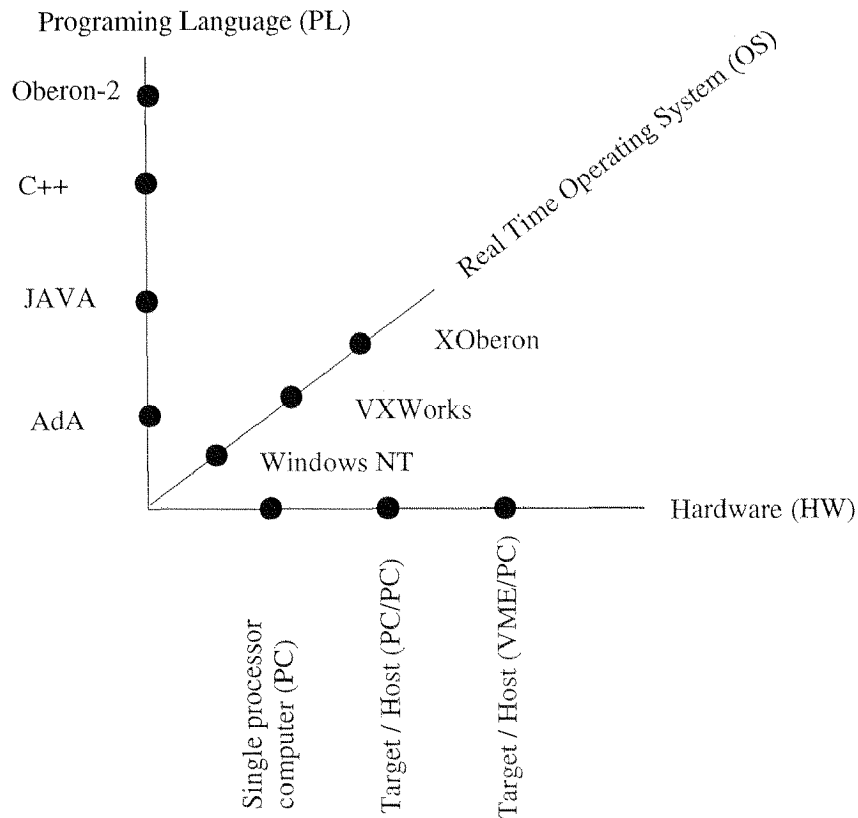
Figure 2.3: The platform space.

With 'platform' in this context we refer to an element of a set which might be viewed as the Cartesian product of the sets computer hardware, operating system, and programming language i.e.

$$Platform \in HW \times OS \times PL. \tag{2.4}$$

Figure 2.3 illustrates that - although not all combinations lead to valid platforms - there are numerous potential combinations. Finding the most suitable platform would in principle require the realization of the system on every platform and perform an a posteriori evaluation. This would be, however, outside of the scope of this thesis and the evaluation had to rely on a priori information instead - taking into account the know how available at our institute of course.

From the specifications R-1 to R-4 we derived the following selection criteria for the platform components

S-1 Industrial standard HW

S-2 Real time OS

S-3 Object oriented (oo) programming language

The industrial standard hardware criterion mainly aims at requirement R-3 on the hardware side. It particularly includes the possibility of a multi processor system.

The term real time is sometimes used to indicate that a system is able to react quickly to external events. Under this perspective our application would probably not fall into the category of real time systems. However, rather than speed real time systems address the problem of predictability [71, 198]. That is operations are not to be performed "fast" but within a guaranteed amount of time. And as we will see in section 2.7.2 there are a number of tasks that require a guaranteed repetition time and therefore also have a termination deadline. In addition real time operating systems usually provide multitasking capabilities. For a prototype system real time like features might be realized by the programmer on a non real time operating system (see e.g. [308]). However, by using an a priori real time operating system, a potential source of implementation errors is eliminated.

Concerning the selection of the programming language it should be mentioned that the problem of software in safety critical system has received increased attention in recent years (see e.g. [420, 485, 161, 283, 199, 392, 202]. Failures in software systems are of a fundamentally different nature than in hardware systems since software does not suffer from aging or wear [183, 59, 199, 202]. The sources of errors are [59]:

- inaccuracies in the problem specification

- errors introduced during software development

- errors introduced during compilation and linking.

Prominent examples of the second type are the ARIANE 5 disaster [124] or the problems in the Pathfinder mission [493]. A less prominent but well studied software problem in a medical application is the Therac-25 incident discussed in [269]. Other software problems of the same type that appeared in medical systems are reported in [52]. For the third type of errors a logically correct source program is translated into incorrect machine code. That is there is an error of the first or second type in the compiler or linker. A short discussion on this type of faults may be found in [59].

Considerable research effort is put into developing formal methods that allow the verification of the correctness of software in a strict mathematical sense. But, there is no satisfactory solution for large software programs [59, 199]. There are ,however, some guidelines for the design of software for safety critical systems (see e.g. [392, 199]).

A first rule is to keep the design as simple as possible [199, 201, 202] since the simpler the design the more intuitive it is and the easier it may be verified. The object oriented design paradigm very much supports this idea [429].

A second rule concerns the restriction of the allowable language constructs. In [420] Oberon$_T$ is introduced as a subset of the standard Oberon language and [392] gives numerous suggestions for how to improve safety by avoiding certain language features in general and for C in particular.
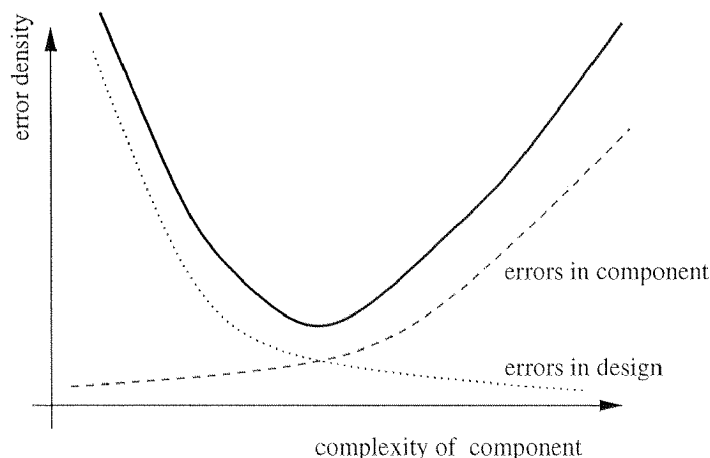
Figure 2.4: We conjecture that there exists an optimal component complexity for a given system complexity.

Finally, [200, 199] reasons that object oriented design inherently improves safety of software systems. Meyer [323] even states that there is no building of mission critical software without oo techniques. The OO criterion in addition supports requirements R-3.

A further aspect for the component selection is shown in figure 2.4. We conjecture that there exist components of optimal complexity to solve a particular problem of given complexity. A similar relation is stated in [204] for the error density in programs versus the average component complexity. We postulate that such a relation holds in general for error density in systems composed of smaller entities. More specific the error density in the final system depends on the errors in the components used (e.g. compiler or operating system) and the errors introduced with the design. The more complex a component the likelier it contains errors. The more components of low complexity are used to build a system the more likely errors are introduce with the design. This basically means that for our system of medium complexity components of adequate (medium) complexity are probably most suited.

In view of all the above aspects we chose a VME/PC Target/Host computer hardware, the XOberon real time operating system (developed at the Robotic Institute of ETH [120, 119, 61]) and the object oriented programming language Oberon-2. A detailed discussion of the properties of all the other possible platform components will be omitted here. First, since any discussion would remain incomplete and second since a lot of the arguments true today are likely to be invalid in a year. We will therefore restrict ourself to briefly introduce the features of each of the chosen components. We will explain how these components satisfy R-1 to R-4 and S-1 to S-3. Comments on how the chosen components are different from other potential choices will be made where appropriate. For some more details the reader is referred to [155].

Redundant Gasmonitor

Mass Flow Controllers

Flow Meters

Touchscreen

Standard Patient Monitor

Electromechanic
Vaporizer

Computer

Emergency Stop Button

Manual Gas Dosing

Breathing
System

Uninterruptable
Power Supply (UPS)
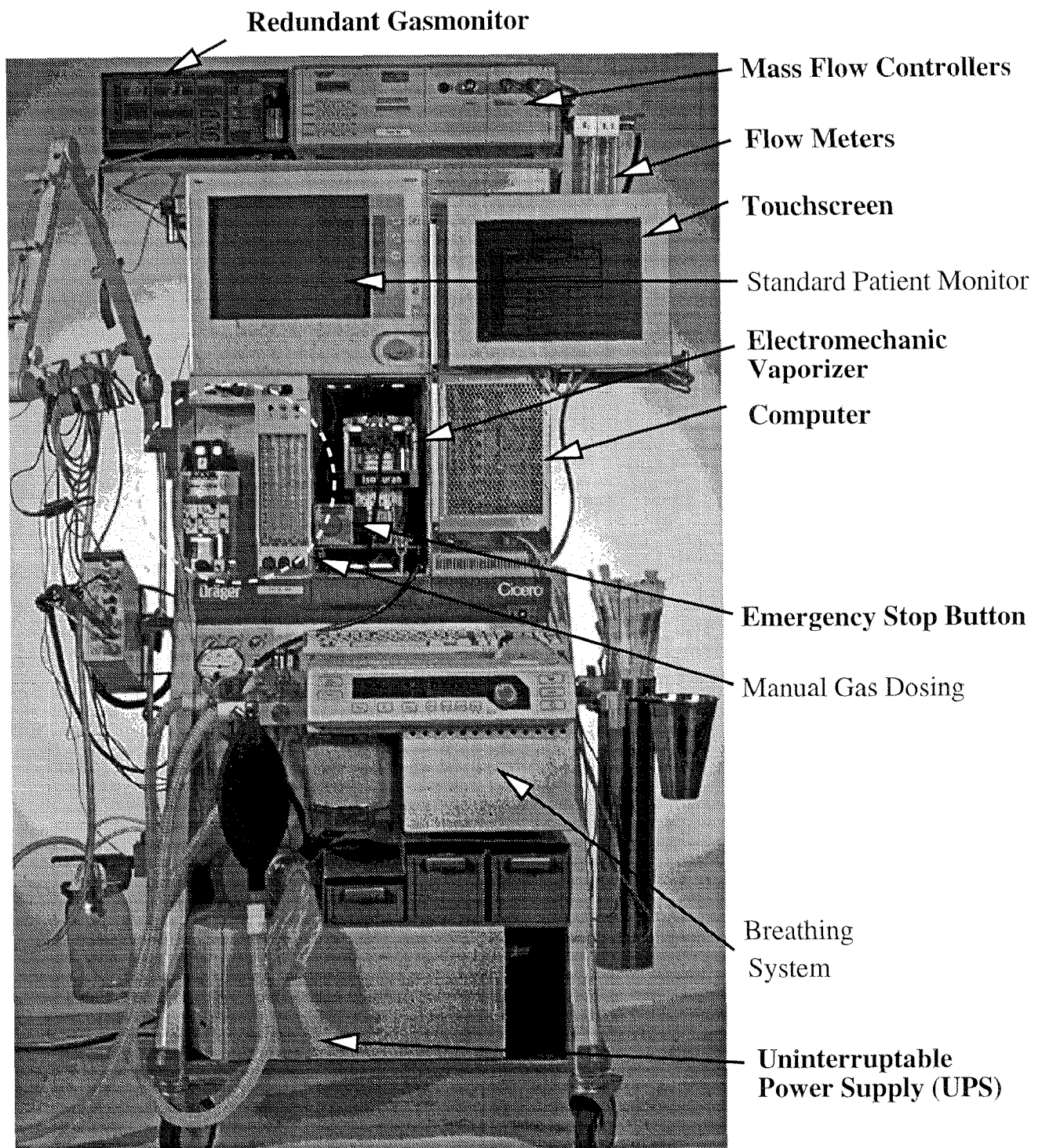
Figure 2.5: Compact integration of the feedback control system on a standard Cicero EM. Non standard elements are labeled in bold face text.

system's / software engineer

- get special log information
- get data flow information
- get target load information
- add new device drivers

control engineer

- choose configurations
- add control algorithm
- compose user interface

anesthetist

- change set values
- choose, switch controllers
- invoke emergency stop
- switch to manual control

local host computer

.xls format

.m format

remote host computer

Ethernet

target computer system

DC Power | analog IO | serial IO | PowerPC | PowerPC

"Divan protocol"

"MEDIBUS"

vaporizer   mass flow controllers

gas dosing device "IfAGADOS"

patient monitor

ventilator "DIVAN"

"MEDIBUS"

serial

serial

gas dosing device "GADOS"

infusion pump

EEG (BIS) monitor

Figure 2.6: Context picture showing the different parts of the system and the different users with their respective use cases.

2.4   Computer Hardware

The computer hardware consists of two computers: a 'target' computer system and a 'host' computer (compare figure 2.6). The target computer system is a VME-Bus system with a PowerPC board. The host computer is a standard Intel Pentium PC. Host and target computers are linked via an Ethernet connection. This provides great flexibility in terms of the location of the different computers. That is the host computer may either be local or remote. The target and a local host computer are mounted on the same frame together with the necessary I/O boards and integrated on a standard anesthesia workplace CiceroEM manufactured by Dräger AG, Lübeck (compare figure 2.5). This eliminates the limitation L-5. The option of a remote host computer is of particular interest during software development. It allows that software development is done at ETH in Zurich while the code is run on the target computer system located at the hospital in Bern.

The real time critical tasks i.e. input and output of data, the control algorithms as well as supervisor functionality are implemented on the target computer. The modularity of the VME system guarantees for the extendibility on the computer hardware side. The host computer hosts the development environment and functionality for data visualization and data storage. This separation of functionality is quite standard. It is for example found in professional systems like Tornado/VxWorks or Matlab's Real-Time-Workshop with RealLink32. During the development phase or for system configuration a keyboard and mouse are used for user interaction while the system is operated through a touchscreen in the OR.

2.5   Operating Systems

Corresponding to the two hardware systems there are two different operating systems.

2.5.1   XOberon (Target)

The XOberon operating system on the target computer provides standard real time features such as parallel processes, priorities, mechanisms for inter process communication and exception handling. The priorities of different processes are assigned in a way very intuitive for control engineers (see figure 2.7).
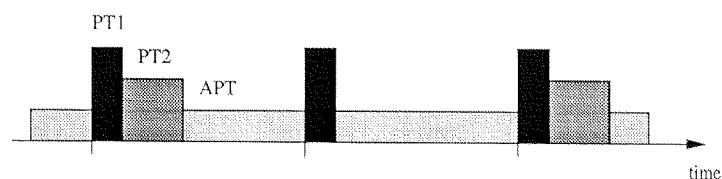
Figure 2.7: Rate monotonic scheduling of XOberon tasks.

The system provides real time (RT), i.e. time critical, and non real time (NRT) tasks. For RT tasks it is further distinguished between periodic (PT) and aperiodic tasks (APT). For the periodic tasks the frequency with which they are to be repeated is specified. The frequency then also determines the priority of the process. That is the operating system regularly interrupts processes of lower frequency to schedule processes with higher frequency. The remaining time between periodic tasks is then divided among non periodic tasks. For any RT task the programmer has to specify a duration and a deadline. The creation of a task can be compared to signing a contract: the handler must guarantee to terminate by consuming at most *duration* microseconds of computation time. The scheduler on the other hand needs to test whether it can guarantee to give the task *duration* microseconds computation time before the deadline passes. The duration thus specifies an obligation of the task handler, while the deadline specifies an obligation of the scheduler which implies

$$period \geq deadline > duration > 0. \tag{2.5}$$

The allocation of computation time to the non real time tasks (threads) is based on a "round robin" scheme. This guarantees that each thread eventually receives a minimum of computation time and avoids priority inversion situations [425].

For data exchange between processes, code segments can be protected from mutual access and signals are provided for inter process synchronization.

An important feature concerning system safety it the handling of exceptions. An exception handler is a procedure which is called by the operating system if a run time error like a reference to un-allocated data or a floating point overflow occur. In its simplest form this procedure switches back from electric to manual dosing (see also section 2.8).

We conclude this introduction to XOberon by briefly mentioning the features that distinguish it from other operating systems that were evaluated. The most important difference between XOberon and the commercial Tornado/VxWorks for our purpose is the way how task priorities are specified. While VxWorks requires that timer interrupts with priorities are defined this mechanisms are nicely encapsulated by XOberon. Particularly with respect to MMI implementations WindosNT represented an interesting alternative. However, the realization of real time features requires considerable low level knowledge about the operating system [336, 197, 456]. This violates the simplicity design criterion.

2.5.2   Oberon System 3 (Host)

The standard Oberon System 3 [393, 495, 394, 192, 138] serves as an operating system for the host computer. The two tasks running on the host computer are data storage and visualization. Both tasks demand an average computation time but no strict timing specifications need to be met. Thus, no real time features are needed here. A main feature of the Oberon System is its graphical interface components called Gadgets some of which are shown in figure 2.13. The use of these Gadgets with Oberon follows the Model-View-Controller (MVC) concept [429, 57]. The MVC methodology was introduced with Smalltalk and its basic idea is to partition the program into three parts (see figure 2.8):
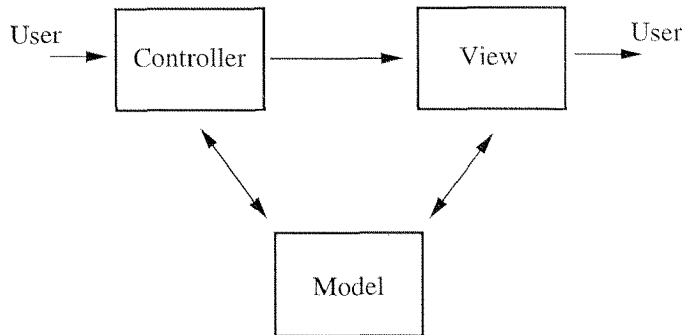
Figure 2.8: The original MVC concept intro-
duced with Smalltalk.
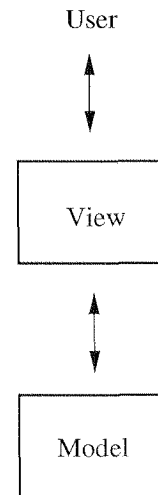
Figure 2.9: The MVC concept used in Oberon
System 3.

- **Model** refers to the core modules of an application. It is responsible for managing the information being manipulated. Model captures some relevant features of some real-world situation. For example, things to be shown in a window have a corresponding data representation. The model then handles this data representation.

- **View** transforms the data handled by the Model into an image that can be seen by the user(s). A Model can be connected to several different views showing the same data but (probably) in different ways.

- The **Controller** coordinates input from user with View and Model. It is thus responsible for coordinating between the Model and the View, so that if one of them changes, it knows how to communicate that fact to the other.

For illustration consider a classical computer system consisting of keyboard, screen, and computer board. And imagine a spread sheet application being run on the computer system. "Controller" in the MVC frame work refers to the program part handling the keyboard and passing the inputs to the program part handling the spread sheet content. That is the part which is referred to as the "Model". "View" refers to the program part responsible for nicely displaying the spread sheet contents on the screen. The control engineer should note that the terms model and controller have a different meaning than in control engineering.

In Oberon this concept is used slightly differently in the sense that Controller and View are combined simply into views. In Oberon System 3 they are referred to as Model and View Gadgets, respectively. The advantage is that the model may be designed independent of how its contents will be displayed. As a simple example consider a variable containing a REAL value. This value may be displayed using a text field or a scroll bar. It is not relevant at the time at which this variable is introduced how it finally will be displayed.

2.6   Programming Language

The decision about the programming language was made in favor of Oberon-2. This choice was strongly influenced by the Oberon-2 know-how available at the automatic control lab. But Oberon-2 has also several objective advantages. Oberon-2 is an object oriented language with similar properties as is ancestors Pascal and Modula II. Features which are important with respect to safety are strong type checking at compile time, runtime type checking, no pointer arithmetic. With these properties Oberon-2 is inherently safer to use (it reduces the probability of occurrence of certain types of faults) than C or C++. Note that also a lot of these properties were later adopted for the design of JAVA [185, 265] as well, which makes JAVA and Oberon-2 very much alike (with respect to their properties not their syntax). The general advantages of JAVA over C++ discussed for example in [22] therefore carry over to the comparison of Oberon-2 and C++. The language Oberon-2 alone is not well suited for real time application [413]. Some extensions are discussed however [494, 193]. The same is true for JAVA [361]. For Oberon-2 only the real time extensions provided by the XOberon compiler render it a suitable alternative to other languages. Another candidate programming language was Ada [354]. Ada was originally designed for the implementation for mission critical software. It inherited several concepts introduced in ALGOL 68 and Pascal [36], it is well structured, modular and strongly type checked. The major disadvantage is that it is very large and complex [198]. A more detailed discussion of some oo programming languages can be found in [404, 409].

2.7   Software design

Choosing suitable platform components is an important step towards fulfilling requirements R-1 to R-4 for an automatic feedback system. Particularly for fulfilling R-2 and R-3 a well structured software is mandatory. The methods for designing oo software are very mature [429, 404, 57] and differ not significantly. They all rely on some kinds of object diagram, class diagram and interaction diagram. Real time systems in addition need to be decomposed into different tasks. Structuring methods for real time systems are described in [184, 69, 88].

[184] suggests to start with a behavioral model where it is assumed that all objects are concurrent. And leave it to a next step to determine which objects are also realized with concurrent tasks. It is thus possible to start with the design of the object structure following the standard procedures and the decision which objects need to be concurrent (or active) and which not is decided afterwards. In identifying the different tasks a tradeoff is to be made. On one hand introducing tasks clarifies and simplifies the design and on the other hand too many tasks may make the implementation too complex and cause considerable scheduling overhead. The approach in [69] is similar. Here the different objects are deemed *passive, active, protected, etc.* already during the design of the object structure. We will here follow [184] by first designing a top level object model which also allows to describe the general system behavior. From there the object and class structure is further detailed and the different tasks are identified.

At the beginning of a design process a context picture (see [429]) helps to get an overview of

the design problem. Figure 2.6 shows such a context picture for our project. The main devices involved are the target and host computers, the respirator, the patient monitor, and an electronic gas dosing device consisting of mass flow controllers and an electrically driven vaporizer. In an earlier project phase a compact electronic gas dosing device (GADOS) from Dräger was in evaluation and in the future an EEG monitor and an infusion pump will be required [418]. Patient monitor and respirator communicate via a serial interface (RS232) while the gas dosage requires three digital-analog converter channels.

We further have the three types of users: system's engineer, control engineer, and anesthetist. Each of them has different requirements towards the software design. The anesthetist is expecting a system which is easy to use. His main requirement concerns the man machine interface. The control engineer occasionally needs to change, alter, or add an algorithm. This may require adding a new device, displaying or storing different variables, and to adjust the user interface. He is expecting to make these alterations on a rather abstract level. The system and software engineer will have to trace and eliminate errors or provide new device drivers.

2.7.1 Object structure

The most important step in oo software design is to determine the objects. The standard oo literature [429, 404, 57] gives some guidelines on how to find the appropriate objects. But eventually there are different object structures that would lead to a successful implementation and we will therefore briefly discuss our reasoning which led to the particular object structure.

From the control systems point of view the essential objects are the input and output signals and in principle it does not matter whether a certain measurement is provided by a device of type "A" or "B". Similar arguments hold for the output signals. Thus a possible design would be to provide measurement variable objects (e.g. an MAP-object or an SpO_2-object) which always provide an up-to-date measurement to the controller, are able to retrieve that measurement from any suitable device and thus 'hide' the device specific aspects from the control engineer. However, although principally it does not matter what device a measurement is derived from, practically it does matter because some device specific information is usually needed for the design of a control algorithm. For example the accuracy (precision) of a measurement plays a role in filter design and knowledge about actuator limits is needed for anti windup measures. Also the dynamic characteristics of the two gas dosing devices mentioned in figure 2.6 are very different which has to be taken into account for controller design. Therefore input/output devices and control algorithms are usually not independent. This reasoning let us conclude that the most intuitive object structure results if reality is mapped into software more or less one to one. Note that this design is also consistent with the guideline given in [429] to have a close map from reality to software structure. Figure 2.10 shows the object on the top level where every input/output device is represented by an individual software object. These device (driver) objects hide the software handshaking and protocol interpretation from the control engineer.

We now have allocated one object for every input or output device. Further, we let mode control logic (see section 4.3) as well as control and fault detection algorithms (see chapters 4 and 7) be represented by individual objects. Control and fault detection algorithms are natural candidates
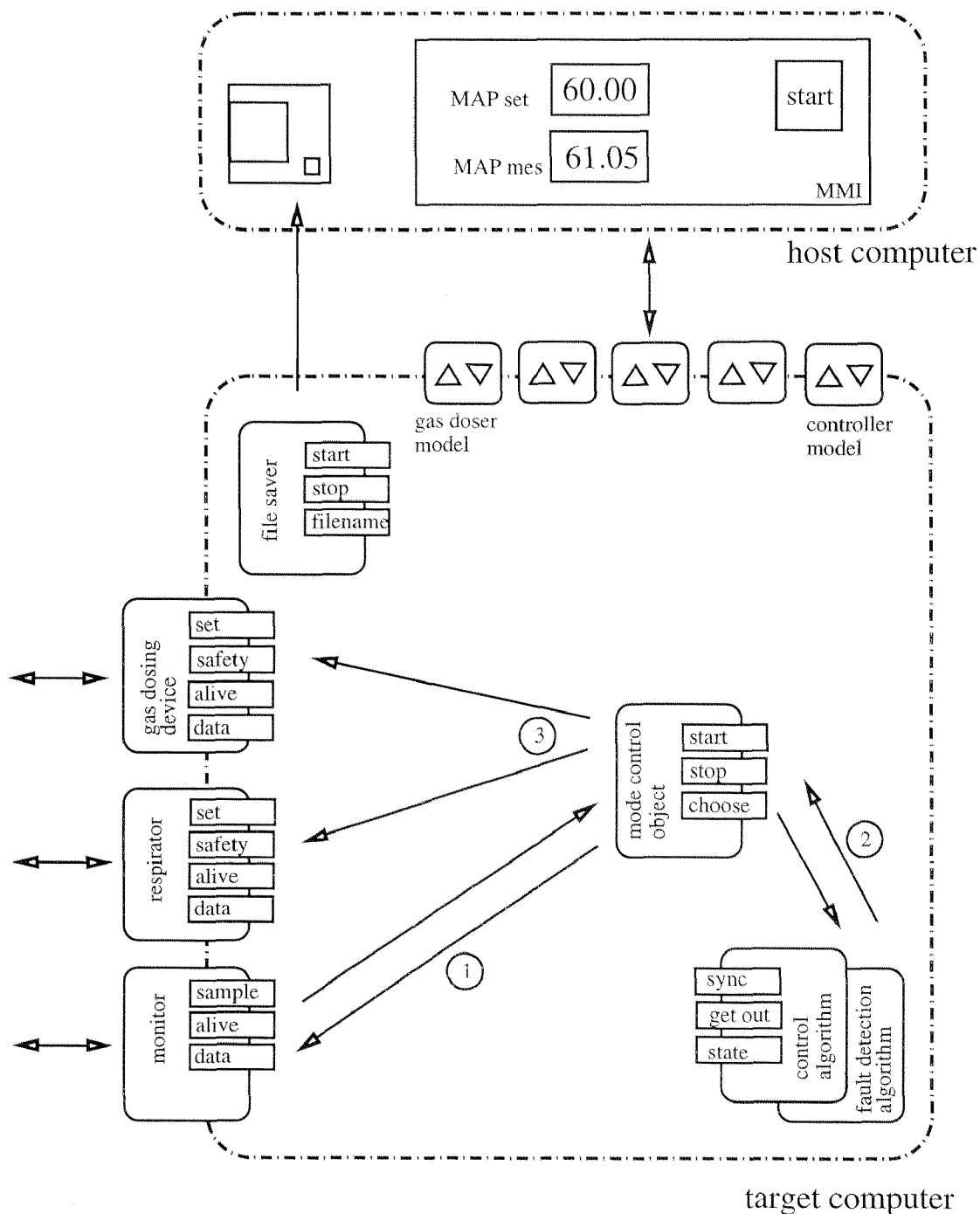
Figure 2.10: Objects at the top level of the object structure.
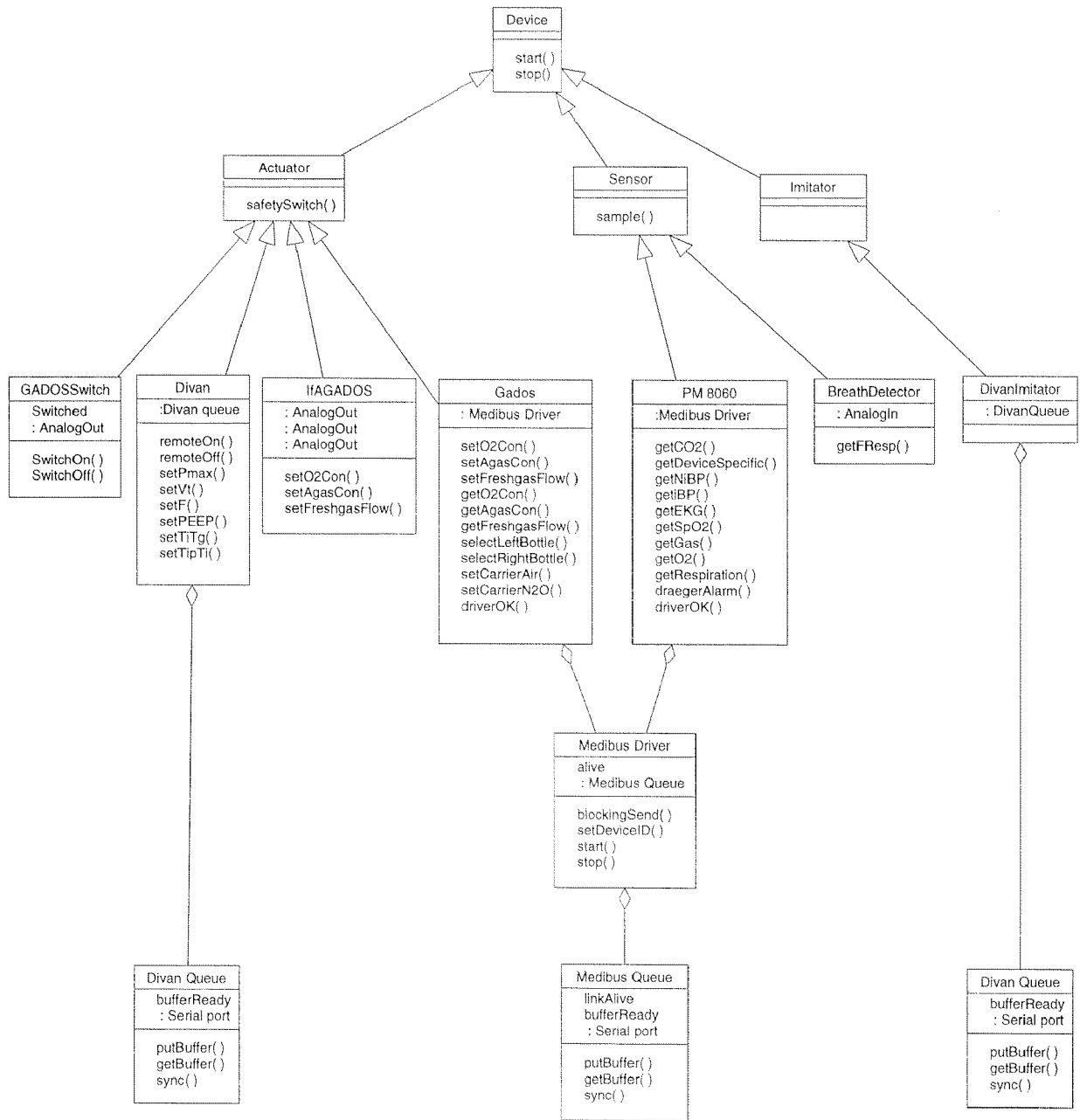
Figure 2.11: Device hierarchy.

for objects since they have a clear defined state and behavior. The same is true for the mode control logic. It represents the central object of a control application and it is essentially the realization of a state automaton. That is it coordinates the sampling from the monitor (1), call of controller methods (2), and writing to the output devices (3). The mode control object thus realizes an important part of the functions that will be allocated to the 'Supervisor' in chapter 5.

Finally there is one model object for every device object, every algorithmic object and the mode control object. The model object may be viewed as being an image of the object it represents. They serve as interface elements between the elements of the user interface on the host and the objects on the target. That is they 'collect' all data available in their original and make it available to view elements located on the host. Their name (model objects) is expressing their function of a model in the MVC concept. The role of these model objects is described in some more detail in section 2.7.4. The primary motivation for this concept is that it allows to decouple the interface design completely from the control application (see also chapter 8).

Figure 2.11 shows the class structure (hierarchy) of the I/O devices. The abstract classes of actuators, sensors and imitators are derived from an abstract device class. From these abstract classes (actuators, sensors, imitators) the concrete I/O device (drivers) are derived.

There is not much in common for these different devices that could be generalized in the abstract classes. Introducing them still has some potential. E.g. for exception handling purpose all actuators may be added to a 'list of actuators'. A shut down procedure then may run through this list and invoke the safety switch method of each device.

The class of imitators seems somewhat odd. Imitators serve to 'calm' devices which have several links of which only some are used by the control system. The PM8060 for example requires links to a gas dosing device and a respirator. In our setup the port originally intended for the gas dosing device is used by our system. The respirator is also connected to our system instead of the monitor. Without a connected respirator, however, the monitor is constantly producing a "VENT COM" alarm. It must be soothed by regularly sending any syntactically correct respirator response. This is done by the DivanImitator class.

A question that arises is whether it could be useful to introduce generic abstract classes for patient monitors, gas dosing device and respirators. Let us discuss this issue for the gas dosing device. A meaningful generic gas dosing device provides the minimum functionality that a gas dosing device must posses. A possible definition of the minimal functionality is to utilize the functionality available in the manual operation mode. By this it will always be possible to functionally replace manual gas dosing with a dosing device extended from the minimal gas dosing device. Utilizing the nomenclature used in figure 2.11 such a minimal device must at least have the methods

- setO2Con()
- setAgasCon()
- setFreshgasFlow()
- setCarrierAir()
- setCarrierN2O().

However, the IfAGados device does not posses all this functionality. It therefore does not make sense to derive IfAGados and GADOS form one generic class of gas dosing devices.

A similar class diagram could be derived for the controllers. However, in [111] no use of the object oriented concepts was made.

2.7.2 Task structure

In [184] guidelines are given which help to determine the task structure from the behavioral diagram where all objects potentially are still concurrent. The following categories of task structuring criteria may be utilized to obtain a suitable task structure:

- **I/O tasks structuring criteria**. This addresses how I/O devices are mapped into tasks which requires a closer look at the different devices. Consider a device that communicates via D/A or A/D channels (e.g. the gas dosing device IfAGADOS). For such devices the driver need not be implemented as a concurrent task. On the other hand there are devices like the patient monitor PM8060 that do not run synchronously with the control application. For such cases it makes sense to implement the corresponding driver objects as concurrent ones. At this point it should be mentioned that multiple inheritance would provide a means to deal with this situation where certain device drivers are also processes. How this concept is implemented in Oberon is discussed in section 2.7.6.

- **Internal task structuring criteria**. These try to identify the internal tasks of the system. According to figure 2.10 potential internal tasks are associated with the mode control object, the algorithmic objects, the storage manager, and the user interaction. Not all of these tasks need to be concurrent as will be discussed next.

- **Task cohesion criteria**. This analysis aims at grouping tasks that exhibit some kind of cohesion. Important here are temporal and sequential cohesion. Temporal cohesion groups tasks which are triggered by the same event and sequential cohesion groups tasks that need to be executed sequentially. Using sequential cohesion arguments shows that mode control objects, algorithmic objects and file saver need not be implemented as concurrent objects. It is namely the mode control task defined in the mode control object which determines the sequential execution of sampling the monitor devices, request of output values of control and fault detection algorithms, and which writes to the actuator devices (see figure 2.10). It makes sense also to let the mode control task initiate the storage of all values since this guarantees the consistency of the data within one control interval.

- **Tasks priority criteria**. Once the different concurrent tasks have been identified their priority needs to be determined. In a first step time critical (RT) tasks are separated from non-time critical tasks and then periodic and aperiodic tasks are distinguished. The only non time critical tasks are the user interactions. In a system with a sampling time of 10 seconds it does not matter whether the display is updated 2 seconds earlier or later. Active (concurrent) device drivers are to be implemented as time critical tasks since the connected devices usually require timing constraints to be met (the PM8060 monitor
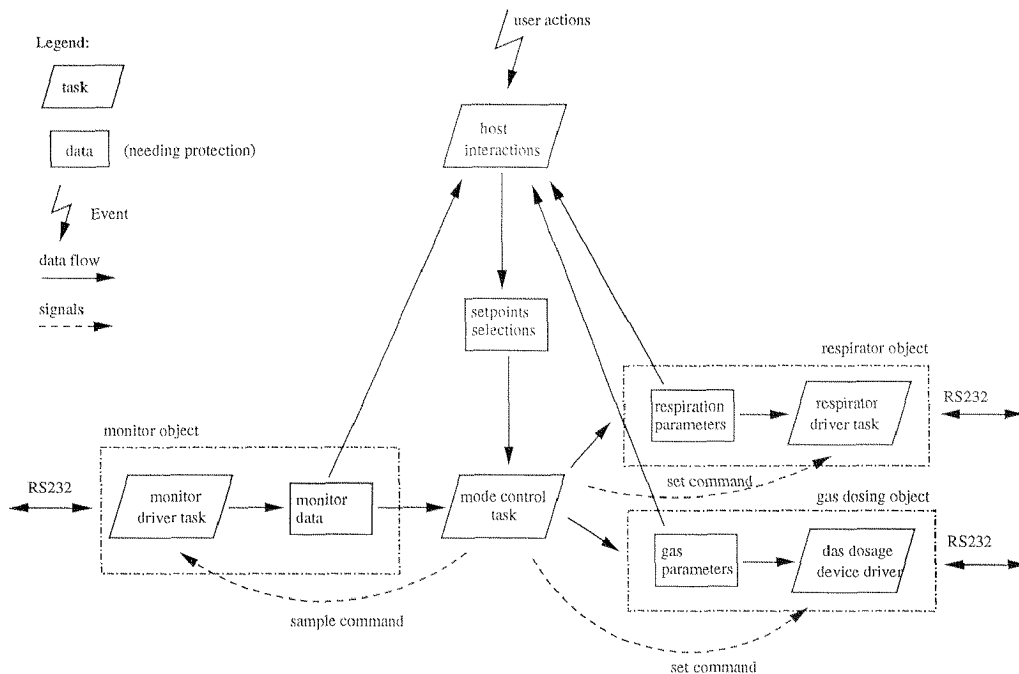
Figure 2.12: The different tasks with their exchanged data and signals.

requires a command to be sent every 2 seconds (at least a NOP) otherwise it falls back into its idle state). The mode control task is time critical also and in general it is periodic with the sampling time. Since the control algorithms developed by Derighetti in [111] need to be synchronized with the breathing cycle this period needs not to be a constant. Such cases might be implemented by generating a new aperiodic time critical task for every sampling period. Alternatively, we mapped these tasks into a high priority thread implementing an endless loop waiting for a synchronization signal from a breath cycle detector.

Figure 2.12 shows the task structure of the system (the notation is taken from [184]) where the three different types of tasks can be distinguished. First there is the mode control task which is defined through the application object and which is responsible for the sampling of the input devices, the call of the control algorithms and the writing to the output devices. Further, every device driver is implemented as a individual periodic process and may thus be viewed as an active object. Finally, there are the asynchronous requests from interface elements of the host computer which are handled as threads by the target operating system. It is also shown what data is exchanged between the different tasks which indicates which data needs to be protected from mutual access. In addition, the signals exchanged among the tasks are shown.

2.7.3 Writing a new control application

Input and output device objects and a skeleton mode control object are provided by the platform. To create a new "control application" (total software package required to use feedback controllers in the OR) this framework needs to be extended which requires the following activities. First
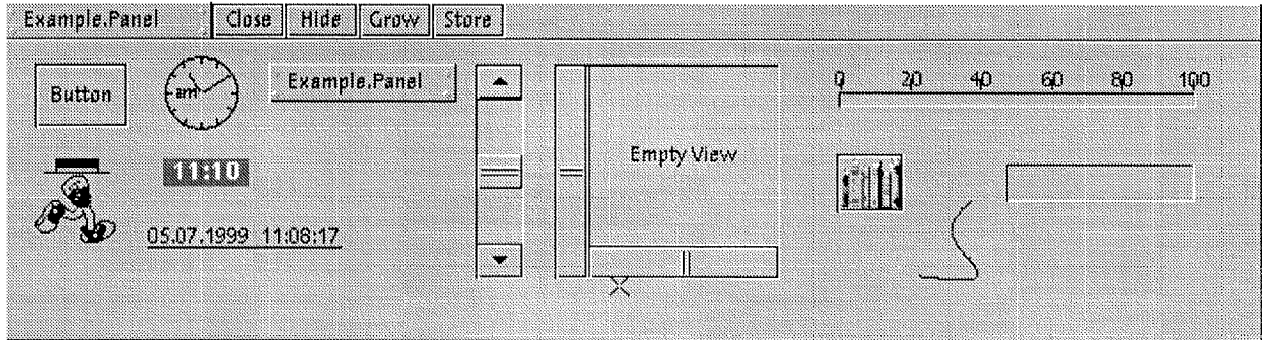
Figure 2.13: A selectin of different View Gadgets available in Oberon System 3.

the new control algorithms must be implemented as a control algorithm object (if not existing). Second, if internal variables of the control algorithm object are to be available for displaying or storing, also a model object corresponding to the control algorithm object must be generated. Finally, a few statements need to be added to the mode control object.

A feature of the XOberon system which proves to be very helpful in the testing and debugging the software is its dynamic loading and linking capability. To test the mode control object only the module defining this class needs to be recompiled, freed and reloaded, the rest stays resident.

2.7.4   Remote gadgets

The Oberon System 3 [192, 191, 138] provides components for the design of graphical user interfaces (GUI) some of which are shown in figure 2.13. It is of course desirable to utilize these existing components for the design of a GUI for our control application. This is not straight forward first since the Gadget system utilizes messages instead of method calls and second since the data to be visualized is localized on the target computer. In this section we will discuss the concepts introduced to allow the use of the System 3 Gadgets with an XOberon application.

To do so we need to introduce briefly the Gadgets messaging system (see figure 2.14). Since we are only able to lay out the very basic concepts the interested reader is referred to [138] for details. Every Gadget (View Gadget or Model Gadget) is an extension of the base class objects. All Gadgets have one message handler (method) and the Gadgets communicate by exchanging messages which are interpreted by the message handler. The messages themselves are record types that are extensions of a generic object message type. This concept makes the Gadgets system very flexible and extendible. The two message types required for the discussion to follow are update messages and attribute messages.

We are now ready to describe the basic concepts required to allow the use of the Gadgets library with an XOberon application. The mechanism is illustrated in figure 2.15. The figure shows the different objects involved if the mean arterial pressure value read from the PM8060 ought to be displayed with a Gadget on the host computer display.
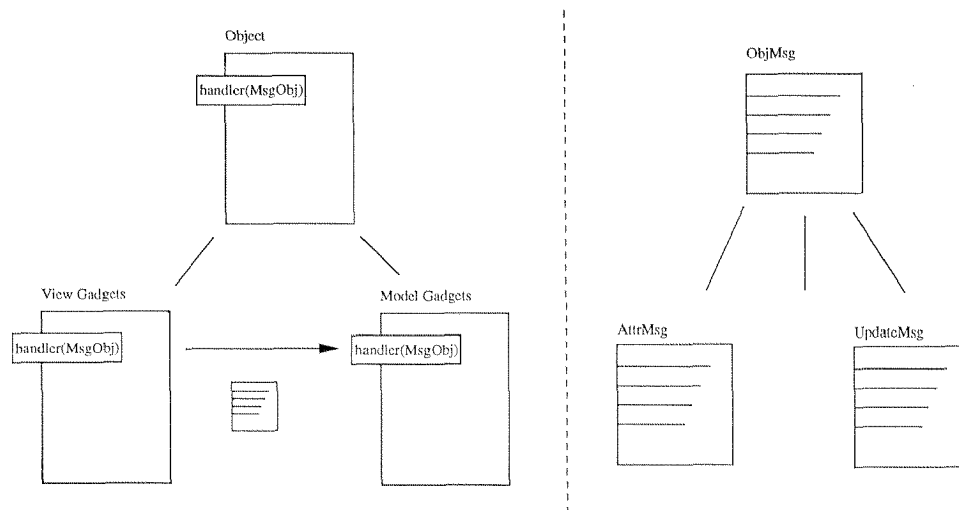
Figure 2.14: The basic ingredients of Oberon System 3 are objects and messages.

On the host side we have a View Gadget located on the display and a remote Gadget. With the Gadgets.Link command of the Oberon operating system a remote Gadget is created and linked to the view Gadget. This remote Gadget has five attributes of interest:

- **IP Nr.**: This attribute specifies the IP number of the target computer.

- **Library**: This attribute specifies the model object on the target computer (compare also figure 2.10).

- **Field**: This attribute specifies which datum of the target object should be displayed.

- **Refresh rate**: This attribute specifies how often a new value shall be requested.

- **Value**: Finally represents the current value of the datum.

The remote Gadget further has an Oberon task. This task is responsible for regularly sending a request for an new value to the target, for polling the connection for the target answer, and after successfully receiving an new value for sending an update message to the display. The display forwards the update message to the view Gadget which upon receipt gets the actual value from the remote Gadget by sending an attribute message.

On the target side we have an inspector daemon, a target object model (the PM8060 model in our example), and the corresponding target object (the PM8060 device object). The inspector daemon is automatically activated by the XOberon operating system upon opening of a connection from the host computer. Such a connection is opened the first time that a remote Gadget sends a data request to the target computer. The daemon re-translates the host data request which arrives in string-format into a Gadget message and sends this message to the model object (the PM8060 model) specified by the library attribute of the remote Gadget. The model gets the required datum (MAP value) from the corresponding device object (the PM8060 device object).

Display

View Gadget

103.50

UpdateMsg

handler

AttrMsg

IP Nr.
Library = PM8060
Field = MAP
Refresh rate
Value

Remote Gadget

Host Computer

Target Computer

handler

getMAP

PM8060 model object

AttrMsg

Inspector Deamon

PM8060

MAP value

PM8060 I/O device object
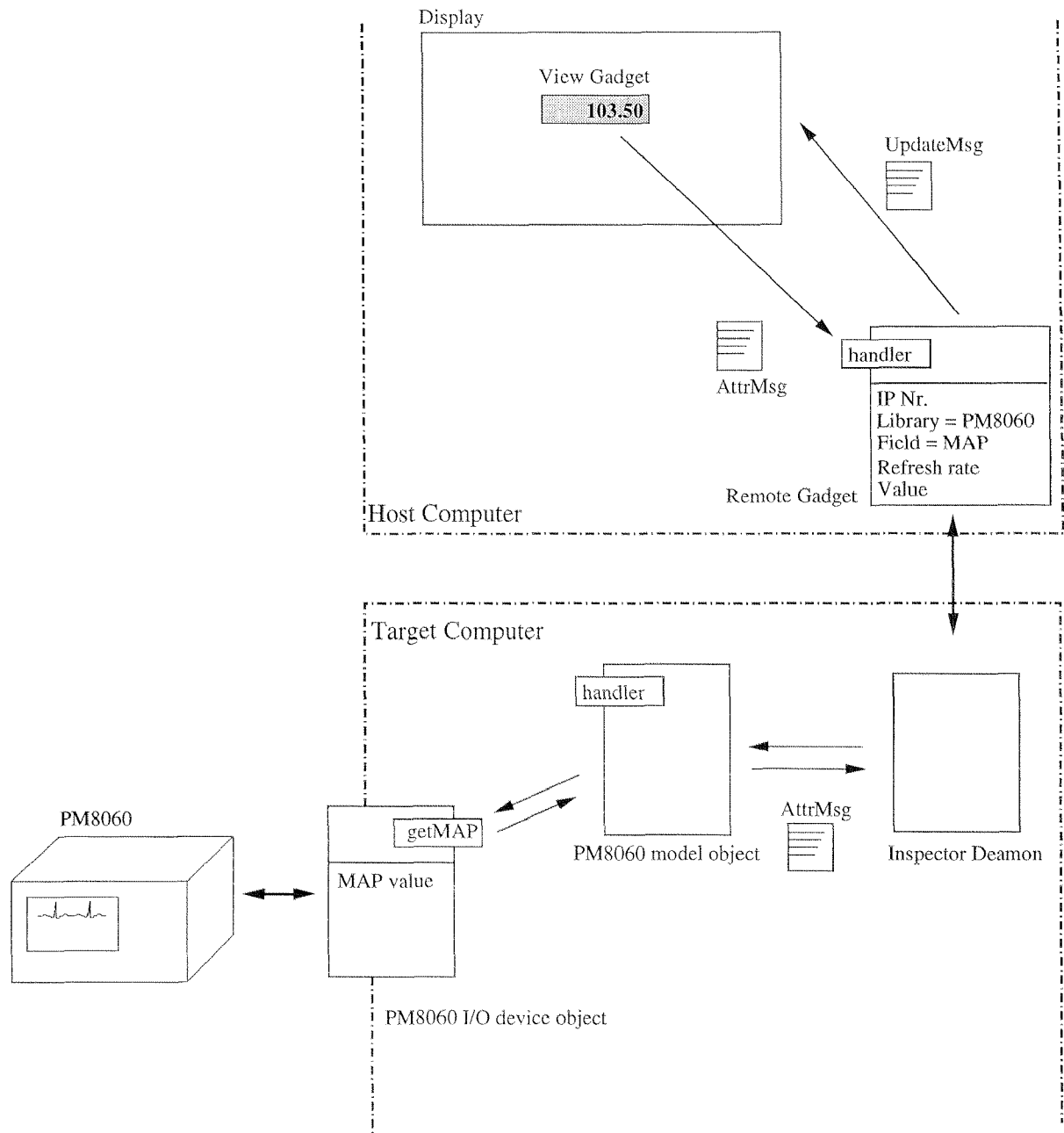
Figure 2.15: Mechanism which allows to display a target datum with an Oberon System 3 View Gadget.

It sends the datum back to the daemon again in the form of a gadget message. The daemon then sends the new value to the host computer in string-format where it is received by the remote Gadget.

2.7.5 Composing user interfaces

Although the mechanisms for target host communication with Gadgets involves several steps (see section 2.7.4) the actual task of composing a graphical user interface (GUI) is not more complicated than with Oberon System 3. The different View Gadgets may be placed on a panel with "drag and drop". After linking the view Gadget to a remote model the Gadgets's Columbus tool might be used to set the required attributes of the remote model (IP Nr., Library, Field, Refresh rate). And that's it.

Clearly, the flexibility in designing GUI's provided by Oberon System 3 carries over to the target host application. In particular the GUI may be designed completely independent from the target application. In principle it would even be possible the modify the GUI at run time on line.

2.7.6 Comments on the use of object orientation

What exactly the key concepts of object oriented software design are depends a bit on the source (see e.g. [404, 57, 334, 204]). The following are generally mentioned:

- **Information hiding or encapsulation:** The complex implementation of data is encapsulated in an object and clients can only access the data via a well defined interface.

- **Abstraction:** An information hiding object so far only exist once. Objects therefore are defined as abstract data types of which multiple instances may be defined.

- **Inheritance:** allows existing abstract data types to be extended to a new type and where this new one inherits all the data and operations from its parent. Existing operations may even be modified. This makes it possible to design semi-finished products and classes that can handle these semi-finite products. An end user might extend these semi-finite products to his needs and may still manipulate them with the existing classes for handling them. A typical example are the base classes of objects and messages of the Oberon System 3 described in 2.7.4.

- **Polymorphism:** If procedures are bound to an object dynamically (at run time) then it is possible to store in a variable of type T not only objects of type T but also any extension of T. Thus variables can be polymorphic. Extensible abstract data types with dynamically bound procedures are called classes. And objects are instances of classes.

[334] summarizes: "Object-oriented programming means programming with abstract data types (classes) using inheritance and dynamic binding". Not all of these concepts are of equal importance for this design.
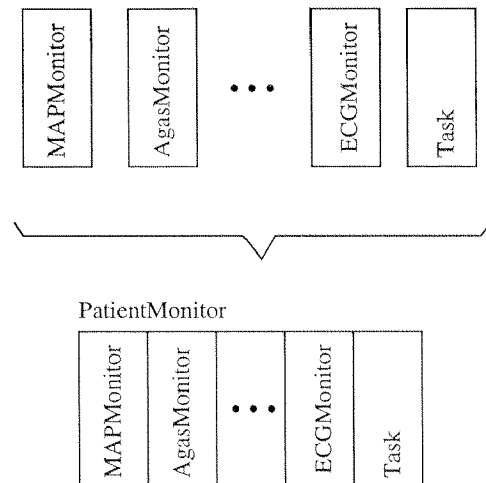
Figure 2.16: Using multiple inheritance to define patient monitors classes.

Most use was made of the encapsulation and abstraction. Encapsulation is the main tool for structuring a system (compare also [429]). It requires to clearly define boundaries and interfaces of software entities (objects) and by this forces to do a lot of thinking before starting implementation. Abstraction plays a role when multiple instances of the same class are desired. It is used in the device hierarchy and controller hierarchy. In the device hierarchy a MedibusDriver object is needed for most Draeger devices. In the controller hierarchy the class of observer based state feedback controllers is defined. Multiple instances of observer based state feedback controller class are used in the endtidal controller and in the MAP override controller.

In section 2.7.1 we have already mentioned where inheritance is of use in defining the device hierarchy. The target object models (figure 2.10) are all extensions of the basic Gadgets object type which enables them to understand the Gadgets messages. Extensions are necessary since their actual behavior depends on the target object that they represent.

It was also mentioned that the device hierarchy would provide a useful application of multiple inheritance (which is not supported by Oberon). Multiple inheritance allows an extension to inherit not just from one class but from several. The problem with multiple inheritance is that it leads to conflicts if the classes are not orthogonal. Multiple inheritance would allow to compose devices from smaller entities. Consider for example a patient monitor and imagine we have defined abstract classes for generic MAPMonitors, AgasMonitors, ECGMonitors, etc. Depending on the actual properties of the monitor a patient monitor might be composed from generic monitor types by means of multiple inheritance. This situation is illustrated in figure 2.16. There is a way around multiple inheritance which is described in [334]. This method was used in our design to realize active devices (see figure 2.17) which are devices and also a real time task. The idea is to define an extension of the device class and add a record field for a real time task and define another extension of the real time class task by adding a field for a device and then to "mate" them by corresponding pointers. Although practical for double inheritance situations we feel that this method is not appropriate for larger combinations.
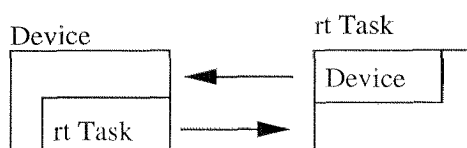
Figure 2.17: Avoiding multiple inheritance for the definition of active devices.

At a number of occasions it is desired to overwrite methods in extended classes. This is for example the case when performing hard ware in the loop simulations where the handler methods of the I/O devices need to be overwritten. It is, however, not required to modify them at run time. In fact, for the whole target software it is true that no use of polymorphism must be made. It is only on the host computer within Oberon System 3 where polymorphism plays an important role.

2.8 Safety aspects at the platform level

In section 2.2 we have listed safety as a major system requirement. In the chapters to follow a number of algorithmic means to increase the safety of this automated anesthesia system will be discussed. A number of faults (e.g. power loss of the target computer), however, can not be handled on an algorithmic level. Furthermore, safety also has to be guaranteed during the development phase of these supervisory algorithms. For such cases safety strategies at platform level have to be provided. These strategies resulted as a direct consequence of a risk analysis [136] which was conducted following [121]. Besides the description of the research platform and the legal aspects the following failure scenarios are identified (the reader is referred to figure 2.5 for reference to the different devices):

FS-1: Failing of any actuator or sensor. For the control loops developed up to now this concerns:

    FS-1a: The mass flow controllers for oxygen or nitrous oxide may either fail to dose the correct amount of gas or pressure reduction valves might break so that the gas enters the respirator at supply pressure.

    FS-1b: The electrically driven vaporizer might be stuck or empty.

    FS-1c: The gas concentration measurements might be wrong.

    FS-1d: The blood pressure measurement might be wrong.

FS-2: Loss of electric power or supply pressure.

FS-3: Malfunctioning of a control algorithm.

Recall equation 2.1 which defines risk. For the scenarios described above risk must be reduced by reducing the harm. This is achieved by the following counter measures. Note that according to the industrial standard [2] the measures only have to deal with single point failures.

CM-1: Counter measures for sensor and actuator failure scenarios.

CM-1a: For the case of an incorrect flow additional flow meters allow an optical verification of the flows by the supervising anesthetist. An emergency button allows to activate manual dosing immediately. The details of this fall back strategy are described below. Damage in the case of broken valves is prevented by the respirator which is equipped with a relief pressure valve.

CM-1b: The position of the electrically driven vaporizer can visually be inspected easily due to additional extra large markings. The level of anesthetic in the vaporizer can be checked with the standard level indicator. Again the emergency button allows to inactivate the electric vaporizer immediately.

CM-1c: A redundant gas monitor allows to verify the PM8060 measurements. The alarm thresholds of this second monitor are to be set.

CM-1d: A fully redundant invasive blood pressure measurement would require a second arterial cannula which is clinically not acceptable. To provide a redundant blood pressure measurement an upper arm cuff must be connected to the PM8060 to enable non invasive blood pressure measurements.

CM-2: There are two possible power loss scenarios, a breakdown of the power supply or an accidental switching off of the computers. The first power failure case is covered by with a uninterruptable power supply (UPS) and in the second case a fall back concept automatically switches to manual control. The same is true for the case of supply pressure loss.

CM-3: In case of a controller with insufficient performance or which is unstable the supervising anesthetist is able to inactivate automatic control by either switching the controller off via the control panel or by pressing the emergency button.

A number of counter measures have been mentioned that rely on a fallback strategy. This strategy is schematically shown in figure 2.18. According to this the gas flow can either be dosed manually or electrically. Switching from one dosing mode to the other occurs with the pneumatically driven valve PV. Where in the pressureless state the manual dosing is active. The pressure supply for the valve PV is controlled through the two valves MV and EV. MV is a manually operated valve located at the rear of the research platform. EV is an electrically operated valve. There are three switches in series that control EV. Of course all of them need to be closed to switch EV. The switch WD denotes the hardware watchdog and the switch EB denotes the emergency button. The switch GS is driven by an analog output of the target computer system. This output is switched at the moment when the control system changes from the state PASSIVE to the state DOSING (see section 4.3 for reference). Thus, the research platform falls back to manual dosing whenever either the watchdog is triggered or the emergency button is pressed or if the control system is in state PASSIVE.

Note that before switching to electronic dosage the anesthetist is able to set a preset flow for the manual dosage which becomes active as soon as the system falls back to manual dosing.
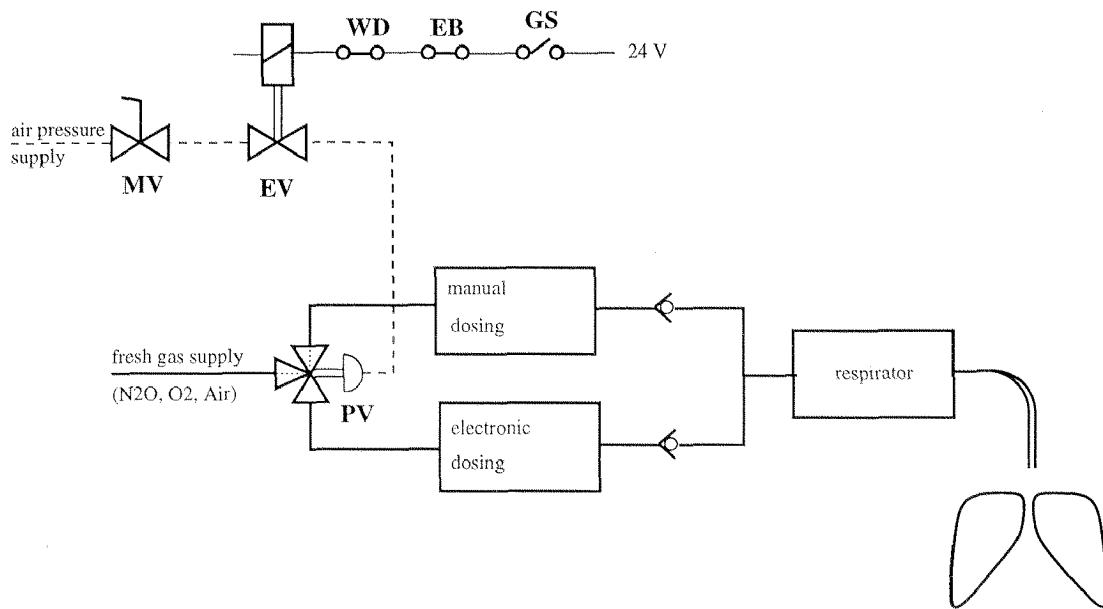
Figure 2.18: Fall back concept at platform level.

2.9 Conclusions

The research platform as shown in figure 2.5 has been used in several clinical studies. The compact integration on a standard workplace and the fact that it can be used for normal manual anesthesia as well as for testing feedback controllers significantly reduces the procedural difficulties encountered with the first prototype system. It allows to use the same workplace from the beginning to the end of surgery and time required until automatic controllers are ready is shortened since no wiring needs to be installed. The experimental system is now at a stage where a instructed anesthetist is able to use the system without engineer's support.

With the XOberon system a non commercial tool was used. Since the number of users (e.g. [421, 476]) and therefore testers is considerably lower than for commercial products one would expect a much higher error density. The fact is that we ran into two nontrivial problems on the XOberon Software level, which were solved by intensive teamwork with the designer. For comparison, we roughly had to spend twice as much time to eliminate software problems on the application level due to implementation errors.

From our experience, caution is required when using classes written for Oberon System 3 applications. In a library developed at our lab which implements matrices and the corresponding operations, extensive use of memory allocations (NEW) is made and a lot of garbage is created. This is not a problem in the standard Oberon System 3 since it is equipped with a garbage collector. In real time tasks, however, memory allocation must be avoided because of its unpredictable duration.

Different use could be made of object oriented programming paradigms. Important were encapsulation and abstraction, polymorphism was negligible.

Extending the MVC concept to the target-host-architecture gives great flexibility in GUI design (see also chapter 8). In particular since future XOberon versions will provide a Web-server on the target it will also be possible to draw from available JAVA libraries like [435] for GUI design.

Chapter 3

The Model

3.1 Introduction

In section 1.2 it has been discussed that the complete description of the system to be considered for - manual of automatic - control during anesthesia results in a large MIMO model. The mathematical models to be discussed in this chapter will, however, only represent a subsystem of that. And since this thesis is concerned with fault tolerant control of mean arterial blood pressure (MAP) via Isoflurane the model will describe the relation between the concentration of anesthetics mixed into the fresh gas stream and the measurements of inspiratory and exspiratory concentrations of anesthetics as well as MAP. In addition the strongest source of disturbance of MAP - the surgical stimulations - is also included in the model. This situation is illustrated in figure 3.1.
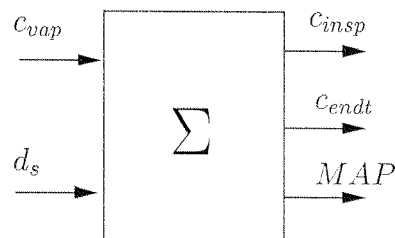
Figure 3.1: Submodel with two inputs and three outputs.

The model in figure 3.1 may be split into the respirator part and the physiology part as shown in figure 3.2, which shall be discussed separately.

Concerning volatile anesthetics and MAP several models may be found in the literature.

For the uptake and distribution of volatile anesthetics, four physiology based models are discussed and compared in [299]. References to earlier models with questionable physiological assumptions

c_{vap} → Ventilator

c_{insp} →

c_{endt} →

d_s → Patient MAP →

Σ
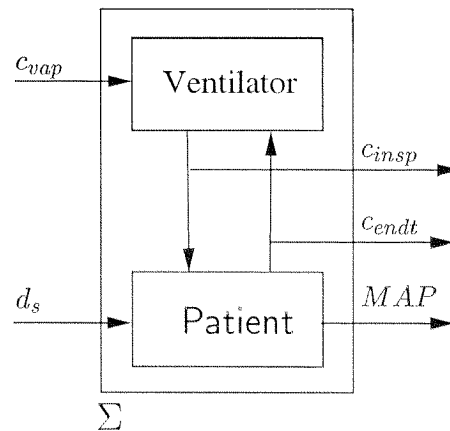
Figure 3.2: Two subparts are to be modeled. One is a technical device (ventilator) and the other represents in vivo physiological processes (patient).

are also given. The four models agree in their way of modeling the different organs in terms of compartments but differ in the way how blood transport in arteries and veins is modeled. For one model, transport phenomena are entirely neglected, two models explicitly introduce transportation delays and the fourth model accounts for the blood transport with a separate arterial and venous compartment (pool). The authors conclude that neglecting circulation times leads to systematic errors mainly in the first few minutes after beginning or termination of drug administration. That is, the difference is pronounced mainly at high frequencies. Little difference was found between the different approaches of modeling arterial and venous blood transport.

A further physiology based model is introduced in [267]. It models the different organs in the same way through compartments as the four models compared in [299] and it accounts for blood transport with separate venous and arterial blood pools leading to a model with 13 body compartments. Pharmacodynamics (cf. definition 3.2.1) and patient dependency of the parameters are neglected but in a broad clinical validation [268] a reasonably good fit was obtained. The largest errors are observed during fast transients, i.e. at high frequencies.

Another model exclusively dealing with the uptake and distribution of volatile anesthetics was introduced by Yasuda et al. in [503, 505, 504]. It is a classical mammillary compartment model as discussed for example in [225] with five compartments. The values of the volumes and exchange rates were derived from step response data. The physiological interpretation of the volumes and time constants was made a posteriori.

Fukui and Smith [157, 158] present a model that combines the effects of a volatile anesthetic (Halothane), ventilation, CO_2, and hemodynamics. The model is very detailed and consequently very complex. It models cardio vascular dynamics beat-to-beat and it includes baroreflex effects. The numerous parameters of the model are unpublished and the effects of surgical stimulations are not modeled.

A model which focuses on the changes of MAP due to inspired Isoflurane is used by the group of Linkens in several simulation studies [273, 274, 280, 279, 293, 297, 296]. The model is of first

order with a time delay, i.e.

$$G(s) = \frac{\Delta MAP(s)}{c_{insp}(s)} = \frac{Ke^{-\tau s}}{(1 + Ts)} \tag{3.1}$$

with

$$\tau = 25\ s = 0.42\ min$$
$$T = 2\ min$$
$$K = -15\ mmHg/\%$$

In the first paper where this model is used [281] they describe, how the parameters are justified. They basically rely on published data by Millard et al. [327].

Smith and Schwede [437] also derive an input/output model to relate a volatile anesthetic (Halothane) and MAP experimentally in dogs. They performed step response and frequency response experiments. For their step response experiments they find that four exponentials (corresponding to a forth order system) are sufficient to characterize the response. In the frequency response they observe little deviations from a first order system.

Concerning the understanding of surgical stimulation and pain perception a lot of work has been done ([379, 380, 499, 479]). In this research the goal is to find a relationship between drug infusion and pain perception during and after surgery. The effects of standardized painful stimuli to physiological reactions is analyzed qualitatively. The main objective of this research is to find optimal strategies of drug administration in critical care. The dynamics of physiological reactions to surgical stimulations was not of interest for this type of research. Concerning the mathematical modeling of pain an overview is given in [62]. The focus of the literature discussed therein is to model the neural aspects of pain, and the authors identify three levels at which the problem has been addressed: the molecular level, the cellular level and the level of large neural networks. The hemodynamic aspects are not discussed. An example of a model for dental pain perception can be found in [142, 143, 144]. In these references the authors derive a linear black box model for the perception of temperature induced dental pain. As a measure of pain they use the finger span voluntarily applied by the subjects under test. That is the subjects were instructed to match their finger-span between thumb and index finger to the perceived pain intensity [142]. The span was then measured with a linear potentiometer. The model thus covers the transfer from afferent nerve activity to the voluntary finger span measure. Unfortunately it is not possible to transfer their results to our problem, first since the authors don't give any physiological interpretation of their transfer function and second since it covers a large portion of the efferent nervous system while the blood pressure response is mainly an effect of the response of the afferent nervous system.

Deriving models for the respiratory circuit is expected to be simpler since it may be done based on first principles. However, not much can be found in the literature. For the development of an adaptive controller for closed circuit anesthesia described in [477] or [226] the authors establish mass balances in the respirator to optimally adjust the fresh gas composition. But the dynamic aspects such as transportation delays are neglected. The model of Leron et al. discussed above [267] also accounts for the ventilation circuit. The authors model the closed circuit system with an additional first order differential equation derived from mass balances.

There is thus no model available describing the relations depicted in figure 3.2. This gap is closed by Derighetti in his thesis [111] where he has derived a model that combines all the above mentioned input and output signals. The model builds on a model for the uptake and distribution of volatile anesthetics introduced by Zwart et al. [524, 438] for Halothane. It was adopted in an MD thesis by Nicolet [344] for Isoflurane and other common volatile anesthetics. This part describing the kinetics of volatile anesthetics has been used successfully for controller design and simulation by other authors [516, 337, 110, 153]. This model was augmented with a model for the influence of surgical stimulations [112] and the dynamics of the respirator [111]. Derighetti used numerical methods to reduce the order of the model. And he successfully used the reduced order model to derive model based controllers. In preparing the controllers of Derighetti for a broad clinical validation and in validating the models for fault detection purposes, however, we discovered several points of refinements and improvement potential. These refinements concern pharmacokinetic and pharmacodynamic parameters of the Isoflurane model, structure and parameters of the model for the effect of surgical stimulations, as well as structure and parameters the model for the respiratory circuit. The aim of this chapter is to present an updated version of the model introduced by Derighetti in his thesis [111]. In contrast to Derighetti our goal is finally to use the model for fault detection purposes. For this it is important to trace the influence of every parameter in the model to allow runtime adjustment of the fault detectors. The ease of having a low order model is much less important. No effort will therefore be spent on model reduction.

We organized the chapter as follows. In section 3.2 the physiological background is provided. The reader will realize that in some cases more background is provided than is later used in the model. This is done intentionally. With this we want to give a clear indication where simplifications were made and we also want to provide starting points if someone intends to improve the model. In section 3.3 the - in our view - relevant physiological aspects are modeled in terms of nonlinear physiology based differential equations. In section 3.6 the parameters of the model are determined and in section 3.7 several validation experiments are provided. A linearization of the model is given in section 3.8 and some remarks on the bandwidth of the model are made in section 3.9. Concluding remarks are given in section 3.10. The equations and the parameters of the model are summarized in section 3.5 and table 3.6, respectively for reference.

3.2 Physiology

In this section the physiological foundations which will be used for the derivation of the model are reviewed. For a more thorough treatment of this matter the interested reader is referred to literature exclusively dealing with the physiological basis of anesthesia. A good reference in this respect is [97].

In studying drugs and their relation to the body it is distinguished between pharmacokinetics and pharmacodynamics. The exact definitions depend a bit on the source [171, 109]. We will use the definition given in [109] which is as follows.

Definition 3.2.1 *Pharmacodynamics (PD) can be defined as the quantitative relationship between*

(observed) plasma and/or tissue concentration(s) of an active substance and the magnitude of the (observed) pharmacological effect(s). In contrast Pharmacokinetics (PK) describes the quantitative relationship between administered drug and (observed) plasma and/or tissue concentration(s). Loosely speaking pharmacokinetics describes what the body does to the drug while pharmacodynamics describe what the drug does to the body [4].

3.2.1 Solubilities, partial pressures, and concentrations

Before going further into physiology some physical facts about gases are briefly reviewed. First, recall that the total pressure of a gas mixture is given by the sum of the partial pressures of every component, i.e.

$$p = \sum_{i=1}^{N} p_i \tag{3.2}$$

where N denotes the number of components in the mixture. If there are two phases, e.g. a liquid phase and a vapor phase, then the partial pressure of every component in the two phases are equal in equilibrium. If they are not equal, molecules move from the phase with higher partial pressure to the phase with lower partial pressure until equilibrium is reached. The driving forces for exchange are thus partial pressures.

If mass balances are to be derived concentrations rather than partial pressures are of interest. The number of molecules per volume in the liquid phase (i.e. the concentration) is described by Henry's law given by

$$c_i = a p_i \tag{3.3}$$

where a denotes the solubility coefficient. For volatile anesthetics this relation is usually stated in terms of partition coefficients (λ) instead of solubilities [129]. The partition coefficient of any two phases (e.g. gas/blood or blood/tissue) describes the ratio of the concentrations in the two phases at equilibrium, i.e.

$$\lambda_{gas/blood} = \frac{c_{gas}}{c_{blood}} \quad [-]. \tag{3.4}$$

In our model gas/blood and gas/tissue partition coefficients will be used. Note that the gas/blood partition coefficients may be related to the solubility coefficients, if the partial pressure is expressed in terms of a concentration.

3.2.2 Physiological background of volatile anesthetics

Most of the physiological mechanisms to be described hold generally for volatile and in particular fluorinated Ether anesthetics like Isoflurane, Enflurane, etc. When discussing aspects that are common we will refer to volatile anesthetics and whenever differences between the different

anesthetics exist we will discuss the particular case of Isoflurane which is used throughout the whole thesis.

Since volatile anesthetics are applied by mixing them into the inspired air during artificial ventilation some aspects of respiratory physiology shall be discussed first. During normal spontaneous and artificial ventilation not the whole lung volume is replaced in every breath. According to figure 3.3 the total lung volume may be partitioned into different volumes based on their physiological importance.
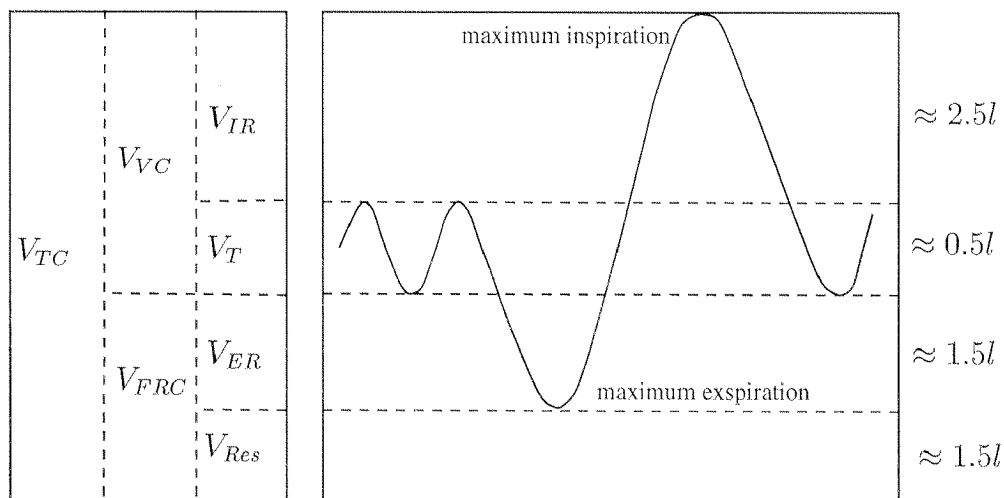
Figure 3.3: Partitioning of the lung volume into parts of different physilogical importance see also the references [23, 431, 145, 230].

The volume exchanged during a normal respiratory cycle is the tidal volume (V_T). Especially during exercise, however, the thorax is expanded much wider such that there is an additional volume that is available during inspiration and which is called the inspiratory reserve volume (V_{IR}). Analogously, additional exspiratory volume is available if the thorax is compressed more than normal. This volume is called the exspiratory reserve volume (V_{ER}). Finally, there is a residual volume (V_{Res}) which can not be removed from the lung. Together with the exspiratory reserve volume it forms the functional residual capacity (V_{FRC}). During artificial ventilation the tidal volume is moved in and out of the lung by a mechanical ventilator. Functional residual capacity stays resident in the lung also during mechanical ventilation. The total ventilation of the lung q_V is specified by the anesthetist in terms of respiratory frequency f_R and tidal volume V_T, i.e.

$$q_V = f_R V_T. \tag{3.5}$$

This product is also referred to as minute volume (MV).

Volatile anesthetics now are carried into the lungs through the normal respiratory mechanism. On the way into the lung the bronchi branch about 20 times until they end in the alveoli. The exchange of gas between inspired air and the blood takes place in the alveoli only. The whole bronchial system does not participate in gas exchange and is referred to as the anatomic dead space. These facts are illustrated in figure 3.4.
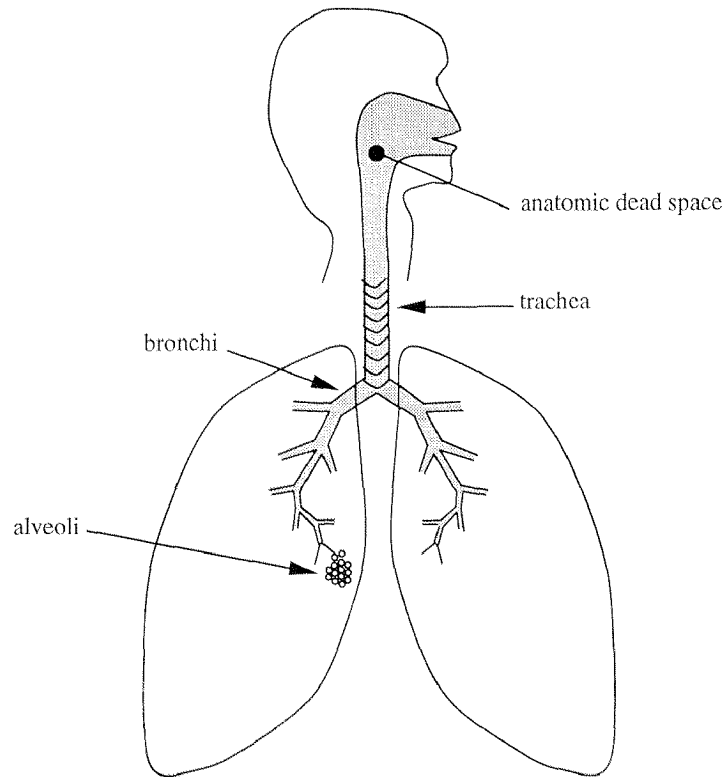
Figure 3.4: See also [431, 66, 230] for reference.

In figure 3.5 the situation in the alveoli is schematically shown. Alveoli have a diameter of about $0.3mm$. They are separated form the capillaries by cells and a membrane of about $0.2 \ldots 0.6 \mu m$. The total area of alveoli is in the range of $50 \ldots 100 m^2$. Recalling Ficks's law (see e.g. [189]) which governs diffusion through a membrane

$$q_{gas} \sim AD\frac{\Delta p}{d} \tag{3.6}$$

where q_{gas} denotes the mass transport across the barrier, A denotes the surface, D denotes the diffusion constant and Δp denotes the partial pressure difference across the barrier of thickness d. The diffusion constant

$$D \sim \frac{\lambda}{\sqrt{m}} \tag{3.7}$$

is proportional to the solubility of the gas in the membrane λ and the square root of the molecular weight m. From this equation it becomes clear that diffusion is a powerful mechanism of transportation at the scales encountered in alveoli.

Further, for gases like nitrous oxide that don't bind to hemoglobin and do not have high solubility in blood, the partial pressure in the blood passing an alveolus rapidly equilibrates with the partial pressure in the alveolus [486]. The time required for equilibration is much shorter than the time required for the blood to pass the alveolus. The transport of such a gas is thus said to be perfusion limited [486]. In contrast carbon monoxide is bound to hemoglobin. This allows a lot of CO to transfer the barrier without significant changes in partial pressure. The time of passing

the alveolus does not allow equilibration. The transport of such gases is said to be diffusion limited [486].

Isoflurane seems to lie between these two extremes. At least [258] gives experimental evidence that no complete equilibration occurs since the authors find a finite alveolar-pulmonary -end-capillary partial pressure difference. They are not able to give a final explanation for this but attribute some of the problems to the large molecular weight of Isoflurane compared to O_2 and CO_2.
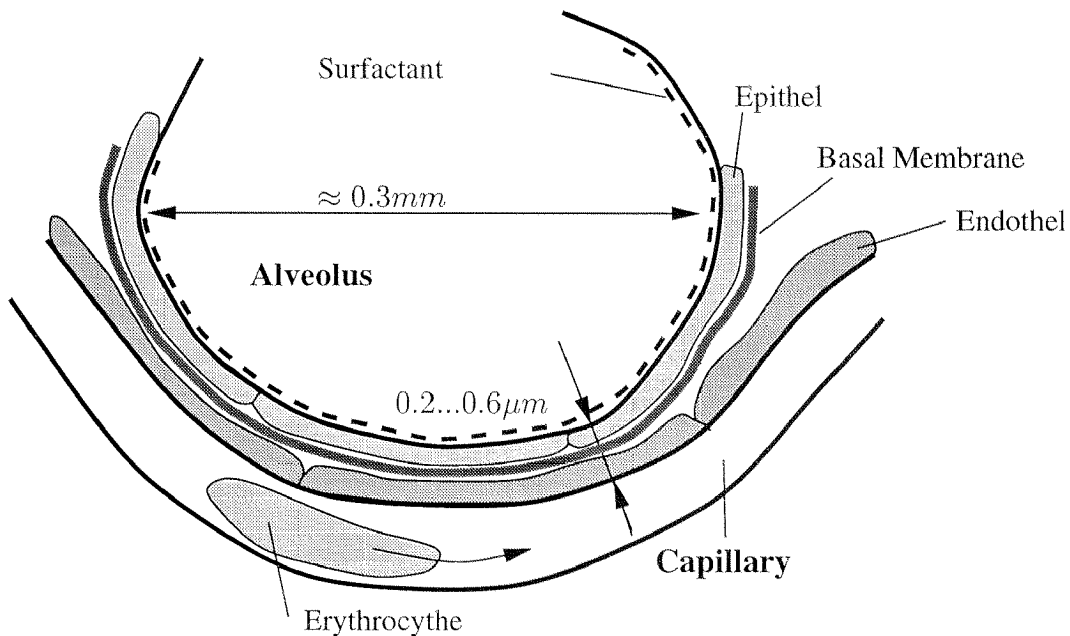
Figure 3.5: Schematic of the anatomic aspects of alvolar gas exchange. See for example [23, 431, 66] for reference.

The amount of anesthetic being carried away in the pulmonary blood is determined by the partial pressure of anesthetic in the blood and its solubility in the blood.

Not all alveoli participate in the gas exchange. In fact, four abnormal situations may be distinguished as illustrated in figure 3.6.

First an alveolus might not be ventilated (A). On the other hand a capillary might not be perfused (B). Third there are ventilated alveoli with perfused corresponding capillaries but where no diffusion occurs due to for example increase diffusion length (C). And finally there are cases where a direct anatomical shunt from the venous side to the arterial side exist (D). The first three cases are pathological and may be a result of a disease of the lung like pneumonia while the last case is a birth defect. The cases where venous blood is transfered to the arterial side without gas exchange are referred to as pulmonary or lung shunt (ls). And the alveoli that are ventilated but do not participate in gas exchange are building the alveolar dead space (V_{AD}). The net alveolar ventilation is thus decreased by alveolar and anatomic dead space, i.e.

$$q_{AV} = f_R(V_T - V_D - V_{AD}).$$ (3.8)
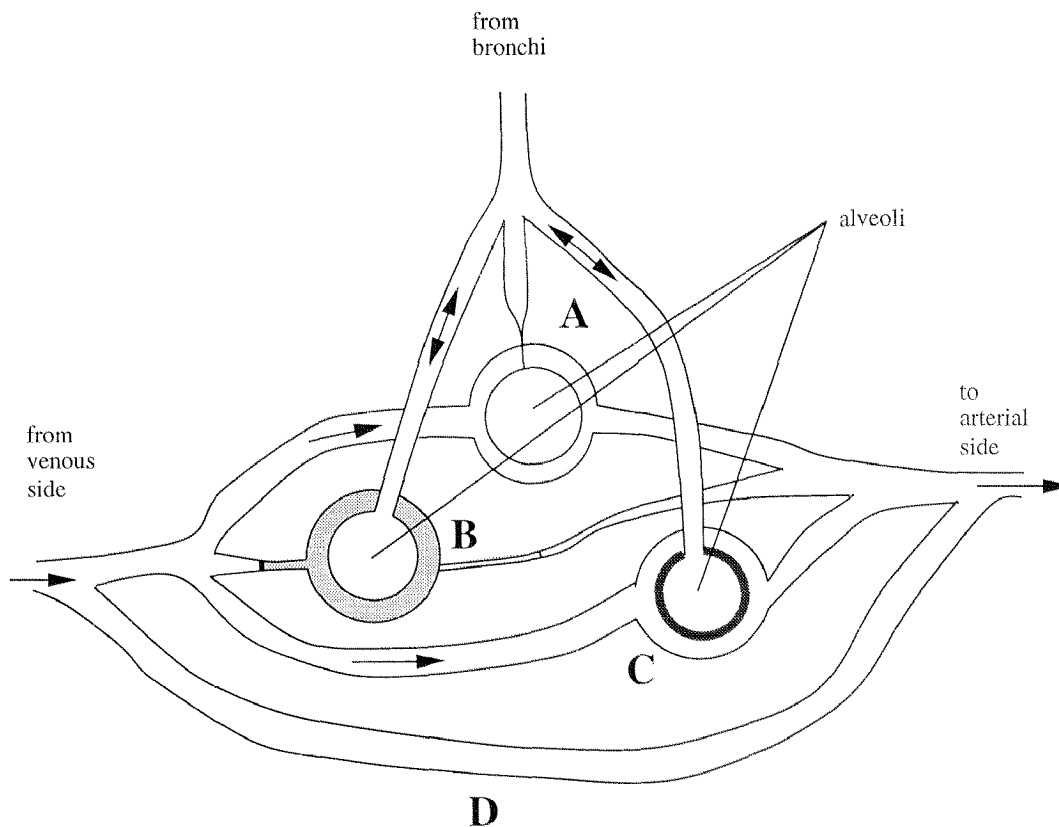
Figure 3.6: Different cases of abnormal gas exchange situations [23, 431, 145].

Volatile anesthetics are carried to the lung and into the alveolar through the normal respiratory mechanisms. In the alveoli diffusion is responsible for the exchange of anesthetics between the alveoli and the blood.

The net uptake of anesthetic is thus determined by (see also [129, 513, 514]):

a) the alveolar ventilation

b) the solubility (blood/gas partition coefficient)

c) the cardiac output

d) the alveolar to venous anesthetic partial pressure difference

e) ventilation or perfusion abnormalities

The anesthetic is then carried to all the different organs by the blood. Similarly to the bronchi the arteries branch several times on the path to an organ. While the aorta has about a diameter of $2...3cm$ the capillaries have a diameter of about $0.9\mu m$ [431]. The corresponding velocity of the blood flow is $60cm/s$ and $0.5cm/s$ respectively [431, 116, 347]. The capillaries in tissues form a meshwork with a roughly uniform distribution of capillaries in local regions of uniform structure and metabolic demand. Each capillary roughly supplies tissue in its neighborhood of

about $0.003...0.0003mm^2$ [225, 348]. At these scales diffusion processes again are responsible for a rapid equilibration of the partial pressure in the blood and the tissue. The main factor determining the uptake of anesthetics by tissue are:
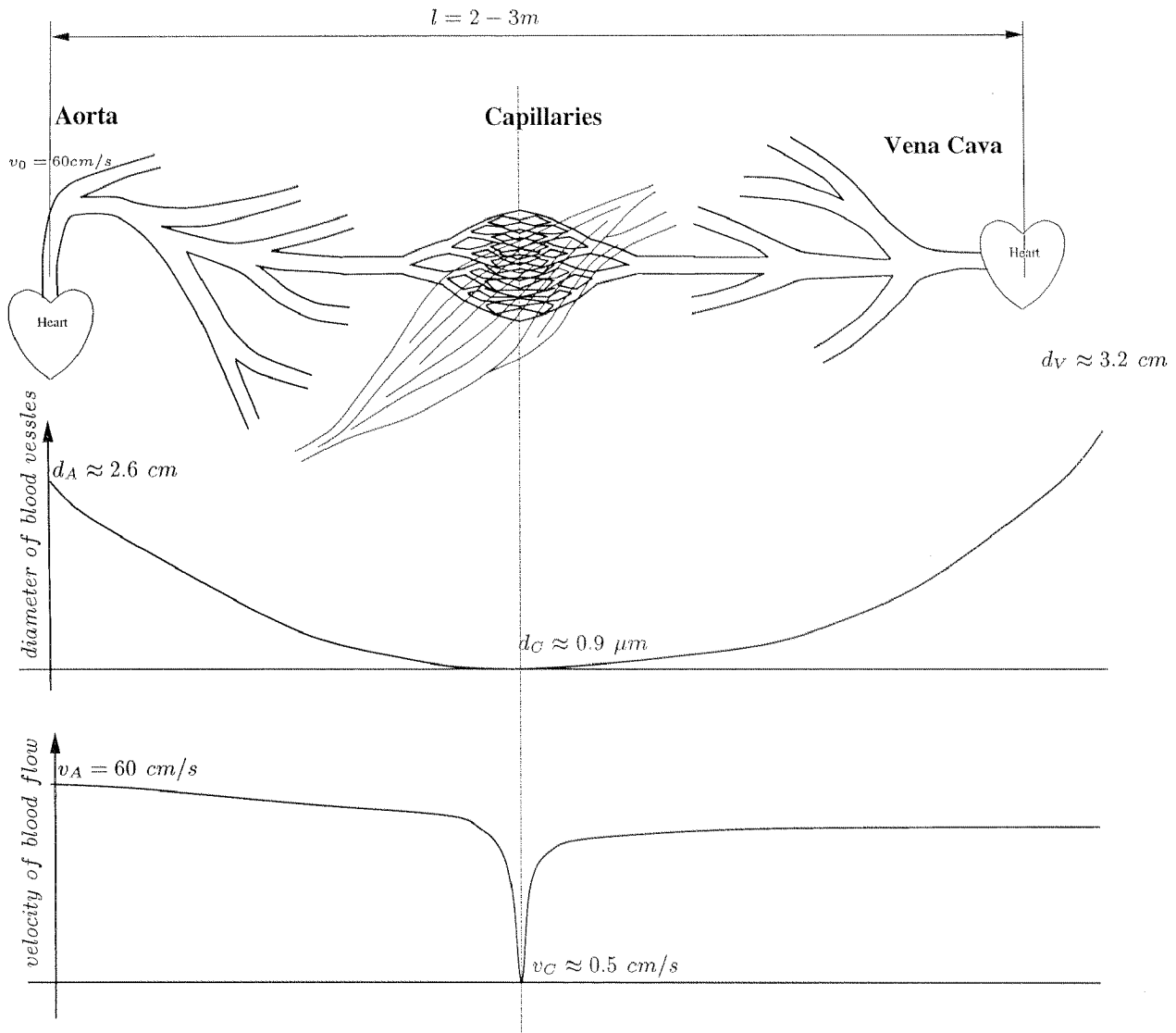
Figure 3.7: The conditions for blood flow through the vascular system change significantly between the ventricles back to the atria of the heart. In the large vessels leading to and from the peripheral capillaries the velocity of blood flow is high compared to the velocity in the capillaries. In a first approximation the pure transportation delay is therefore usually neglected. See also [431] or [66] [347] for reference.

a) the size of the tissue

b) the affinity of the tissue for anesthetic (tissue/blood partition coefficient)

c) perfusion of the organ

d) the partial pressure difference between blood and tissue

And the tissue capacity relative to blood flow determines the amount of anesthetic taken up and thus the rate at which the partial pressure in the tissue changes (see e.g. [129, 513, 514]).

Volatile anesthetics are metabolized at different rates [100]. For Isoflurane the metabolization rate is less than 3% [100]. And since the elimination of anesthetics through the skin is negligible [512] exspiration is the main source of elimination for most volatile anesthetics.

Up to now we have discussed what happens with volatile anesthetics that enter the body, that is the pharmacokinetics. But anesthetics also act on the body. This is described by the pharmacodynamics.

A first effect of volatile anesthetics is a reversible paralysis of the central nervous system (CNS) [66]. The main results of this are unconsciousness and a decrease of the reflex effectuality. The actual degree of suppression of the CNS functions is dose dependent. The fact that volatile anesthetics affect the CNS activity was used in several attempts to derive an indicators for anesthetic depth. A number of depth indicator have been derived from spontaneous EEG signals. [386] gives an overview on spontaneous EEG features used in anesthesia. The first studies [173] concentrated on time domain features to asses anesthetic state. Later with digital computers making fast Fourier transform (FFT) practical also frequency domain features were analyzed. Typical features are the energy content in different frequency bands and parameters from the bispectrum [20, 430]. Several depth indicators combine time and frequency domain features as for example [313]. The latest indicator of this type is the bispectral index (BIS) [285] introduced by Aspect Medical Systems Inc. Alternatively to spontaneous EEG, activity of the EEG evoked by external stimulations might be used. Most common is the EEG potential evoked by auditory stimuli as used in [277] for control purposes.

The exact mechanisms behind the narcotic effects of volatile anesthetics are not yet completely understood [66]. It is established that there does not occur a blocking of any receptors by the anesthetics. This becomes obvious from the fact that Xenon as a noble gas exhibits similar anesthetic effects as the fluorinated ether anesthetics. It is thus very likely that some physical phenomenon is responsible for the CNS palsy. Empirically it was found that there is a correlation between lipid solubility and anesthetic potency [449, 452, 402]. It is conjectured that the effect is due to the solution of anesthetics in neural membranes [66].

Of further interest for our purposes are the hemodynamic effects of volatile anesthetics. All the halogenated ether anesthetics qualitatively act in the same manner with the exception of Halothane. They decrease MAP [103, 100] which is caused by a decrease of cardiac output (CO) as well as peripheral resistance [100]. The peripheral resistance decreases as a result of the vasodilating properties of most halogenated ether anesthetics.

As the CO is given by

$$CO = HR \cdot SV \tag{3.9}$$

i.e. as the product of heart rate (HR) and stroke volume (SV) the effects on those hemodynamic variables need to be discussed separately. While increasing HR ether anesthetics also decrease SV so that a net decrease in CO results [100] at steady state. The increase of HR is a result of the sympatho mimetic effect of some ether anesthetics [128, 483]. This effect consequently

also leads to increased norepinephrine levels in the plasma under Isoflurane anesthesia [483, 343] and it is modified by opioids [508]. The reduced stroke volume is a consequence of the reduced myocardial contractility [290].

3.2.3 The physiology of surgical stimulations

Surgical stimulations are very stressful incidences to which the body reacts heavily. During anesthesia these reactions might be modulated by different drugs but they qualitatively occur also under anesthesia. In particular, in absence of analgesics the hemodynamic response under Isoflurane anesthesia was shown to be almost independent of the level of anesthesia [519].
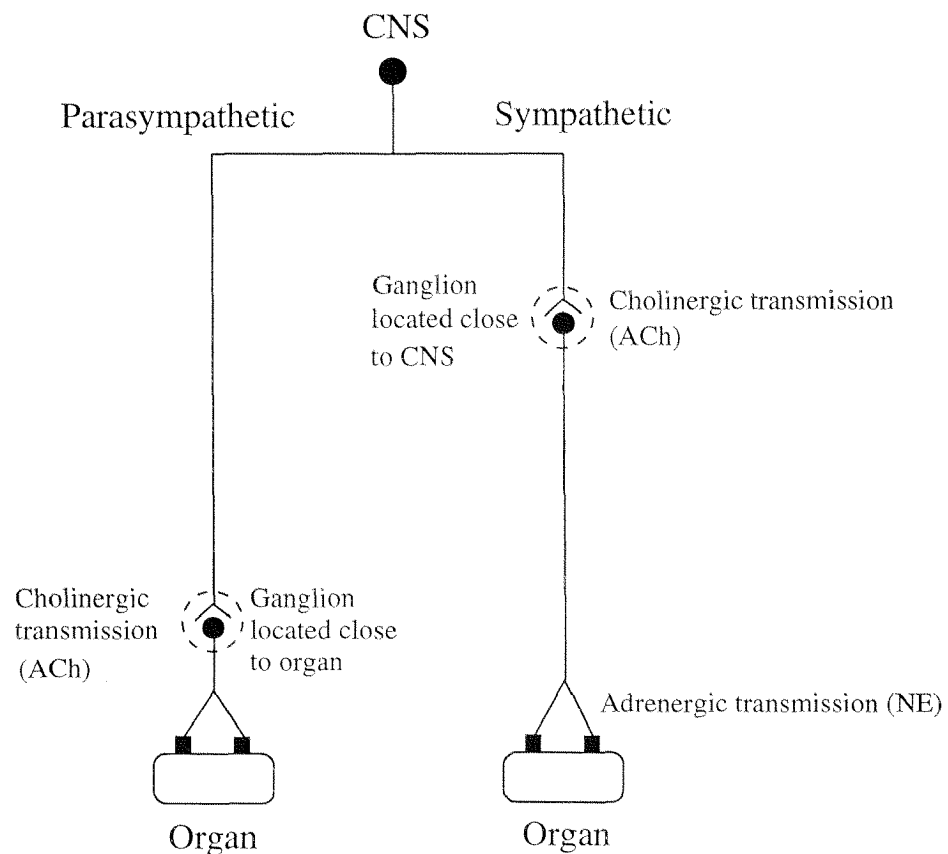
Figure 3.8: Schematic representation of the parts of the autonomous nervous system. Similar diagrams might be found in the textbooks [453, 431, 96]

The stress response of the body to surgical stimulations is an involuntary reaction of the autonomous nervous system. The effector part is divided into two components: the sympathetic and the parasympathetic part, as shown in figure 3.8. Both parts are composed of two neurons. One neuron carries the neural impulse from the CNS to a ganglion where the impulse is transferred to a second neuron innervating the effector organ. The neuron closer to the CNS is consequently called the preganglionic and the one further from the CNS is called the postganglionic neuron. Most organs are innervated by sympathetic as well as parasympathetic fibers. Despite these similarities the two systems differ in several ways. The main differences are [453]:

- origin of the preganglionic neuron in the CNS

- location of the ganglion

- the chemical transmitters involved

- the effects on the effector organ.

The stress response triggers the sympathetic part of the autonomous nervous system. This system can be considered as an emergency mechanism usually activated under conditions of stress, infection, hemorrhage and of course pain. The stimulation prepares the body for critical situations. It leads to physiological reactions such as pupil widening, increase of heart rate and blood pressure (leading to better blood flow in the main organs) and contraction of skin vessels (to decrease blood loss in case of injury). Generally speaking the human body is being prepared for "fight or flight" [162]. The qualitative aspects of surgical stress response interesting for our model are qualitatively summarized in figure 3.9. These facts may be for example derived from physiology textbooks like [145, 96, 162].

Concerning the hemodynamics the sympathetic system triggers a neural and a humoral reaction. The neural reaction of sympathetic activity leads to norepinephrine release from the associated nerve endings into the synaptic cleft (the space between the nerve endings and the effector cells) and the released transmitter then activates specific adrenoceptors located in the membrane of the postsynaptic effector cell producing the characteristic response of the effector organ. The sympathetic activity further leads to epinephrine and norepinephrine release from the adrenal medulla which is under direct sympathetic control of the central nervous system (CNS) (see e.g. [207]). These hormones are discharged into the blood stream and exert their effects when they are carried to the effector cells.

With respect to our work the changes in cardiac output and peripheral resistance are of interest. In the following sections the different aspects of the sympathetic response will be discussed.

3.2.4   The neuronal reaction

The details concerning the neural activity discussed in this section are illustrated in figure 3.10. General references describing the mechanisms of adrenergic neurons are [70, 365, 96].

At adrenergic nerve endings norepinephrine is synthesized and stored in vesicles. The arriving nerve impulses trigger the release of norepinephrine in the synaptic cleft through exocytosis, i.e. fusion of the vesicle with the cell membrane in such a way that the vesicle interior becomes continuous with the extracellular space. The release in the individual nerve ending is thus quantized. But the average amount of norepinephrine released increases linearly proportional to the logarithm of the frequency of arriving nerve impulses [215]. Upon release norepinephrine diffuses across the synaptic cleft to the effector cell where the stimulation of receptors leads to the cell specific response. There are different adrenergic receptors (α, β) invoking the different cell responses as will be discussed in section 3.2.6.
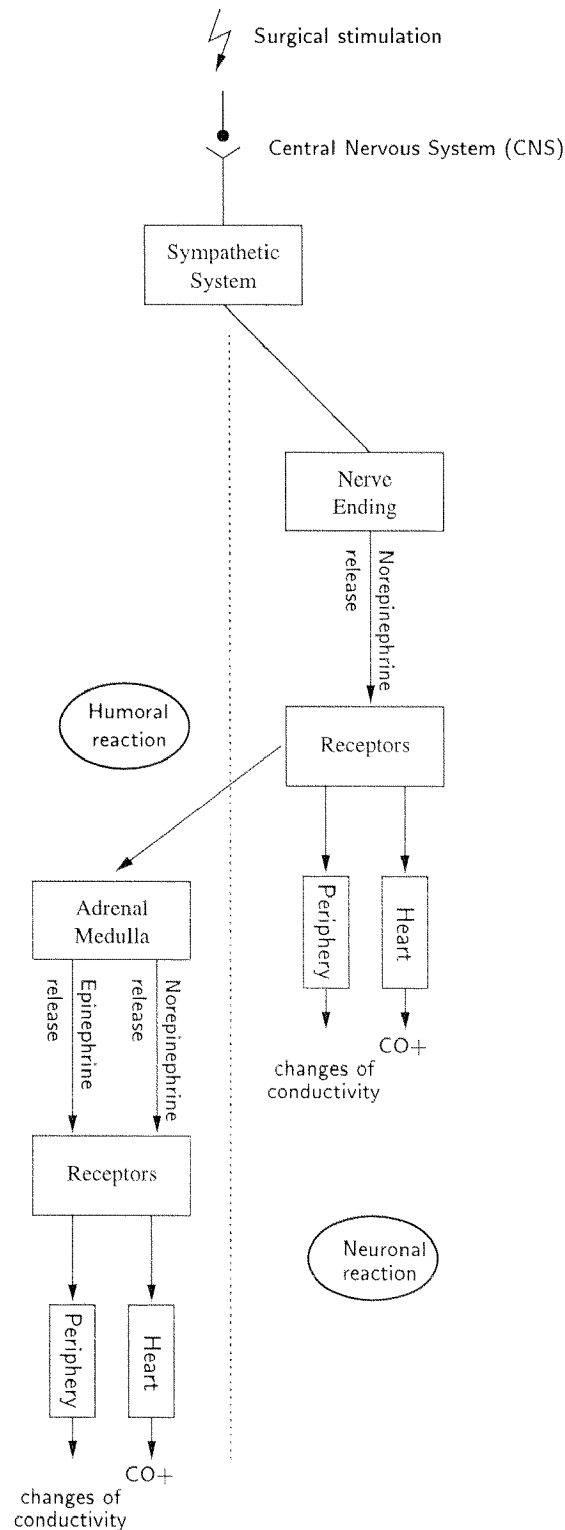
Figure 3.9: Qualitative description of the physiology of how surgical stimulation affect MAP. A stimulus propagates through the nervous system from the origin of the stimulation to the CNS followed by a stimulation of the sympathetic system. The sympathetic nervous system evokes a neuronal and humoral reaction which causes specific reactions of effector cells. The hemodynamic reactions of importance are changes in peripheral resistance and cardiac output (CO).

As soon as the neuronal reaction is terminated there is a rapid decrease of norepinephrine in the sympathetic cleft due to a very fast absorption of epinephrine by the nerve ending. That is 90 % of released norepinephrine is reabsorbed by the nerve ending [363, 96] where it is either restored in vesicles or inactivated by monamine oxidase (MAO). This ensures the locally restricted action of synaptic NE . A second mechanism of deactivation is the destruction of norepinephrine molecules not recaptured and that are metabolized by the enzyme catechol-o-methyl-transferase (COMT) [96]. Finally some of the released norepinephrine diffuses into the blood vessels. This phenomenon is referred to as "spill over".

The release and re-uptake of norepinephrine in the nerve ending is modulated by several local mechanisms. Epinephrine positively influences norepinephrine release via stimulation of β_2 receptors at the nerve ending [339, 444]. Stimulation of α_2 receptors at the nerve ending by synaptic norepinephrine acts as a negative feedback on the norepinephrine release [70, 365].
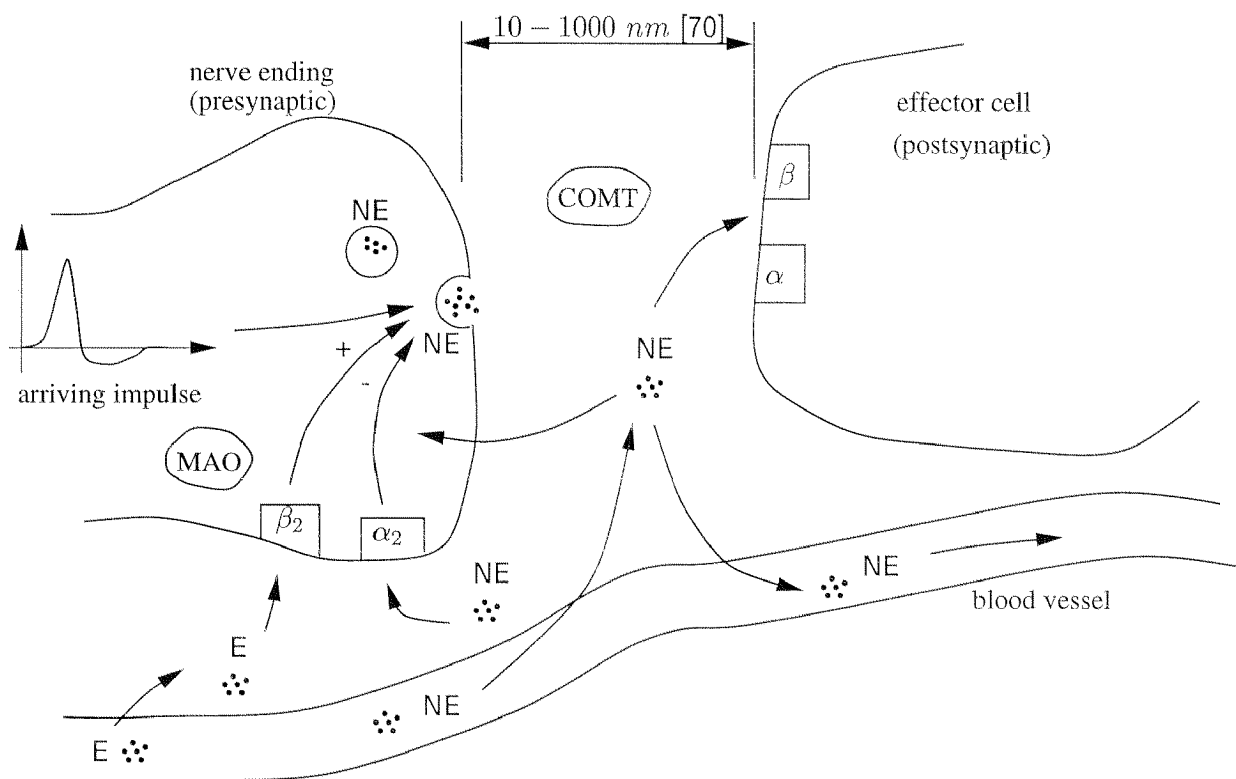
Figure 3.10: Schematic drawing of the details of adrenergic transmission. Similar representations can be found in several texts like [70, 145, 96].

3.2.5 The humoral reaction

The adrenal medulla synthesizes and stores the catecholamines E and NE . Analogously to the situation in nerve endings the storage is in vesicles at a ratio of 4:1. The adrenal medulla is under direct sympathetic control [484, 207] receiving direct innervation from preganglionic fibers [96]. Sympathetic activity causes the discharge of E and NE into the venous blood [471]. The ratio of E and NE released is not fixed and the release can be modulated by other drugs [471, 484].

Receptor	α_1-Receptor	α_2-Receptor	β_1-Receptor	β_2-Receptor
Sensitivity	NE hi [496, 453] E hi [453] E > NE [96]	NE hi [496, 453] E hi [453] E ≥ NE [96]	NE hi [453] E hi [453] E = NE [239, 96]	NE low [496, 453] E hi [453] E ≫ NE [239, 96]
Heart	increased contractility		increased heart rate	
Smooth vascular muscles	constriction	constriction		relaxation
Smooth broncheolar muscles	constriction	constriction		relaxation

Table 3.1: Table showing the effects of the stimulation of the different adrenergic receptors. The information is extracted for [431] pg. 57 [97] pg. 293 and [145] pg. 130.

From the adrenal medulla these catecholamines first pass through the lung and then through the periphery. Both have the ability to uptake and store catecholamines [471].

Physiologically the lung is not just responsible for gas exchange. In addition it performs important metabolic functions [139, 49]. With respect to the catecholamines it is of importance that the lung removes about 35 % of the traversing NE while E passes unaffected [176, 471]. Responsible for the elimination are the endothelean cells (cf. figure 3.5) through transcellular transport and subsequent metabolization by MAO [49].

The passage through the vascular bed finally removes more than 80 % of the circulation E and NE [176, 471]. There are several mechanisms responsible for this rapid removal. First there is the uptake by sympathetic nerve fibers. [176, 471] reasons that this only accounts for a small part of the removal and that the gros amount is removed by uptake and metabolization in other cells (smooth muscle cells [471] or erythrocythes [141] and others). Finally there is some evidence that the clearance is decreased under normal levels of anesthesia [108].

3.2.6 Receptors

The interaction of catecholamines and the effector cells occurs by means of adrenergic receptors. Of importance for the cardiovascular effects of E and NE are α and β-receptors [496] among which α_1, α_2, β_1, β_2 receptors may be distinguished. α_1 and β_1 are excitory while α_2 and β_2 are inhibitory [96]. For our work we only need to discuss the qualitative and quantitative effects of receptor stimulation. Readers interested in the physiological details are referred to the specific literature, e.g. [239, 53, 371, 6].

The response to E or NE of depends on:

- the site (organ) where the receptor is located

- the sensitivity of a receptor to either hormone

For example stimulation of cardiac β_1-receptors causes an increase in heart rate [496] while β_2-stimulation in the peripheral vascular beds causes vasodilation [496]. And E possesses α_1- and β-adrenergic activity while NE possesses α- and β_1-adrenergic activity. The effect of α and β receptor stimulation on different organs is summarized in table 3.1.

The net effect of synaptic or circulatory E or NE on an effector organ consequently depends on:

- the amount of E and NE present at the site

- the number of receptors of a certain type [363, 496].

This leads to qualitatively different responses for E and NE .

3.2.7 Autoregulation Mechanisms

There are several autoregulation mechanisms for control of circulation. A detailed physiological discussion may be found in [117]. A brief and more engineering oriented summary of the different mechanisms may be found for example in [194] and a nice illustration is given in [92] (pg. 8). The reference [194] also provides information on the effectiveness (reaction time and gain) of the different control mechanisms. The most important ones are briefly summarized here:

- The **baro reflex** is the fastest and a very strong auto regulation [194]. It is for example responsible for a fast blood pressure increase when rising from horizontal position. It is also the probably best studied and well modeled mechanism [25, 26, 10, 24, 378, 87, 17, 118, 86].

  Increase of arterial pressure excites stretch receptors located in carotid sinuses and the wall of the aortic arch [162]. There is evidence that different types of receptors exist [378]. Type I receptors are sensitive to changes in the mean and type II receptors are sensitive to the derivative of the pulse wave. The receptor signals trigger the response of the parasympathetic part of the autonomous nervous system [162] with a subsequent reduction of CO via decrease in HR. If arterial pressure falls below normal this mechanisms operates in reverse.

- The **chemo reflex** regulation mechanism is somewhat slower and weaker than the baro reflex [194]. It is triggered when pressure falls to reasonably low values ($< 80mmHg$) [194]. If blood pressure falls to such values chemoreceptor cells do not receive enough oxygen and accumulate carbon dioxide. These changes in gas concentrations cause the chemo sensitive cells to transmit signals to the brain which in turn leads to an increase in cardiac activity and peripheral vaso constriction.

- The **central nervous system ischemic response** is again somewhat slower (response time on the order of several 10 seconds) but very potent [194]. It is activated at very low values of arterial pressure (especially below $40mmHg$) through direct excitation of the vasomotor center of the CNS. It also leads to increase of cardiac activity and peripheral vaso constriction. It's main purpose is to ensure adequate perfusion of the CNS.

- The **stress relaxation** of the circulation is considerably slower (response times of several 10 min) and also less potent then the previously mentioned [194]. This mechanism is local and causes vessels to stretch when blood pressure increases.

- There are further auto regulation mechanisms [194] which either are much slower or less potent then the ones described so far and which therefore will not be discussed here.

Not all of these auto regulation mechanisms have been studied under anesthesia. The baro reflex has and [249] quantifies how the baroreflex is decreased during Isoflurane anesthesia. [471] finds that circulating catecholamines appear to have no effect on the baro reflex.

3.3 Physiology based nonlinear local grey box model

We are now ready to develop the mathematical model for the the combination of volatile anesthetics, surgical stimulations and mean arterial pressure as shown in figure 3.1. In this context mathematical model means a description in terms of differential equations. The model equations are physiologically motivated. Since in some cases just phenomena are modeled it is not a true first principles model. On the other hand it is also not a complete black box, because of the physiological interpretation of most of the parameters. It will thus be referred to as a grey box model.

Something else must be kept in mind when building, identifying and validating models. A model is always an abstraction of reality. Its purpose is to describe and predict certain aspects of interest of reality while other aspects are neglected. Thus there does not exist a "true" model. And model quality can only be assessed with respect to the purpose of the model. This facts is probably best captured by the phrase "as simple as possible but as complex as necessary". Some discussion along this line is provided in [35] concerning models in anesthesia. General texts on physiological modeling are [171, 225, 460, 396, 93].

The central aspect of the model is a circulation model describing the hemodynamics (see figure 3.11). Static pharmacodynamic equations describe the effect of anesthetics and the stimulations on the circulation model. Pharmacokinetics then define the time evolution of anesthetic concentrations (see figure 3.13) and sympathetic activity (see figure 3.17). Finally, the equations accounting for the respirator dynamics are added.

As pointed out in the introduction this model is a refined version of the model used by Derighetti in his thesis [111]. The structure of PK of volatile anesthetics are unchanged but some parameters were adjusted. For the hemodynamic model, however, an important modification is made by consistently including the sympathomimetic effect of Isoflurane. The PK/PD of the stress response model are built on the same ideas but otherwise the model is completely changed. The respirator dynamics at last are described by a model of lower order than Derighetti's.

1	myocard (heart muscle)
2	brain gray matter
3	brain white matter
4	well perfused organs
5	poorly perfused organs
6	splanchincus (stomach,intestine)
7	skeletal muscle
8	fat
9	skin shunt
L	lung
A	arterial system
V	venous system

Table 3.2: List of the different compartments

3.3.1 The hemodynamics (circulation model)

The circulation model (figure 3.11) is used to model the hemodynamics. It describes the blood flows in all different compartments and their relation to MAP and CO. The average blood flowing out from the heart (i.e. the cardiac output denoted by CO) is distributed among different parts of the body (referred to as compartments). The different compartments considered in this model are listed in table 3.2. Each of these compartments exhibits a certain conductance to blood flow denoted by g_i. MAP, CO and g_i are now related analogously to voltage U, current I, and conductance G in Ohm's electrical law:

$$MAP(t) = \frac{CO(t)}{\sum_{i=1}^{9} g_i(t)}. \tag{3.10}$$

This equation suggests that $CO(t)$ and the $g_i(t)$ must be measurable for the continuous computation of $MAP(t)$. Although they are not the equation is not useless. If it is possible to compute $CO(t)$ and the $g_i(t)$ from secondary variables equation (3.10) might still be used to compute $MAP(t)$. The dependence of $CO(t)$ and the $g_i(t)$ from other variables is discussed in the next sections.

3.3.2 Modeling the auto regulation

In section 3.2.7 we have listed the various blood pressure auto regulation mechanisms. Taking all of these into account would over complicate the final model and we thus make the following simplifying assumptions:

A-1 *The auto regulation of blood pressure can be modeled as a single mechanism.* This assumption seems justified since closed loop identification of the baro reflex as performed e.g. in [10] is not able to distinguish between the effects of the different mechanisms and that
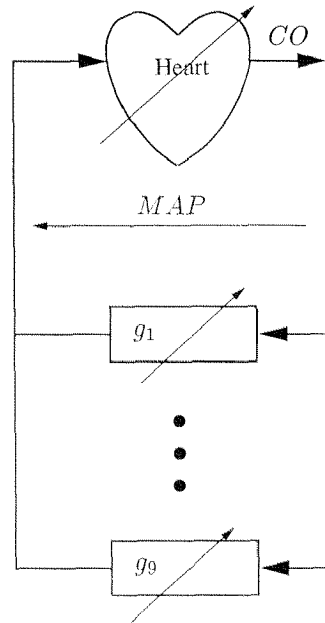
Figure 3.11: The circulation model models the hemodynamics. The variable CO denotes cardiac output and the g_i denote conductivities.

thus these experimental models include the effects of all mechanisms. This is also implied e.g. by [25] where all neural regulation effects are allocated into one transfer block. This basically amounts to modeling the most dominant i.e. the baro reflex and neglecting the less effective ones.

A-2 *The auto regulation does not interfere with the sympathetic nervous system.* According to [194, 162] the baro reflex works via invocation of the parasympathetic system.

This feedback acts decreasingly on CO via the heart rate in response to deviations of MAP from its base line as shown in figure 3.12. In the literature the baro reflex response has often been identified as a linear transfer function [25, 509, 10, 24, 457, 328, 17, 86] which shows mainly first order behavior [25, 509, 10]. Some scepticism towards a linear baro reflex model might arise at this point. Note, however, that there is evidence that local feedback mechanisms seem to have linearizing effects on the baro reflex [464].

The gain is usually expressed in $[k_{BR}] = \frac{ms}{mmHg}$. That is, it expresses by how many ms the heart period is prolonged per $mmHg$ of change in blood pressure. Consequently the baro reflex is modeled equation wise through

$$CO(t) = \frac{CO_0}{1 + k_{BR}HR_0 r_b} \tag{3.11}$$

and

$$\dot{r}_b(t) = \frac{1}{\tau_{BR}} \left(\Delta MAP(t) - r_b \right) = \frac{1}{\tau_{BR}} \left(MAP(t) - MAP_0 - r_b \right) \tag{3.12}$$

where k_{BR} denotes the baro reflex gain, τ_{BR} denotes the time constant of the reflex, and r_b denotes the associated state. Note that equation (3.12) implies $[r_b] = mmHg$.
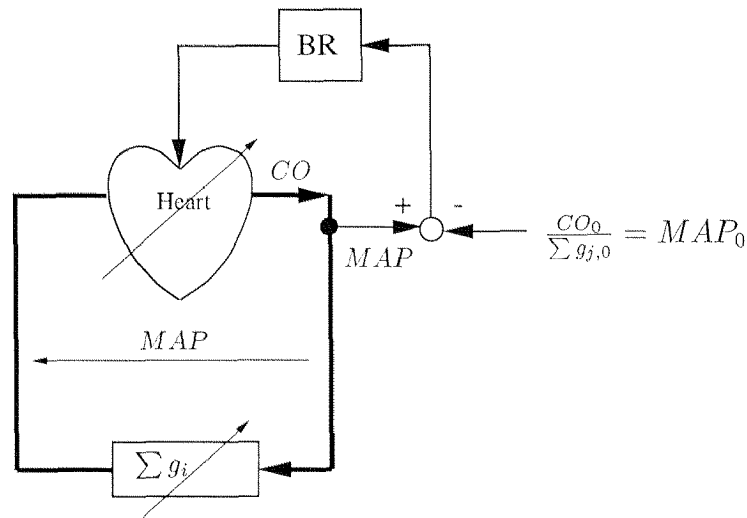
Figure 3.12: Schematic drawing of the blood pressure auto regulation mechanism.

Equation (3.11) is derived as follows

$$CO(r_b) = SV \cdot HR(r_b) = \frac{SV}{T_0 + \Delta T(r_b)} = \frac{SV}{T_0 + k_{BR}r_b} = \frac{SV}{T_0(1 + \frac{1}{T_0}k_{BR}r_b)}$$

$$= \frac{CO_0}{1 + k_{BR}HR_0 r_b} \tag{3.13}$$

where T_0 denotes the nominal heart rate period.

3.3.3 The pharmacodynamics

The pharmacodynamic relations describe how cardiac output CO and the compartmental conductances g_i change as functions of other underlying variables. It is through the time dependence of these underlying variables that the time dependence of $CO(t)$ and $g_i(t)$ are induced. Following the physiological facts described in section 3.2 three components need to be considered, these are the effects of the anesthetic agent, of the neural activity, and of the humoral activity. In establishing these PD relations the following assumptions were made:

A-3 *The humoral component of the stress response can be modeled through the E concentration only.* This assumption is based on the following observations. First, Cryer [102] studied E and NE plasma concentrations under different physiological and pathophysiological conditions. He finds that plasma NE concentrations during surgery are far below plasma concentrations required to produce measurable hemodynamic effects. Plasma E concentrations are in a range, however, where they produce measurable hemodynamic effects. Second, [471] suggests that NE has little significance as a circulating hormone. Consequently, also the spill over from synaptic cleft into blood vessels is neglected since this only influences the NE concentrations in the plasma. Note, however, that there might be other vasoactive substances involved with the body stress response (see e.g. [484]) which would need to be subsumed in that humoral component.

A-4 *The pharmacodynamic effects of the stress factors and of anesthetics are additive.* This assumption basically says that volatile anesthetics do not interact with the receptors that are stimulated by E and NE . This assumption is supported by a study of Zbinden et al. [519] where the authors study the hemodynamic response to different noxious stimuli and where they find that "Isoflurane used as a sole agent depresses pre-stimulation blood pressure, but the blood pressure response *per se* to stimulation is virtually concentration independent".

A-5 *The pharmacodynamic effects of the the neural and the humoral component may also be described by affine functions.* This implies that the amount of receptors stimulated at the effector cells and the subsequent response of the cells is proportional to the concentration of E or NE present at the site. This assumption does certainly not hold in general since the activation of receptors usually exhibits saturation effects at high concentrations in the form of the Michaelis-Menten-kinetic [445] or a Hill [460] equation. However, studies such as [102] suggest that plasma epinephrine and norepinephrine concentrations during anesthesia are still low compared to plasma concentration during heavy exercise or under pathological conditions. Note that this corresponds to an implicit linearization of the above mentioned nonlinear relations. The use of linearizations is only justified since the concentrations are far below the saturating concentrations.

A-6 *The pharmacodynamic effects of the of the volatile anesthetics may be described by affine functions [524].*

A-7 There is no adaption to anesthetic agent, circulating E or neural activity. This means that the PD relations do not change over time.

With these assumptions we get the following pharmacodynamic equations for the compartmental conductance and the cardiac output:

$$g_i = g_{i,0}(1 + \beta_i p_i + \gamma_i c_P + \kappa_i n) \tag{3.14}$$

$$CO = CO_0 (1 + \alpha_1 p_1 + \alpha_3 p_A + \alpha_4 c_P + \alpha_6 n) \tag{3.15}$$

In these equations CO_0 and $g_{i,0}$ denote the initial values for CO and g_i without surgical stimulation and anesthetic agent. This implies that the E concentrations $c(t)$ and the neural activity $n(t)$ are to be understood as deviations from a base line. p_i denotes the partial pressure of anesthetic agent in the corresponding compartment, c_P denotes the E concentration in the periphery, and n denotes the neural sympathetic activity. Note that the PD coefficients α_i and β_i must not be confused with the α- and β-receptors described in section 3.2.6.

The conductance (g_i) of a certain compartment is according to equation 3.15 depending on the partial pressure of volatile anesthetics in the compartment (p_i), the peripheral E concentration (c_P), and the neural activity (n). The neural and the humoral activity are fast messaging systems whose activities are activated and deactivated equally rapidly in all regions of the body. In contrast different body regions exhibit very different capabilities in taking up and storing volatile anesthetics. Thus, while the time evolution of the partial pressure of volatile anesthetics are modeled separately for every compartment the E concentration and the neural activity are modeled as being equal in all the compartments. For more details about the PK model of n and c_P it is

referred to sections 3.3.5 and 3.3.6 as well as figure 3.17. The different factors β_i, γ_i, and κ_i account for the compartment specific strength of the response.

The pharmacodynamic equation for the cardiac output 3.14 has four influencing terms. The anesthetic partial pressure in the heart (p_1), the arterial partial pressure (p_A), the peripheral E concentration (c_P), and the neural activity (n). The original Halothane model by Zwart et al [524] proposed three influencing anesthetic partial pressure terms, that is those in the heart, in the brain, and in the arterial blood. The influence of the anesthetic partial pressure in the heart represents the direct effect of the anesthetic on the contractility of the myocardial fibers [290]. The influence of the brain partial pressure represents the sympatho mimetic effect exhibited by some anesthetics [483]. The influence of the arterial partial pressure might be explained by effects as a result of the direct contact of myocardial tissue and arterial blood in the heart chambers. The model used by Derighetti [111] was extended by Derighetti et al [112] with neural and humoral components to

$$CO = CO_0 \left(1 + a_1 p_1 + [a_2 p_2] + a_3 p_A + a_4 c_E + [a_5 c_{NE}] + a_6 n\right). \tag{3.16}$$

This modification resulted from the modeling of surgical stimulations. The influence of neural activity represents the effects of sympathetic activity. And the two humoral components represent the effects excreted by the circulating E and NE released from the adrenal medulla.

The arguments for simplifying equation (3.16) to (3.14) are as follows. First, by assumption A-3 circulating NE is neglected. Second, the sympatho mimetic effect should for consistency be included in the neural (sympathetic) activity.

The time evolution of these individual influencing terms will now be discussed in the following sections.

3.3.4   Uptake and distribution of volatile anesthetics

In this section the model for uptake and distribution of anesthetics will be introduced. It is a one to one translation of the model for Halothane by Zwart et al. [524] to Isoflurane. The only change is an additional output representing the endtidal concentration measurements. This output will be modeled following [489] which is slightly different from how it was modeled by Derighetti [111]. In view of figure 3.2 this model describes the anesthetic's part of the patient block where the inspiratory concentration (c_{insp}) represents the system input and the endtidal concentration (c_{endt}) represents the system output. For the model we will use the following convention concerning concentrations and partial pressures. If it is referred to a measurement provided by the patient monitor (e.g. c_{insp} or c_{endt}) it is done in terms of a concentration. To the state variables inside of the body we will refere to in terms of partial pressures. We do this since the governing forces are the partial pressures while measurements are usually displayed in terms of concentrations. In deriving this part of the model the following assumptions are made.

A-8 *The model can be realized with a finite number of compartments.* It is common practice in physiological modeling to lump different organs and group of organs together that have
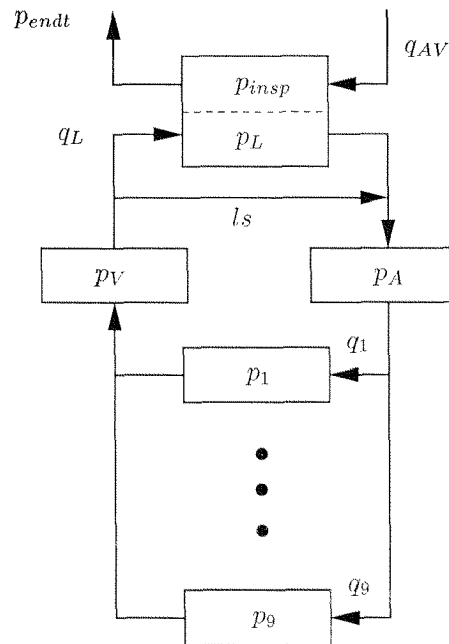
Figure 3.13: The physiological model describes uptake and distribution of volatile anesthetics. The variables p_i denote drug concentrations, the q_i denote blood flows and ls denotes the lung shunt (i.e. blood that passes the lung unaffected).

similar properties with respect to the phenomenon to be modeled. This implies that there is complete mixing in the capillary bed and the exchange between capillary blood and tissue is rapid enough so that blood and tissue volume can be lumped (see [74, 225, 460, 93] for a more fundamental discussion of compartmental modeling). The list of compartments chosen here is given in 3.2 and their interconnection is shown in figure 3.13.

A-9 *Ventilation and blood flow can be described as nonpulsatile phenomena since equilibration times are large compared to cardiac and respiratory cycles.* This assumption is standard in compartmental modeling. Consequently the input and output signals (c_{insp}, c_{endt}) are modeled continuously also. In reality however, inspired and endtidal concentration measurements are sampled from a continuous curve at discrete time instances as shown in figure 3.14. That is, the monitor is continuously sampling gas from the Y-piece at the patients mouth and it thus analyses a continuous gas stream representing the inspiratory phase as well as exspiratory phase. The inspiratory concentration measurement (c_{insp}) represents the concentration during the inspiratory phase and the endtidal concentration measurement represents the concentration at the end of the exspiration phase. The input and output signals $c_{insp}(t)$ and $c_{endt}(t)$ may then be viewed as the continuations of the discrete time signals $c_{insp}(k)$ and $c_{endt}(k)$.

A-10 *Transportation times can be neglected.* Recall figure 3.7 which illustrates the fact that blood flow velocity is relatively high in the connecting part of the vascular system. In addition Mapleson showed in [299] that an arterial pool compartment accounts well for the transportation delay which justifies this assumption.
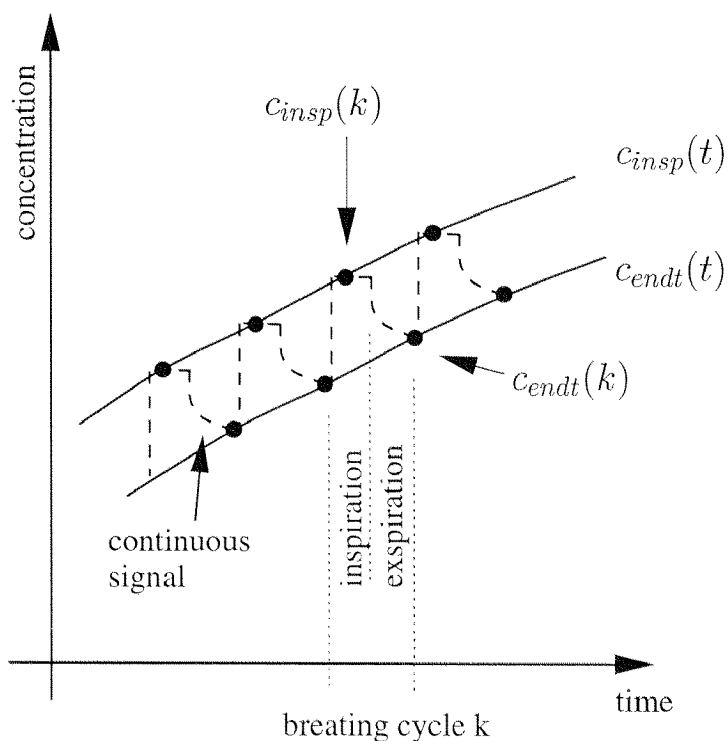
Figure 3.14: Although inspiratory and endtidal concentrations are values valid at discrete time instances they are modeled like continuous signals.

A-11 *Ventilation is kept constant.* Although not always true in practice this assumption at least holds over long time intervals since ventilation parameters are adjusted not very frequently. In this model alveolar ventilation would need to be adjusted in this case. Note also, that this aspect needs especially be taken into account when running an automatic CO_2 controller in parallel which frequently adjusts ventilation parameters.

A-12 *There is no other way of exchange between different compartments than transport by the blood.*

A-13 *Equilibration within a compartment is instantaneous.* This assumption is common when deriving pharmacokinetic models and is also referred to as "well mixedness" assumption [93].

A-14 *The inhalation agent is not metabolized.* This assumption is justified because Isoflurane is only marginally metabolized ($\sim 3\ \%$) [100].

Each compartment consists of a tissue part and a blood part (see figure 3.15). Anesthetics enter the compartment with the blood steam and partial pressure p_A. The blood and the tissue part of the compartment instantaneously equilibrate so that blood leaves the compartment with the compartmental partial pressure p_i.
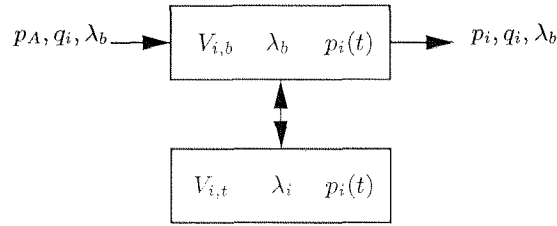
Figure 3.15: The model for a normal tissue compartment consists of a blood part and a tissue part with volumes $V_{i,b}$ and $V_{i,t}$ respectively. Each part has different solubility λ_b and λ_i but (by assumption 13) the same drug concentration.

This description leads to the following equation for the evolution of anesthetic partial pressure in a normal body compartment [524] (indices 1 to 9):

$$\dot{p}_i(t) = \frac{\lambda_b q_i(t)}{\lambda_b V_{i,b} + \lambda_i V_{i,t}} \left[p_A(t) - p_i(t) \right]. \tag{3.17}$$

In this equation $q_i(t)$ denotes the blood flow through the compartment, $V_{i,b}$ and $V_{i,t}$ denote blood and tissue volume and λ_b and λ_i denote the corresponding solubilities. The flow $q_i(t)$ is governed by

$$q_i(t) = g_i(t) \; MAP(t). \tag{3.18}$$

The lung compartment has a slightly different structure. There is in addition to the blood and tissue volumes the functional residual capacity that has to be taken into account and there is a second way (besides transportation with the blood) how anesthetics can enter the compartment. This leads to the equation [524]:

$$\dot{p}_L(t) = \frac{1}{\lambda_b V_{i,b} + \lambda_i V_{i,t} + V_{FRC}} \left\{ \lambda_b q_L(t) \left[p_V(t) - p_L(t) \right] + q_{AV}(t) \left[p_{insp}(t) - p_L(t) \right] \right\} \tag{3.19}$$

where $q_{AV}(t)$ denotes the alveolar ventilation given by equation (3.8).

Arterial and venous compartments differ from the normal compartments in the balance equations since there are different streams that enter and leave the compartment. The equations are:

$$p_A(t) = \frac{\lambda_b CO(t)}{\lambda_b V_{i,b} + \lambda_A V_{A,t}} \left[p_V(t) ls + p_L(1 - ls) - p_A(t) \right] \tag{3.20}$$

$$p_V(t) = \frac{\lambda_b}{\lambda_b V_{i,b} + \lambda_V V_{V,t}} \left[\sum_{i=1}^{9} q_i(t) p_i(t) - CO(t) p_V(t) \right] \tag{3.21}$$

where ls the lung shunt, that is the portion of CO which passes the lung without participating in gas exchange. The different contributions to the shunt have been discussed with figure 3.6.

It remains to state the output equation for the endtidal concentration measurement which is following [489]

$$p_{endt}(t) = \frac{V_{AD}}{V_A} p_{insp}(t) + \left(1 - \frac{V_{AD}}{V_A} \right) p_L(t) \tag{3.22}$$
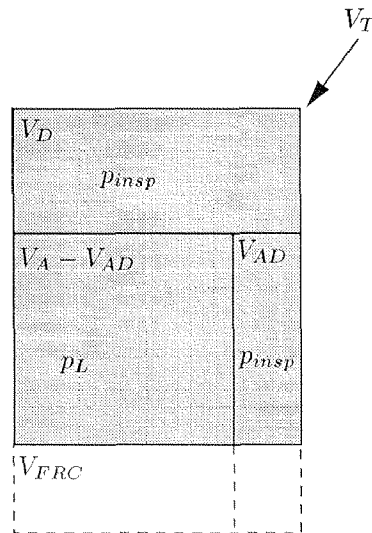
Figure 3.16: Partitioning of the tidal volumes according to different contributions to gas exchange.

where V_{AD} denotes the alveolar dead space and V_A denotes the total alveolar space. For an intuitive understanding of this equation consider the partitioning of the tidal volume during exspiration according to figure 3.16. Of the total tidal volume (V_T) a portion filled the anatomic dead space (V_D). This gas did not participate in gas exchange which exclusively occurs in the alveoli. The composition of this gas remains therefore unchanged. This gas leaves the lung at the beginning of the exspiration phase and contains anesthetic still at the partial pressure p_{insp}. The remaining portion of V_T (V_A) reaches the alveoli. There it equilibrates with resident gas of the functional residual capacity (V_{FRC}). Of the total number of alveoli a certain fraction does not participate in gas exchange. They form the alveolar dead space (see section 3.2.2). The gas composition is assumed not to change. In those alveoli that do participate in gas exchange equilibration between gas, tissue and blood occurs. That is the anesthetic partial pressure reaches p_L. Now at the end of the exspiration phase the alveolar gas leaves the lung. This gas is a mixture of gas from the alveoli that did participate in gas exchange and from alveoli that did not. Consequently the endtidal concentration is a combination of p_{insp} and p_L weighted with the respective volumes $V_A - V_{AD}$ and V_{AD}, respectively.

Derighetti modeled the endtidal partial pressure with

$$p_{endt}(t) = K_s p_{insp}(t) + p_L(t) \tag{3.23}$$

where K_s is postulated as a gas shunt, i.e. "gas amount that will not be mixed in the lung and flows directly into the endtidal path" [111]. No physiological interpretation for K_s is given, however.

3.3.5 The neuronal activity

At the very fine scale of the single neuron and the single synaptic cleft the neural activity is a quantized process. To simplify the respective model we make the assumption:

A-15 *The neural activity can be modeled as a continuous process where the dominating dynamic element results in a first order linear process.* The continuous process assumption is based on the fact that numerous neurons are involved to a achieve a certain effect so that the average firing rate of the whole ensemble of neurons is quasi continuous. The first order process assumption seems arbitrary. It will be, however, justified by the experiments to be presented in section 3.6.2.

Further simplifications are made by assuming that:

A-16 *The modulating effects of the circulating plasma catecholamines on the neural activity are neglected.*

A-17 *The effects of surgical stimulations and anesthetics (sympatho mimetic effect) are additive.*

Under these assumptions the dynamics of the neural activity $n(t)$ are given by equation 3.24.

$$\tau_n \dot{n}(t) \;\; = \;\; -n(t) + f_n\left[\tilde{d}_s(t - T_n)\right] + \tilde{\alpha}_2 p_2 \tag{3.24}$$

The response of an effector cell at the nerve ending depends on the amount of NE in the cleft. The variable $n(t)$ could therefore be interpreted as the mean NE concentration in the ensemble of synaptic clefts. This approach was taken by Derighetti [111]. However, this concentration has never been measured. In addition, it is not certain, whether indeed the synaptic cleft is determining the observed first order dynamic. The variable $n(t)$ is thus to some extent hypothetical. In view of this we prefer not to assign units to $n(t)$, i.e. $[n(t)] = [-]$. τ_n describes the activation time constant of the neural activity. The surgical stimulation is denoted by $\tilde{d}_s$ and the time required for the nerve signal to travel through the nervous system is denoted by T_n. Finally, $f_n(\cdot)$ is a possibly nonlinear function relating the stimulation and neural activity. It accounts among others for the logarithmic relation between NE release and the firing rate [215]. $\tilde{d}_s$ is an unknown and unmeasurable disturbance input. The quantity $f_n[\tilde{d}_s(t - T_n)]$ is therefor also unknown and it is also not measurable. Both $\tilde{d}_s$ and $f_n[\tilde{d}_s(t - T_n)]$ may thus equally well serve as disturbance input for the model. For simplicity we let $d_s = f_n[\tilde{d}_s(t - T_n)]$ represent the disturbance input.

3.3.6   The release and distribution of the catecholamines

In an earlier model [112] the distribution of catecholamines E and NE was modeled utilizing the same 12 compartments as those listed in table 3.2 for the volatile anesthetic. However, while anesthetics are taken up and stored by tissue no such storage happens for catecholamines. The circulating catecholamines NE and E might be viewed as a broadcast messaging system. They are released form the adrenal medulla selectively pass the lung and are almost completely removed by the periphery [471]. We thus make the following simplifying assumption:
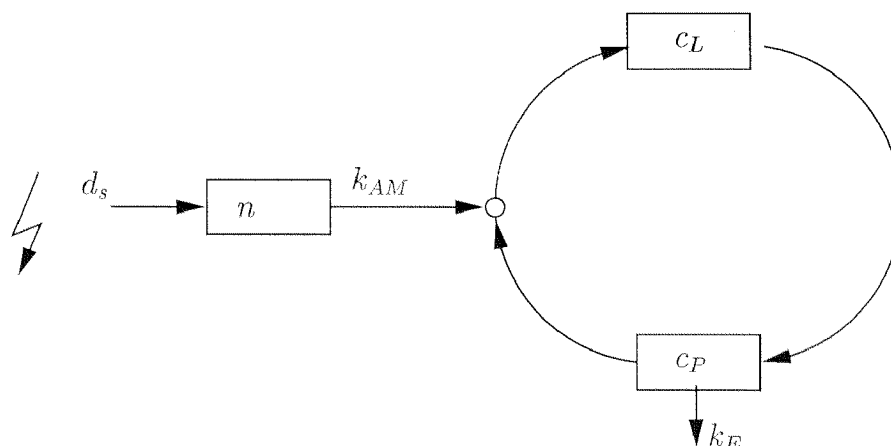
Figure 3.17: The physiological model for the pharmacokinetics related to surgical stimulations.

A-18 *The kinetics of E can be modeled by means of two compartments - the lung and the periphery.* Although there is no elimination of E from the lung it still introduces a lag which will be modeled by a compartment in the general sense.

A-19 Metabolism by enzymes is usually governed by a Michaelis-Menten-model (see e.g. [445]). *However, applying the arguments used with assumption A-5 we will replace the nonlinear kinetic with a linear intrinsic clearance.*

A-20 *The concentration is uniform on the venous side from right atrium to pulmonary arterial and on the arterial side from pulmonary vein to arterial tree.* This assumption is also made by Mari for the insuline model [301, 302] and it simplifies our model by eliminating the arterial and venous compartment. The assumption may be justified further by noting that the time the blood spends in the large arteries and veins is small compared to the time spent in the peripheral parts of the body. In the model for the circulation of the volatile anesthetics in section 3.3.4, the venous and arterial compartments mainly served to combine the individual blood streams after lung and periphery respectively.

A further assumption is:

A-21 *The release of E from the adrenal medulla into the venous pool is proportional to the neural activity $n(t)$.*

With the above assumptions we are left with two compartments as shown in figure 3.17 that is the lung and a combined peripheral compartment. Note that the same structure is for example used in [301, 302] to model glucose kinetics.

The dynamic equations for the concentration of E may be written:

$$\dot{c}_L(t) \quad = \quad \frac{CO(t)}{\tilde{V}_L}[c_P(t) - c_L(t)] + \frac{k_{AM}}{\tilde{V}_L}n(t) \tag{3.25}$$
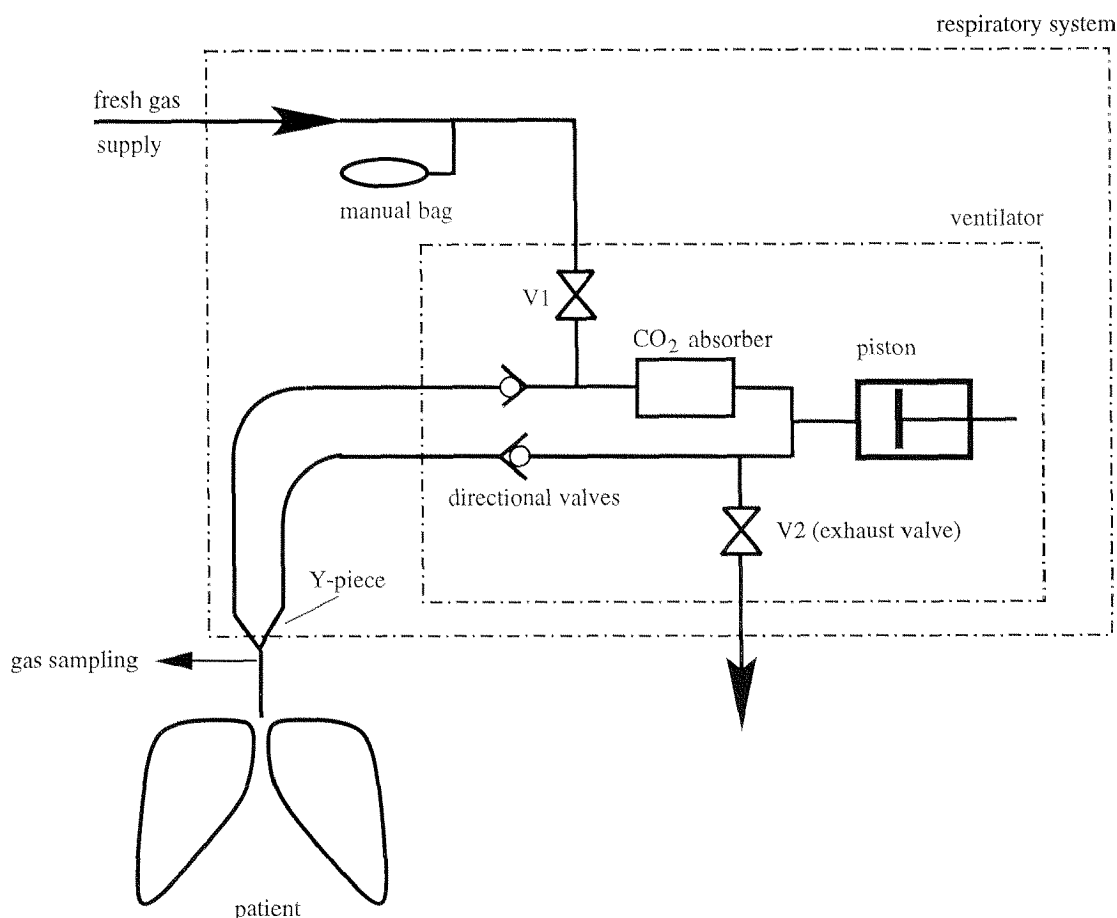
Figure 3.18: Schematic drawing of the whole respiratory system.

$$\dot{c}_P(t) \quad = \quad \frac{CO(t)}{\tilde{V}_P}\left[c_L(t) - c_P(t)\right] - k_E c_P \tag{3.26}$$

Where $c_L(t)$ and $c_P(t)$ denote the E concentration in the lung and peripheral compartment respectively. $\tilde{V}_L$ and $\tilde{V}_P$ denote the corresponding distribution volumes. And k_E models the linear intrinsic clearance in the periphery compartment (A-19).

3.4   Modeling the respiratory system

According to figure 3.18 the term "respiratory system" refers to the actual ventilator device plus all the connecting tubes and other external elements that need to be considered when deriving the mathematical relationship between inspiratory anesthetic concentration (c_{insp}), the vapor position which is proportional to c_{vap} and the endtidal concentration (c_{endt}). Figure 3.18 depicts this setup schematically. For a more detailed description one might consult the manual [125].

It operates as follows. The piston is moving the gas mixture in and out of the lung according to the

anesthesia techinque	flow	typical compositions
minimal flow	0.5 l/min	O_2: 0.3 l/min, N_2O: 0.2 l/min
low flow	1 l/min	O_2: 0.5 l/min, N_2O: 0.5 l/min
high flow	$\geq$ 4 l/min	-

Table 3.3: Anesthesia techniques defined based on the total fresh gas flow taken from [31].

desired respiration frequency. With the specific location of direction valves the air flows through the upper branch during inspiration and it flows through the lower branch during exspiration. Thus if there was no external supply or no exhaust the gas mixture would circulate in this loop built by pump, lung and the two connecting branches of tubes.

With every breath a fraction of the O_2 in the inspired air is replaced by CO_2 and is subsequently removed when passing through the CO_2-absorber located in the inspiration branch. In addition there is a net uptake of volatile anesthetic agents. A fresh gas stream entering on the inspiratory branch compensates for this consumption of volume. At steady state of an oxygen/nitrous oxide anesthesia this consumption is about $0.38l/min$ [31]. It is roughly $0.25l/min$ of O_2 and the rest is N_2O [31]. Depending on the total fresh gas flow different anesthesia regimes are distinguished which are summarized in table 3.3. The excessive gas is exhausted from the exspiration branch through valve V_2 which is open in the exspiration phase. Clearly the larger the fresh gas flow the more is replaced every time unit and the faster the reaction to composition changes of the fresh gas. When working with low and minimal flow as in our case the dynamics associated with the respiratory circuit become important and must thus be included in a model for controller design.

In his thesis Derighetti [111] developed two different models for the respiratory circuit. The first takes into account various nonlinearities as well as any state (pressure) dependent switching of valves. The resulting differential equations for this nonlinear hybrid system are very stiff and can only be treated with specialized simulation software. The model may serve to study certain circuit configurations but it is too complex for controller design. Derighetti also derived a simplified model that neglects the pressure dynamics and models only mass transport. It is, however, still of order 8. In this section we propose a first order model derived from average mass balances. The main difference to Derighetti's model is that pure time delays resulting from transportation are neglected. In his model [111, 113] he includes such delays for the transport of the gas to the ventilator, from the ventilator to the patient, and from the patient back to the ventilator. The consequences of these simplifications are discussed in section 3.9.

The main simplifying assumption for is

A-22 *The respiration circuit may be modeled by a single storage volume.* This amounts to lumping all volumes of the circuit (pump, tubes, absorber, ...) into one single volume and assume an average anesthetic partial pressure. For this volume the 'well stirredness' assumption might seem unjustified. However, since both valves V_1 and V_2 are only open during exspiration phase a partial mixing of exspired gas and fresh gas is achieved. In addition, the comparison with the model derived by Derighetti which attempts to model also the recirculation revealed small enough differences.

The mass balance yields the following equation for the partial pressure in this lumped respiratory circuit volume

$$V_R \, \dot{p}_R(t) = FFp_{vap}(t) \quad + \quad f_R(V_T - V_D - V_{AD}) \left[p_L(t) - p_R(t)\right]$$

$$-(FF - Q_\Delta) \left[\frac{V_{AD}}{V_A} \, p_{insp} + (1 - \frac{V_{AD}}{V_A}) \, p_L\right] \qquad (3.27)$$

The terms of this equation have the following interpretation. With $p_R(t)$ denoting the average anesthetic partial pressure in the respiratory circuit $V_R \, \dot{p}_R(t)$ represents the change of mass of anesthetics in the circuit. With FF denoting the fresh gas flow $FFp_{vap}(t)$ represents the anesthetic delivered with the fresh gas stream. The term

$$f_R(V_T - V_D - V_{AD}) \left[p_L(t) - p_R(t)\right] = q_{AV}(t) \left[p_{insp}(t) - p_L(t)\right] \qquad (3.28)$$

denotes the net transfer of anesthetics to the patient. For interpretation of the right hand side recall figure 3.16. The last term accounts for the exhausted anesthetics. The net flow exhausted is given by $(FF - Q_\Delta)$ where Q_Δ denotes the net uptake. The exhausted mixture carries anesthetic gas with partial pressure p_{endt}. It is so since in the early phase of expiration the piston is pulling the dead space so that during the time when V_2 is open a portion of the alveolar mixture is exhausted.

With the simplification of modeling an average partial pressure in the respiratory system we have

$$p_{insp}(t) = p_R(t). \qquad (3.29)$$

To comply with figure 3.2 equation (3.27) may also be written as

$$\dot{p}_R(t) = -\frac{f_R V_A}{V_R} p_R(t) + \frac{FF}{V_R} p_{vap}(t) + \frac{1}{V_R} \left(FF - Q_\Delta + f_R V_A\right) p_{endt}(t). \qquad (3.30)$$

3.5 The Summarized Model

In this short section we summarize all the equations required to describe the relation in the MIMO system depicted in figure 3.1. We also list all the parameters required for the complete characterization of the system. This list of parameters will then serve as the starting point for the parameter determination in section 3.6.

We will utilize the general description for nonlinear systems i.e.

$$\begin{aligned} \dot{\mathbf{x}}(t) &= \mathbf{f}(\mathbf{x}(t), \mathbf{u}(t)) \\ \mathbf{y}(t) &= \mathbf{h}(\mathbf{x}(t), \mathbf{u}(t)) \end{aligned} \qquad (3.31)$$

where the inputs and their units are

$$\mathbf{u}(t) = \begin{bmatrix} c_{vap}(t) & d_s(t) \\ [\%] & [-] \end{bmatrix} \qquad (3.32)$$

the outputs and their units are

$$\mathbf{y}(t) = \begin{bmatrix} c_{insp}(t) & [\%] \\ c_{endt}(t) & [\%] \\ MAP(t) & [mmHg] \end{bmatrix} \tag{3.33}$$

and the states and their units are

$$\mathbf{x}^T(t) = \begin{bmatrix} p_R(t) & p_1(t) & \vdots & p_9(t) & p_L(t) & p_A(t) & p_V(t) & r_b(t) & n(t) & c_L(t) & c_P(t) \\ [\%] & [\%] & \vdots & [\%] & [\%] & [\%] & [\%] & [mmHg] & [-] & \left[\frac{pg}{ml}\right] & \left[\frac{pg}{ml}\right] \end{bmatrix}. \tag{3.34}$$

The different components of the function $\mathbf{f}(\cdot, \cdot)$ are given by:

respirator circuit	$$\dot{p}_R = \frac{FF}{V_R} p_{vap} + \frac{f_R(V_T - V_D - V_{AD})}{V_R} [p_L - p_R]$$ $$- \frac{(FF - Q_\Delta)}{V_R} \left[\frac{V_{AD}}{V_T - V_D} p_R + (1 - \frac{V_{AD}}{V_T - V_D}) p_L \right] \qquad (3.35)$$
normal tissue	$$\dot{p}_i = k_i g_{i,0} CO_0 \frac{(1 + \beta_i p_i + \gamma_i c_P + \kappa_i n)(1 + \alpha_1 p_1 + \alpha_3 p_A + \alpha_4 c_P + \alpha_6 n)(p_A - p_i)}{(1 + k_{BR} HR_0 r_b) \sum_{j=1}^{9} g_{j,0}(1 + \beta_j p_j + \gamma_j c_P + \kappa_j n)} \quad (3.36)$$
lung	$$\dot{p}_L = k_L \left\{ \lambda_b (1 - ls) \frac{CO_0(1 + \alpha_1 p_1 + \alpha_3 p_A + \alpha_4 c_P + \alpha_6 n)}{(1 + k_{BR} HR_0 r_b)} (p_V - p_L) \right.$$ $$\left. + f_R(V_T - V_D - V_{AD})(p_R - p_L) \right\} \qquad (3.37)$$
arteries	$$\dot{p}_A = k_A \frac{CO_0(1 + \alpha_1 p_1 + \alpha_3 p_A + \alpha_4 c_P + \alpha_6 n)}{(1 + k_{BR} HR_0 r_b)} [p_V ls + p_L(1 - ls) - p_A] \qquad (3.38)$$
veins	$$\dot{p}_V = k_V \frac{CO_0(1 + \alpha_1 p_1 + \alpha_3 p_A + \alpha_4 c_P + \alpha_6 n)}{(1 + k_{BR} HR_0 r_b)} \left[\frac{\sum_{j=1}^{9} g_{j,0}(1 + \beta_j p_j + \gamma_j c_P + \kappa_j n) p_j}{\sum_{j=1}^{9} g_{j,0}(1 + \beta_j p_j + \gamma_j c_P + \kappa_j n)} - p_V \right]$$ $$(3.39)$$
auto regulation	$$\dot{r}_b = \frac{1}{\tau_{BR}} \left(CO_0 \frac{(1 + \alpha_1 p_1 + \alpha_3 p_A + \alpha_4 c_P + \alpha_6 n)}{(1 + k_{BR} HR_0 r_b) \sum_{j=1}^{9} g_{j,0}(1 + \beta_j p_j + \gamma_j c_P + \kappa_j n)} - MAP_0 - r_b \right) \quad (3.40)$$
neural activity	$$\dot{n} = \frac{1}{\tau_n} (-n + d_s + \tilde{a}_2 p_2) \qquad (3.41)$$
lung epinephrine	$$\dot{c}_L = \frac{CO_0(1 + \alpha_1 p_1 + \alpha_3 p_A + \alpha_4 c_P + \alpha_6 n)}{(1 + k_{BR} HR_0 r_b)\tilde{V}_L} [c_P - c_L] + \frac{k_{AM}}{\tilde{V}_L} n \qquad (3.42)$$
peripheral epinephrine	$$\dot{c}_P = \frac{CO_0(1 + \alpha_1 p_1 + \alpha_3 p_A + \alpha_4 c_P + \alpha_6 n)}{(1 + k_{BR} HR_0 r_b)\tilde{V}_P} [c_L - c_P] - k_E c_P \qquad (3.43)$$

With

$$k_i = \frac{\lambda_b}{\lambda_b V_{i,b} + \lambda_i V_{i,t}}, \quad k_L = \frac{1}{\lambda_b V_{L,b} + \lambda_i V_{L,t} + V_{FRC}}$$

$$k_A = \frac{\lambda_b}{\lambda_b V_{A,b} + \lambda_A V_{A,t}}, \quad k_V = \frac{\lambda_b}{\lambda_b V_{V,b} + \lambda_V V_{V,t}}.$$

And the output equations are:

inspiratory measure-ment	$p_{insp}(t) = p_R(t)$	(3.44)
exspiratory measure-ment	$p_{endt}(t) = \frac{V_{AD}}{V_T - V_D} \, p_R + (1 - \frac{V_{AD}}{V_T - V_D}) \, p_L$	(3.45)
MAP equation	$MAP = \dfrac{CO_0(1 + \alpha_1 p_1 + \alpha_3 p_A + \alpha_4 c_P + \alpha_6 n)}{(1 + k_{BR} HR_0 r_b) \sum\limits_{j=1}^{9} g_{j,0}(1 + \beta_j p_j + \gamma_j c_P + \kappa_j n)}$	(3.46)

For the parameters it will be distinguished between pharmacokinetic (PK) and pharmacodynamic (PD) parameters. Following definition 3.2.1 parameters describing an effect will be viewed as PD parameters and the others will be allocated to PK parameters.

3.6 Estimation of the model parameters

The aim of this section is to provide estimates for the model parameters listed in table 3.4. There are two distinct ways how such estimates can be obtained. First, one might perform experiments and identify the parameters from input-output data. Or one might retrieve them from the published physiological literature. Both paths have their limitations. An experiment which excites the system such that all parameters can be identified accurately would require several hours. For example Yasuda el al. [505, 504] had to perform a three hour experiment to estimate the kinetics of Isoflurane with a single step response. On the other hand normally not all parameters can be determined from published sources. We will therefore follow an intermediate path. That is, parameters will be taken from literature sources wherever reliably available. Parameters not available will be obtained from experimental data.

The result of this parameter estimation section will be summarized in table 3.6. Note that these parameters are now specific to Isoflurane.

3.6.1 PK and PD parameters of the baro reflex

There are two parameters to be determined that is the time constant τ_{BR} and the gain k_{BR}. As pointed out in section 3.3.2 a number of publications present identification results concerning auto regulation of blood pressure. Estimates for the auto regulation (baro reflex) gain under Isoflurane anesthesia are published in [249] and [481]. According to [249] we have

$$k_{BR} = \frac{25 \ ms}{mmHg} \tag{3.47}$$

at 1.3 % Isoflurane. This is in agreement with [481]. The two publication do not provide estimates for the time constant. Such an estimate is provided in [86] with

$$\tau_{BR} \approx 5 \ s. \tag{3.48}$$

3.6.2 Parameters for the dynamic response to surgical stimulations

The parameters of the disturbance model will be estimated before estimation of the PK and PD parameters for Isoflurane because the parameters associated with sympathetic activity reappear in the later model. Concerning the quantitative dynamic aspects of surgical stimulations on hemodynamics not much can be found in the literature. Typically only isolated characteristics like maximum MAP increase after stimulation [519] or average plasma concentrations of E [102] are studied. It was therefore necessary to perform experiments that would allow to estimate these parameters [374, 214]. For the experiment a well defined painful stimulus was applied to volunteers under Isoflurane anesthesia. The stimulus consisted of a 5 s train of electric pulses. Each pulse had a duration of 0.25 ms, a current of 60 mA, and it was repeated every 20 ms. Arterial pressure, ECG and plethysmography (perfusion measurement) were recorded during the

Parameter	Description, Interpretation	unit
PK parameters of the anesthetic agent		
CO_0	(nominal) cardiac output at rest	$[\ell/\text{min}]$
$g_{i,0}$	(nominal) compartment conductivity at rest	$[\ell/\text{min mmHg}]$
$V_{i,t}$	volume of tissue part of compartment	$[\ell]$
$V_{i,b}$	volume of blood part of compartment	$[\ell]$
λ_i	solubility of anesthetic in compartment tissue	[-]
λ_b	solubility of anesthetic in blood	[-]
ls	lung shunt	[-]
V_{FRC}	functional residual capacity	$[\ell]$
f_R	respiratory frequency	$[1/\text{min}]$
V_T	tidal volume	$[\ell]$
V_D	anatomic dead space	$[\ell]$
V_{AD}	alveolar dead space	$[\ell]$
PD parameters of the anesthetic agent		
α_1	CO effect parameter heart compartment	$[1/\%]$
$\tilde{\alpha}_2$	CO effect parameter heart compartment	$[1/\%]$
α_3	CO effect parameter arterial compartment	$[1/\%]$
β_i	parameters describing the effects on the conductivities	$[1/\%]$
PK parameters of the neural activity		
τ_n	activation / deactivation time constant	$[1/\text{min}]$
PD parameters of the neural activity		
α_6	sympathetic effect on cardiac output	[-]
κ_i	sympathetic effect on compartment conductivity	[-]
PK parameters of the baro reflex		
τ_{BR}	baro reflex time constant	$[\text{min}],[\text{s}]$
PD parameters of the baro reflex		
k_{BR}	heart period prolongation constant of the baro reflex	$[\text{ms/mmHg}]$
PK parameters of epinephrine		
$\tilde{V}_L$	distribution volume of the lung	$[\ell]$
$\tilde{V}_P$	distribution volume of the total periphery	$[\ell]$
k_E	intrinsic clearance of epinephrine in the periphery	$[1/\text{min}]$
k_{AM}	release constant for epinephrine from the adrenal medulla	$[\text{pg/min}]$
PD parameters of epinephrine		
α_4	effect of epinephrine on cardiac output	$[\ell/\text{pg}]$
γ_i	effect of epinephrine on compartment conductivity	$[\ell/\text{pg}]$
(PK) parameters of the respiratory circuit		
FF	fresh gas flow	$[\ell/\text{min}]$
V_R	volume of respiratory circuit	$[\ell]$
Q_Δ	net uptake by patient	$[\ell/\text{min}]$

Table 3.4: List of model parameters.

experiment. And blood samples were taken every 30 s after stimulation and plasma epinephrine and norepinephrine concentrations were determined. For illustration the results obtained from one volunteer are shown in figure 3.19 to 3.22.
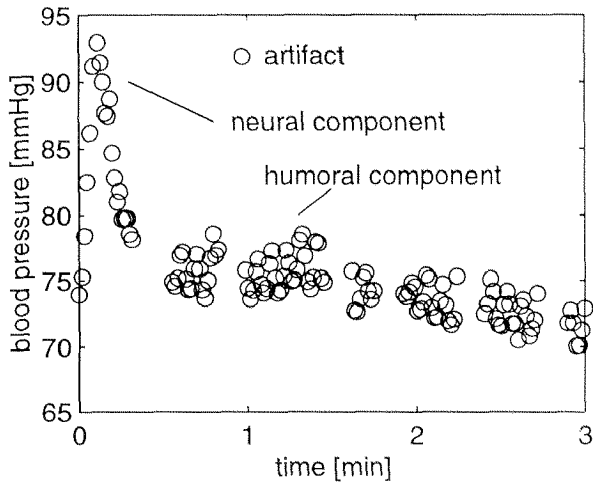
Figure 3.19: Beat-to-beat MAP values after stimulation. The oscillatory behavior represents the pressure variations due to the respiration. The gaps in the recording were caused by the removal of blood sampling artifacts.
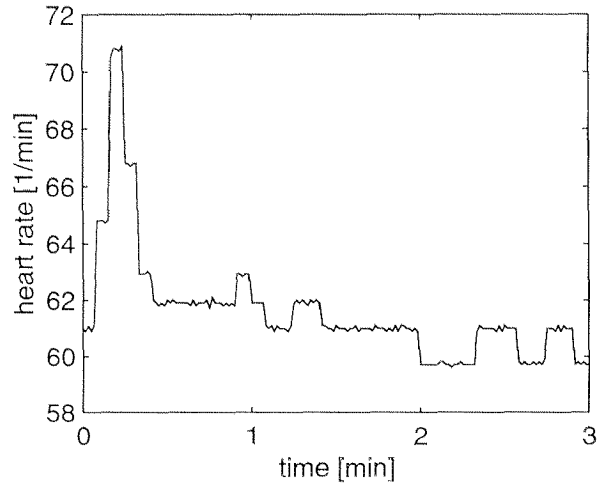
Figure 3.20: Heart rate recording after stimulation. The stair case like graph results from the fact that the monitor only computes integer valued heart rates.
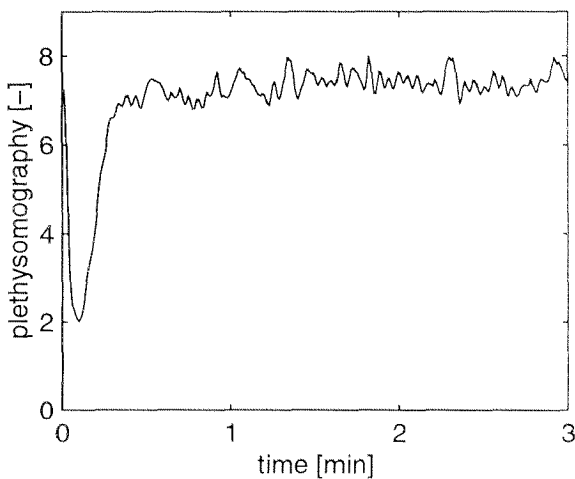
Figure 3.21: Plethysmography curve measured via the absorption in pulseoximetry.
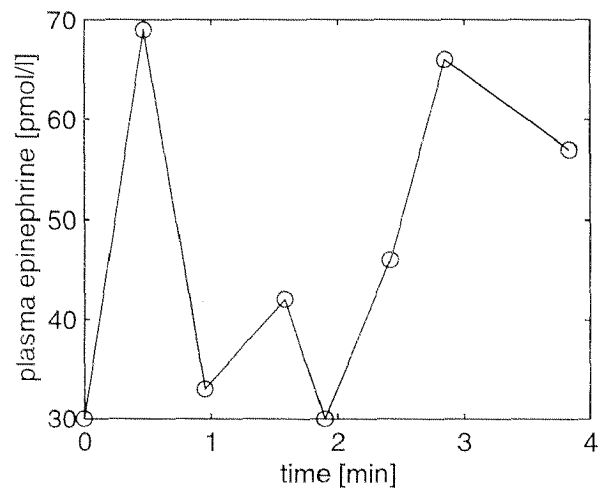
Figure 3.22: Plasma E concentrations recorded after stimulation. The rather erratic behavior must probably be attributed to the insufficiency of the laboratory method.

From figure 3.19 showing the beat-to-beat MAP values the neural and the humoral component may clearly be distinguished. This clear separation will be utilized for estimation of the parameters associated with either component. Figure 3.20 shows the heart rate recording after stimulation. Due to the quantization and averaging over several beats the humoral component may not

as clearly be recognized. Figure 3.21 shows the plethysmography curved measured with the pulseoximeter. It is derived from the absorption measured by the oximeter [468, 140] and it mainly represents a measure for the peripheral resistance. Finally, figure 3.22 shows the sampled plasma epinephrine concentrations. Unfortunately they do not show the expected behavior. At the current state of knowledge we have to attribute this to the insufficient laboratory method.

3.6.3 PK and PD parameters of the sympatho-neural activity

The parameters to be estimated are τ_n, α_6, and κ_i. An estimate for the neural time constant τ_n can directly be obtained from the MAP response curve as shown in figure 3.23. For the eight patients studied

$$\tau_n = 9.5 \pm 0.9 \ s \tag{3.49}$$

proved to be a good choice. To get an estimate for α_6 we first recall equation 3.9 and note that according to [96] the stimulation of β_1 and α_1 receptors by NE increase both heart rate and contractile force. If we assume

A-23 *HR and SV are equally affected by stimulations of β_1 receptors through E or NE .*
       This is supported by table 17-8 in [96].

Then an estimate for α_6 is given by

$$\alpha_6 = \frac{2}{n_{max}} \frac{\Delta HR}{HR}, \tag{3.50}$$

For the seven test persons where $\frac{\Delta HR}{HR}$ could be evaluated an average of 0.1628 ± 0.0294 was obtained which yields

$$\alpha_6 = 0.6291 \pm 0.1190. \tag{3.51}$$

For the κ_i two sources are combined. First, from [96] the relative effect on the conductances of the different compartments $\tilde{\kappa}_i$ is determined. To obtain absolute effects κ_i, data from the experiment is utilized again. A rough estimate for the relative effects $\tilde{\kappa}_i$ may be obtained from table 17-8 in [96]. The table lists the receptor types located in the arterioles of different organs and the strength of a constrictive or dilative response on a scale from "+" to "+++". Table 3.6.3 summarizes these facts. Translating "+" with $\tilde{\kappa}_i = -1$, "++" with $\tilde{\kappa}_i = -3$, and "+++" with $\tilde{\kappa}_i = -10$ and taking into account the fact that NE has little effect on β_2 receptors we estimate

$$\tilde{\kappa}^T = \begin{bmatrix} -1 & 0 & 0 & -10 & -10 & -10 & -3 & -10 & -10 \end{bmatrix}. \tag{3.52}$$

where $i = 1 \cdots 9$ corresponds to the nine compartments listed in table 3.2. To obtain the absolute effects $\kappa_i = \frac{\tilde{\kappa}_i}{K_\kappa}$, the normalization K_κ can be found by matching the peak value of the blood pressure response which is given by

$$MAP_{max} = \frac{CO_{max}}{\sum\limits_{j=1}^{9} g_{i,pre}\left(1 + \frac{\tilde{\kappa}_i}{K_\kappa} n_{max}\right)} \tag{3.53}$$
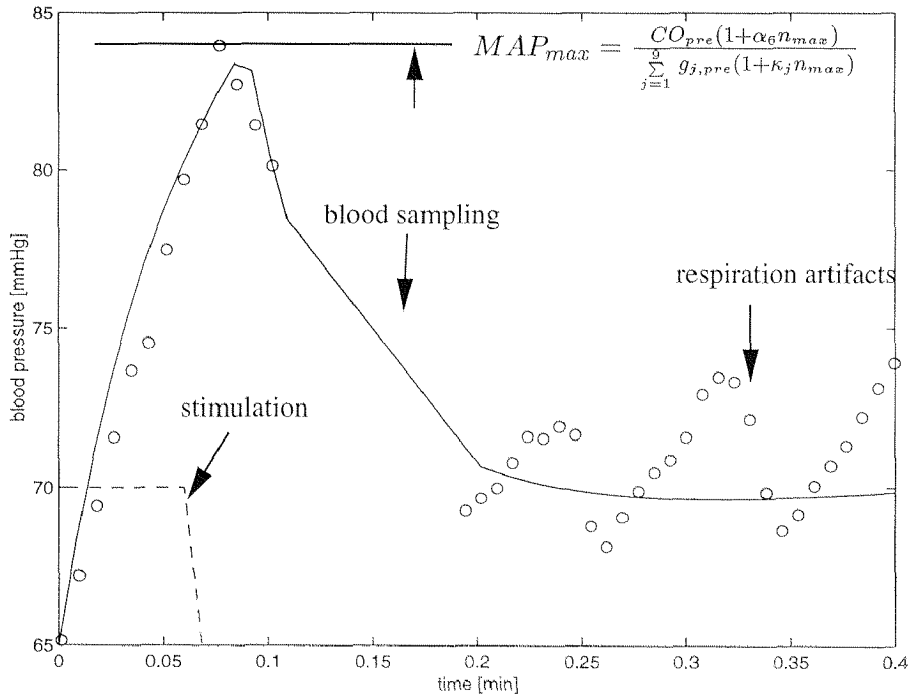
Figure 3.23: Typical stimulation response used for parameter identification.

from where we obtain

$$K_\kappa = \frac{MAP_{max} \sum\limits_{j=1}^{9} g_{i,pre}\tilde{\kappa}_i n_{max}}{CO_0(1 + \alpha_6 n_{max}) - MAP_{max} \sum\limits_{j=1}^{9} g_{i,pre}} \qquad (3.54)$$

and where $g_{i,pre}$ denotes the pre-stimulation conductivity considering the Isoflurane influence. It is computed according to 3.14. From the experimental data K_κ is estimated. $K_\kappa = 37.6 \pm 2.0$ yields

$$\kappa^T = \begin{bmatrix} -0.0266 & 0 & 0 & -0.2660 & -0.2660 & -0.2660 & -0.0798 & -0.2660 & -0.2660 \end{bmatrix}.$$
$$(3.55)$$

3.6.4 PK and PD parameters of epinephrine

There are six parameters that need to be determined which are $\tilde{V}_L$, $\tilde{V}_P$, k_E, k_{AM}, α_4, and γ_i. Again different sources will be utilized.

The distribution volumes $\tilde{V}_L$ and $\tilde{V}_P$ may be obtained from $V_{i,b}$ and $V_{i,t}$ through

$$\tilde{V}_L = \lambda_E V_{L,t} + V_{L,b} \quad \text{and} \quad \tilde{V}_P = \sum_{i=1}^{9} \left(\lambda_E V_{i,t} + V_{i,b} \right). \qquad (3.56)$$

| Arterioles | Receptors | Effect | |
		Constriction (α_i)	Dilation (β_i)
Coronary	$\alpha_1, \alpha_2; \beta_2$	$+$	$++$
Cerebral	$\alpha_1; -$	≈ 0	
Renal	$\alpha_1, \alpha_2; \beta_1, \beta_2$	$+++$	$+$
Salivary glads	$\alpha_1, \alpha_2; -$	$+++$	
Abdomnial Viscera	$\alpha_1; \beta_2$	$+++$	$+$
Skeletal Muscle	$\alpha_i; \beta_2$	$++$	$++$
Skin and Mycosa	α_1, α_2	$+++$	
Pulmonary	$\alpha_1; \beta_2$	$+$	$+$

Table 3.5: Excerpt from table 17-8 in [96] summarizing the effects of α- and β-stimulation on peripheral resistance in different organs.

How $V_{i,t}$ and $V_{i,b}$ may be determined is discussed in section 3.6.5. λ_E accounts for the ability of tissue to uptake and store adrenaline [471]. A value of

$$\lambda_E = 5.1 \pm 0.4 \tag{3.57}$$

was determined based on the localization of the peak of humoral activity.

The intrinsic clearance k_E may be computed from the total body or organ clearance. Clearance describes drug elimination at steady state. It is defined as [172]

$$Cl = q \frac{c_{in} - c_{out}}{c_{in}} \tag{3.58}$$

where c_{in} is the plasma concentration of the blood entering the organ and c_{out} the concentration in the blood leaving the organ, and q denotes the blood flow through the organ. To relate total clearance Cl and intrinsic clearance k_E consider the differential equation describing the time evolution of the concentration in an ideal compartment given by

$$\dot{c} = -k_E c + \frac{q}{V}(c_{in} - c_{out}) \tag{3.59}$$

with $c_{out} = c$ at steady state we obtain

$$k_E = \frac{q}{V} \frac{c_{in} - c_{out}}{c_{out}} \tag{3.60}$$

which can be expressed in terms of the clearance as

$$k_E = \frac{Cl}{V} \frac{q}{q - Cl}. \tag{3.61}$$

From the fact that the elimination for epinephrine in the periphery is $\gtrsim 0.9$ [471] we estimate for $Cl := 0.96$

$$k_E = 0.3614. \tag{3.62}$$

which is in agreement with a halftime constant of $2 \cdots 3\ min$ suggested in [363].

To determine the excretion rate of E from the adrenal medulla, plasma concentration measurements are required. The measurements obtained in [374, 214], however, do not allow to compute such an estimate. But since a mismatch in k_{AM} linearly affects the epinephrine concentrations c_L and c_P, such a mismatch might be compensated by adjusting α_4 and γ_i accordingly. Physiologically meaningful values for k_{AM} might be obtained by relying on catecholamine concentrations published in the literature. Publications studying the catecholamine changes during anesthesia are [102, 271, 5, 209, 351]. The papers explicitly comparing catecholamine concentrations before and after painful stimulations [210, 271, 209] observe an increase of plasma epinephrine from $45\frac{pg}{ml}$ to $140\frac{pg}{ml}$ for heavy stimulations like skin incision. In view of these facts we chose to set

$$k_{AM} := 3 \quad [\frac{pg}{min}] \tag{3.63}$$

which leads to plasma E concentration increases of about $40\frac{pg}{ml}$. With assumption A-23 we may estimate α_4 analogously to equation 3.50 as

$$\alpha_4 = \frac{2}{c_{P,max}} \frac{\Delta HR}{HR} = 0.3112 \pm 0.0524. \tag{3.64}$$

where ΔHR is now measured at the time of $c_{P,max}$. For estimating the γ_i the same procedure as for the κ_i is applied. First from table 3.6.3 rough estimates for the relative values $\tilde{\gamma}$ are derived. Considering the dilating effect of β-stimulation through epinephrine

$$\tilde{\gamma}^T = \begin{bmatrix} 3 & 0 & 0 & -3 & -10 & -3 & 0 & -10 & -3 \end{bmatrix}. \tag{3.65}$$

is obtained. With a time constant of $\tau_n = 10s$ the neural activity has practically decayed completely when $c_P(t)$ achieves its maximum value $c_{P,max}$ so that

$$MAP_{max} = \frac{CO_{max}}{\sum\limits_{j=1}^{9} g_{i,pre}(1 + \frac{\tilde{\gamma}_i}{K_\gamma} n_{max})} \tag{3.66}$$

from where the normalization constant K_γ may be computed as

$$K_\gamma = \frac{MAP_{max} \sum\limits_{j=1}^{9} g_{i,pre}\tilde{\gamma}_i c_{P,max}}{CO_{max} - MAP_{max} \sum\limits_{j=1}^{9} g_{i,pre}}. \tag{3.67}$$

From the experimental data records $K_\gamma = 5.5 \pm 3.12$ was found. Thus

$$\tilde{\gamma}^T = \begin{bmatrix} 0.75 & 0 & 0 & -0.75 & -2.5 & -0.75 & 0 & -2.5 & -0.75 \end{bmatrix} [\frac{ml}{pg}]. \tag{3.68}$$

is obtained.

3.6.5 PK parameters of Isoflurane

There are three sources that allow to determine the PK parameters. First, CO_0, $g_{i,0}$, $V_{i,t}$, and $V_{i,b}$ are anatomic parameters and they may be taken form the corresponding literature. Second,

V_T and f_R are parameters set by the anesthetist and are therefore known. Finally, λ_i, λ_b, ls, V_{FRC}, V_{AD}, and V_D are found in physiology texts specialized to anesthesia. In principle ls, V_{FRC}, V_{AD}, and V_D would be anatomic parameters also. As will be discussed, however, they are to some extent gas dependent.

From Brody's relation [63] CO_0 may be estimated from the body weight with

$$CO_0 = 0.2 m_{[kg]}^{\frac{3}{4}} \qquad [\frac{l}{min}] \tag{3.69}$$

where $m_{[kg]}$ denotes the value of the body weight measured in kg. For estimation of the conductivities published data on the distribution of blood flow to the different organs [41, 524, 299, 431, 116] is utilized. Based on the flow distribution we obtain

$$g_{i,0} = \frac{CO_0}{MAP_0} \mathcal{P}_{q,i}. \tag{3.70}$$

Stacked into a vector the values for the flow distribution based on [41, 524, 299, 431, 116] are

$$\mathcal{P}_q^T = \begin{bmatrix} 5 & 11.5 & 3.5 & 25 & 2.5 & 23.5 & 18.5 & 2.5 & 8 \end{bmatrix} [\%]. \tag{3.71}$$

This is in agreement with [524]. Blood and tissue volumes of the different compartments are given by

$$V_{i,t} = k_t \mathcal{P}_{t,i} m \quad [l] \quad \text{and} \quad V_{i,b} = k_b \mathcal{P}_{b,i} m \quad [l] \quad \text{where} \quad i = 1, ..., 9, L, A, V. \tag{3.72}$$

In equations 3.72 $\mathcal{P}_{t,i}$ and $\mathcal{P}_{b,i}$ denote the distribution of the total blood and tissue volume to the different compartments. k_t and k_b are constants relating body weight with total tissue volume and total blood volume respectively. Written in vector form the partitions are according to [524]

$$\mathcal{P}_t = \begin{bmatrix} 0.5 & 0.9 & 1.7 & 0.6 & 10.7 & 6.7 & 56.9 & 21.0 & 0.0 & 1.0 & 0.0 & 0.0 \end{bmatrix} [\%] \tag{3.73}$$
$$\mathcal{P}_b = \begin{bmatrix} 2.7 & 6.8 & 1.9 & 16.1 & 2.1 & 17.9 & 7.5 & 2.9 & 7.3 & 6.8 & 17.6 & 10.4 \end{bmatrix} [\%]. \tag{3.74}$$

Similar values are found in [23]. The factors for total tissue and blood volumes are according to [344]

$$k_t = 0.9 \quad [\frac{l}{kg}] \quad \text{and} \quad k_b = 0.08 \quad [\frac{l}{kg}]. \tag{3.75}$$

The solubilities of Isoflurane have experimentally be determined by several authors [506]. Summaries of these results are given in [513, 514, 512]. We note that for some compartments the values published are not consistent between the different sources. For example the blood/brain partition coefficient has been estimated between 1.6 and 2.6 [513]. Here we work with

$$\lambda_i = \begin{bmatrix} 1.60 & 1.60 & 1.60 & 1.30 & 2.40 & 1.90 & 4.40 & 64.00 & 0 & 2.40 & 1.46 & 0 \end{bmatrix} \tag{3.76}$$

where again $i = 1, ..., 9, L, A, V$ and with

$$\lambda_b = 1.46. \tag{3.77}$$

Values for the functional residual capacity are provided in [97]

$$V_{FRC} = 2.57 \pm 0.43 \ [l].$$ (3.78)

Values for the anatomic dead space are provided by most physiology textbooks [95, 431, 23]. According to these sources

$$V_D = 0.3 \ V_T.$$ (3.79)

For determining ls and V_{AD} we refer to the discussion in section 3.2.2 and [258]. [258] provides average values for ls and V_{AD} where V_{AD} is computed from CO_2 partial pressure measurements and ls is computed from O_2 content measurements. If these values for V_{AD} and ls are used to calculate ideal alveolar and pulmonary end capillary Isoflurane concentrations an unexpectedly large difference is obtained. The authors of [258] attribute this effect to possibly non ideal equilibration of Isoflurane in the alveoli due to its relatively large molecular weight. This fact is also described in [129]. Due to a non ideal equilibration the partial pressure of Isoflurane is not uniformly at partial pressure p_L in the alveolus at the beginning of exspiration. While the partial pressure next to the membrane is indeed at partial pressure p_L the partial pressure towards the opening of the alveolus to the bronchi is still at p_{insp}. The average partial pressure in the active alveoli thus lies between p_L and p_{insp}. This fact may be accounted for by modeling an enlarged V_{AD}. The data provided in [258] allows to reasonably select a value for V_{AD}. The paper provides measurements for inspired, endtidal, arterial and mixed venous partial pressure after about 25 min of applying a constant inspired anesthetic concentration. Figure 3.24 compares the average values published in [258] and the predictions of our model with

$$V_{AD} := 0.35 \ V_T.$$ (3.80)

[258] also provides an estimate for ls of

$$ls = 14.8 \pm 4.74 \ [\%].$$ (3.81)

The value obtained for V_{AD} is by a factor three larger than what is normally estimated through CO_2 partial pressure measurements for patients under anesthesia [258]. That is non ideal mixing reduces the active alveolar space considerably. Note also that Derighetti obtained a similar result. For his "gas shunt" coefficient in equation 3.23 he provides a value of $K_s = 0.3$.

3.6.6   PD parameters for Isoflurane

From equations (3.14) and (3.15) there are the PD parameters α_1, α_3, and β_i with $i = 1 \cdots 9$ for the direct influence of Isoflurane partial pressure on $CO(t)$ and $g_i(t)$. In addition from equation (3.24) there is $\tilde{\alpha}_2$ for the influence of Isoflurane on the sympathetic neural activity. To estimate these parameters experimental data and published data is combined to a regression problem.

To be able to set up the estimation problem on experimental data we make several approximations. First, we will neglect the lag between the Isoflurane partial pressure in the CNS $(p_2(t))$ and the
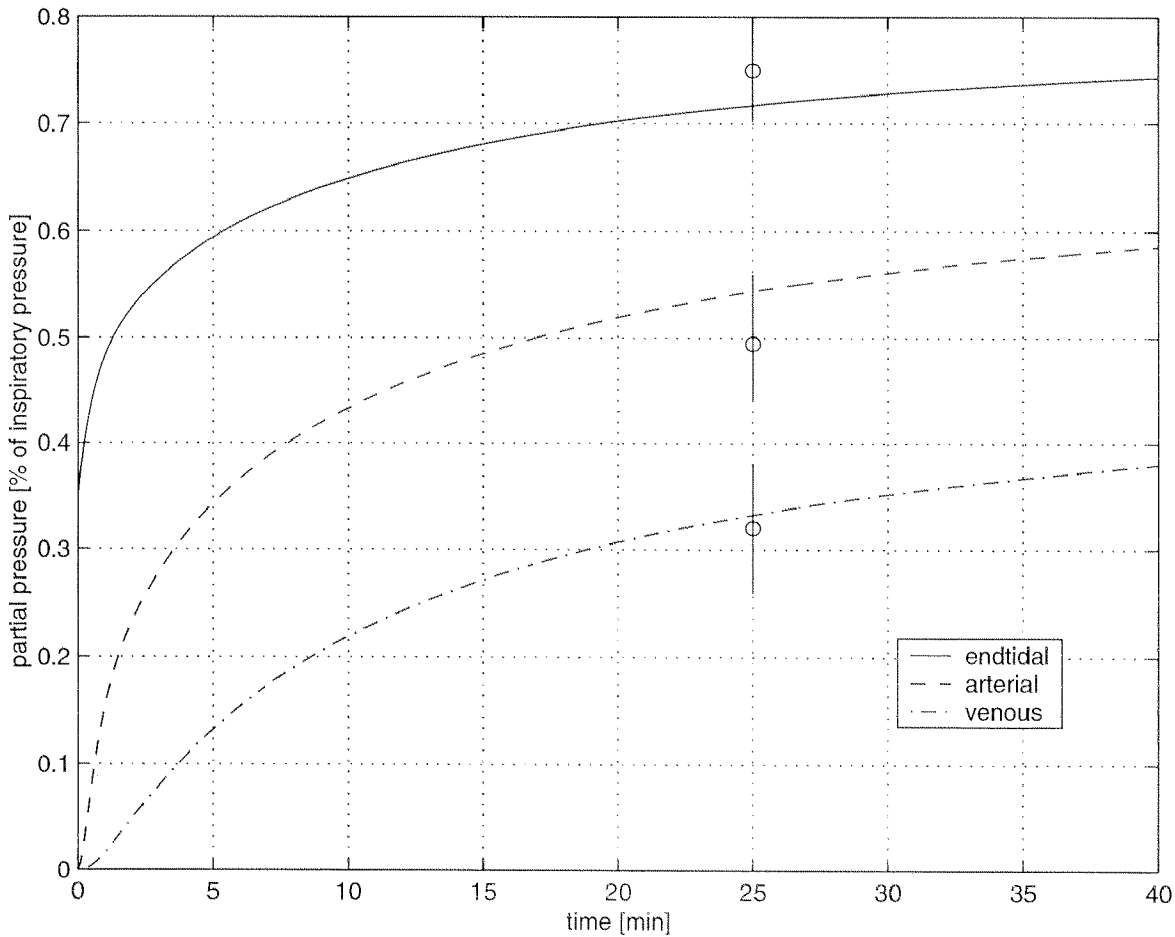
Figure 3.24: Responses of endtidal, arterial, and mixed venous partial pressure to constant inspired concentration. Average values and standard deviations for measurements of these responses after about $25\ min$ as provided by [258] are shown for comparison.

neural activity $(n(t))$. This is justified due to the fast time constant of the neural activity. With this approximation the CNS partial pressure enters the PD equations directly through $\alpha_6\tilde{\alpha}_2$ and $\kappa_i\tilde{\alpha}_2$, respectively. The influence of the circulating epinephrine will be neglected in view of the dominating neural influence. We also neglect the lag in the baro reflex since it is fast compared to changes of the partial pressure variables. With these approximations the MAP equation may be written as

$$MAP = \frac{CO_0(1 + \alpha_1 p_1 + \alpha_6\tilde{\alpha}_2 p_2 + \alpha_3 p_A)}{(1 + k_{BR}HR_0\Delta MAP)\sum\limits_{j=1}^{9} g_{j,0}(1 + \beta_j p_j + \kappa_i\tilde{\alpha}_2 p_2)}. \tag{3.82}$$

To transfer equation (3.82) into an estimation problem the p_i must be obtained first. These variables may be estimated with a PK model using the nominal parameters CO_0 and $g_{i,0}$. This is justified since the changes in the compartment flows for low Isoflurane partial pressures ($<$ $0.5\ MAC \triangleq 0.65\ \%\ vol$) are on the order of $0 \cdots \pm 20\%$ [288, 166, 165, 130] only. With measurements for MAP and estimates for $p_i(t)$ available the estimation of the PD parameters

may be formulated as a regression problem of the form

$$\min_{\theta} \quad |\Phi\theta - Y| \tag{3.83}$$

$$\text{s.t.} \quad S\theta = B. \tag{3.84}$$

The design matrix Φ is given by

$$\Phi = \begin{bmatrix} g_{1,0}p_1(0) & \cdots & g_{9,0}p_9(0) & \left(\sum_{j=1}^{9} g_{i,0}\kappa_i - \frac{CO_0\alpha_6}{\widetilde{MAP}(0)}\right)p_2(0) & -\frac{CO_0p_1(0)}{\widetilde{MAP}(0)} & -\frac{CO_0p_A(0)}{\widetilde{MAP}(0)} \\ \vdots & \vdots & \vdots & \vdots & \vdots & \vdots \\ g_{1,0}p_1(t) & \cdots & g_{9,0}p_9(t) & \left(\sum_{j=1}^{9} g_{i,0}\kappa_i - \frac{CO_0\alpha_6}{\widetilde{MAP}(t)}\right)p_2(t) & -\frac{CO_0p_1(t)}{\widetilde{MAP}(t)} & -\frac{CO_0p_A(t)}{\widetilde{MAP}(t)} \\ \vdots & \vdots & \vdots & \vdots & \vdots & \vdots \end{bmatrix} \tag{3.85}$$

the vector θ is

$$\theta^T = \begin{bmatrix} \beta_1 & \beta_2 & \cdots & \beta_9 & \tilde{\alpha}_2 & \alpha_1 & \alpha_3 \end{bmatrix} \tag{3.86}$$

and the observation vector is given by

$$Y^T = \begin{bmatrix} \frac{CO_0}{\widetilde{MAP}(0)} - \sum_{j=1}^{9} g_{i,0}, & \cdots & \frac{CO_0}{\widetilde{MAP}(t)} - \sum_{j=1}^{9} g_{i,0} & \cdots \end{bmatrix}. \tag{3.87}$$

The short hand notation $\widetilde{MAP}(t)$ was used to denote $MAP(1 + k_{BR}HR_0\Delta MAP)$.

The constraints $S\theta = B$ defined by equation (3.84) mainly apply to the conductivity changes and are of the form

$$\beta_i + \kappa_i\tilde{\alpha}_2 = B_i. \tag{3.88}$$

One constraint concerns the change in cardiac output and is of the form

$$\alpha_1 + \alpha_6\tilde{\alpha}_2 + \alpha_3 = B_0. \tag{3.89}$$

The constraints B_i and B_0 result from steady state information available in the literature. Note that B_0 represents the steady state change in CO at 1 % Isoflurane. From [97]

$$B_0 = -0.05[1/\%] \tag{3.90}$$

may be obtained. Similarly the constraints B_i represent the conductivity changes at 1 % Isoflurane. They might be obtained from sources like [288, 165, 166, 130, 211]. Note that since Derighetti [111] did not account for the conductivity changes induced by the sympathomimetic effect (i.e. the terms $\tilde{\alpha}_2\alpha_6$) the values of the B_i's are equal to the β_i published in [111]. They are computed according to

$$B_i = \frac{\frac{MAP}{MAP(p_{test})}\frac{q_i(p_{test})}{q_{i,0}} - 1}{p_{test}} \tag{3.91}$$
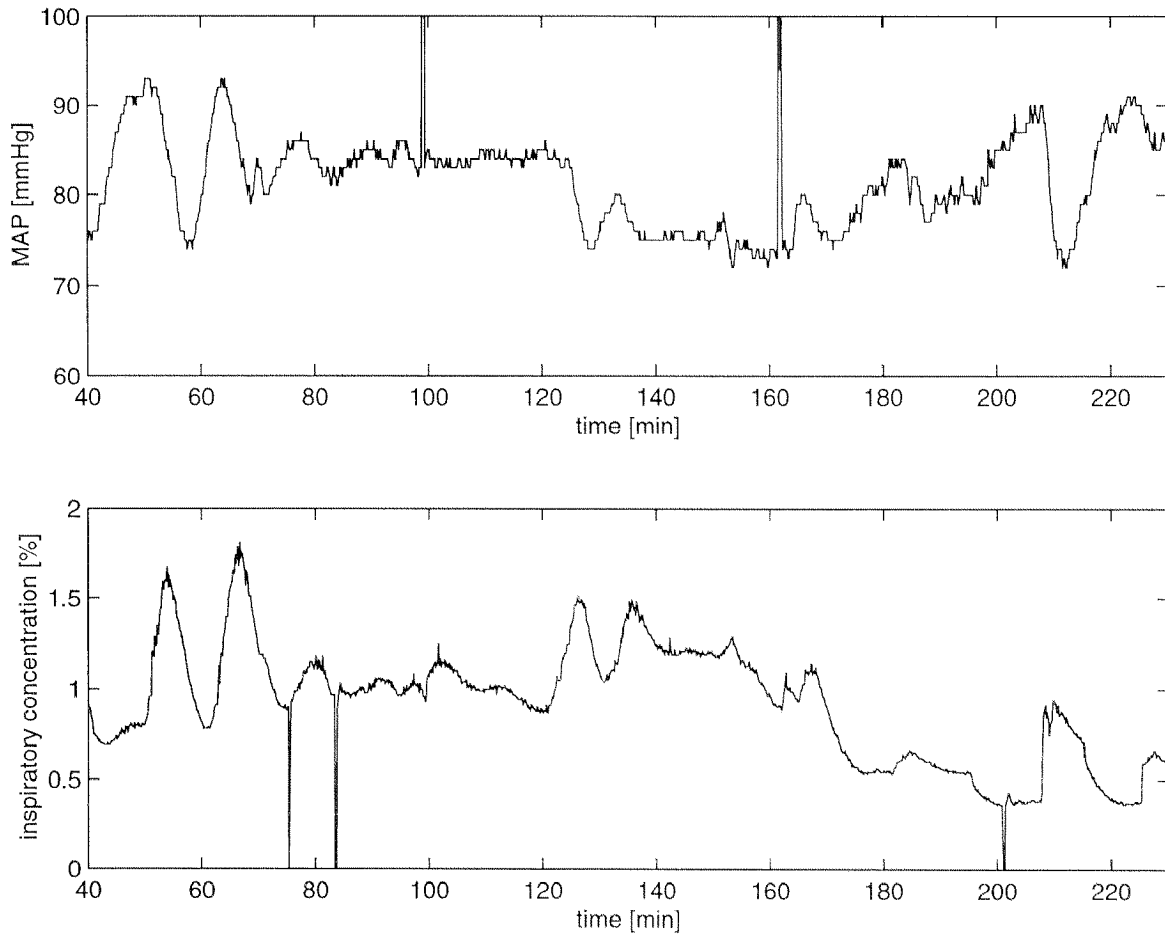
Figure 3.25: An blood pressure episode with almost no disturbance influence allows to estimate the Isoflurane PD parameters.

where p_{test} denotes the steady state test concentration at which $MAP(p_{test})$ and $q_i(p_{test})$ are measured. From the data published we obtain in agreement with [111]

$$B^T = \begin{bmatrix} 0.52 & 0.48 & 0.48 & 0.17 & 0.17 & 0.22 & 0.52 & 0 & 0.78 \end{bmatrix} [1/\%]. \qquad (3.92)$$

Experimental data to be used for estimating the PD parameters according to equation (3.83) should be free from disturbances and persistently excited through the input like the sequence shown in figure 3.25.

The estimation yields

$$\alpha_1 = -4.4454 \qquad (3.93)$$
$$\tilde{\alpha}_2 = 6.9757 \qquad (3.94)$$
$$\alpha_3 = 0.0175 \qquad (3.95)$$

and

$$\beta = \begin{bmatrix} 0.70 & 0.47 & 0.47 & 2.00 & 2.00 & 2.05 & 1.07 & 1.83 & 2.61 \end{bmatrix} [1/\%]. \qquad (3.96)$$

Note that these values are the result of a single case. Due to the lack of undisturbed blood pressure records it was not possible to perform estimates on a broader basis. Some conclusions might, however, still be drawn from this example (section 3.9).

3.6.7 Parameters of the respiratory circuit

The fresh gas flow is set by the anesthetist and therefore known. The volume of the respiratory circuit is easily measurable and is in our case $V_R = 3.0$ $[l]$. The consumption of gas through net uptake of O_2 is given by [31]:

$$\dot{V}_{O_2} = 10 m_{[kg]}^{3/4} \quad [ml/min]. \tag{3.97}$$

The consumption of gas through net uptake of N_2O is given by the approximation due to Severinghaus [31]:

$$\dot{V}_{N_2O} = 1000 \cdot t^{-1/2} \quad [ml/min] \tag{3.98}$$

where $t = 0$ denotes the start of drug application. It should be noted that this equation is only valid under low flow conditions (see table 3.3). The total consumption Q_Δ is then given by

$$Q_\Delta = \dot{V}_{O_2} + \dot{V}_{N_2O}. \tag{3.99}$$

This agrees with average values provided by [466, 97].

3.6.8 Parameters summarized

Table 3.6 summarizes the results of the different parameters estimation steps.

Parameter	Source	Value / Equation	Unit
PK parameters of the anesthetic agent			
CO_0	[63]	(3.69)	[ℓ/min]
$g_{i,0}$	[111]	(3.70)	[ℓ/min mmHg]
$V_{i,t}$	[524, 344]	(3.72)	[ℓ]
$V_{i,b}$	[524, 344]	(3.72)	[ℓ]
λ_i	[513, 514, 512, 506]	(3.76)	[-]
λ_b	[513, 514, 512, 506]	1.46	[-]
ls	[258]	0.1	[-]
V_{FRC}	[97]	2.57	[ℓ]
f_R	set by anesthetist	$9 \cdots 11$	[1/min]
V_T	set by anesthetist	$0.4 \cdots 1.2$	[ℓ]
V_D	[258]	(3.79)	[ℓ]
V_{AD}	[258]	(3.80)	[ℓ]
PD parameters of the anesthetic agent			
α_1	[288, 166, 165, 130]	(3.83)	[1/%]
$\tilde{\alpha}_2$	[288, 166, 165, 130]	(3.83)	[1/%]
α_3	[288, 166, 165, 130]	(3.83)	[1/%]
β_i	[288, 166, 165, 130]	(3.83)	[1/%]
PK parameters of the neural activity			
τ_n	[152]	10	[s]
PD parameters of the neural activity			
α_6	[152]	0.6291	[-]
κ_i	[96]	(3.55)	[-]
PK parameters of the baro reflex			
τ_{BR}	[86]	5	[s]
PD parameters of the baro reflex			
k_{BR}	[249, 481]	25	[ms/mmHg]
PK parameters of epinephrine			
$\tilde{V}_L$	[524, 344, 152]	(3.56)	[ℓ]
$\tilde{V}_P$	[524, 344, 152]	(3.56)	[ℓ]
k_E	[471]	0.3641	[1/min]
k_{AM}	[152]	300	[pg/min]
PD parameters of epinephrine			
α_4	[152]	0.3112	[ℓ/pg]
γ	[96]	(3.68)	[ℓ/pg]
(PK) parameters of the respiratory circuit			
FF	set by anesthetist	1.0	[ℓ/min]
V_R	device specific	3	[ℓ]
Q_Δ	[31]	(3.99)	[ℓ/min]

Table 3.6: List of model parameters with their values and source. The reference [152] denotes this thesis.

3.7   Model validation

This section provides a number of validation experiments for the model given by equations (3.35) to (3.46) and the parameters according to table 3.6.

3.7.1   Validation of the model for volatile anesthetics

The most straight forward validation experiment is to compare measured and simulation predictions for the endtidal anesthetic concentration. The typical result of such a comparison is shown in figure 3.26. The second plot showing the simulation errors reveals larger errors during transients. This indicates larger modeling errors at high frequencies. A fact that must be taken into account for threshold selection in fault detection.
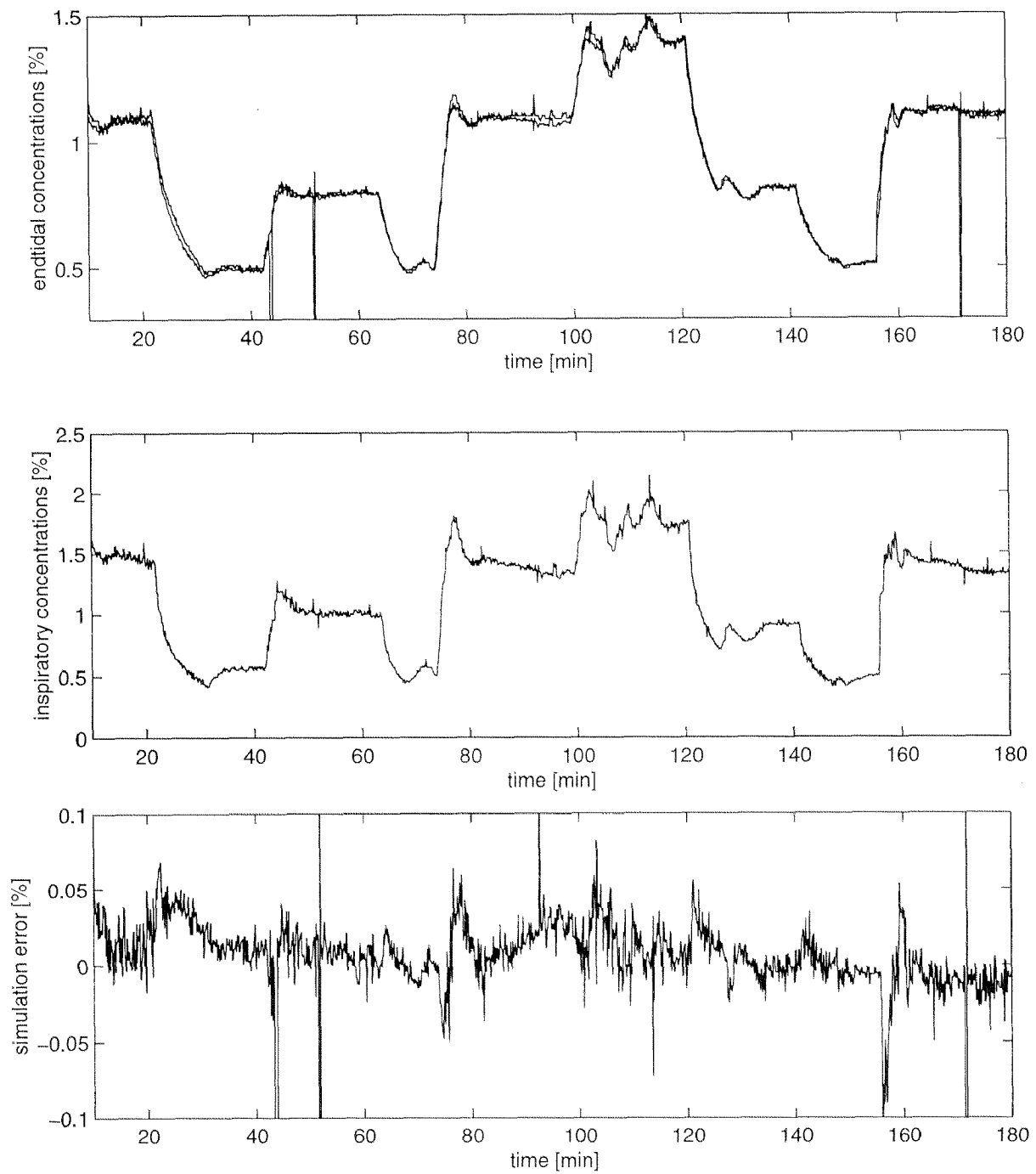
Figure 3.26: Comparison of simulated and measured endtidal concentrations.

A further validation is provided in figure 3.27 where simulation predictions for the arterial partial pressure are compared with arterial partial pressure measurements. The predictions obtained with Derighetti's model are also shown for comparison. Note that the offset present in Derighettis model (figure 2.9 in [111]) could be removed with the modified value for V_{AD} and ls given by equation (3.80) and (3.81).
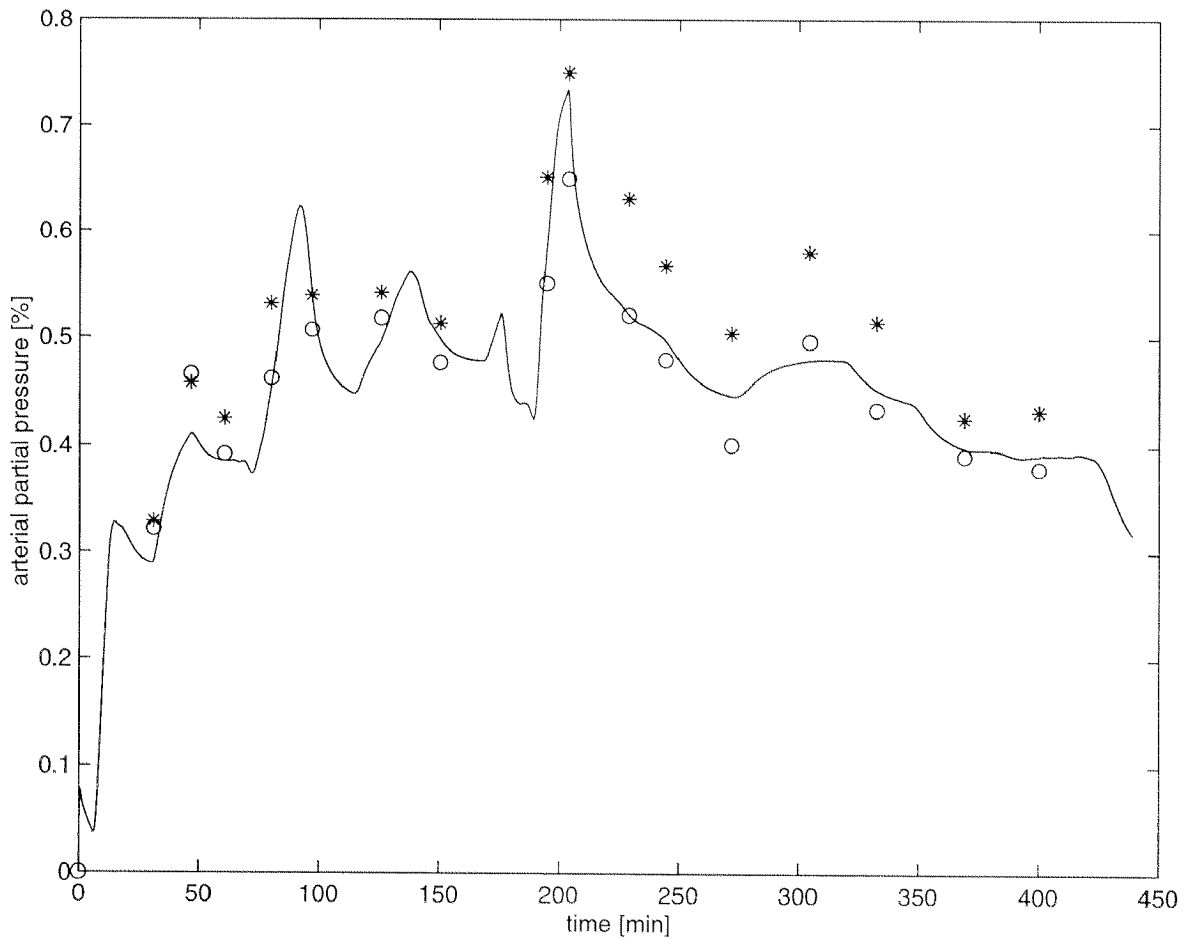
Figure 3.27: Comparison of arterial blood samples with the simulation prediction for the arterial partial pressure. The solid lines denote the prediction obtained with our model, the 'o' denote the arterial measurements, and the '*' denote the predictions obtained by Derighetti.

Yet another validation is made based on EEG measurements. In section 3.2.2 we have argued that brain activity is expected to be correlated with the suppression of the CNS function through volatile anesthetics. EEG measures of brain activity are thus expected to be correlated with the anesthetic brain partial pressure. A parameter assessing the brain activity to obtain an unconsciousness measure is the bispectral index (BIS) [20, 285]. It provides an indicator between 0 and 100. 100 corresponds to the awake state and the lower the value the deeper the level of unconsciousness. A device providing this measure is the BIS-monitor form Aspect Medical Devices. Our model does not include this BIS-measurement since the BIS-monitor became available in our project just recently. The index still allows a partial validation of our model for volatile anesthetics. More precisely by assessing the correlation between BIS values and brain partial pressure predictions a measure of the ability of the model to correctly predict brain concentrations is obtained. Such a correlation plot is shown in figure 3.28. The clear correlation provides confidence about the correct prediction of brain concentrations with our model.
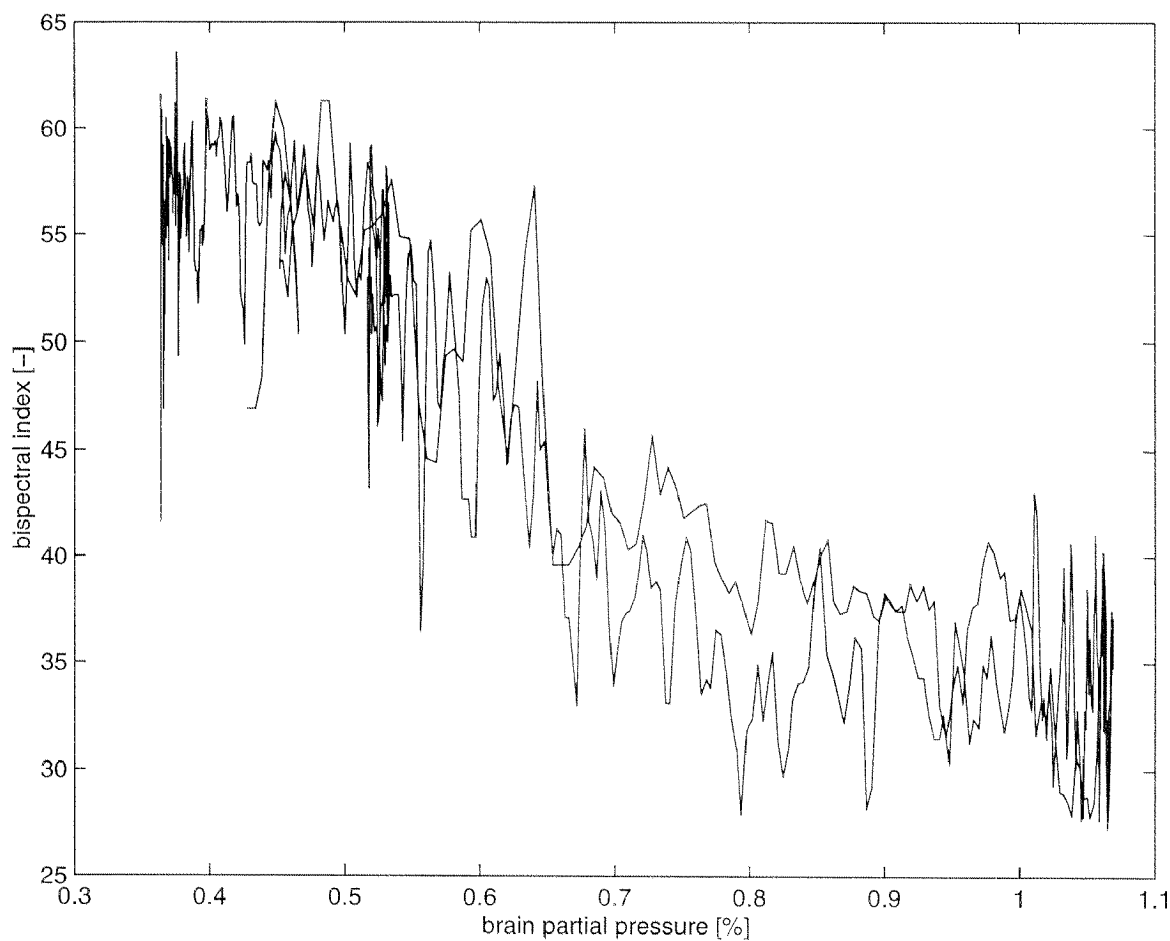
Figure 3.28: BIS measurements plotted against model based predictions of brain partial pressure. The presented data was collected during a one hour period of automatic blood pressure control.

Finally, we provide a direct validation of the PD parameters of the model for volatile anesthetics in terms of an MAP response. This is done by comparing the response of our model to published data form a clinical study. In this study Weiskopf et al. [483] recorded the MAP response to a rapid increase of endtidal anesthetic concentrations. The procedure was that volunteers were kept at $0.55 \ MAC \ \triangleq 0.71 \ \%$ vol of Isoflurane for 32 minutes. In this time MAP stabilized at $64 \pm 1mmHg$. Then the endtidal concentration was increased to $1.66 \ MAC \ \triangleq 2.21 \ \%$ vol within 100 seconds. MAP measurements were obtained during this transient phase. The data of the study is shown in figure 3.29. The figure compares the experimental response the the response of our model under the same conditions. This validation shows that the model is good in the sense that its response lies within the statistical accuracy of the experimental data.
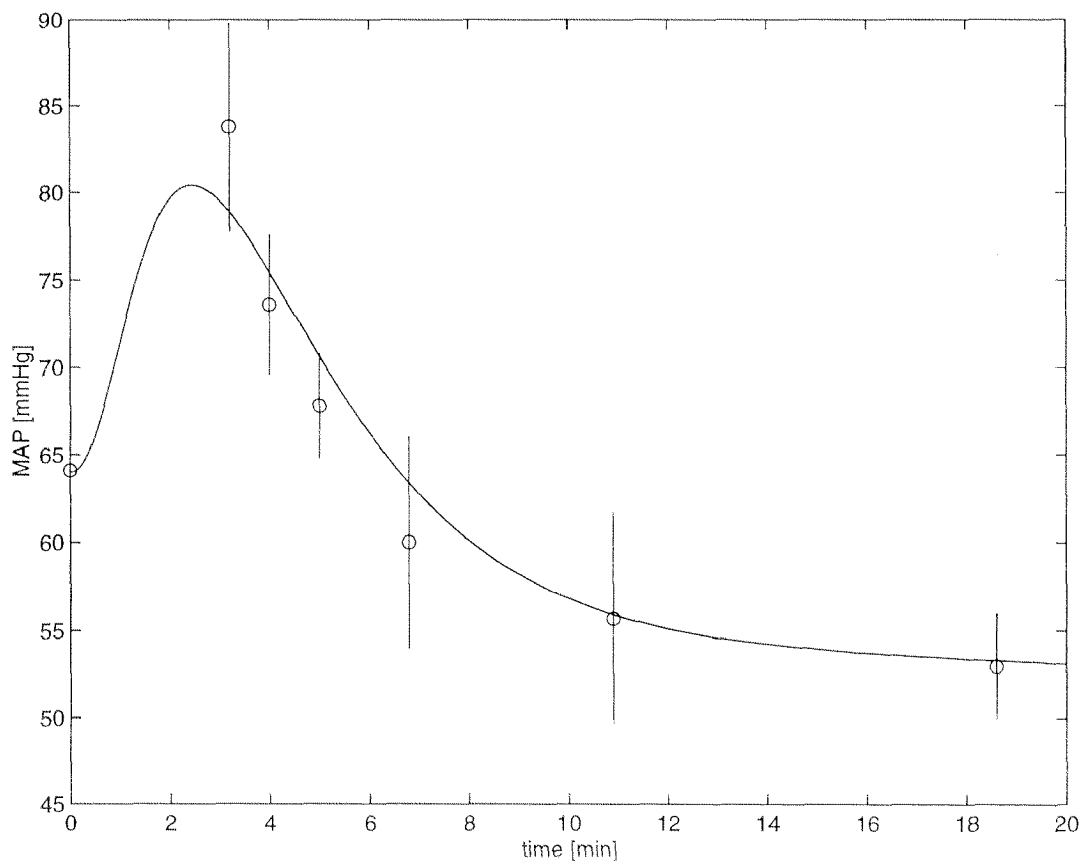
Figure 3.29: Comparison of experimental data and model response to a rapid increase of endtidal Isoflurane concentration. The 'o' denote the means and the vertical lines denote the standard deviations over the twelve volunteers. The solid line represents the model response.

3.7.2 Validation of the model for the respiratory system

A first validation will be made in terms of step responses. For this experiment an artificial plastic lung instead of a patient was connected to the system. The artificial lung has mechanical properties equal to those of a real lung. CO_2 production is mimicked by adding CO_2 during the expiration phase. O_2 is not removed. Uptake of anesthetics is not modeled. Figure 3.30 compares the measurements of inspired and expired anesthetic concentration determined experimentally with those obtained by simulating the appropriately modified respiratory system (3.35) and lung equations (3.37). The model is able to capture the dominant dynamics. The neglected transportation delays lead to errors in particular in the initial phase of the response. The consequences of this will be discussed in section 3.9.
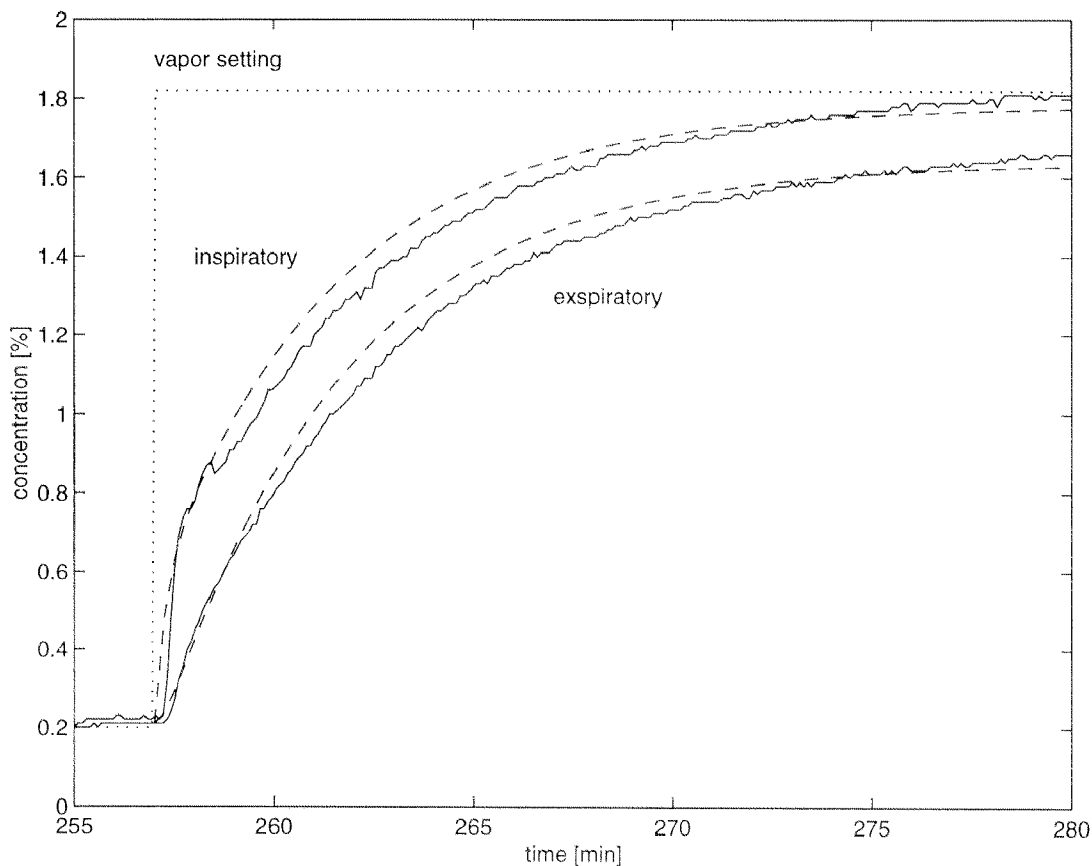
Figure 3.30: Step response validation of the respiratory circuit model. The experiment was performed with the parameters $FF = 1$ ℓ/min, $f_R = 10$ $1/min$, and $Vtidal = 0.6$ ℓ.

The experiment was performed with $FF = 1$ ℓ/min, $f_R = 10$ $1/min$, and $Vtidal = 0.6$ ℓ which represents a typical parameter set in our applications. The fresh gas flow FF is the parameter determining the dominant time constant. The higher this flow the shorter the time constant. Tidal volume V_T and the respiratory frequency f_R determine the minute volume. The minute volume determines the exchange rate between respiratory circuit and lung. Increasing the minute volume will decrease the dead time at the beginning of the response. It will also decrease the inspiratory / endtidal gradient. Decreasing the minute volume has the opposite effect.

3.8 A linear model for controller and detector design

Since procedures for controller or fault detector design are much more mature for linear than for nonlinear systems it is desirable to work with a linear system description whenever possible. Using nonlinearity measures Derighetti [111] showed that the system is only weakly nonlinear. This allows to work with linear model approximations instead of the nonlinear model. Linear model approximations are usually obtained by linearizing the nonlinear system dynamics at an equilibrium point

$$\mathbf{f}(\bar{\mathbf{x}}, \bar{\mathbf{u}}) = 0. \tag{3.100}$$

Derighetti further showed [111] that there is only one physiologically meaningful equilibrium point. For the volatile anesthetic pressures this is

$$\bar{p} = p_i = p_R = p_L = p_A = p_V = \frac{FF}{FF - Q_\Delta} p_{vap}. \tag{3.101}$$

This equilibrium pressure is independent of the equilibrium of the other variables. The equilibrium concentration for epinephrine $\bar{c}_P$ and $\bar{c}_L$ are readily derived from equations (3.25) and (3.26). They are

$$\bar{c}_P = \frac{k_{AM} \bar{n}}{\tilde{V}_P k_E} \tag{3.102}$$

and

$$\bar{c}_L = k_{AM} \bar{n} \left(\frac{1}{\tilde{V}_P k_E} + \frac{1}{\overline{CO}} \right). \tag{3.103}$$

Note that $\overline{CO} \neq f(\bar{c}_L)$. The equilibrium neural activity is given by

$$\bar{n} = \bar{d}_s + \tilde{\alpha}_2 \bar{p}_2. \tag{3.104}$$

Finally, the equilibrium of the dynamic state associated with the baro reflex is given by

$$\bar{r}_b = 0. \tag{3.105}$$

The linearized systems equations are then given by

$$
\begin{aligned}
\delta \dot{\mathbf{x}}(t) &\approx \left. \frac{\partial \mathbf{f}}{\partial \mathbf{x}} \right|_{\bar{\mathbf{x}}, \bar{\mathbf{u}}} \delta \mathbf{x}(t) + \left. \frac{\partial \mathbf{f}}{\partial \mathbf{u}} \right|_{\bar{\mathbf{x}}, \bar{\mathbf{u}}} \delta \mathbf{u}(t) \\
\delta \mathbf{y}(t) &\approx \left. \frac{\partial h}{\partial \mathbf{x}} \right|_{\bar{\mathbf{x}}, \bar{\mathbf{u}}} \delta \mathbf{x}(t) + \left. \frac{\partial h}{\partial \mathbf{u}} \right|_{\bar{\mathbf{x}}, \bar{\mathbf{u}}} \delta \mathbf{u}(t).
\end{aligned}
\tag{3.106}
$$

The structure of the different matrices is given on the next page and the coefficients are provided in appendix A.

$$\frac{\partial \mathbf{f}}{\partial \mathbf{x}}\Big|_{p_0,u_0} =$$

$$\left[\begin{array}{ccccccccccccccccc}
\partial f^1_{R,R} & 0 & 0 & 0 & 0 & 0 & 0 & 0 & 0 & 0 & \partial f^2_{R,L} & 0 & 0 & 0 & 0 & 0 & 0 \\
0 & \partial f^3_{1,1} & 0 & 0 & 0 & 0 & 0 & 0 & 0 & 0 & 0 & \partial f^3_{1,A} & 0 & 0 & 0 & 0 & 0 \\
0 & 0 & \partial f^3_{2,2} & 0 & 0 & 0 & 0 & 0 & 0 & 0 & 0 & \partial f^3_{2,A} & 0 & 0 & 0 & 0 & 0 \\
0 & 0 & 0 & \partial f^3_{3,3} & 0 & 0 & 0 & 0 & 0 & 0 & 0 & \partial f^3_{3,A} & 0 & 0 & 0 & 0 & 0 \\
0 & 0 & 0 & 0 & \partial f^3_{4,4} & 0 & 0 & 0 & 0 & 0 & 0 & \partial f^3_{4,A} & 0 & 0 & 0 & 0 & 0 \\
0 & 0 & 0 & 0 & 0 & \partial f^3_{5,5} & 0 & 0 & 0 & 0 & 0 & \partial f^3_{5,A} & 0 & 0 & 0 & 0 & 0 \\
0 & 0 & 0 & 0 & 0 & 0 & \partial f^3_{6,6} & 0 & 0 & 0 & 0 & \partial f^3_{6,A} & 0 & 0 & 0 & 0 & 0 \\
0 & 0 & 0 & 0 & 0 & 0 & 0 & \partial f^3_{7,7} & 0 & 0 & 0 & \partial f^3_{7,A} & 0 & 0 & 0 & 0 & 0 \\
0 & 0 & 0 & 0 & 0 & 0 & 0 & 0 & \partial f^3_{8,8} & 0 & 0 & \partial f^3_{8,A} & 0 & 0 & 0 & 0 & 0 \\
0 & 0 & 0 & 0 & 0 & 0 & 0 & 0 & 0 & \partial f^3_{9,9} & 0 & \partial f^3_{9,A} & 0 & 0 & 0 & 0 & 0 \\
\partial f^4_{L,R} & 0 & 0 & 0 & 0 & 0 & 0 & 0 & 0 & 0 & \partial f^5_{L,L} & 0 & \partial f^6_{L,V} & 0 & 0 & 0 & 0 \\
0 & 0 & 0 & 0 & 0 & 0 & 0 & 0 & 0 & 0 & \partial f^7_{A,L} & \partial f^8_{A,A} & \partial f^9_{A,V} & 0 & 0 & 0 & 0 \\
0 & \partial f^{10}_{V,1} & \partial f^{10}_{V,2} & \partial f^{10}_{V,3} & \partial f^{10}_{V,4} & \partial f^{10}_{V,5} & \partial f^{10}_{V,6} & \partial f^{10}_{V,7} & \partial f^{10}_{V,8} & \partial f^{10}_{V,9} & 0 & 0 & \partial f^{11}_{V,V} & 0 & 0 & 0 & 0 \\
0 & \partial f^{12}_{b,1} & \partial f^{13}_{b,2} & \partial f^{13}_{b,3} & \partial f^{13}_{b,4} & \partial f^{13}_{b,5} & \partial f^{13}_{b,6} & \partial f^{13}_{b,7} & \partial f^{13}_{b,8} & \partial f^{13}_{b,9} & 0 & \partial f^{14}_{b,A} & 0 & \partial f^{15}_{b,b} & \partial f^{16}_{b,n} & 0 & \partial f^{17}_{b,P} \\
0 & 0 & \partial f^{18}_{n,2} & 0 & 0 & 0 & 0 & 0 & 0 & 0 & 0 & 0 & 0 & 0 & \partial f^{19}_{n,n} & 0 & 0 \\
0 & \partial f^{20}_{L,1} & 0 & 0 & 0 & 0 & 0 & 0 & 0 & 0 & \partial f^{24}_{L,L} & \partial f^{21}_{L,A} & 0 & \partial f^{22}_{L,b} & \partial f^{23}_{L,n} & 0 & \partial f^{25}_{L,P} \\
0 & \partial f^{26}_{P,1} & 0 & 0 & 0 & 0 & 0 & 0 & 0 & 0 & \partial f^{30}_{P,L} & \partial f^{27}_{P,A} & 0 & \partial f^{28}_{P,b} & \partial f^{29}_{P,n} & 0 & \partial f^{31}_{P,P}
\end{array}\right],$$

$$\frac{\partial \mathbf{f}}{\partial \mathbf{u}}\Big|_{\bar{x},\bar{u}} =
\left[\begin{array}{ccc}
\partial f^{32}_{R,V} & 0 & 0 \\
0 & 0 & 0 \\
\vdots & \vdots & \vdots \\
0 & 0 & \partial f^{33}_{n,d} \\
0 & 0 & 0 \\
0 & 0 & 0
\end{array}\right],$$

$$\frac{\partial \mathbf{h}}{\partial \mathbf{x}}\Big|_{\bar{x},\bar{u}} =
\left[\begin{array}{ccccccccccccccccc}
\partial h^1_{i,R} & 0 & 0 & 0 & 0 & 0 & 0 & 0 & 0 & 0 & 0 & 0 & 0 & 0 & 0 & 0 & 0 \\
\partial h^2_{e,R} & 0 & 0 & 0 & 0 & 0 & 0 & 0 & 0 & 0 & \partial h^3_{e,L} & 0 & 0 & 0 & 0 & 0 & 0 \\
0 & \partial h^4_{m,1} & \partial h^5_{m,2} & \partial h^5_{m,3} & \partial h^5_{m,4} & \partial h^5_{m,5} & \partial h^5_{m,6} & \partial h^5_{m,7} & \partial h^5_{m,8} & \partial h^5_{m,9} & 0 & \partial h^6_{m,A} & 0 & \partial h^7_{m,b} & \partial h^8_{m,n} & 0 & \partial h^9_{m,P}
\end{array}\right],$$

$$\text{and} \quad \frac{\partial \mathbf{h}}{\partial \mathbf{u}}\Big|_{\bar{x},\bar{u}} =
\left[\begin{array}{ccc}
0 & 0 & 0 \\
0 & 0 & 0 \\
0 & 0 & 0
\end{array}\right].$$

The structural aspects of the linearized model can be emphasized by partitioning the system states. This structural representation will reveal some of the properties that Derighetti implicitly assumed. Namely the missing coupling between the partial pressure states and the states of the stress response model. And it will help to discuss FDI aspects.

To do so let

$$\mathbf{x}_R = \begin{bmatrix} p_R \end{bmatrix} \tag{3.107}$$

$$\mathbf{x}_{Gas} = \begin{bmatrix} p_1 & p_2 & \cdots & p_L & p_A & p_V \end{bmatrix} \tag{3.108}$$

$$\mathbf{x}_D = \begin{bmatrix} r_b & n & c_L & c_P \end{bmatrix}. \tag{3.109}$$

That is $\mathbf{x}_R$ corresponds to the respiratory circuit state, $\mathbf{x}_{Gas}$ collects all the partial pressure states of the volatile anesthetic, and $\mathbf{x}_D$ collects the remaining states. The linear model description may then be written as

$$
\begin{bmatrix} \dot{\mathbf{x}}_R \\ \dot{\mathbf{x}}_{Gas} \\ \dot{\mathbf{x}}_D \end{bmatrix} =
\begin{bmatrix} \mathbf{A}_R & \mathbf{A}_{R,Gas} & 0 \\ \mathbf{A}_{Gas,R} & \mathbf{A}_{Gas} & 0 \\ 0 & \mathbf{A}_{D,Gas} & \mathbf{A}_D \end{bmatrix}
\begin{bmatrix} \mathbf{x}_R \\ \mathbf{x}_{Gas} \\ \mathbf{x}_D \end{bmatrix} +
\begin{bmatrix} \mathbf{B}_R & 0 \\ 0 & 0 \\ 0 & \mathbf{B}_D \end{bmatrix}
\begin{bmatrix} p_{vap} & d_s \end{bmatrix}
$$

$$
\begin{bmatrix} p_{insp} \\ p_{endt} \\ MAP \end{bmatrix} =
\begin{bmatrix} \mathbf{C}_{insp,R} & 0 & 0 \\ \mathbf{C}_{endt,R} & \mathbf{C}_{endt,Gas} & 0 \\ 0 & \mathbf{C}_{MAP,Gas} & \mathbf{C}_{MAP,D} \end{bmatrix}
\begin{bmatrix} \mathbf{x}_R \\ \mathbf{x}_{Gas} \\ \mathbf{x}_D \end{bmatrix} \tag{3.110}
$$

3.9 Bandwidth restrictions

An important characterization of a control system is the closed loop bandwidth. For observer based controllers as we will use them in chapter 4 one important restriction for the achievable closed loop bandwidth is introduced by the bandwidth of the model. This is so since for good closed loop control performance it it required that the bandwidth of the observer is by a factor of 2 to 3 larger than the closed loop bandwidth. The bandwidth of the model should ideally itself have a bandwidth that is larger than the observer bandwidth. A rough upper bound for the model bandwidth may be estimated by looking at the dynamics that were neglected in the model.

The bandwidth of the model has also consequences for FDI. Conceptually FDI is based on comparing measured and predicted system outputs (see section 7.8). Faults are detected based on the excursions in these so called residuals. Clearly, any un-modeled dynamic will also contribute to these residual signals. Thus, the more un-modeled dynamics the less powerful a detector will be (see also section 3.7.1).

A further restriction for the achievable closed loop bandwidth of the blood pressure control loop is the non-minimum phase characteristic of the MAP output.

The next sections quantify these restrictions further.

3.9.1   Un-modeled dynamics

The following list summarizes the most important un-modeled dynamics.

- **Blood transport:** With assumption A-10 we explicitly neglected the transportation of blood in the large vessels. From the values provided in figure 3.7 it may be seen that the pure transportation delay is of the order of 5-6 seconds. Since the idealizing assumptions for compartments do not hold in reality these compartments only account for a part of the lag introduced in the capillary bed.

- **Continuous ventilation:** With assumption A-9 we neglect the fact that changes vaporizer settings do not become effective continuously. In the worst case time delays on the order of the respiration period are introduced here.

- **Lumped respiratory circuit:** With the simplification A-22 we neglected the transportation delays in the respiratory circuit. From the experiment shown in figure 3.30 it can be seen that these delays are on the order of 20 to 30 seconds.

Considering these facts we conclude that the model is questionable above frequencies of $2 - 3\ rad/min$.

3.9.2   Non-minimum phase zeros

Inverse response behavior as exhibited by the MAP output shown in figure 3.29 are - in linear systems - caused by non-minimum phase zeros [150]. That is, zeros of the transfer function from the input (c_{vap}) to the output (MAP) that lie in the right half plane. The pole/zero plot for this transfer function is shown in figure 3.31. It reveals indeed a zero that lies at

$$s_0 = 0.0996 \tag{3.111}$$

in the s-plane. A rule of thumb states that the achievable closed loop bandwidth is less than the real part of that non-minimum phase zero, i.e.

$$BW \leq \Re(s_0). \tag{3.112}$$

That is the upper bound for the bandwidth of blood pressure control is on the order of $0.1\ rad/min$ which requires an open loop model bandwidth of $0.3 - 0.5\ rad/min$.

3.10   Conclusions

This chapter derived a physiology based dynamic MIMO model that relates the inputs 'vaporizer concentration' and 'surgical stimulations' to the outputs 'inspired anesthetic concentration', 'endtidal anesthetic concentration', and 'mean arterial pressure' as shown in figure 3.1. Different
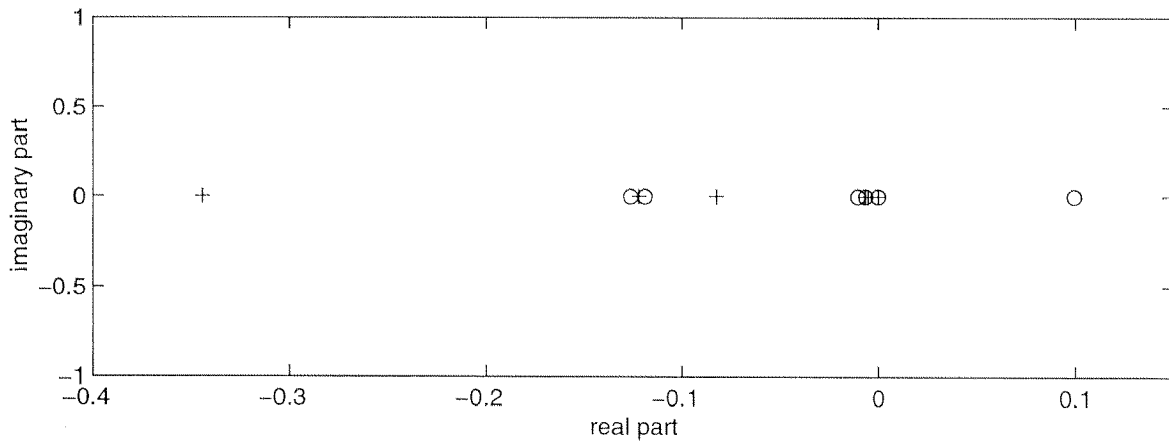
Figure 3.31: Poles ('+') and zeros ('o') of the transfer function from c_{vap} to MAP. Note that there are a number of close pole/zero locations. This indicates a potential for model reduction.

unmodeled phenomena limit the valid frequency range to $0.5 - 3\ rad/min$. This restriction has consequences for the achievable bandwidth for closed loop control as well as for the effectiveness of fault detectors. The non-minimum phase characteristic observed for the MAP-output will further limit the closed loop control bandwidth.

The model is of 16th order and has numerous physiological parameters. Other authors have proposed models of lower order [503, 505, 504, 111] based on either numerical order reduction [111] or by black box identification from experimental data [503, 505, 504]. In both cases it becomes difficult to trace the effect of changing physical, physiological or patho-physiological conditions on the model parameters. We therefore prefer to stay with the high order model where these influences easily can be traced.

A final comment shall be made about the weight dependence of the system dynamics. From any of the differential equations governing the evolution of the partial pressures in the body, i.e. equations (3.17) to (3.21), it is possible to factor out an $m^{\frac{3}{4}}$ in the numerator and an m in the denominator. The factor $m^{\frac{3}{4}}$ in the numerator originates from equation (3.69) and the factor m in the denominator originates from equation (3.72). The dynamic equations consequently may be written as

$$\dot{x}_{Gas} = m^{-\frac{1}{4}}\bar{f}_{Gas}\left(x_{Gas}\right) \tag{3.113}$$

where we have used x_{Gas} according to equation (3.108) to combine all partial pressure states of the body. That is, the system dynamics only weakly depend on the weight of the patient. This explains why other authors [503, 505, 504] are able to successfully derive PK models without introducing this weight dependency.

Chapter 4

Control Algorithms

4.1 Introduction

In section 1.4 a broad overview about automatic control applied to anesthesia was given. In this chapter we will first have a closer look at published controllers dealing with control of MAP or endtidal concentrations through volatile anesthetics. In particular a valuation of Derighetti's work will be given. The focus of this chapter, however, lies with the clinical validation of the control algorithms developed by Derighetti in his thesis [111]. These validation results are presented in section 4.4 for the endtidal controller and in section 4.5 for the MAP controller. Before that the control algorithms are described in section 4.2. Up to some extensions that will be pointed out in detail they are identical to those described in Derighetti's thesis. It will therefore be avoided to go through every detail of the controller development process. However, enough information is provided for reproduction of the algorithms. Section 4.3, finally, describes the supervisor logic control introduced for the clinical validation.

4.1.1 Blood pressure regulation through volatile ether anesthetics

Control algorithms for regulation of MAP by means of volatile anesthetics have been published in [416, 327, 329, 318, 390, 293, 459, 515, 114, 296]. Various control algorithms have been proposed by these different authors. They include bang-bang [416], Fuzzy Logic [280, 318, 459, 515, 114], neural networks [390], generalized predictive [296, 292], as well as classical self tuning control [327, 329].

The use of a bang-bang controller is motivated by the relatively narrow constraints on the input variables. If fast changes in MAP are desired this normally leads to saturation of the control signal. The algorithm suggested in [416] uses a simple second order model to determine the optimal switching times by means of online optimization. While the bang-bang strategy yields

good results during transients it is less suited for quasi steady state operation. Figures 6, 7, and 8 in [416] show that the control signal is "chattering" during these phases. Nevertheless, the authors successfully tested the control on dogs.

The arguments for Fuzzy Logic control are the classical ones. It is referred to the nonlinear dynamics, to the inter and intra patient variability and the fact that the human anesthetist's experience may be utilized. Similar arguments are used to motivate the use of neural networks [390]. All authors [280, 318, 459, 293, 515, 114] use PID- or PD-like Fuzzy controllers. Derighetti [114] suggests an interesting variation by cascading Fuzzy controllers for inspired concentration, endtidal concentration and MAP. The authors provide different degrees of validation for their controllers. While Linkens [278, 279, 293] uses simulation tests, others report ten [515] and more [459] clinical trials.

The use of self tuning control is mainly motivated by inter and intra patient variability which are said to be difficult to capture in a model [327]. The authors report 34 successful clinical applications of their controller [329].

The group of Linkens published numerous simulation studies for the use of generalized predictive control (GPC). It is a predictive control scheme which uses ARMAX models for prediction [90, 91]. In the first approach a unconstrained linear quadratic setup was used [281, 292]. Later constraints on the manipulated variables were introduced [279, 296]. We feel that the explicit handling of input constraints should be one of the main motivations for using GPC (or MPC).

4.1.2   Control of endtidal concentrations of volatile anesthetics

Applications of automatic control of endtidal concentration of anesthetics are described in [406, 450, 333, 84, 489, 477]. The suggested algorithms include open loop model based [406], heuristic [450, 333], PI- [489], and predictive control [477].

The early open loop control application [406] uses a fifth order compartmental model to predict the endtidal concentration. The predicted concentration is then used in the feedback control algorithm resulting in an open loop control scheme. No details about the model nor about the controller are provided. Acceptable performance is demonstrated in a series of animal experiments.

The heuristic controller [450, 333] also represents an early control application. The control scheme identifies some patient characteristics during an initial uptake phase. [333] argues that it would not be possible to derive these characteristics from patient data. Still they use the model of Zwart et al. [524] to validate their controller. After the identification phase a modified proportional control law is used. And after 90 breathing cycles it is switched to a PI-like control law. The controllers are validated in several clinical trials.

In [489] a PI controller is designed for the control of endtidal Halothane concentration. It is validated on the model by Zwart et al. [524] and on eight dogs [516].

Finally, [477] proposes a predictive controller with a horizon of one step. The formulation leads to a simple linear control law. The model used for prediction is of second order and captures

respiratory circuit and lung dynamics. The parameters of the model are estimated online and the model is updated continuously. The algorithm was clinically validated in five dogs.

4.1.3 Control of inspiratory concentrations of volatile anesthetics

Some controllers for the inspiratory concentration of volatile anesthetics are also reported [397, 226, 104]. The techniques used are PID [397], model based predictive [226], and Fuzzy Logic [104] control.

The PID controller [397] was validated on five dogs and the Fuzzy controller [104] was validated on 30 patients.

For the predictive control algorithm [226] a cost function based on the output prediction k-steps in the future is used. A formulation which leads to a simple linear feedback law. As validation the authors provide simulation experiments.

4.1.4 Derighetti's contribution

Summarizing these publications one observes that initially Halothane or Enflurane was used and as Isoflurane was introduced in the clinic it also came in use for automatic control applications. It further becomes apparent that as the availability of digital computers increased more sophisticated algorithms were introduced. But throughout the whole development process variability and nonlinearity arguments are used to motivate control algorithms that do not rely on mathematical models.

For his thesis [111] Derighetti initially also started with successful applications of fuzzy logic control [110, 104]. However, he reports difficulties in the tuning of the controllers for performance and their adaptation to new conditions (e.g. change from high flow to low flow anesthesia). These difficulties motivated the use of a mathematical model with parameter that have a clear physical or physiological interpretation. He utilizes this model to derive model predictive (MPC) and observer based state feedback (OBSF) controllers. His contribution is thus to show in pilot studies that controllers derived from a tailored model perform well in a clinical environment.

4.2 Control algorithms

4.2.1 Observer based state feedback controllers

The generic structure for an OBSF controller as it is used here is shown in figure 4.1. Several augmentations to the classical state feedback with observer [235, 9] were made. First, a feed forward term (F) is added for better setpoint tracking. Second, integral action (k_i) is added

to compensate for disturbances and modeling errors. And finally, an anti windup compensation (k_{AW}) is added to cope with the severe input constraints.
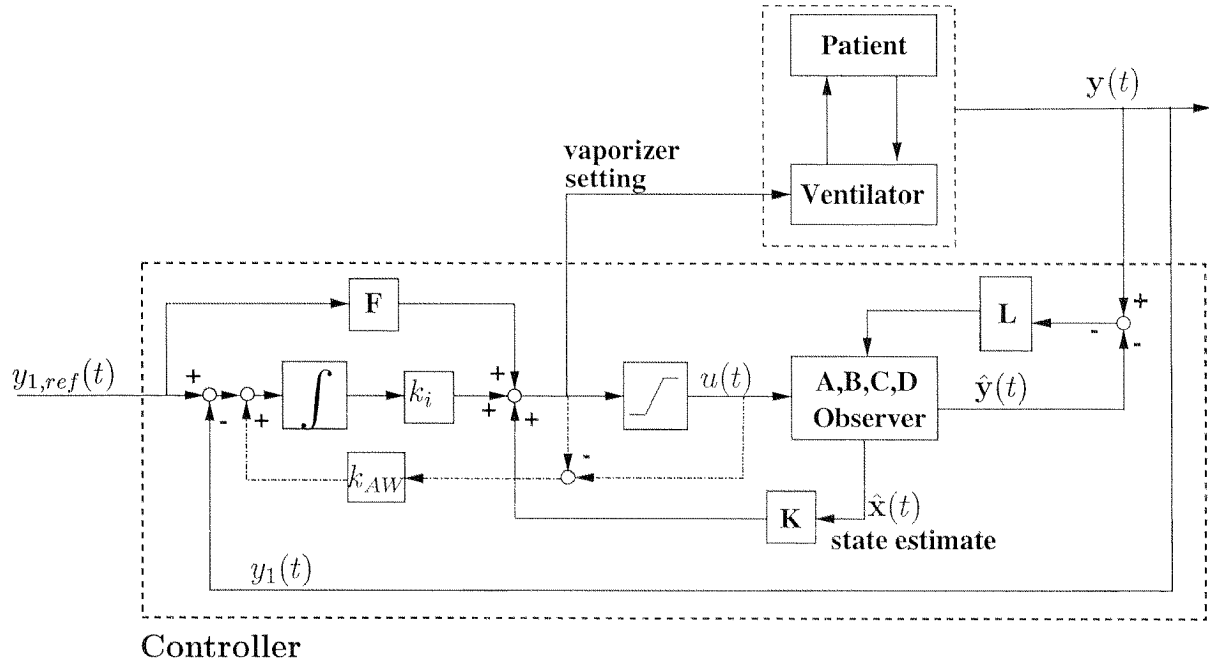

Figure 4.1: Structure of the OBSF controller used in [111].

The tuning parameters of this controller are therefore the state feedback $(\mathbf{K},\ k_i)$, the output injection $(\mathbf{L})$, the feed forward $(\mathbf{F})$, and the anti windup compensation (k_{AW}). The parameters $\mathbf{K},\ k_i$, and $\mathbf{L}$ result as the solution of a linear quadratic regulator (LQR) problem. The generic LQR problem is formulated as follows

$$\min_{\mathbf{u}(t)} \int_0^\infty \left\{ \mathbf{x}^T(t)\mathcal{Q}\mathbf{x}(t) + \mathbf{u}^T(t)\mathcal{R}\mathbf{u}(t) \right\} dt$$
$$\text{s.t.} \quad \dot{\mathbf{x}}(t) = \mathcal{A}\mathbf{x}(t) + \mathcal{B}\mathbf{u}(t). \tag{4.1}$$

It is well known [65] that for this problem a solution in the form of a constant state feedback exists, i.e.

$$\mathbf{u}(t) = -\mathcal{K}\mathbf{x}(t) \tag{4.2}$$

where $\mathcal{K}$ results from solving a Riccati equation. To obtain the parameters $\mathbf{K},\ k_i$, and $\mathbf{L}$ the two LQR problems specified through $\mathcal{A},\mathcal{B},\mathcal{Q}$, and $\mathcal{R}$ are suitably set up.

The problem formulation for the state feedback parameters $(\mathbf{K},\ k_i)$ is as follows:

$$\mathcal{A} = \begin{bmatrix} 0 & -\mathbf{C}_1 \\ 0 & \mathbf{A} \end{bmatrix} \quad \mathcal{B} = \begin{bmatrix} 0 \\ \mathbf{B} \end{bmatrix}$$

$$\mathcal{Q} = \check{\mathbf{C}}^T \mathbf{Q} \check{\mathbf{C}} \quad \mathcal{R} = \mathbf{R} \tag{4.3}$$

Where

$$\breve{\mathbf{C}} = \mathbf{I} - \breve{\mathbf{C}}^T \left(\breve{\mathbf{C}} \breve{\mathbf{C}}^T \right)^{-1} \breve{\mathbf{C}} \tag{4.4}$$

with

$$\breve{\mathbf{C}} = \begin{bmatrix} \gamma & \mathbf{C}_1 \end{bmatrix} \tag{4.5}$$

and where the matrices $\mathbf{A}$, $\mathbf{B}$, and $\mathbf{C}$ refer to the standard description for LTI systems. Note that $\mathbf{C}_1$ denotes the row of $\mathbf{C}$ which generates the controlled output $y_1(t)$. This formulation results from requiring trajectory tracking and integral action [111, 9]. The tuning parameters for the state feedback are thus $\mathbf{Q}$, $\mathbf{R}$, and γ. The integrator feedback coefficient k_i is given by

$$k_i = \mathcal{K}(1) \tag{4.6}$$

and the state feedback vector $\mathbf{K}$ is given by

$$\mathbf{K} = \mathcal{K}(2 : n + 1). \tag{4.7}$$

The problem formulation for the output injection matrix $\mathbf{L}$ is as follows

$$\begin{aligned} \mathcal{A} &= \mathbf{A}^T & \mathcal{B} &= \mathbf{C}^T \\ \mathcal{Q} &= \rho \mathbf{B} \mathbf{B}^T & \mathcal{R} &= \mathbf{R}. \end{aligned} \tag{4.8}$$

This formulation results form a loop transfer recovery (LTR) design [405]. The output injection matrix $\mathbf{L}$ is given by

$$\mathbf{L} = \mathcal{K}^T \tag{4.9}$$

and the tuning parameter for $\mathbf{L}$ are ρ and $\mathbf{R}$.

Finally, the feed forward term $\mathbf{F}$ is given by

$$\mathbf{F} = \left[\mathbf{C}(\mathbf{B}\mathbf{K} - \mathcal{A})^{-1} \mathbf{B} \right]^{-1} \tag{4.10}$$

and the anti windup parameter was set

$$k_{AW} := 1 \tag{4.11}$$

by Derighetti.

4.2.2 Observer based state feedback control of endtidal anesthetic concentration

In the setup for the endtidal controller the measurement vector $\mathbf{y}(t)$ contains the inspired and endtidal anesthetic concentration measurement. The controlled output $y_1(t)$ is of course the endtidal concentration.
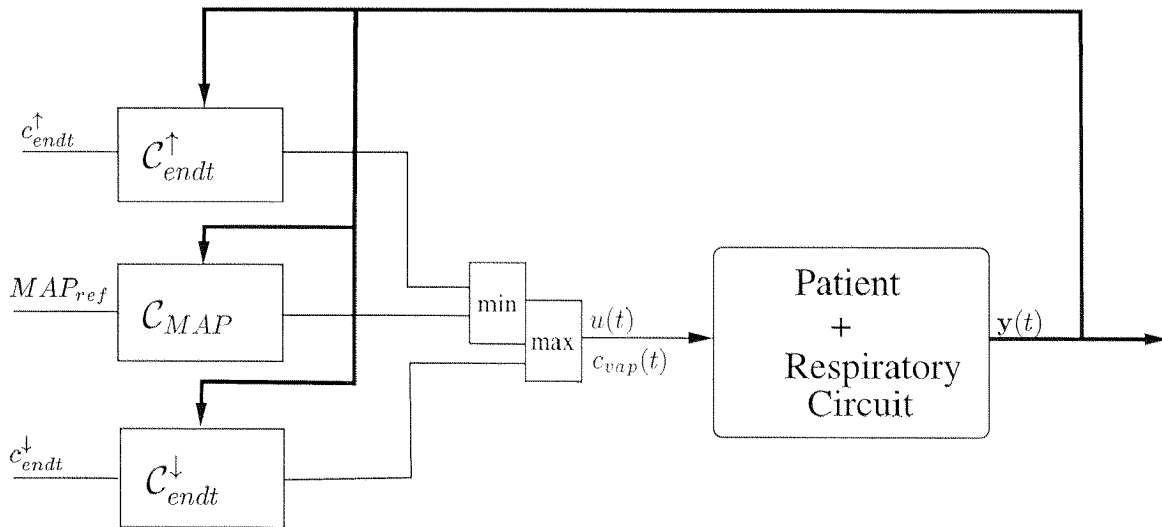
Figure 4.2: Override control structure for MAP control.

Tuning parameters chosen for the feedback design are

$$\mathbf{Q} = 1, \quad \mathbf{R} = 0.05, \quad \text{and} \quad \gamma = 3. \tag{4.12}$$

The tuning parameters chosen for the observer design are

$$\mathbf{R} = \begin{bmatrix} 1 & 0 \\ 0 & 0.1 \end{bmatrix}, \quad \text{and} \quad \rho = 100. \tag{4.13}$$

4.2.3 Observer based state feedback control of MAP with endtidal override

The structure of the MAP control algorithm is somewhat more complex than the one for the endtidal concentration. Schematically it is shown in figure 4.2. The main MAP controller C_{MAP} is an OBSF controller as described in section 4.2.1. The measurement vector $\mathbf{y}(t)$ contains the inspired and endtidal anesthetic concentration measurement and the mean arterial pressure. The controlled output $y_1(t)$ is of course mean arterial pressure. Tuning parameters chosen for the feedback design are

$$\mathbf{Q} = 1, \quad \mathbf{R} = 0.005, \quad \text{and} \quad \gamma = 0.3. \tag{4.14}$$

And the tuning parameters chosen for the observer design are

$$\mathbf{R} = \begin{bmatrix} 10 & 0 & 0 \\ 0 & 0.5 & 0 \\ 0 & 0 & 100 \end{bmatrix}, \quad \text{and} \quad \rho = 100. \tag{4.15}$$

For MAP control constraints have not just to be imposed on the control signal $c_{vap}(t)$ but also on the endtidal concentration. An upper limit $c_{endt}^{\uparrow}$ has to be imposed because a high Isoflurane

concentration may lead to a hypotonic crisis, cardiac arrhythmias, or even cardiac arrest. To comply with this upper limit Derighetti introduced an override controller $\mathcal{C}^{\uparrow}_{endt}$. This override controller is in itself a complete OBSF controller. The minimum selector applied to the control signals of MAP controller $(\mathcal{C}_{MAP})$ and endtidal controller $(\mathcal{C}^{\uparrow}_{endt})$ ensures that the upper limit $c^{\uparrow}_{endt}$ is complied with. The analysis of override structures may done according to [179, 178, 248].

At least equally important, however, is that a minimum endtidal concentration $c^{\downarrow}_{endt}$ is guaranteed since a low endtidal concentration may lead to light anesthesia and awareness. For the clinical evaluation of the MAP controller we therefore also introduced an override controller $(\mathcal{C}^{\downarrow}_{endt})$ to ensure a minimum endtidal concentration.

Note that in this structure each of the three controllers is a complete OBSF controller with an observer of its own. This makes sense, since each of the observers is obtained form a system linearization valid at a different operating point.

4.2.4   Closed loop bandwidth

An important characterization of feedback controllers is the achieved closed loop bandwidth. It determines how fast the closed loop system is able to react to changes in the reference signal. Figures 4.3 and 4.4 shown the frequency response plots for the closed loops of endtidal and MAP control, respectively. The $3\ dB$ bands are shown for reference with dashed-dotted lines.

It can be seen that the bandwidth for endtidal control is about $1\ rad/min$. This is only somewhat lower than the postulated model bandwidth of about $3\ rad/min$ and must therefore be viewed as an upper limit of achievable bandwidth. For MAP control two frequency responses are shown. The dashed response corresponds to a controller obtained by utilizing the pharmacodynamic parameters published by Derighetti. The plot shows the effect of the non-minimum phase property which Derighetti did not model. It leads to a resonance like gain increase at about $0.3\ rad/min$ which leads to poor loop performance. This poor performance is documented in figure 3.25. If the controller is designed for the non-minimum phase plant instead, the closed loop bandwidth is reduced considerably. This case is shown with solid lines. Note that the bandwidth of about $0.2\ rad/min$ lies in the range of the real part of the zero location

$$\Re(s_0) = 0.0996 \tag{4.16}$$

as postulated in section 3.9.

4.2.5   Controller parameterization

Derighetti automated the controller design in such a way that given the relevant model parameters the tailored controller can be computed in a couple of minutes. The procedure is implemented in Matlab. The different steps of the design process are illustrated in figure 4.5. Sequentially this involves the linearization of the model equations, an order reduction using the balanced
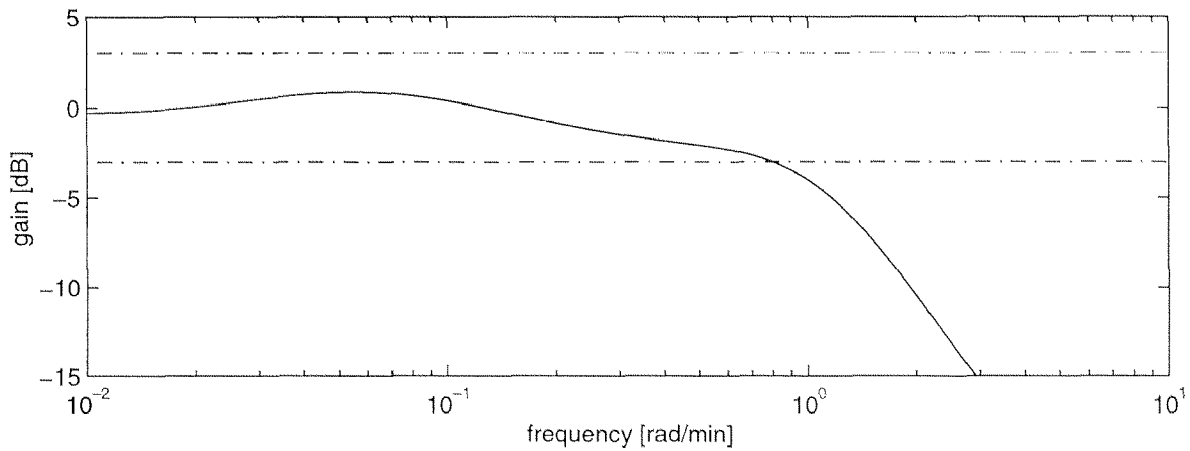
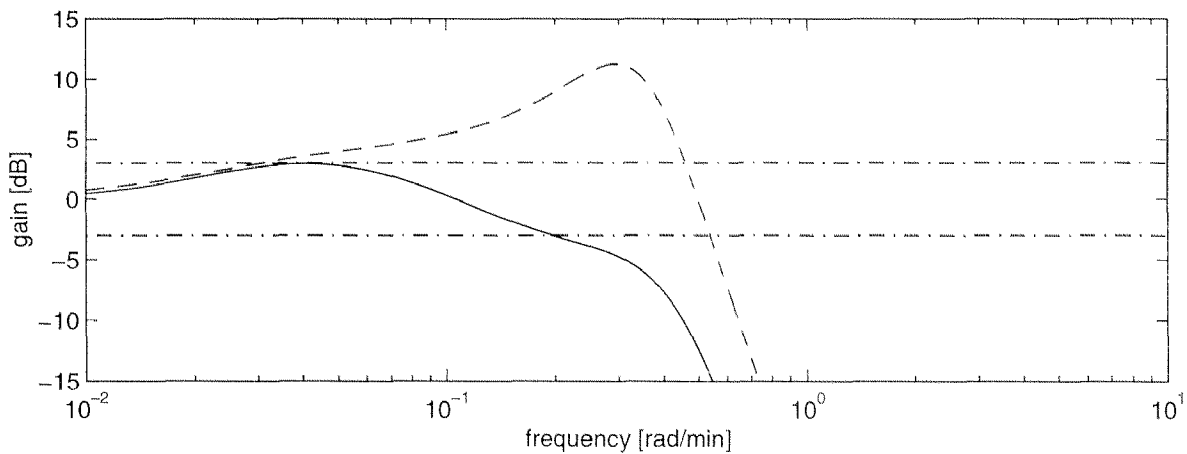Figure 4.3: Closed loop frequency response of the endtidal controller.

Figure 4.4: Closed loop frequency response of the MAP controller.

truncation by Moore [330], the controller design using the LQR-LTR procedure [405], and finally the discretization of the controller. The result is stored directly as Oberon source code files.

During the pilot study phase controllers for a patient were computed as soon as the relevant parameters were known. This happened normally on the evening before the planned operation. For the clinical evaluation, however, it was rather desired to have the possibility to compute the controller online. For this the implementation of the whole design process on the target computer in Oberon would have been one option. Only since a number of non trivial numeric steps are involved this would have been a major challenge. It was therefore preferred to perform an a posteriori parameterization of the controllers. For the continuous parameters FF and m this is done by means of polynomial approximation of every individual controller parameter. And for the discrete parameter f_R a set of controllers is provided from where the appropriate one is selected at run time (see next section). The dependency of the controllers from the tidal volume was removed by using the common rule of thumb

$$V_T = 0.01 \cdot m_{[kg]} \quad [l].$$ \hfill (4.17)

These modifications allow to compute the controller parameters online without going through
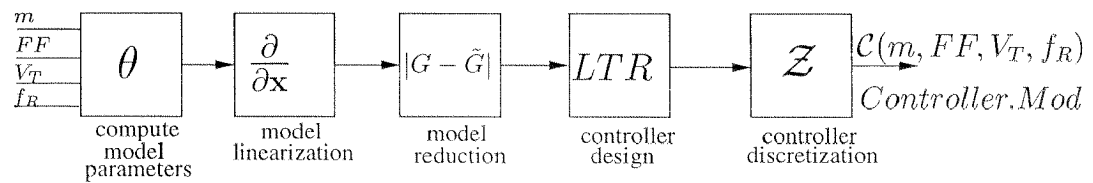
Figure 4.5: The different steps involved in the design process of the OBSF controllers.

the whole design process of figure 4.5.

4.2.6 Switching controllers

For clinical practice it is not realistic to assume that control relevant parameters stay unchanged during an operation. In particular for the adjustment of ventilation it is occasionally necessary to adjust the respiratory frequency. Since the respiratory frequency determines the sampling rate of the controller a change of the respiratory frequency requires an adjustment of the controller. For our controllers this requires a change of the controller parameters. Derighetti reports a nice example for the effects of a misadjusted respiratory frequency (figure 7.16 in [111]). If the parameters of the OBSF controller are changed the question remains how to initialize the states of the observer. Derighetti suggests to update the observer with past data. That this approach must lead to suboptimal results is illustrated in figure 4.6.
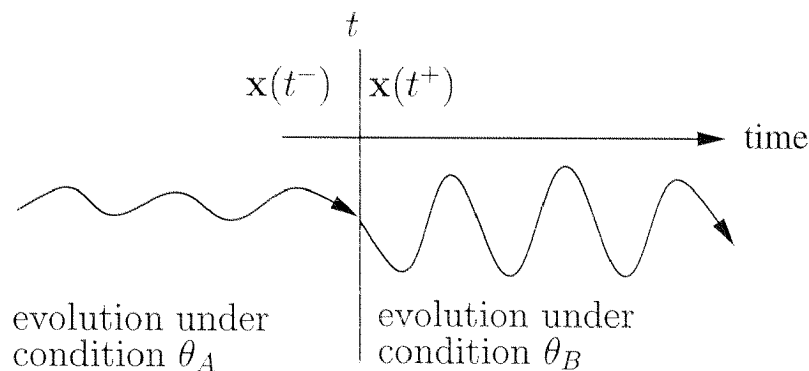
Figure 4.6: The values of the states variables are the consistent information describing the system at the instance of switching.

Assume that up to time t a system evolves under environmental conditions θ_A and that these conditions change to θ_B at time t. To comply with the new environment θ_B the controller parameters are changed at time t. However, updating the observer which has been designed for environment θ_B with data collected under conditions θ_A only under special circumstances (like steady state operation) yields correct results. If we assume that the state of the system $x(t)$ is not able to change abruptly (which is the case for our system) then the states before $(x(t^-))$ and after $(x(t^+))$ the parameter change are equal i.e. $(x(t^-) = x(t^+))$. The consistent initialization

of the controller states is thus to transfer the values of the states of the old controller to the new states.. A successful switching of controllers is shown in figure 4.7. Note that a switch during a transient phase occurs without noticeable effects on the controlled output.

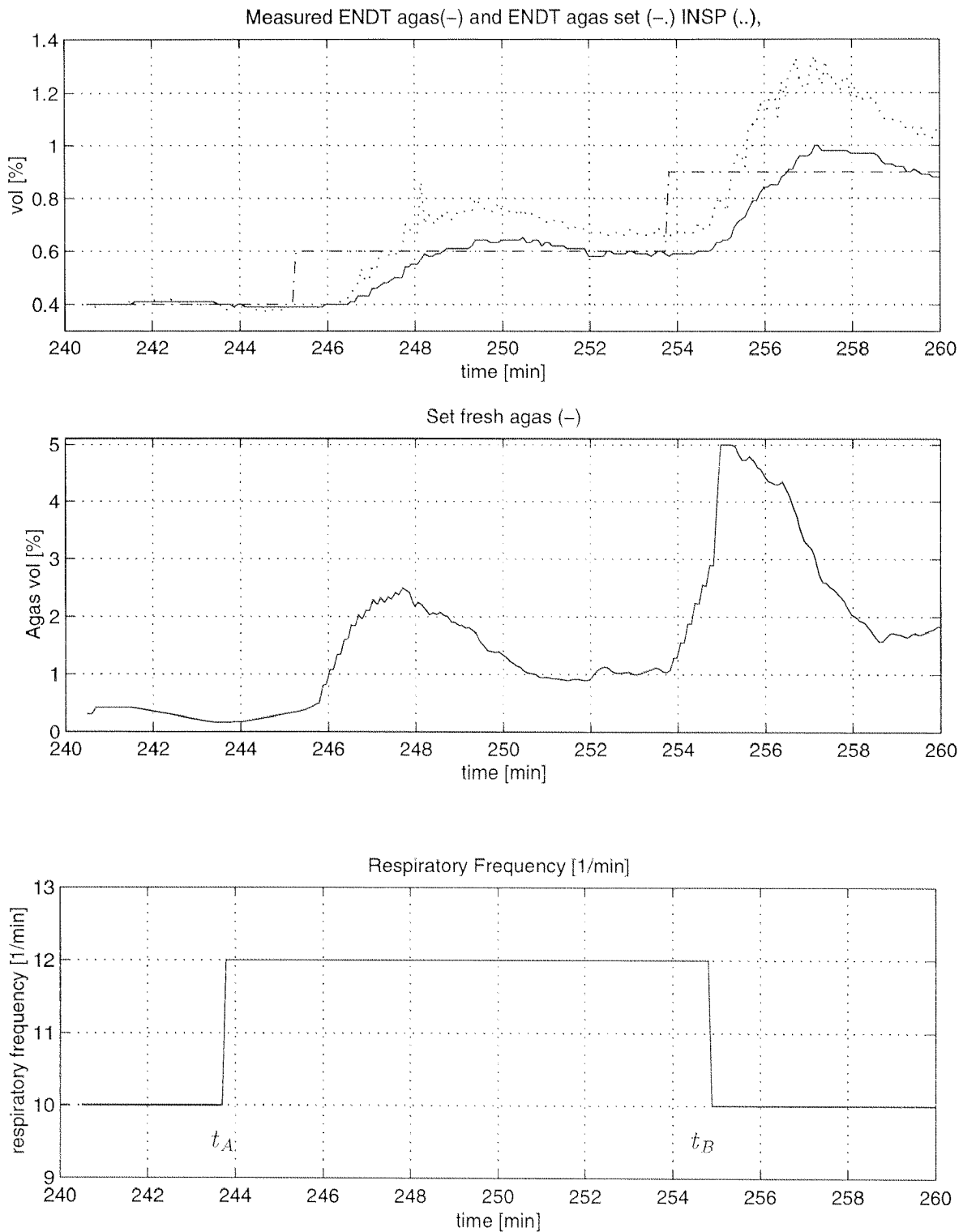Figure 4.7: Example of controller switching due to change in respiratory frequency. Up to time t_A the controller runs with a cycle time of 6 s. Between t_A and t_B it runs with a cycle time of 5 s. And after t_B it again runs with a cycle time of 6 s. At times t_A and t_B the switching of the controller occurs.

4.3   Supervisory logic control (SLC)

For a control engineer the pre-conditions for activating the different controllers are self-evident. But it is not surprising that for the anesthetist conducting the pilot studies this was not the case. For example, while for the control engineer it is clear what parameters have to be set before controller parameters can properly be initialized this is not necessarily the case for an anesthetist.

To ensure that all actions are only executed if the preconditions are satisfied a supervisory control logic was implemented in the form of a finite state automaton (FSA). The diagram of this automaton is shown in figure 4.8. According to this the system has four main states. These are "PASSIVE", "DOSING", "ENDTCTRL", and "MAPCTRL". The characterization of these states is as follows:

PASSIVE   All the software objects are initialized and running. The monitor is sampled every 6 seconds. The MMI is updated regularly. No commands except those required for synchronization are sent to the actuator devices. Gas flow and vaporizer are controlled manually. I.e. the anesthetist conducts anesthesia manually and the control system only records the data.

DOSING   The electronic branch of the gas delivery is active (compare figure 2.18). That is O_2- and N_2O-flow as well as vaporizer position are set via the user interface panel. The control and FDI algorithms are updated with the actual values. This allows the observer to converge while the anesthesia is performed manually electronically by the anesthetist.

ENDTCTRL   The endtidal controller is active. The vaporizer is set by the controller and no possibility to act on the vaporizer via the control panel is given. FDI findings are checked regularly. The MAP control algorithm is updated with the actual values. This ensures that it is possible to switch to MAP control at any time.

MAPCTRL   The MAP controller is active. The vaporizer is set by the controller and no possibility to act on the vaporizer via the control panel is given. FDI findings are checked regularly. The endtidal control algorithm is updated with the actual values. This ensures that it is possible to switch to endtidal control at any time.

Note that the states "PASSIVE" and "DOSING" could alternatively be named "READY" and "MANUAL". To avoid confusion with the manual control mode where the anesthetist is not using the research platform we prefer this terminology.

Orthogonal to these states are the two states "SAVING" and "NOSAVING". In the "SAVING" mode the software runs through all the model objects (see figure 2.10 for reference) and sends any available datum to the host computer where it is written to a file. It may be activated in
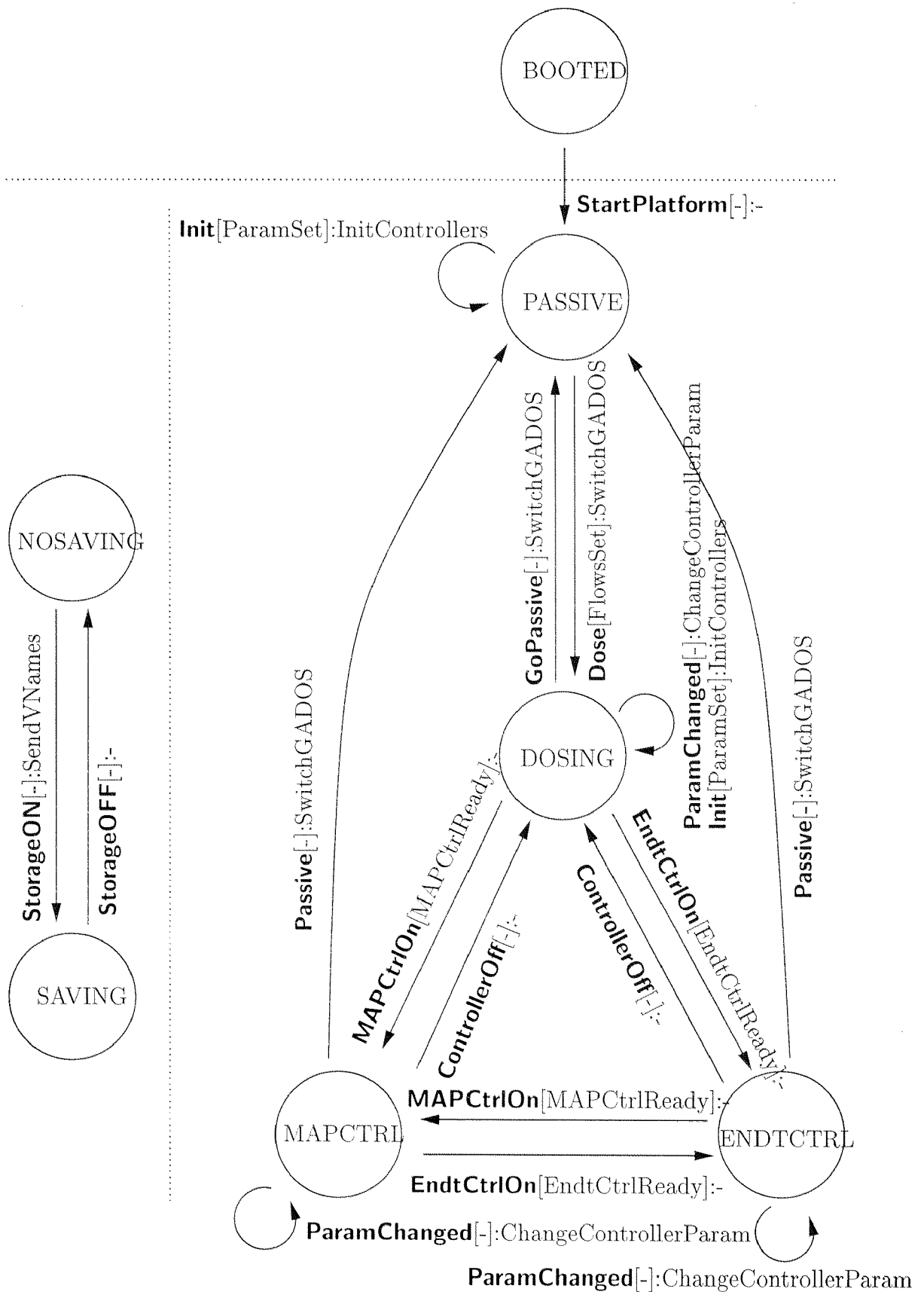
Figure 4.8: Finite state automaton implementation of the SLC for the combined endtidal/MAP controller application.

any of the four main states.

The "BOOTED" state is special. It can only be entered from the outside so to speak and it is a transient state that is entered exactly once. The system is in this state as the target computer has booted. In this state all the software modules have been loaded but only the FSA process is running. This state also implies that the host computer has successfully booted since the target is requesting its bootfile from the host computer.

The transitions between the different modes are triggered by events. Typically these are external events resulting from commands issued via the control panel. In combination with fault tolerant control (see chapter 7) these events may alternatively be triggered by fault events. Certain transitions are only possible if the corresponding preconditions are satisfied. Some transitions also execute an action. E.g. during the transition from "PASSIVE" to "DOSING" the magnetic valve (see figure 2.18 for reference) is switched from the manual dosing to the electronic dosing branch. Using the notation from [404] such a transition is formally written as

$$\textbf{event}[condition] : action. \tag{4.18}$$

The meaning of the command events and the transition actions of the FSA in figure 4.8 are clear from their naming. The transitions conditions, however, require some discussion. They will be given here in mathematical form in one to one correspondence to how they are implemented in Oberon.

$$FlowsSet = TotalFlowSet \wedge O_2FlowSet \wedge AgasConcSet \tag{4.19}$$

The interpretation of this equation is also clear from the naming of the variables. The condition $EndtCtrlReady$ is given by

$$EndtCtrlReady = ControllerInitialized \wedge ObserverReady \wedge EndtReferenceSet. \tag{4.20}$$

where $ObserverReady$ denotes the condition that the observer error has to have converged sufficiently before the controller may be switched on. The $ControllerInitialized$ condition is "TRUE" after the execution of the initialization command

$$\textbf{Init}[ParamSet] : InitControllers. \tag{4.21}$$

Here $ParamSet$ denotes the condition that the parameters m, FF, and f_R have to be specified before the controller parameters can be computed using the polynomial approximations. Finally,

$$\begin{aligned} MAPCtrlReady \;=\; & ControllerInitialized \wedge ObserverReady \wedge MAPRefSet \\ & \wedge UpEndtRefSet \wedge LowEndtRefSet \wedge FallbackEndtSet \\ & \wedge UpEndtCtrlReady \wedge LowEndtCtrlReady. \tag{4.22} \end{aligned}$$

This condition means that all three controllers in the override structure have to be ready before MAP control may be started. Note that $UpEndtCtrlReady$ and $LowEndtCtrlReady$ are conditions analogously to condition (4.20). Of course all necessary reference values have to be specified. The fallback endtidal reference is not used yet. It will play a role for fault tolerant control (see section 7.7.2).

	Group A (manual control first)	Group B (automatic control first)	
Sex			
# Male	7	5	NS
# Female	4	6	NS
Age (yr)	40.18 ± 17.41	53.64 ± 14.21	NS
Weight (kg)	75.64 ± 17.33	70.36 ± 14.35	NS
Duration of Surgery (min)	233.64 ± 121.94	204.09 ± 63.95	NS

Table 4.1: Patient characteristics and average durations of surgery. NS denotes a statistically not significant difference between the two groups. Age, body weight and duration of surgery were compared by using Student's t-test [423, 395] after data were tested for normal distribution. Normality of distribution was tested by using the Kolmogorov- Smirnov test [423, 395]. Sex was compared by using the Fisher Exact Test [423, 395].

4.4 Clinical evaluation of the endtidal controller performance

4.4.1 Patients

After approval by the institutional ethical committee, and after having obtained written, informed consent from each, 22 ASA physical status I to III patients (see e.g. [332] for a definition of ASA classes) undergoing elective surgical procedures (neurosurgery, ear-nose-throat (ENT) surgery, abdominal and orthopedic surgery) were studied. Exclusion criteria were: history of coronary artery disease, poorly controlled arterial hypertension. The patients were premedicated with lorazepam 1-2 mg orally 30 minutes prior to induction of anesthesia. Anesthesia was induced with fentanyl ($2\ \mu g/kg$) and thiopental ($3\text{-}5\ mg/kg$). The trachea was intubated after muscle relaxation with vecuronium ($0.1\ mg/kg$). Additional doses of vecuronium were given to maintain 0 - 2 responses of TOF stimulation at the ulnar nerve. After tracheal intubation, controlled ventilation was adjusted to maintain the endtidal carbon dioxide at 4.5% , and anesthesia was maintained with 70% N_2O in oxygen, Isoflurane and boluses of fentanyl ($1\text{ - }2\ \mu g/kg$) as necessary. After tracheal intubation the fresh gas flow was set to 6 l/min. Ten minutes later the flow was reduced to 1 l/min and at the end of the surgery reset to 6 l/min in both groups. The control system was started after the beginning of the operation. An equilibration period of 5 min was allowed for convergence of the observer before step changes of the endtidal Isoflurane concentration were performed. Anesthesia was conducted by experienced anesthestists (more than two years of special training) only. These anesthetists were responsible for all aspects of anesthesia including the tracking of the endtidal reference changes in the manual phase.

The patients were randomly (by lot) assigned to one of the two following treatment groups for the first phase of anesthesia. Group A patients were anesthetized using manual adjustment of the concentration of Isoflurane. Group B patients were anesthetized using an automatic feedback control system to adjust the endtidal Isoflurane concentration. In both groups, the anesthetist was asked to perform four step changes of the target endtidal Isoflurane concentration, either manually or by setting the target value for the feedback controller. Before the first step change and after each following step, an equilibration period of approximately 10 min was allowed for

maintaining a constant endtidal concentration. The endtidal target concentration was increased in two steps (plus 0.3 and 0.6 % vol) and decreased in two steps (minus 0.3 and 0.6 % vol) in each patient. The sequence of the four step changes was chosen by the anesthetist, according to the need of the intraoperative situation, but the chosen step change had to be kept for a minimal equilibration period of 10 min. If the mean arterial blood pressure decreased more than 20% after an increasing step-change, a single dose of ephedrine (5 mg iv) was allowed or an equivalent decreasing step-change of the endtidal Isoflurane concentration was sought. If the mean arterial pressure increased more than 20% after a decreasing step-change, additional amounts of fentanyl (1 - 2 $\mu g/kg$) were allowed. After this first phase of four step changes, the method of adjusting the endtidal Isoflurane concentration was switched in a crossover manner in the second phase, i.e. patients randomized to Group A (manual control) were now assigned to the automatic feedback control system for the following four step changes, and vice versa for Group B patients.

4.4.2 Performance evaluation

There is no common agreement on what measure should be used to evaluate the performance of automatic controllers in anesthesia. A list of possible criteria is given in [182]. In view of this control performance of manual and automatic control was compared based on the ability to track step changes in the target endtidal Isoflurane concentration in terms of the following criteria:

PC-1 **rise time**: For increasing step changes: time required from 10% to 90% of the step height (e.g. for an increasing step change of 0.6%, from 0.5% to 1.1%, the rise time would be defined as the time to reach 1.04% from 0.56%) For decreasing step changes: time required from 10% to 90% of the step height (e.g. for a decreasing step change of 0.3%, from 0.8% to 0.5%, the rise time would be defined as the time to reach 0.53% from 0.77%)

PC-2 **maximum overshoot**: Maximum amount the system output overshoots or undershoots its target value, expressed as a percentage of the step height. Observation starts after the target value has been reached for the first time.

PC-3 **regulation performance**: Deviation of the measured endtidal Isoflurane concentration from the target value, expressed as percentage frequency distributions of the deviation measured - desired of the endtidal Isoflurane concentration. Observation starts after the target value has been reached for the first time.

PC-4 **number of changes of the vaporizer setting**: Only changes ≥ 0.05 vol% were recorded. In the manual phase this criterion gives a measure for how much attention the anesthetist must pay to the control task. Comparing the number for manual control to the number for automatic control gives an indication on how much additional wear of the actuator is introduced by automatic control. Note that for automatic control this value will be influenced by two factors, the measurement noise and the actual control movements.

4.4.3   Results

There were no significant differences between the two groups with respect to sex, age, weight and duration of surgery (table 4.1). In both groups, two patients had only one series of step changes studied because the operation was finished early. The remaining 18 patients were studied following the protocol, i.e. they all had 4 step changes performed in the manual as well as the automatic mode. Thus a total of 80 step changes were analyzed in each group.

The statistical evaluation of the experiments are summarized in tables 4.2 and 4.3. Representative recordings of experiments are shown in figures 4.9 to 4.12.

From tables 4.2 and 4.3 we see that the performance of the feedback control was superior to the manual control in terms of overshoot and regulation performance, with increasing as well as decreasing step changes. The response time for the increasing step changes was shorter in the automatic mode for the larger steps only, but for the smaller steps it was shorter in the manual mode. The response time for the decreasing step changes was not statistically different between the two groups. The automatic control of the endtidal Isoflurane concentration resulted in higher numbers of changes of the vaporizer setting, for increasing as well as decreasing step changes (only with decreasing steps of 0.6 vol% the difference was not statistically significant).

From visual inspection of the results presented in figures 4.9 to 4.12 it is not reasonable to assume that the larger number of vapor changes for automatic control is only due to noise. It is rather conjectured that the superior control performance is achieved at the expense of more control moves.

From a control engineering point of view it is interesting to notice the asymmetry in the response to positive and negative steps. It is a consequence of the asymmetry in the available control input. Symmetric responses are only obtained when negative steps start at relatively high concentrations like in figure 4.12.

A final comment shall be made concerning the handling of the input constraints. In section 4.2 it was mentioned that the control algorithms needed special anti-windup measures to cope with the severe input constraints. Note now that the anesthetists seem to have problems with these input constraints also. This appears very clearly towards the end of both negative steps shown in figure 4.9 but is also present in figures 4.10 and 4.12.

| | + 0.3 vol % step change | | + 0.6 vol % step change | |
	automatic control	manual control	automatic control	manual control
rise time (sec)	116 ± 20*	71 ± 34*	149 ± 32*	205 ± 57*
maximum overshoot (%)	19.8 ± 3.7*	30.7 ± 13.2*	14.7 ± 3.7	18 ± 8.1
regulation performance < - 0.25 %	0	0	0	0
≥-0.25% - < -0.15 %	0	0	0	0.51 ± 1.34
≥-0.15% - <-0.05 %	0.12 ± 0.37*	10.53 ± 16.20*	1.4 ± 2.31*	12.93 ± 11.11*
≥-0.05% - <+0.05 %	95.53 ± 4.93*	81.61 ± 18.04*	87.89 ± 6.85*	79.49 ± 14.50*
≥+0.05% - <+0.15 %	4.35 ± 4.97	7.44 ± 7.32	10.7 ± 6.11	7.02 ± 9.30
≥+0.15% - < +0.25 %	0	0.41 ± 1.31	0	0.06 ± 0.25
≥+0.25 %	0	0	0	0
number of changes of vaporizer setting	49.9 ± 7.4*	14.7 ± 13.9*	66.3 ± 11.9*	14.4 ± 7.7*

Table 4.2: Increasing step changes. The numerical variables in the two groups were compared by paired t-test when data were normally distributed, otherwise the Wilcoxon Signed Rank Test [395] was used. A P value < 0.05 was considered statistically significant. Differences that have been found statistically significant are marked with *.

| | - 0.3 vol % step change | | - 0.6 vol % step change | |
	automatic control	manual control	automatic control	manual control
rise time (sec)	248 ± 169	320 ± 260	485 ± 230	492 ± 190
maximum overshoot (%)	9.5 ± 3.3*	14.2 ± 6.3*	4.8 ± 1.7*	7.2 ± 4.1*
regulation performance < - 0.25 %	0	0	0	0
≥-0.25% - < -0.15 %	0	0	0	
≥-0.15% - <-0.05 %	0.14 ± 0.60	2.92 ± 6.65	0	0.43 ± 1.43
≥-0.05% - <+0.05 %	99.86 ± 0.60*	92.98 ± 9.40*	99.89 ± 0.49	97.03 ± 7.39
≥+0.05% - <+0.15 %	0	4.1 ± 7.56	0.11 ± 0.49	2.54 ± 6.79
≥+0.15% - <+0.25 %	0	0	0	0
≥+0.25 %	0	0	0	0
number of changes of vaporizer setting	20.2 ± 14.3*	8.7 ± 6.2*	12.7 ± 7.7	9.6 ± 4.1

Table 4.3: Decreasing step changes. The numerical variables in the two groups were compared by paired t-test when data were normally distributed, otherwise the Wilcoxon Signed Rank Test [395] was used. A P value < 0.05 was considered statistically significant. Differences that have been found statistically significant are marked with *.

Reference endtidal (-.) / measured endtidal (–) / inspiratory (..)

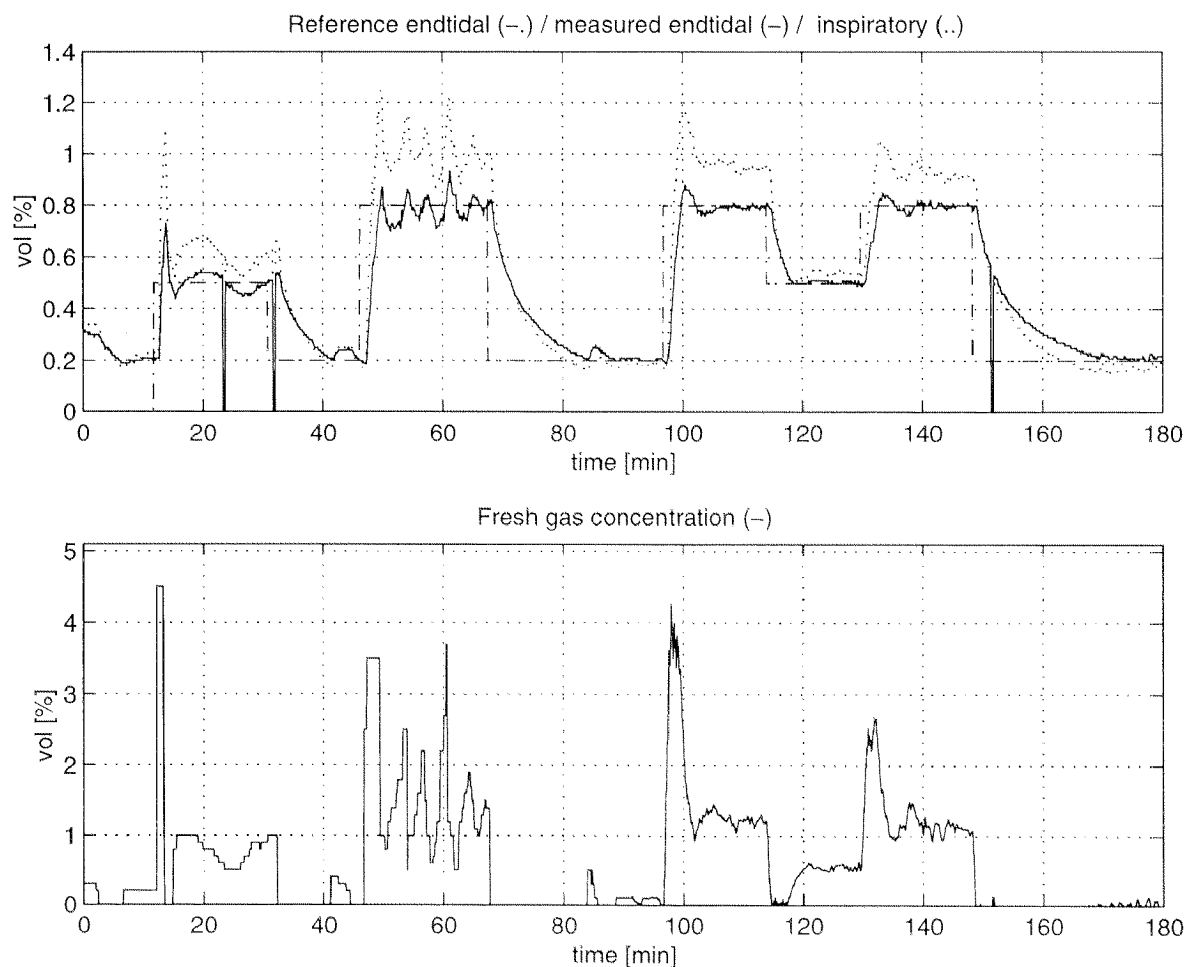
Fresh gas concentration (–)

Figure 4.9: Comparison of manual/automatic control of the endtidal Isoflurane concentration (experiment Jan 01 1999). Automatic control starts at minute 95. This example shows a very poor and "nervous" human control performance. The recording also illustrates the difficulties of the anesthetist to handle the severe input constraints. This is indicated by the bumps in the endtidal concentration towards the end of the negative steps during manual control.
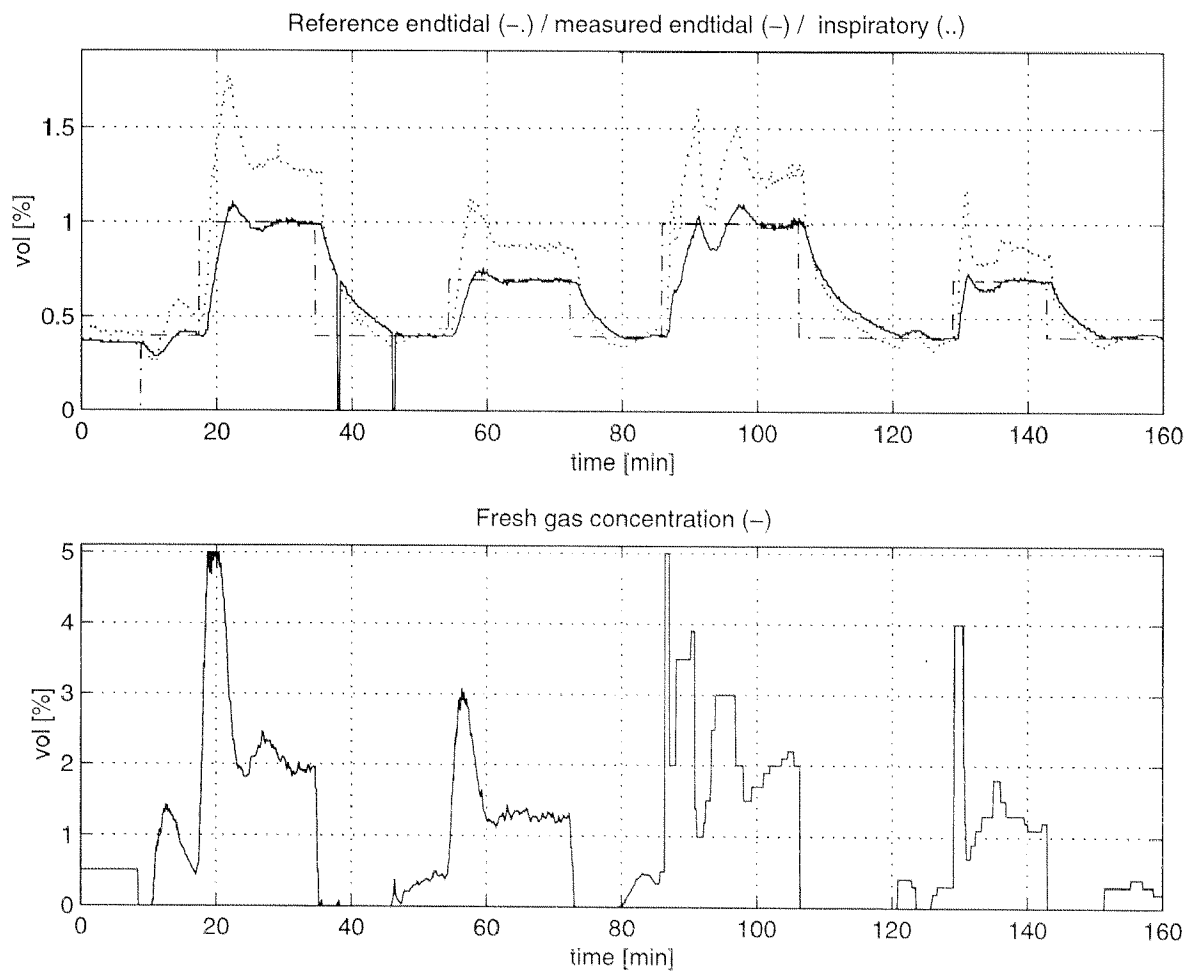
Figure 4.10: Comparison of automatic/manual control of the endtidal Isoflurane concentration (experiment Sep 22 1998). Manual control starts at minute 85. This example shows nicely a certain training effect of the anesthetist. In performing the first step change the anesthetist does not open the vaporizer long enough resulting in slow response. For the second step the anesthetist opens the vaporizer longer. Resulting in a comparably fast response.

Reference endtidal (-.) / measured endtidal (–) / inspiratory (..)
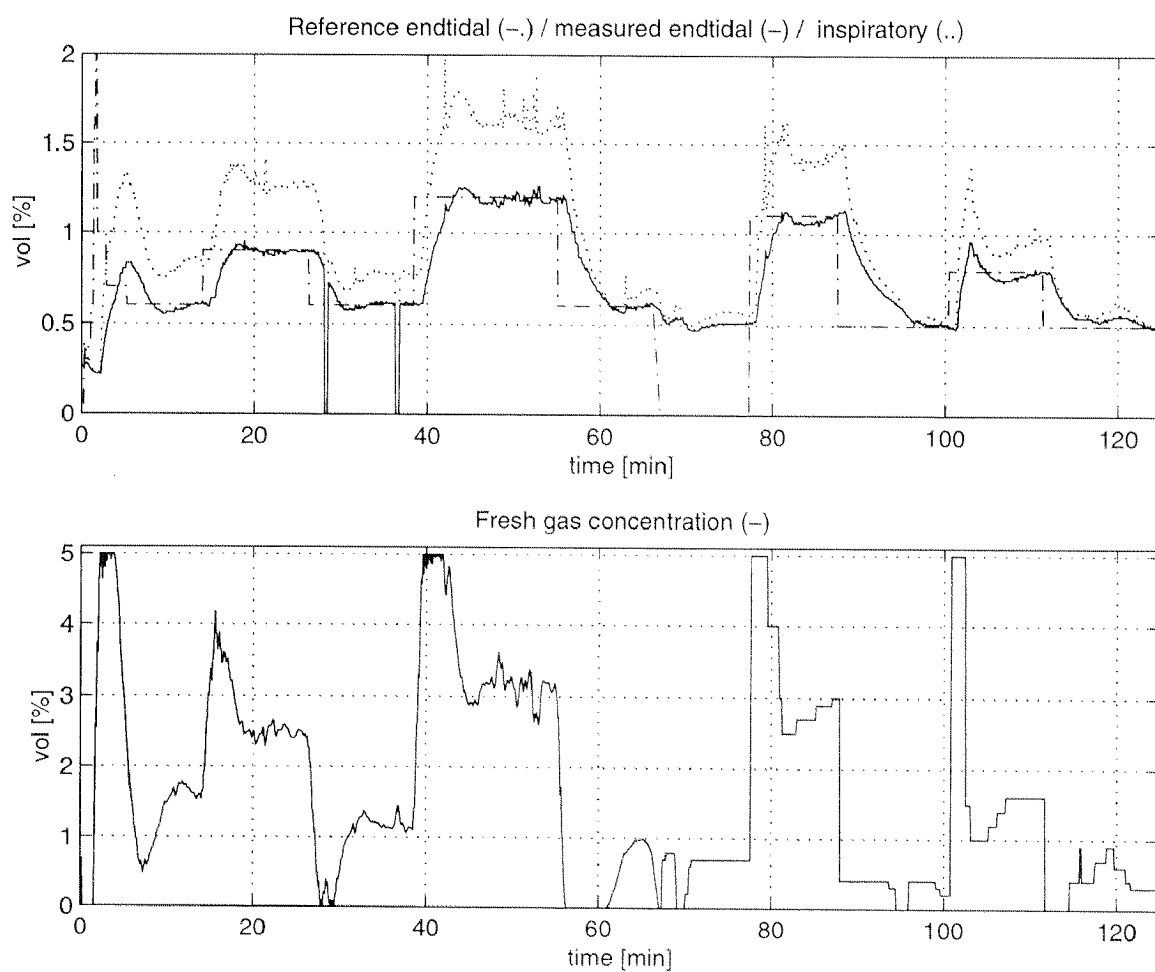

Fresh gas concentration (–)

Figure 4.11: Comparison of automatic/manual control of the endtidal Isoflurane concentration (experiment Oct 21 1998). Automatic control ends at minute 67. This example shows one of the best manual control examples.
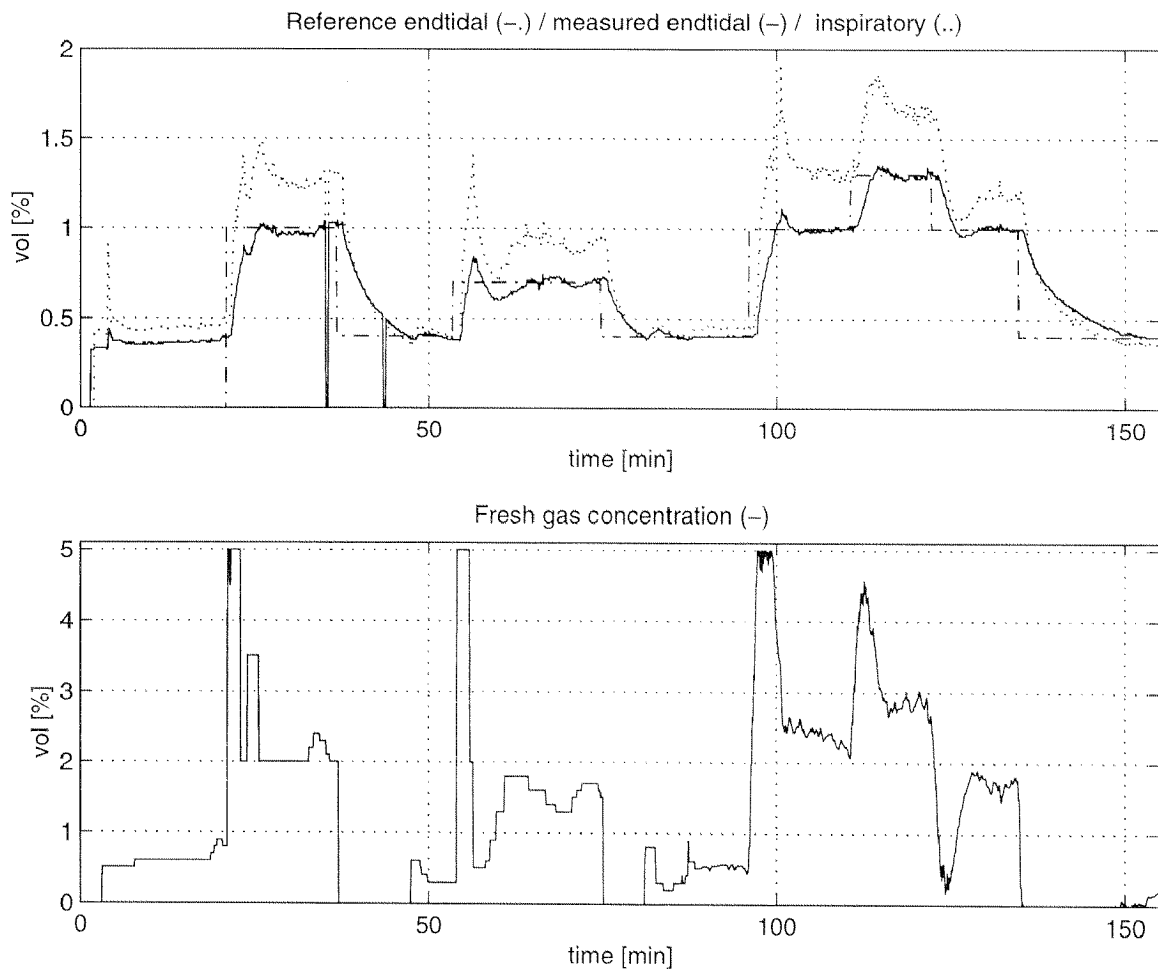
Figure 4.12: Comparison of manual/automatic control of the endtidal Isoflurane concentration (experiment Jan 12 1999). Automatic control starts at minute 88. This example also demonstrates a training effect of the anesthetist. Namely during the first step the vaporizer concentration is reduced too early. The same "mistake" is not made during the second step. It further shows automatic control performance for a different sequence of steps than the previous examples.

4.5 Clinical evaluation of the MAP controller performance

4.5.1 Study protocol

For the evaluation of the performance of the MAP controller a similar study is in progress. That is forty ASA-class I to III patients aged 20 to 65 (see e.g. [332] for a definition of ASA classes), scheduled for elective abdominal, orthopedic, thoracic or neuro-surgery, are enrolled in the study after written informed consent. Exclusion criteria are a history of coronary artery disease or uncontrolled arterial hypertension (diastolic blood pressure > 100 $mmHg$). Patients receive $1 - 2.5$ mg lorazepam one hour before induction of anesthesia. After arrival in the OR patients are monitored with ECG, arterial blood pressure using an intravenous catheter inserted in the radial artery (usually of the non-dominant arm), and pulse oxymetry. After intubation endtidal CO_2 and volatile anesthetics are measured at the Y-piece using a Datex Capnomac monitor. Anesthesia is induced with propofol with a dosage according to the desire of the anesthetist in charge. A continuous infusion of the short acting opioid alfentanil is initiated using the Stanpump program to obtain a plasma target concentration of 100 ng/ml supplemented with a bolus of $400\mu g$ for the intubation. After intubation, the feedback control system is started but just for data acquisition in order to start convergence process of the observers. Anesthesia is maintained with alfentanil 100ng/ml target concentration, vecuronium according to clinical requirements, and feedback controlled Isoflurane in oxygen at 1 ℓ/min fresh-gas flow. Two $ml/kg/h$ of Ringer's lactate are infused as a basis infusion, supplemented with additional Ringer's lactate, colloids and/or blood according to clinical needs. If total blood loss exceeds 1.5 ℓ (or approximately 30% of blood volume), the study is stopped. The patients are initially ventilated at a frequency of 10 min^{-1} and tidal volumes of 10 ml/kg, the frequency being adjusted to obtain normoventilation (endtidal PCO_2 of approximately 35 $mmHg$). The blood pressure measured at the arrival of the patient in the OR is used as target blood pressure value. The patients are randomly (by drawing a lot) assigned to an initial phase with either feedback - controlled blood pressure or with manually controlled blood pressure. After ten minutes allowed for convergence of the observers, feedback control or manual control is started. When an endtidal Isoflurane concentration of less than 0.4 $vol\%$ is required, the alfentanil continuous infusion is decreased so that the target concentration drops by 25 ng/ml and five minutes are allowed for adaptation before the next adjustment of the alfentanil target concentration is made. If endtidal Isoflurane is again higher than 0.5 $vol\%$, the alfentanil target concentration is again set to 100 ng/ml. The same is done reciprocally when an Isoflurane concentration of higher than 1.5 $vol\%$ would be needed, then the alfentanil target concentration is increased by 25 ng/ml. After 60 minutes of observation, the control mode is switched from feedback control to manual control and vice versa. The performance will be evaluated based on the following criteria.

- Duration of periods with mean arterial blood pressure within a bandwidth of target control blood pressure 10%.

- Duration of periods with blood pressure measurements that are higher or lower than 20 % of the desired target blood pressure.

- Number of changes of infusion rate of alfentanil infusion and mean of alfentanil infusion

rate.

- Artifact handling: artifacts in the measurement of blood pressure (e.g. blood sampling, calibration) and gas measurement (disconnection of the sampling line, calibration) are observed and the ability of the supervisor system to detect and eliminate them is determined.

- Number and type of critical incidents in both groups. These are periods with $MAP < 65\ mmHg$ or $systolic\ BP > 160\ mmHg$ or $HR > 110\ bpm$.

Besides the evaluation of controller performance the benefit of automatic control in the daily routine will be evaluated. To analyze the structure and characteristics of the anesthesiologist's job, human factor techniques such as task analysis and workload assessment will be used and the results will be compared between the two modes of MAP control, manual and automatic. Methodology used could consist of the following: time-motion analysis (to generate quantitative measures such as task duration and task density), secondary task probing and subjective workload assessment.

4.5.2 Results

Since the study is still in progress no statistical evaluation can be provided and only example trials are shown in figures 4.13 to 4.15.

For all the figures the upper most plot shows the reference and actual MAP signals. The second plot shows the vaporizer signal. The third plot shows the endtidal concentration along whit the corresponding upper and lower limit. The lowest plot shows the active controller. A value of -1 denotes the lower endtidal controller, a value of $+1$ denotes the upper endtidal controller and 0 denotes the MAP controller being active.

Figure 4.13 is the recording of an automatic control application during a liver surgery. Between periods of good regulation performance an episode with a heavy surgical stimulation occurs. To compensate for this disturbance an endtidal concentration larger than $c^{\uparrow}_{endt}$ would be required. Which activates the upper endtidal override controller. During the period of good regulation the MAP controller is dominating. The controller successfully compensates for disturbances occurring at minute 38, 89, and 94.
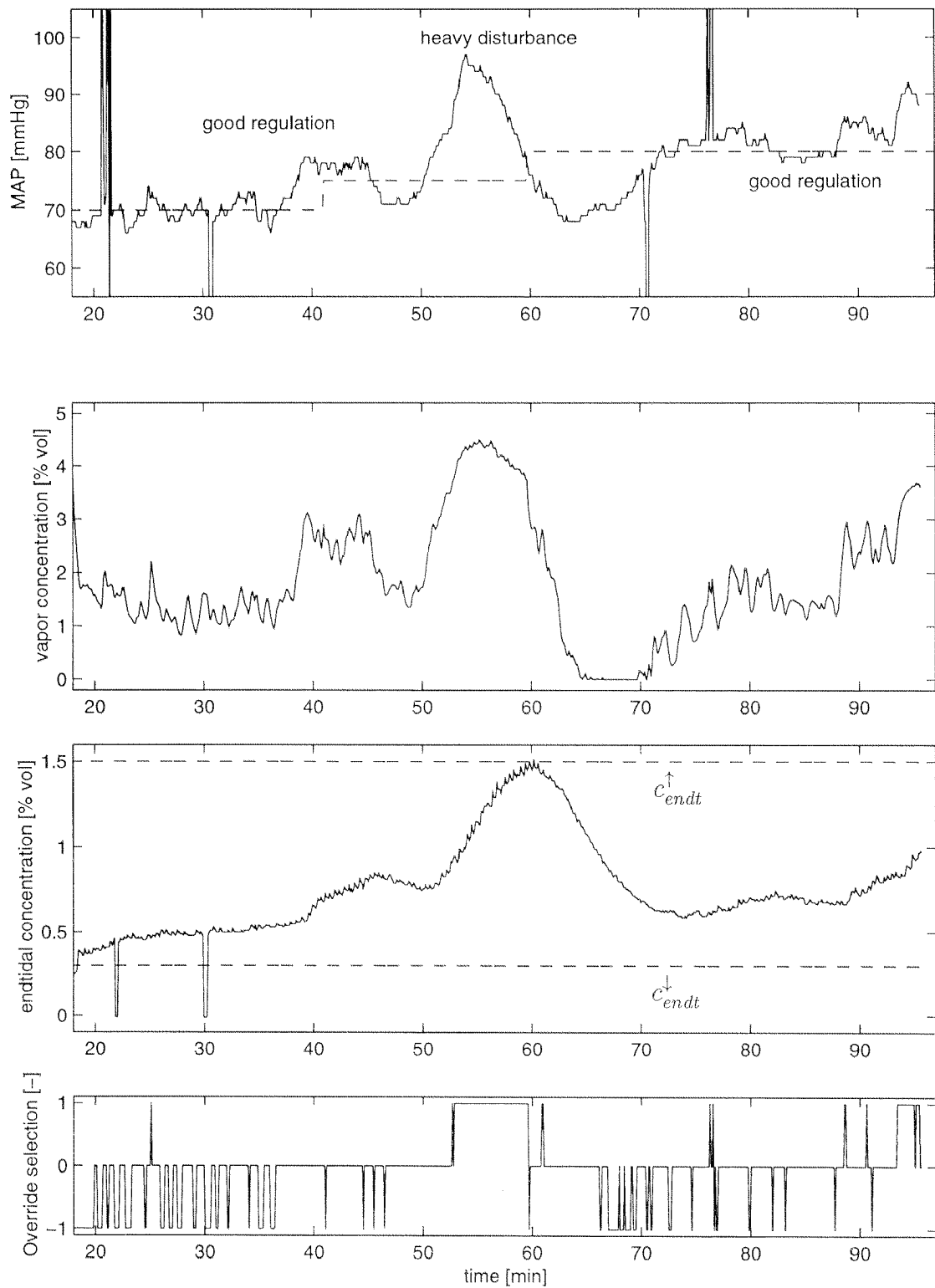
Figure 4.13: Recording of an automatic MAP regulation application during a liver surgery. (experiment Aug 20 1999). No manual control phase was included in this pilot study. Note the successful compensation of "light" disturbances occurring at minutes 38, 89, and 94.

The experiment shown in figure 4.14 was conducted during an ENT surgery. Here a manual and an automatic regulation period are compared. Up to minute 192 anesthesia was conducted manually (in the "PASSIVE" mode). The reason for not conducting the manual control in the "DOSING" mode was that for the workload study no artificial element was desired. From minute 192 to minute 210 manual control was conducted in the "DOSING" mode to allow fro the convergence of the observer. At minute 210 automatic control starts. This manual control phase is dominated by a heavy disturbance and an episode of good regulation. Due to the potentially different disturbance profiles it is not possible to compare the regulation performance based on a single trial. Note that from the plot showing the endtidal concentrations it seems that the controller tends to make more use of the bandwidth of allowed endtidal concentrations.
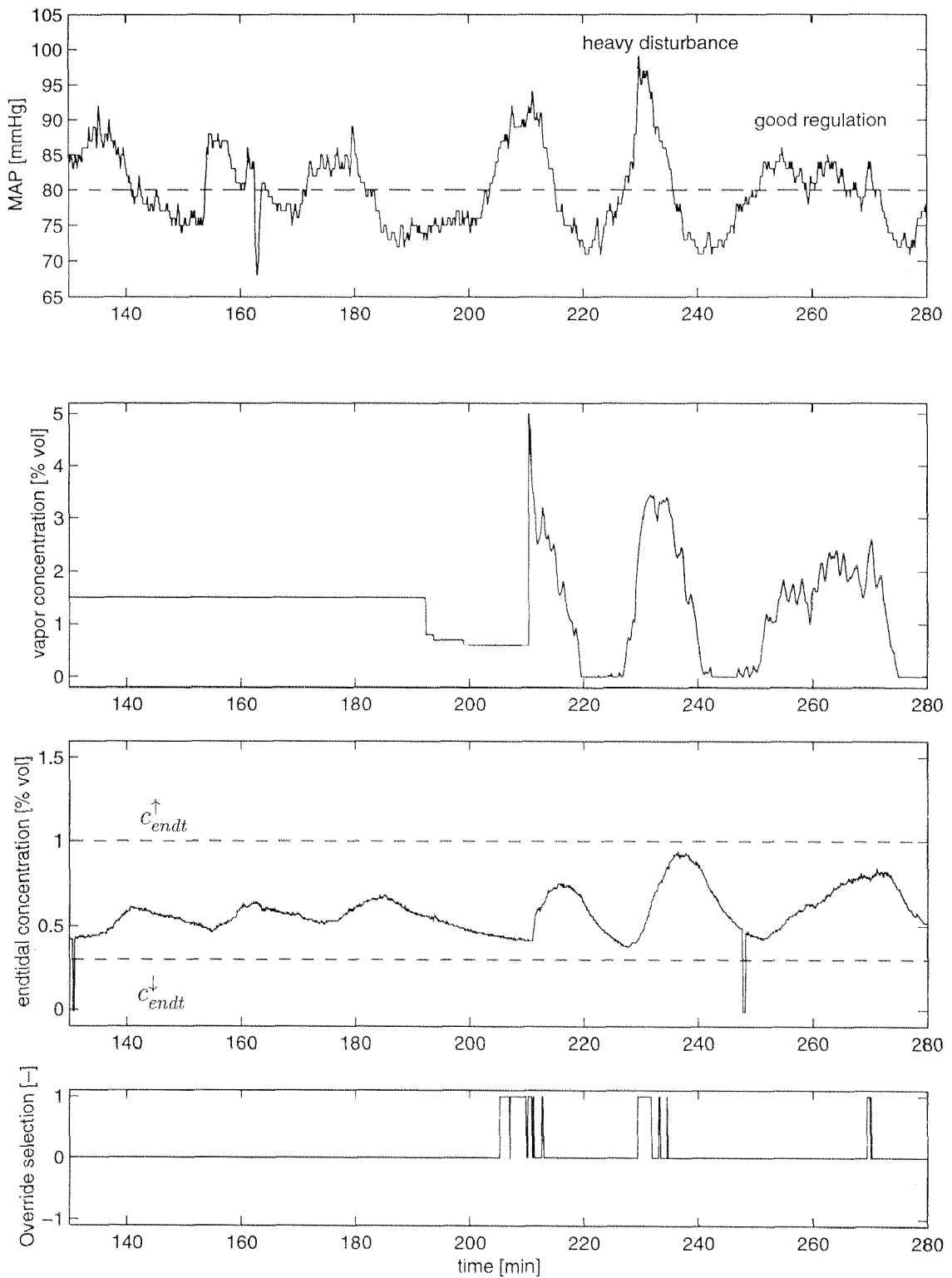
Figure 4.14: Comparison of manual and automatic regulation of MAP during ENT surgery (experiment Jan 20 2000). Automatic control starts at minute 210.

Figure 4.15 shows a comparison of manual and automatic control during an ENT surgery also. The operation began with a phase of heavily stimulating preparations inside the mouth. Then there was a 20 minutes pause until skin was opened at minute 138. It can be seen that the controller is doing a fairly good job in compensating for the blood pressure increase after beginning of the operation. It makes thereby use of the total allowed span of endtidal concentrations. During the pause a very nice example of an active lower endtidal controller is shown. After skin incision it is switched to manual control at minute 138.
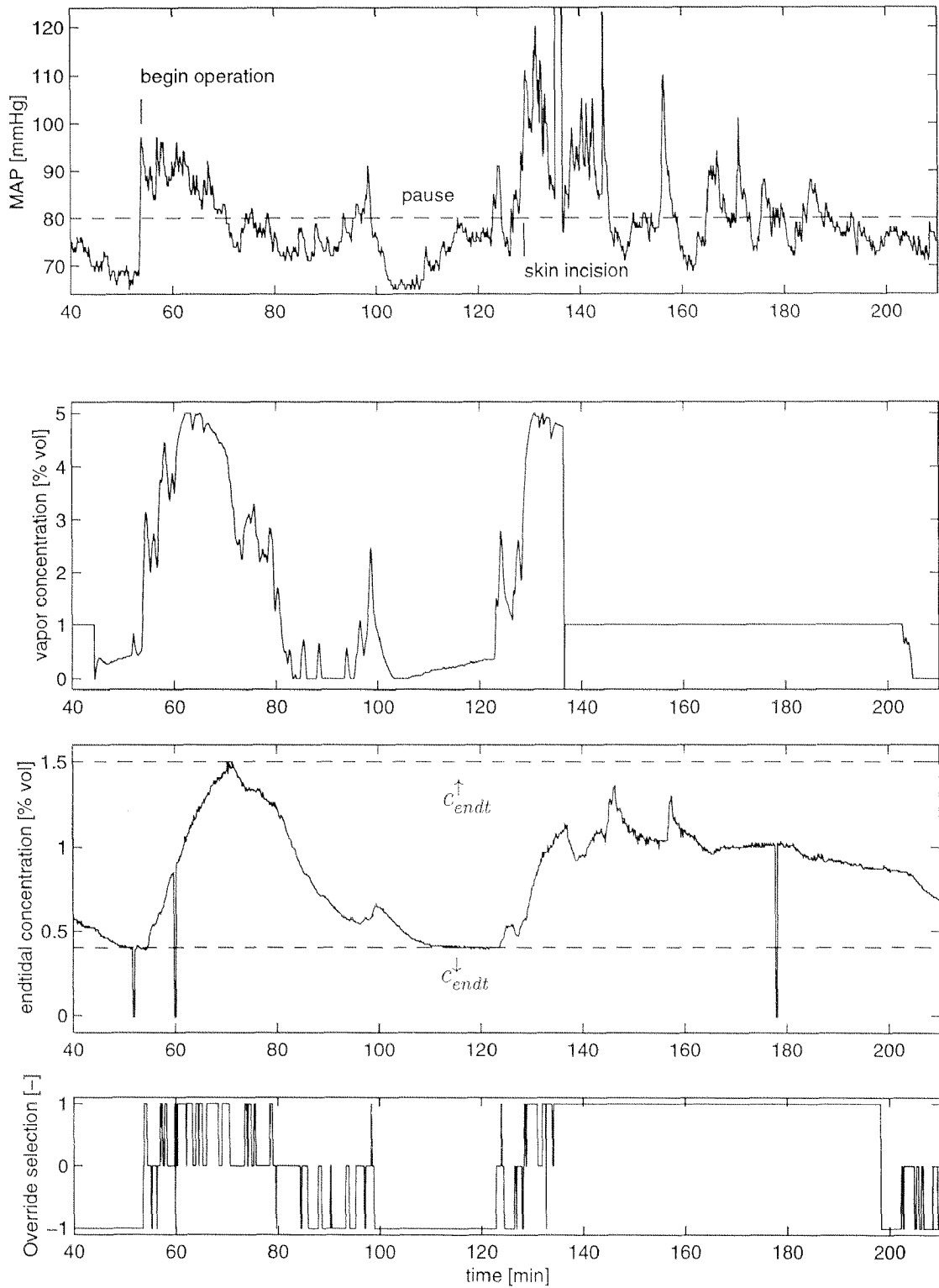
Figure 4.15: Comparison of automatic and manual control during ENT surgery (experiment Jan 26 2000). Manual control starts at minute 137.

4.6   Conclusions

The extensive clinical validation of the endtidal controller lets us conclude that model base control of endtidal Isoflurane concentration is feasible and superior to manual control in a clinical environment. The procedure for artifact suppression which will be discussed in chapter 6 successfully handled all artifacts that occurred during the study. A limiting factor in the application turned out to be the observer. That is several minutes are required for the observer to converge before automatic control may be started.

For the model based MAP controller less definite statements are possible. From the several successful experiments we draw the following conclusions. The controller is successfully able to compensate for "light" disturbances as shown in figure 4.13. The limited control action and the fast disturbance dynamics seriously limit the ability to compensate "heavy" disturbances. These limitations also apply for manual control. Therefore we expect that the difference between manual and automatic control is less pronounced than for endtidal control. An intuitive way for improving blood pressure regulation is to provide the controller with advance information about major future disturbances like skin incision. A case study exploring this potential is provided in appendix B.

Supervisor Structure

This short chapter serves two purposes. First, it outlines what supervision in the context of this thesis means. And second it will outline the content and scope of the next chapters.

5.1 Structure outline

The classical notion of supervisory control theory was introduce by Ramadge and Wohnham [384, 385]. It is meant as a formal framework for analyzing discrete event systems at a logic level. Although continuous extensions to the theory are added [250, 253] it still hasn't found its way to broad application. Some reasons for this are discussed in [14]. Often control of discrete event systems (DES) and hybrid systems are generally referred to as supervisory control. Analysis and control thereby is addressed by different methods like petri nets [252], graphchart [11], or lattice theory [94].

A special class of hybrid systems are fault tolerant control systems (see chapter 7). In this context supervisor logic refers to a function that receives fault detection and isolation information and which determines and executes corrective remedial actions [224]. The definition of supervision in [45] is somewhat narrower in the sense that the supervisor problem addresses the redefinition of control objectives in case of faults. Supervisors for FTC systems are normally designed without the rigorous mathematical framework of supervisory control theory. Rather engineering common sense is used.

Our understanding of a supervisor very much aligns with the interpretation common in fault tolerant control [224]. It includes some additional aspects, however. These different aspects are illustrated in figure 5.1 and will be discussed next.

According to the figure the supervisor functionality may be understood as the sum of all the necessary functions that have to be "wrapped" around the basic feedback control algorithms
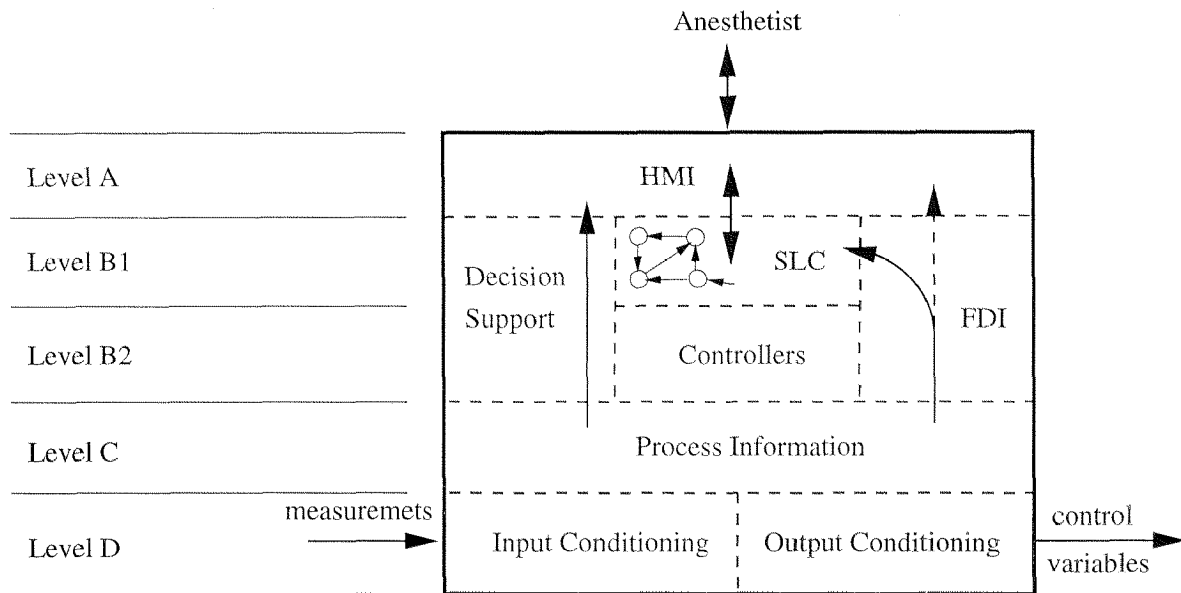
Figure 5.1: The different ingredients of the supervisor for automatic control applications in anesthesia.

to make the controllers routinely applicable in the OR. Martin [303] also uses the term "safety shell". Four main layers can be identified.

D **Input and output conditioning:** This layer is the most process oriented layer and it is therefore drawn as the lowest layer. Entering the anesthesia system the measurements pass an input conditioning stage. This task includes any preprocessing of the signals, such as filtering, selection of the most trusted one out of a set of multiple measurements, and in particular the rejection of measurement artifacts. Leaving the system the control signals pass through a comparable output conditioning stage. Typical tasks of this post processing stage are, shaping of test inputs for FDI, the min-max selection of an override controller or the manual/automatic selection, etc. The strict separation of input/output conditioning and control algorithms is not always unique. This is for example the case for the artifact tolerant controllers or the override selection. Consider for example the artifact rejection problem. In chapter 6 different approaches to the problem will be discussed. In particular signal based and model based approaches will be distinguished. For the signal based approaches artifact rejection represents a (nonlinear) filtering block clearly separated from the controllers. For the model based approach presented in section 6.4 this is not the case since the output injection represents an integral part of the OBSF controller. Only its nonlinear modification is introduced because of the artifacts. Similar reasoning may be deployed concerning the min-max selection of the control signals.

C **Process information:** This represents the sum of all data available about the state of the process including for example controller states. Typically this information is stored in data bank. From there it is accessed for storage or to be displayed. In our architecture (recall chapter 2) this function is provided by the model objects.

B **Algorithmic layer:** This incorporates feedback controllers, supervisor logic control (SLC), fault detection and isolation (FDI) algorithms, as well as decision support functions. The separation into a layer B1 and B2 separates dynamic and logic control. The SLC (see also section 4.3) may be viewed as the core of the supervisor. It fuses the available information from the surrounding blocks into a discrete state (also mode) of the system with well defined activities and transition conditions. FDI functions are responsible for detecting faults in the system. This may include equipment faults like disconnected sensors or leaks. But also the detection of critical physiological patient states like excessive blood loss is handled here. If the FDI results directly lead to events that cause mode transitions of the SLC the classical fault tolerant control setup is implemented. Alternatively the FDI results may only be communicated to the anesthetist along with suggestions for mode transitions. The FTC feedback loop may be viewed as being closed manually in this case. This strategy will be explored during the test phase of FTC. Only after successful completion of tests in this assistance mode the FTC feedback loop will be closed automatically. FTC aspects are discussed in chapter 7. The FDI results are communicated via the HMI anyway. In contrast to FDI decision support (DC) does not interact with the state automaton but it rather makes suggestions to the anesthetist on how to optimize the anesthetic procedure. It provides information that can not directly be read off from monitors. Typical examples are the estimated time required for the patient to wake up after termination of drug application, the estimated concentration of anesthetics in the brain or awareness monitoring [12].

A **Human machine interface (HMI):** This is the most user oriented layer and is therefore drawn as the top layer of the supervisor structure. Every information from the system to the operator (anesthetist) and vice versa has to pass through the HMI. The HMI is typically implemented by a graphical user interface (GUI) but any acoustic alarm is also part of the HMI. Details about the HMI are discussed in chapter 8.

Note that all these functions are found in similar form in similar structure in any process control system.

Of these ingredients artifact tolerant control aspects are discussed in chapter 6. Fault tolerant control will be discussed in chapter 7. Decision support functions will briefly be discussed in section 5.4. Finally, details on the HMI will be described in chapter 8.

5.2 Supervisor applications in anesthesia

Supervisor aspects in anesthesia are not only discussed in connection with control applications. It is also an independent area of interest for monitoring in anesthesia.

An important reason is that the current alarm situation of general anesthesia workplaces is unsatisfactory [415, 482, 51, 352]. In an extensive recent study [51] it was found that many clinicians turn off alarms to avoid the annoyance of frequent false alarms. [383, 353] also reports a high rate of nuisance and false alarms. The problem is attributed to the fact that every physiologically relevant signal (e.g. heart rate or blood pressure) is treated isolated in terms of

alarm limit setting and alarm generation [447]. Often not even sufficient artifact detection is implemented [447, 33]. As a consequence several authors postulate a systems approach to the monitoring problem [33, 34, 360, 488, 164, 338, 447, 352]. This means instead of processing and monitoring individual signals the correlation among the different physiological variables and in particular drug application should be taken into account. [447] sums this up by: "From signal to patient-state monitoring". Different techniques to tackle this problem are suggested. [415] proposes a knowledge based system, [359], [488], [338] and [448] use an artificial neural network, [467] uses Fuzzy learning of expert rules, [451] and [352] propose expert systems. The use of mathematical models, however, has not been explored in this context so far.

The need for supervisor functionality for automatic control application in anesthesia has clearly been recognized by a number of researchers. However, the maturity to which the supervisors have been developed differ greatly. Some authors declare it as subjects of future research [159, 254] while others have implemented supervisor functionality [307, 304, 305]. The overview articles [355, 220, 497] also address supervisor aspects. But they only briefly outline what the authors think were necessary supervisor functions. [156], [303] and [304] also provide a collection of requirements. The list of tasks includes

ST-1 rejection of measurement artifacts

ST-2 generation of probing signals

ST-3 limit the control signals

ST-4 adapt controllers

ST-5 supervise adaptation

ST-6 detect critical patient conditions

These tasks may all be allocated to one of the supervisor function blocks in figure 5.1. So while the cited publications list the requirements in a unstructured list figure 5.1 puts them in a consistent order.

5.3 Artifacts and faults

In the next two chapters procedures for handling artifacts and faults will be discussed. It is therefore necessary to distinguish faults and artifacts with the following definitions.

Definition 5.3.1 *Artifacts are normally occurring situations which temporarily make the nominal system description appear to be invalid.*

Definition 5.3.2 *Faults are abnormal situations which permanently invalidate the nominal system description.*

Examples for both will be given in chapters 6 and 7, respectively. Note the following about these definitions.

Definition 5.3.1 is narrower than what is broadly encountered in literature. In particular aliasing effects [428], respiration artifacts in the blood pressure signal [270, 13, 85], power line interference [218], or "ringing" artifacts in catheter manometers [64] are not covered by this definition. They all represent signals contaminated by another (periodic) signal and are easily treated with linear notch or anti aliasing filters.

Since artifacts represent normal operating conditions and since the system description is only temporarily invalid the control system - in contrast to faults or disturbances - must not react to artifacts. Except perhaps by giving an artifact indication signal.

According to definition 5.3.2 (see also [223]) failures must be viewed as a subset of faults. While in case of a failure a device fails to operate completely [223] it might only fail to operate according to the specifications in case of a fault.

It has not yet been specified what "temporary" means in the context of definition 5.3.1. In chapter 6 typical artifacts will be shown. There normal duration is on the order of 10 to 30 seconds. In extreme cases blood sampling artifacts and calibration artifacts can last up to two minutes (see figures 6.3 and 6.17, respectively). In view of this anything of duration less than two minutes is considered temporary. And any "artifact" of duration of more than two minutes will be treated as a fault by the SLC.

5.4 Comments on decision support

We have mentioned the estimation of the time required to wake up and the estimation of the brain concentration of anesthetics as typical decision support functions. No separate chapter will be devoted to this subject only some comments are made here.

The estimation of the "wake-up-time" requires PK models for the drugs that have an influence on the wake-up-time. That is, using the PK models it is possible to predict the decay of drug concentrations after termination of drug application. Wake up is then predicted when the drug combination transgresses a "wake-up-limit". With Isoflurane as a single agent our PK model would allow to estimate the wake-up-time. However, generally a combination of agents is used. And in particular in combination with opioids the wake-up-time depends to a great extent on the concentration of the opioids. This aspect of decision support is therefore not further explored in this thesis.

In section 3.7.1 we have shown that a good prediction of brain partial pressure with our model may be obtained. The estimate for the "brain concentration" may thus for example be taken form the observer used for FDI (see section 7.8.6).

Seite Leer /
Blank leaf

Artifact Tolerant Control

This chapter first discusses effects of artifacts on the controlled system. Then sources of artifacts that are important in the Isoflurane-MAP control context are studied. And then the different means of treating the artifact problem are provided. Finally, several examples of successfully suppressed artifacts are documented.

6.1 Motivational Example

The need for artifact treatment in automatic control applications during anesthesia has been recognized by several authors [403, 391, 156]. It is best illustrated with an example like the one shown in figure 6.1. Here a model based endtidal controller is supposed to lower endtidal Isoflurane concentrations from 1.3% to 0.7% as indicated by the dashed line. During this maneuver an automatic calibration of the monitor occurs during which a zero value is provided for the concentration measurement. This sudden change in the controlled output causes the controller to fully open the vaporizer. Although the artifact terminates after 20 s still enough Isoflurane has been supplied to the system to considerably overshoot and prolong the maneuver. Very nice examples of untreated artifacts are also shown in Derighetti's thesis [111] (page 177).

The situation illustrated in figure 6.1 represents a deterioration of the controller performance but a situation is not critical for the patient here. However, artifacts in blood pressure controllers might lead to a critical decrease of blood pressure. A very nice example of such critical transients is documented by Fukui and Musuzawa in [156]. Luckily we are not able to document such a situation.

Note also that the artifact is not just of interest with respect to automatic control applications. The problem also needs to be addressed for monitoring [482, 470] or record keeping purposes [319, 373].
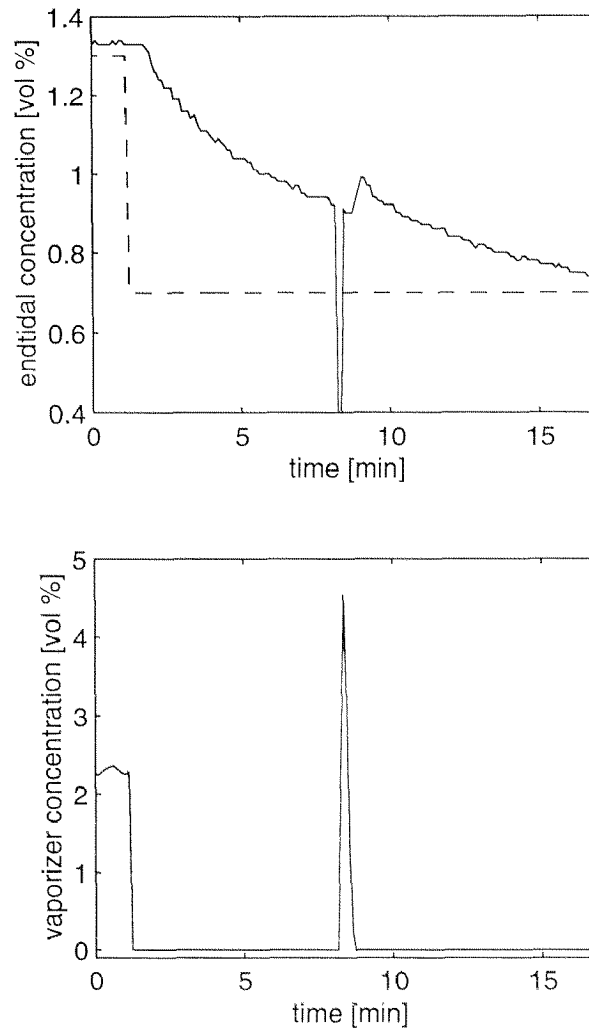
Figure 6.1: Example of an untreated artifact occurring during automatic control of endtidal anesthetic concentration.

6.2   Sources of artifacts

Recalling the MIMO system description figure 3.1, artifacts in gas concentration and blood pressure measurements must be distinguished. The different sources of artifacts in either of the measurements are discussed next.

6.2.1   Artifacts in invasive blood pressure measurements

Before listing and discussing the different artifacts in the blood pressure signal the measurement set up for invasive blood pressure monitoring should briefly be described. It will help to understand the effects of certain routine manipulations on the measured blood pressure signal. A more detailed introduction to invasive blood pressure monitoring may be found in [163, 468, 174].
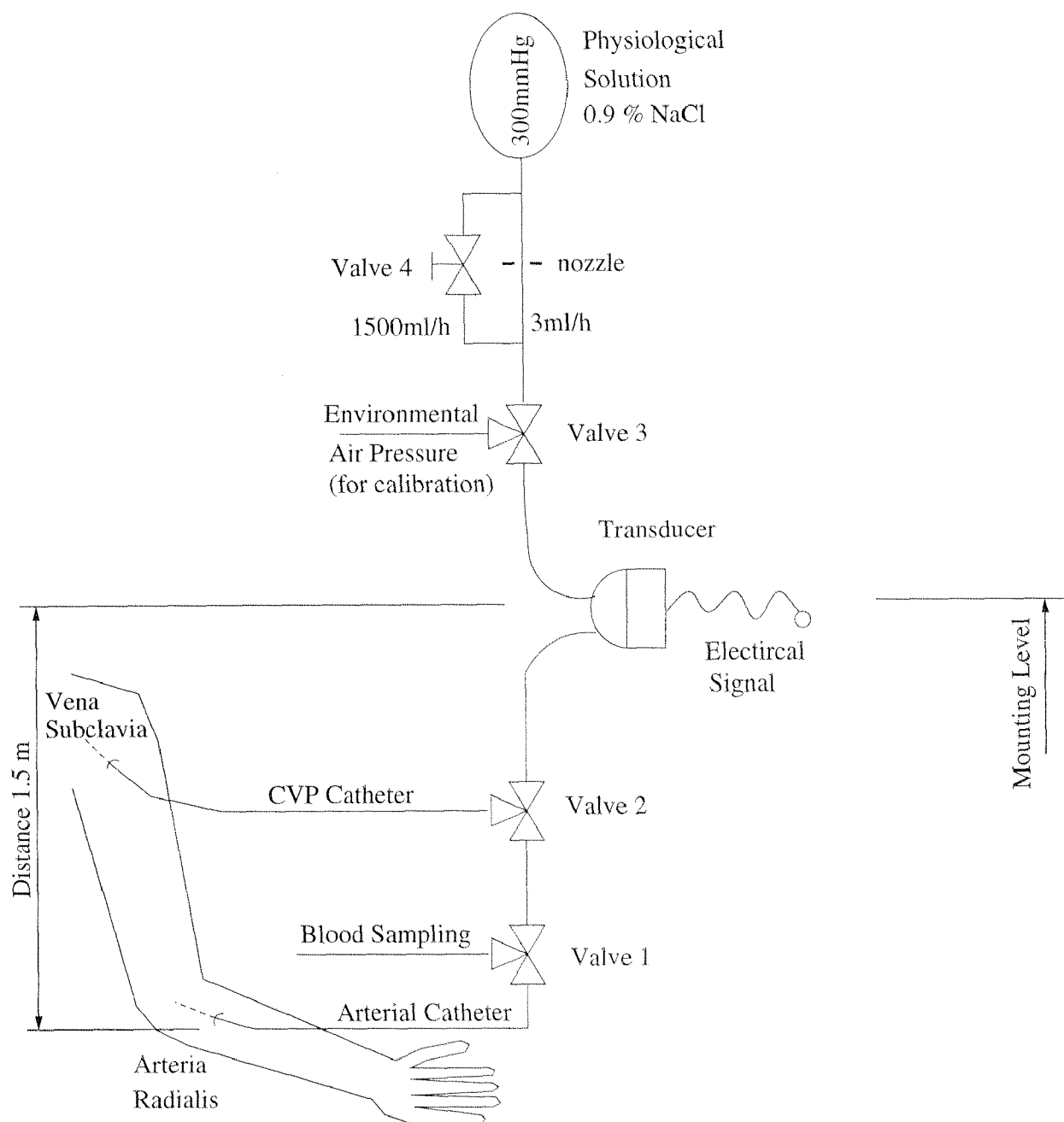
Figure 6.2: Schematic Drawing of the invasive blood pressure monitoring system with external transducer

Figure 6.2 shows a schematic drawing of the system. During normal operation the positions of valves number Valve 1 and Valve 2 are such that the arterial blood pressure is measured by the transducer. Valve 4 is closed and the position of Valve 3 is such that the whole system is flushed with a constant rate of about $3ml/h$ with a physiological $NaCl$-solution (0.9% NaCl). The purpose of this flushing is to prevent the catheter from clogging. This steady flow is supplied by a container that contains physiological $NaCl$-solution which is maintained at a pressure of $300mmHg$ through a cuff similar to the one used for non-invasive blood pressure measurements. A nozzle is mounted to control the flow. Switching from this normal operation mode to an exceptional operation mode typically leads to an artifact in the blood pressure signal. The most important ones will be discussed next. Note that due to the control cycle the signals are sampled at ten seconds intervals.

Taking arterial blood samples

The arterial catheter inserted for invasive blood pressure measurement is usually also used to sample arterial blood if such samples are desired. To do so the position of Valve 1 is changed such that arterial blood can be sampled from the catheter. Since the steady flow for flushing is interrupted pressure builds up in the upper part of the system. The pressure build up approximately follows an exponential with final value equal to the reservoir pressure. Such a blood sampling artifact is shown in figure 6.3. Taking a blood sample normally takes about 30 seconds. This example has an unusually long duration which might be due to a distraction of the anesthetist. It is difficult to provide a rate of occurance for this type of artifact because it heavily depends on the surgery. For some types of surgeries there might no samples to be taken while for others (e.g. for research purposes) blood samples are to be taken periodically.

Flushing the catheter system

The continuous flushing of the system with about $3ml/h$ is usually sufficient to prevent the catheter from clogging, however there might be occasions where is not. For such cases Valve 4 provides a possibility to flush the system with a high flow rate of about $1500ml/h$. In that case the transducer will of course measure the container pressure minus the pressure drop across the nozzle. The duration of such a flush procedure can vary. It depends on the anesthetist's judgment on what is needed to clean the catheter. Some characteristics are however common for these kind of artifacts. The signal typically rises rapidly to about $200mmHg$ and at the end of the flush procedure the signal undershoots which is due to the fact, that the system behaves like a weakly damped oscillator. Figure 6.3 shows a possible artifact pattern where a flushing of the catheter is performed prior to blood sampling.

Calibration

Calibration of the measuring system can be done during normal operation. This might be necessary if the measurements are not trusted for some reason. To do this Valve 3 is changed such
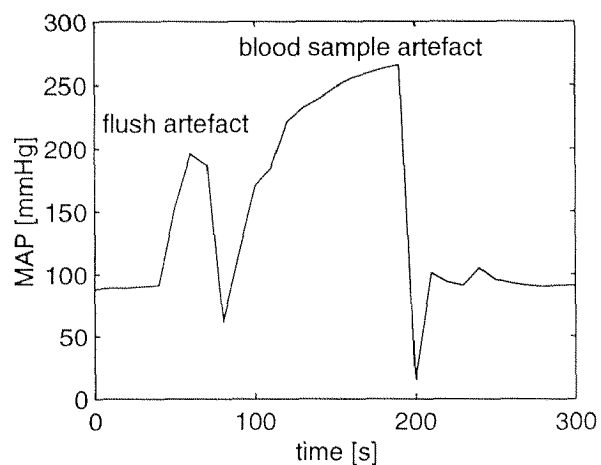
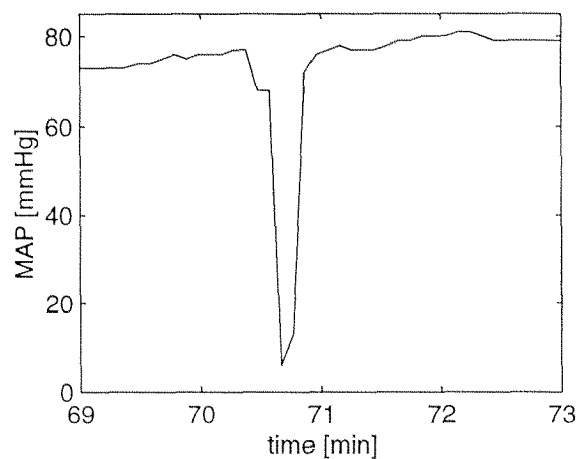Figure 6.3: Typical artifact for catheter flushing and blood sampling.

Figure 6.4: Typical artifact occurring during CVP measurement.
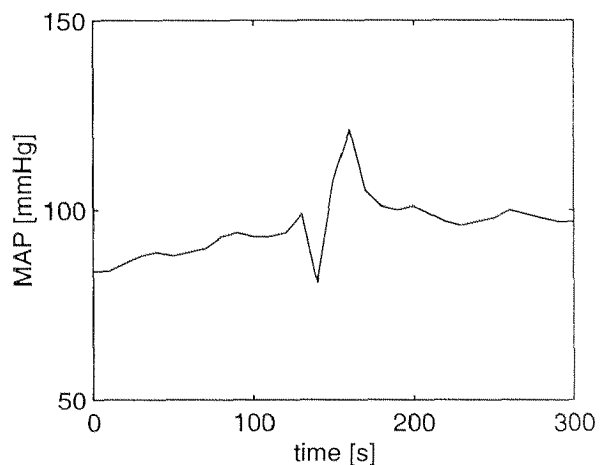

Figure 6.5: Typical artifact occurring if someone bumps against the system.
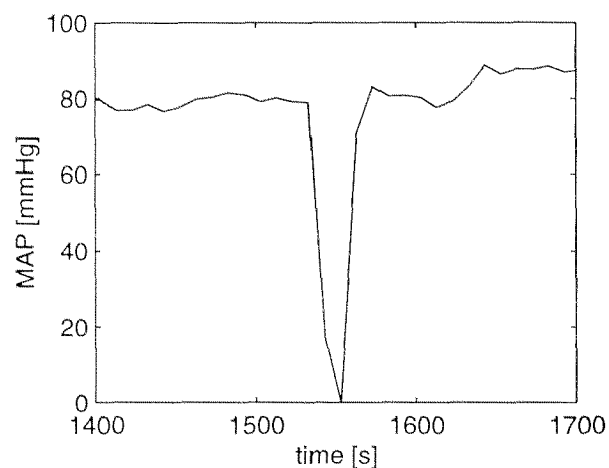
Figure 6.6: Typical artifact occurring during calibration.

that the normal environmental air pressure is measured by the transducer. In that case the blood pressure signal drops to zero. Calibration takes about 30 seconds like the one shown in figure 6.6.

Switch to central venous pressure (CVP) monitoring

The pressure transducers are disposable devices. They therefore represent a non negligible cost factor. To reduce the number of pressure transducers required blood pressure monitoring systems are set up such that a single transducer may be used to measure arterial as well as central venous pressure. This is done by changing the position of Valve 2 . During CVP measurement the pressure signal drops to about $3 - 12mmHg$. A typical episode is shown in figure 6.4.

Bumps

If during normal operation someone bumps against the transducer system strong oscillations on the blood pressure signal can be observed. Sampling such a "bumpy" episode every ten seconds might produce a signal like the one given in figure 6.5.

6.2.2   Other complications and faults in invasive monitoring systems

Clogging of the catheter

Clogging of the catheter happens rather slowly and is therefore difficult to detect. Typical signs for clogging are slowly drifting measurements or a smoothened blood pressure signal [259]. Clogging does not fall into the category of artifacts according to our definition 5.3.1 since it represents a permanent phenomenon. More precisely we consider it a fault. It will thus be dealt with in the next section.

Changing the level of the transducer mounting

The transducer may not be mounted at the correct level and might have to be adjusted during anesthesia. This will result in a sudden and permanent change of the mean arterial blood pressure. For these events no action is required since it is after the occurance of this manipulation that the correct MAP values are obtained.

Air bubble trapped in the catheter system

Air bubbles are usually introduced by inadequate handling of the system. Due to the compressibility of the air they lead to a weakly damped transmission of the pulse waves [163, 174]. Note that air bubbles which do not yet represent a threat to the patient still affect the transmission properties. Since they also represent permanent changes they also fall into the class of faults rather than artifacts.

6.2.3   Artifacts in concentration measurements

For the measurement signal of the anesthetic inspired and exspired concentration three main artifacts are of concern: the calibration artifact, and disconnections of the sampling line or Y-piece.
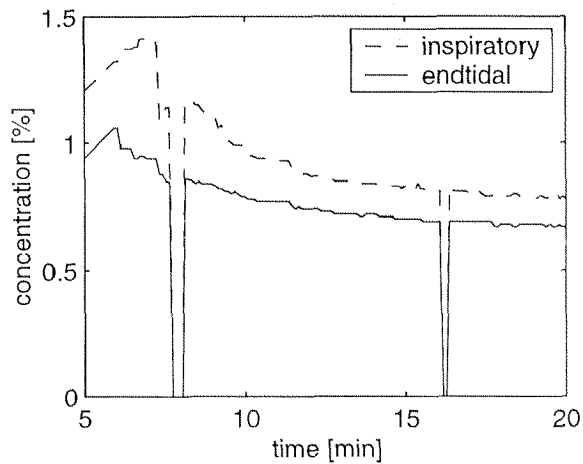
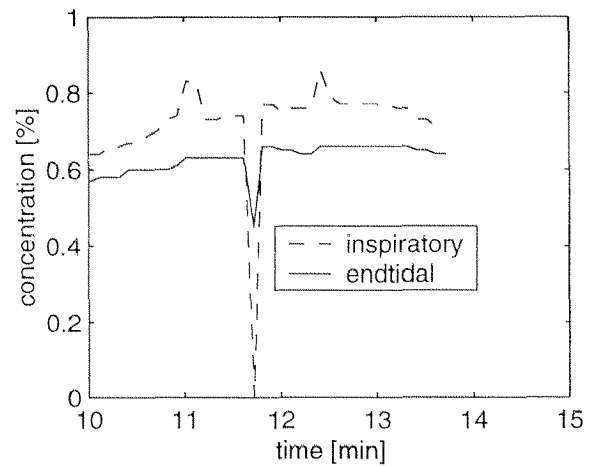Figure 6.7: Typical calibration artifact in a gas measurement.

Figure 6.8: Artifact in the gas measurements caused by a temporary disconnect of the sampling line.

Calibration of the gas sensor

A very frequent artifact occurs during calibration. While calibration of the pressure transducer is initiated by an anesthetist the calibration of the gas sensor is initiated automatically. During calibration zero value is provided by the monitor as shown in figure 6.7.

Disconnection of the sampling line

If it is necessary to relocate the patient, often tubes and wires also have to be relocated. In these situations it is possible that the line sampling gas mixture from the Y-piece (see figure 3.18 for reference) is temporarily disconnected. Such a disconnection typically lasts less than one minute. During this time environmental air is aspired and analyzed. This causes the concentration to drop to nearly 0 as shown in the example 6.8. The reason why the endtidal measurement signal does not drop to zero in this example is most likely due to disconnecting in the exspiratory phase.

Disconnection of the Y-piece

Similarly the disconnection of the Y-piece may occur after or during patient relocation. The resulting artifacts are very similar to those occurring in case of a sampling line disconnect. The duration is also typically less than one minute.
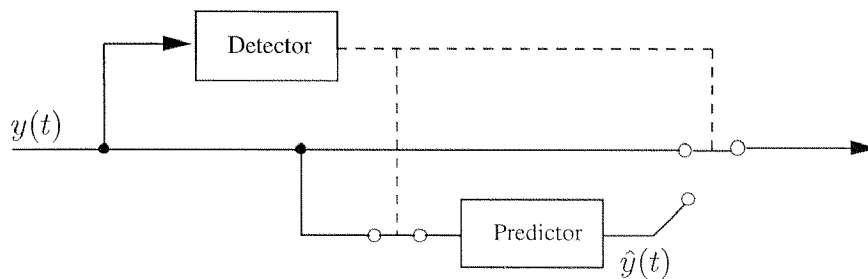
Figure 6.9: For control applications the problem of artifact handling represents a detection and a prediction problem.

6.2.4   Artifacts caused by actuators

In principle artifacts must also be expected to occur in actuators. However, neither for the vaporizer nor for the ventilator artifacts were encountered in the past.

6.3   Solutions to the artifact problem

For control applications the artifact suppression problem might be decomposed into an artifact detection and a signal prediction problem as illustrated in figure 6.9. An explicit detection of artifacts is necessary since the strongest artifacts have considerable contents in the frequency range where good controller performance is desired. This excludes solutions based on linear filtering approaches. The prediction problem results from the fact that a meaningful output must be provided by the controller while the artifact is occurring. According to figure 6.9 the actual measurement is then replaced with a prediction whenever an artifact occurs. In the simplest case the prediction keeps the controller output unchanged during an artifact.

For the signals considered here the detection and prediction problem might be attacked at different levels of processing the signal: The quasi analog signals (sampled at a high rate), the processed signals (e.g. period to period mean), or model based (combination of several signals). Meaningful detector/predictor combinations in this context are marked in figure 6.10. An x denotes a practical detector/predictor combination and (x) denotes a possible combination. The reasoning is as follows. A prediction over dozens of periods based on a period to period quasi analog signal does not make much sense. Better predictions may be obtained by utilizing trends of means etc. or by means of a model. Intuitively it is clear that using less information for detection than for prediction or vice versa is always suboptimal which explains the (x) markings.

Before presenting our approach to the detection and prediction problem a brief summary of the published literature shall be provided. All the published approaches found to the detection problem are signal based solutions. One publication [391] solves the detection problem of artifacts in blood pressure measurements from the quasi analog signal. The characteristics of the blood pressure waveform are used to separate artifacts and valid blood pressure periods. Since the publication deals with closed loop control a prediction problem must also have been solved. However, no

	Detection		
Prediction	quasi analog	processed	model based
quasi analog			
processed	X	X	(X)
model based	(X)	(X)	X

Figure 6.10: Meaningful detector predictor combinations.

details are provided.

Several publications may be found which solve the problem for processed signals like R-R intervals of the ECG signal or MAP. Two publications [319, 373] deal with the artifact problem for record keeping purpose. The detection is performed off line. The null hypothesis (valid signal) is characterized by a mean $\bar{x}$ and standard deviation σ. An artifact is detected if a measurement deviates more than 3σ from the mean. No prediction problem is solved in these applications. The publications [156, 433, 304, 472, 308] all solve detection and prediction problems. [156, 304, 308] apply it in a closed loop control frame work.

[156] takes a knowledge based approach to the detection problem. Details on how the prediction for closed loop purpose is solved are not provided. [433] applies a multi stage Kalman filter to detect physiological trends and artifacts. [304] uses a signal based detection and a model based prediction scheme without providing details, however. [472] adaptively identifies an auto regressive (AR) signal representation which is used for prediction and detection. [308] uses a three sample length median filter to detect the artifact. By "pausing" the controller during artifacts the prediction problem is implicitly solved by keeping the plant input constant. Finally, [115] introduces a decision signal composed of a linear combination of the deviations from a reference value and the signal trend. The authors refer to this scheme as a modified proportional derivative (PD) algorithm. Although applied for alarm generation under normal operating conditions it would work also for artifact detection with slight modifications.

The fact that little use has been made of dynamic models for solving the artifact problem is our main motivation to attack the problem from this perspective.
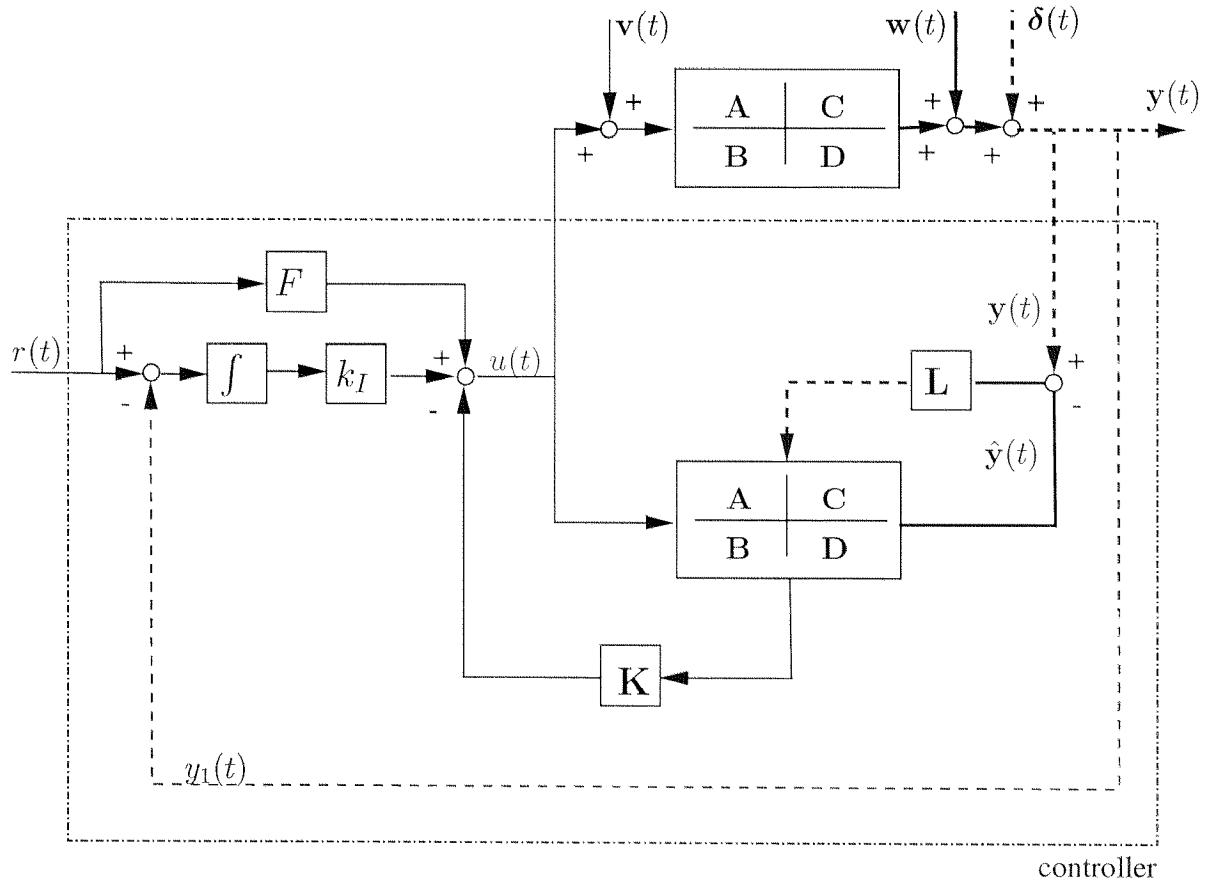
Figure 6.11: Artifacts lead to an "offsetting" of observer and integrator states.

6.4 Artifact tolerant observer based state feedback controllers

This section describes our approach to artifact tolerant control for observer based control schemes in more detail. Although we are treating observer based state feedback controllers with augmented integral action the ideas are also applicable to other observer based control algorithms like MPC.

Before presenting the solution to the artifact problem it is studied how artifacts deteriorate controller performace. Figure 6.11 serves for illustration. In developing the strategy we will work with a linear time invariant approximation of the system to be controlled as given by equations 3.106:

$$
\begin{aligned}
\dot{\mathbf{x}}(t) &= \mathbf{A}\mathbf{x}(t) + \mathbf{B}\mathbf{u}(t) + \mathbf{v}(t) \\
\mathbf{y}(t) &= \mathbf{C}\mathbf{x}(t) + \mathbf{D}\mathbf{u}(t) + \mathbf{w}(t) + \delta(t)
\end{aligned}
\tag{6.1}
$$

where $\mathbf{x}(t) \in \mathbb{R}^n$ denotes the state vector of the system, $\mathbf{u} \in \mathbb{R}^m$ is a vector of system inputs, $\mathbf{y}(t) \in \mathbb{R}^p$ is the vector of system outputs, $\mathbf{v}(t)$ and $\mathbf{w}(t)$ are process and measurement noise vectors respectively, and $\mathbf{A}, \mathbf{B}, \mathbf{C}$ and $\mathbf{D}$ are matrices of appropriate dimension, and where finally $\delta(t)$ represents the artifacts.
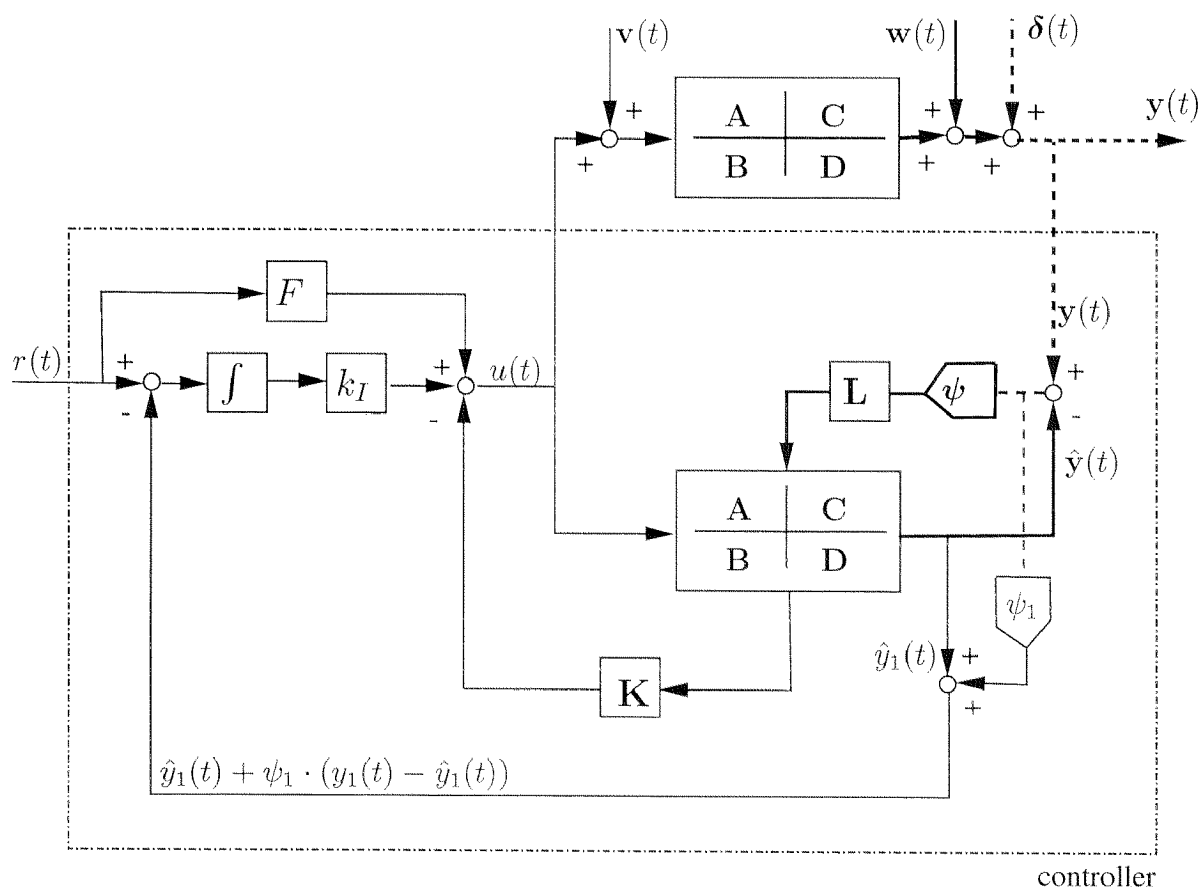
Figure 6.12: Nonlinear elements (ψ) such as saturations prevent the artifacts from offsetting the observer and integrator states.

The observer equations are

$$
\begin{aligned}
\dot{\hat{\mathbf{x}}}(t) &= \mathbf{A}\hat{\mathbf{x}}(t) + \mathbf{B}\mathbf{u}(t) + \mathbf{L}(\mathbf{y} - \hat{\mathbf{y}}) \\
\hat{\mathbf{y}}(t) &= \mathbf{C}\hat{\mathbf{x}}(t) + \mathbf{D}\mathbf{u}(t).
\end{aligned}
\tag{6.2}
$$

They serve to estimate the states ($\hat{\mathbf{x}} \in \mathbb{R}^n$) of the system (6.1). The state estimate is then used in the control law

$$
\mathbf{u}(t) = Fr(t) + k_I x_I - \mathbf{K}\hat{\mathbf{x}}(t)
\tag{6.3}
$$

to compute the input signal to the plant, where $r(t)$ denotes the reference trajectory, and x_I denotes the state of the integrator part of the controller. The dynamic equation describing the integral action is

$$
\dot{x}_I(t) = r(t) - y_1(t)
\tag{6.4}
$$

The output injection matrix $\mathbf{L}$ is computed considering process and measurement noise characteristics (e.g. Kalman filter design) as done in [111]. Artifacts $\delta(t)$, unlike white measurement or process noise, heavily affect the controller in two ways. First, through the output injection matrix $\mathbf{L}$ artifacts lead to a mismatch between observer states and system states. Second, they lead to an offset of the integral part of the controller. This mismatch between controller states and reality could according to [247] be viewed as a "controller wind up". However, if the artifacts $\delta(t)$ were true delta-functions observer states and integrator were set to new values at the instance where the artifact occurs. We will therefore rather use the term "offsetting" to denote this phenomenon. These effects are drawn with dashed lines in figure 6.12. The controller offsetting leads to the observed performance degradation. And a remedy for this problem has to make sure that the artifacts $\delta(t)$ do not enter the observer equation (6.2).

If the observer is designed in a stochastic framework i.e. as a Kalman filter the error signal $\mathbf{e}_y(t) = \mathbf{y}(t) - \hat{\mathbf{y}}(t)$ represents a vector valued zero mean and white stochastic process [16] assuming that $\mathbf{v}(t)$ and $\mathbf{w}(t)$ are zero mean white noise processes. If now an artifact occurs $\mathbf{e}_y(t)$ is not zero mean but has a mean of $\delta(t)$. The detection of an artifact based on the innovations signal $\mathbf{e}_y(t)$ is thus equivalent to detecting a sudden shift in the mean of $\mathbf{e}_y(t)$. Since $\mathbf{e}_y(t)$ is a stochastic signal the test for hypothesis "zero mean" versus the hypothesis "non zero mean" may be formulated as a statistical decision based on the actual value of $\mathbf{e}_y(t)$. For more details se e.g. [490]. Assuming that $\delta(t)$ affects the different components of $\mathbf{y}(t)$ independently the decision may be performed separately for every component of $\mathbf{e}_y(t)$. In case of an artifact the corresponding output injection vector is set to $\mathbf{L}_i = 0$ which prevents the artifact to enter the observer equation (6.2). Such a component wise statistical decision may be represented by a diagonal nonlinear block $f(\mathbf{e}_y(t))$ multiplying the innovations $\mathbf{e}_y(t)$ that is

$$
f_i(e_{y_i}(t)) \cdot e_{y_i}(t) = \left\{
\begin{array}{lll}
e_{y_i}(t) & , & e_{y_i}(t) \leq threshold \\
0 & , & e_{y_i}(t) > threshold \,.
\end{array}
\right.
\tag{6.5}
$$

With a more general nonlinearity

$$
\psi(\mathbf{e}_y(t)) = \mathrm{diag}(\psi_1(e_{y_1}(t)), \cdots, \psi_p(e_{y_p}(t)))
\tag{6.6}
$$

with (typically) unimodal functions $\psi_i(e_{y_i}(t))$ for which $\psi_i(0) = 1$ and $\psi_i(-\infty) = \psi_i(\infty) = 0$ the observer dynamics then become

$$\dot{\hat{\mathbf{x}}}(t) \;=\; \mathbf{A}\hat{\mathbf{x}}(t) + \mathbf{B}\mathbf{u}(t) + \mathbf{L}\psi(\mathbf{e_y}(t))\mathbf{e_y}(t). \tag{6.7}$$

The integrator offsetting may be prevented in a analogous way by feeding back

$$\hat{y}_1(t) + \psi_1(e_{y_1}(t))e_{y_1}(t) \tag{6.8}$$

instead of $y_1(t)$ as shown in figure 6.12. Note that

$$\hat{y}_1(t) + \psi_1\left\{e_{y_1}(t)\right\}e_{y_1}(t) = \hat{y}_1(t) + \psi_1\left\{y_1(t) - \hat{y}_1(t)\right\} \cdot [y_1(t) - \hat{y}_1(t)] \tag{6.9}$$

which leads to feeding back $\hat{y}_1(t)$ if $[y_1(t) - \hat{y}_1(t)]$ is large and feeding back $y_1(t)$ if $[y_1(t) - \hat{y}_1(t)]$ is small.

The total system equations then become

$$\begin{aligned}
\dot{\mathbf{x}}(t) &= \mathbf{A}\mathbf{x}(t) + \mathbf{B}\mathbf{u}(t) + \mathbf{v}(t) \\
\mathbf{y}(t) &= \mathbf{C}\mathbf{x}(t) + \mathbf{D}\mathbf{u}(t) + \mathbf{w}(t) + \delta(t)
\end{aligned}$$

$$\begin{aligned}
\dot{\hat{\mathbf{x}}}(t) &= \mathbf{A}\hat{\mathbf{x}}(t) + \mathbf{B}\mathbf{u}(t) + \mathbf{L}\psi(\mathbf{e_y}(t))\mathbf{e_y}(t) \\
\hat{\mathbf{y}}(t) &= \mathbf{C}\hat{\mathbf{x}}(t) + \mathbf{D}\mathbf{u}(t)
\end{aligned}$$

$$\begin{aligned}
\dot{x}_I(t) &= r(t) - \hat{y}_1 + \psi_1(e_{y_1}(t))e_{y_1}(t) \\
\mathbf{u}(t) &= Fr(t) + k_I x_I - \mathbf{K}\hat{\mathbf{x}}(t) \tag{6.10}
\end{aligned}$$

With this nonlinear modification the stability of the feedback system must be checked anew. To analyze the stability of the overall system defined by equations (6.10) it is useful to bring the system into the following form (see also Figure 6.13)

$$\begin{aligned}
\mathbf{e_y} &= G(s)\tilde{\mathbf{e}} + \mathbf{z}_1 \\
\tilde{\mathbf{e}} &= \Delta(\mathbf{e_y}) + \mathbf{z}_2 \tag{6.11}
\end{aligned}$$

where $G(s)$ incorporates the linear time invariant parts of the closed loop system and Δ contains the nonlinear weighting functions. Different approaches can be taken to prove the stability of the interconnection (6.11). A very powerful tool is the analysis in terms of integral quadratic constraints (IQC)[315]. In this frame work the Δ-block might also contain time varying or uncertain system parts which makes up the power of this method.

The different elements in (6.11) are related to (6.10) as follows. $G(s) = \mathcal{C}(s\mathbf{I} - \mathcal{A})^{-1}\mathcal{B} + \mathcal{D}$ is given in state space notation by

$$\mathcal{A} = \begin{bmatrix} \mathbf{A} & -\mathbf{BK} & \mathbf{B}k_I \\ \mathbf{0} & \mathbf{A} - \mathbf{BK} & \mathbf{B}k_I \\ -\mathbf{MC} & \mathbf{0} & \mathbf{0} \end{bmatrix} ; \quad \mathcal{B} = \begin{bmatrix} \mathbf{0} \\ \mathbf{L} \\ \mathbf{0} \end{bmatrix} ; \quad \mathcal{C} = \begin{bmatrix} \mathbf{C} & -\mathbf{C} & \mathbf{0} \end{bmatrix} ; \quad \mathcal{D} = [\mathbf{0}] \tag{6.12}$$
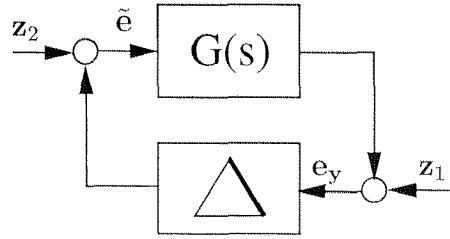
Figure 6.13: Feedback interconnection for the nonlinear stability analysis.

where $\mathbf{M} = \begin{bmatrix} 1 & 0 & \cdots & 0 \end{bmatrix}$, $\mathbf{e_y} = \mathbf{y} - \hat{\mathbf{y}}$, $\tilde{\mathbf{e}} = \psi(\mathbf{e_y}(t))\mathbf{e_y}$, $\mathbf{z}_2 = 0$, and

$$\mathbf{z}_1 = G(s) = \mathcal{C}(s\mathbf{I} - \mathcal{A})^{-1}\mathcal{E}\mathbf{d} \tag{6.13}$$

with

$$\mathcal{E} = \begin{bmatrix} \mathbf{B}F & 0 & \mathbf{I} \\ \mathbf{B}F & \mathbf{L} & 0 \\ 1 & 0 & 0 \end{bmatrix}, \text{ and } \mathbf{d} = \begin{bmatrix} r \\ \mathbf{v} \\ \mathbf{w} \end{bmatrix}. \tag{6.14}$$

The matrix $\mathbf{M}$ is introduced for technical purposes. It servers to extract the first row of $\mathbf{C}$ which generates $y_1(t)$.

For the analysis it is first necessary to find a matrix function $\Pi(j\omega)$ which characterizes Δ in terms of an inequality (an IQC) of the form

$$\int_{-\infty}^{\infty} \begin{bmatrix} \mathbf{e}(j\omega) \\ \tilde{\mathbf{e}}(j\omega) \end{bmatrix}^* \Pi(j\omega) \begin{bmatrix} \mathbf{e}(j\omega) \\ \tilde{\mathbf{e}}(j\omega) \end{bmatrix} d\omega \geq 0 \tag{6.15}$$

where $\mathbf{e}(j\omega)$ and $\tilde{\mathbf{e}}(j\omega)$ denote the Fourier transform of e and $\tilde{e}$ respectively and * denotes the conjugate transpose. Suitable functions $\Pi(j\omega)$ are known for most common nonlinearities. The memory less nonlinearity restricted to a sector, for example, satisfies an IQC with

$$\Pi(j\omega) = \begin{bmatrix} -2\alpha\beta & \alpha+\beta \\ \alpha+\beta & -2 \end{bmatrix} \tag{6.16}$$

where α denotes the lower and β denotes the upper sector bound. Then under some not very restrictive conditions the feedback interconnection of $G(s)$ and Δ is stable if there exist an $\epsilon > 0$ such that

$$\begin{bmatrix} G(j\omega) \\ \mathbf{I} \end{bmatrix}^* \Pi(j\omega) \begin{bmatrix} G(j\omega) \\ \mathbf{I} \end{bmatrix} \leq \epsilon\mathbf{I}, \quad \forall \omega \in \mathbb{R}. \tag{6.17}$$

The problem of solving (6.17) can be formulated in terms of linear matrix inequalities (LMIs) which can very efficiently be solved numerically [160].

Deriving the LMI for our set up is straight forward. It is easy to see that if equation (6.16) for the single nonlinear diagonal element then

$$\Pi(j\omega) = \begin{bmatrix} -2\alpha\beta\mathbf{I} & (\alpha+\beta)\mathbf{I} \\ (\alpha+\beta)\mathbf{I} & -2\mathbf{I} \end{bmatrix} \tag{6.18}$$

holds for the whole nonlinear block in equation 6.11. Note that equation (6.5) implies $\alpha = 0$ and $\beta = 1$. With this equation 6.17 becomes

$$G(j\omega)^* + G(j\omega) - 2\mathbf{I} \leq \epsilon\mathbf{I}, \quad \forall\omega \in \mathbb{R}. \tag{6.19}$$

which is equivalent to requiring

$$\mathbf{I} - G(j\omega) \quad \text{s.p.r. (strictly positive real)} \tag{6.20}$$

Which is exactly the stability condition obtained by the circle criterion [242, 132]. The condition (6.20) may be written in terms of LMIs as [196, 58, 179]

$$\mathbf{P} > 0 \ , \quad \begin{bmatrix} \mathcal{A}^T\mathbf{P} + \mathbf{P}\mathcal{A} & \mathbf{P}\mathcal{B} - \mathcal{C}^T \\ \mathcal{B}^T\mathbf{P} - \mathcal{C} & -2\mathbf{I} \end{bmatrix} < 0. \tag{6.21}$$

Equations (6.20) and (6.21) are only valid for minimal realizations $\mathcal{A}, \mathcal{B}, \mathcal{C}, \mathcal{D}$ and $\mathcal{A}$ Hurwitz [58, 242]. To treat system (6.12) the pure integrator has to be substituted for a lag i.e.

$$\frac{1}{s} \rightarrow \frac{1}{s+\epsilon}. \tag{6.22}$$

For cases where $G(s)$ in equation (6.11) is a SISO system the circle criterion (equation (6.21)) has a nice graphical representation [242]. The application of the artifact suppression scheme to the endtidal controller leads to a $G(s)$ of dimension 3×3. The application to the MAP controller leads to a $G(s)$ of dimension 4×4. Instead of a graphical test a numerical verification of equation (6.21) must thus be performed. This test was performed for endtidal and MAP controller with positive result.

6.4.1 Determining the ψ_i

The nonlinear modifications $\psi_i(e_{y_i})$ of the output injection have to be chosen such that the performance of the observer does not suffer in the artifact free case. More precisely they must be chosen such that the normal noise on the signal (e_{y_i}) does not lead to an inactivation of the observer corrections. Therefore a look at the distribution of the amplitude of e_{y_i} is necessary. Estimates obtained from recordings during clinical trials of these distributions for the different signals (errors for the predictions of inspired and endtidal concentrations, as well as MAP) are shown in figures 6.14 to 6.16 in the form of histograms. Into the same figures the functions $\psi_i(e_{y_i})$ are plotted. The are all of the form

$$\psi_i(e_{y_i}) = \begin{cases} \frac{a}{(e_{y_i}(t)+b)^2+a} & , \quad e_{y_i}(t) \leq -b \\ 1 & , \quad -b < e_{y_i}(t) \leq b \\ \frac{a}{(e_{y_i}(t)-b)^2+a} & , \quad e_{y_i}(t) > b \end{cases} \tag{6.23}$$

with different choices of a and b for the different innovation signals. The values are summarized in table 6.1.

	a	b
inspiratory controller	0.005	0.1
endtidal controller	0.0005	0.02
MAP controller	10.0	10.0

Table 6.1: Parameters for the nonlinear weighting functions.
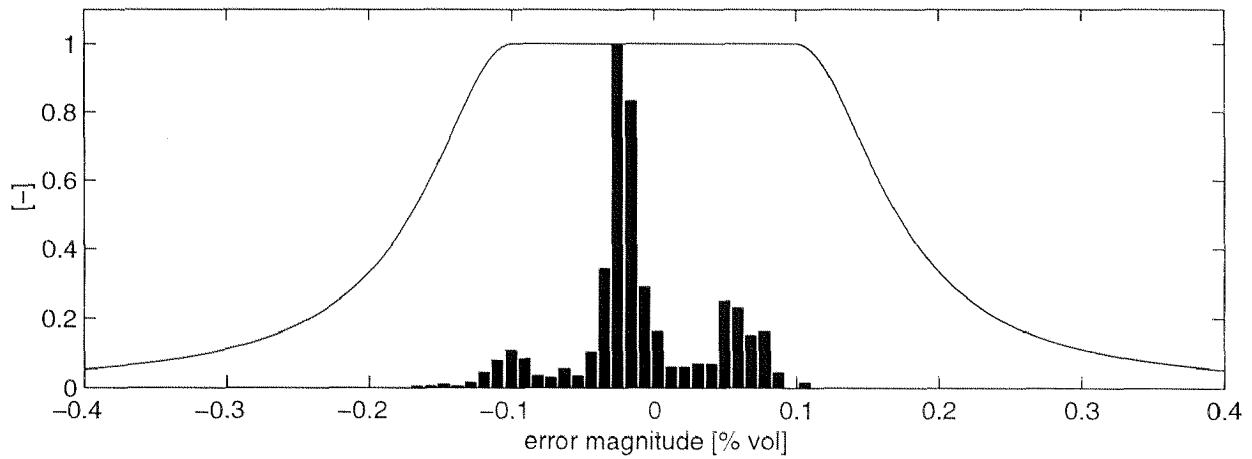
Figure 6.14: Histogram and $\psi_i(\cdot)$ for the observer error of the inspiratory anesthetic concentration.
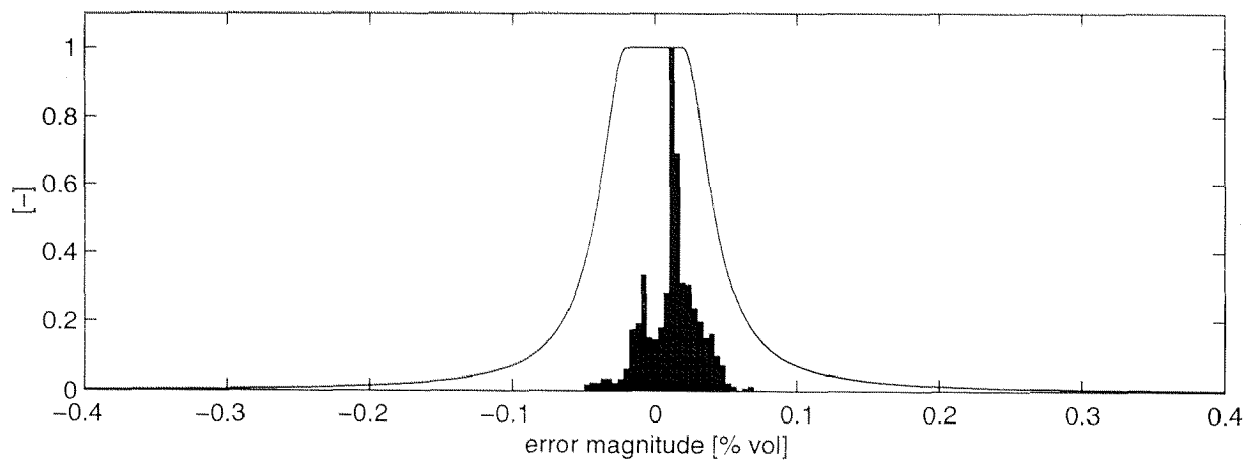
Figure 6.15: Histogram and $\psi_i(\cdot)$ for the observer error of the endtidal anesthetic concentration.
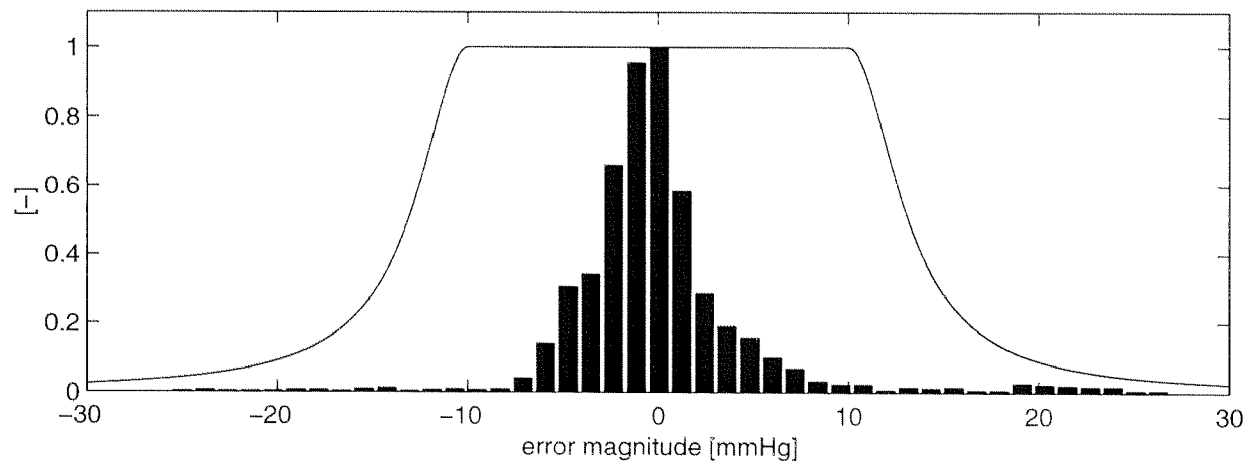
Figure 6.16: Histogram and $\psi_i(\cdot)$ for the observer error for MAP.

6.4.2 Application of the artifact tolerant control scheme to endtidal control

The artifact suppression scheme was extensively tested during the clinical validation of the model based endtidal controller described in 4.4. The series of plots in figure 6.17 shows typical cases. Note that artifacts of different duration occurring during various control maneuvers were successfully suppressed.
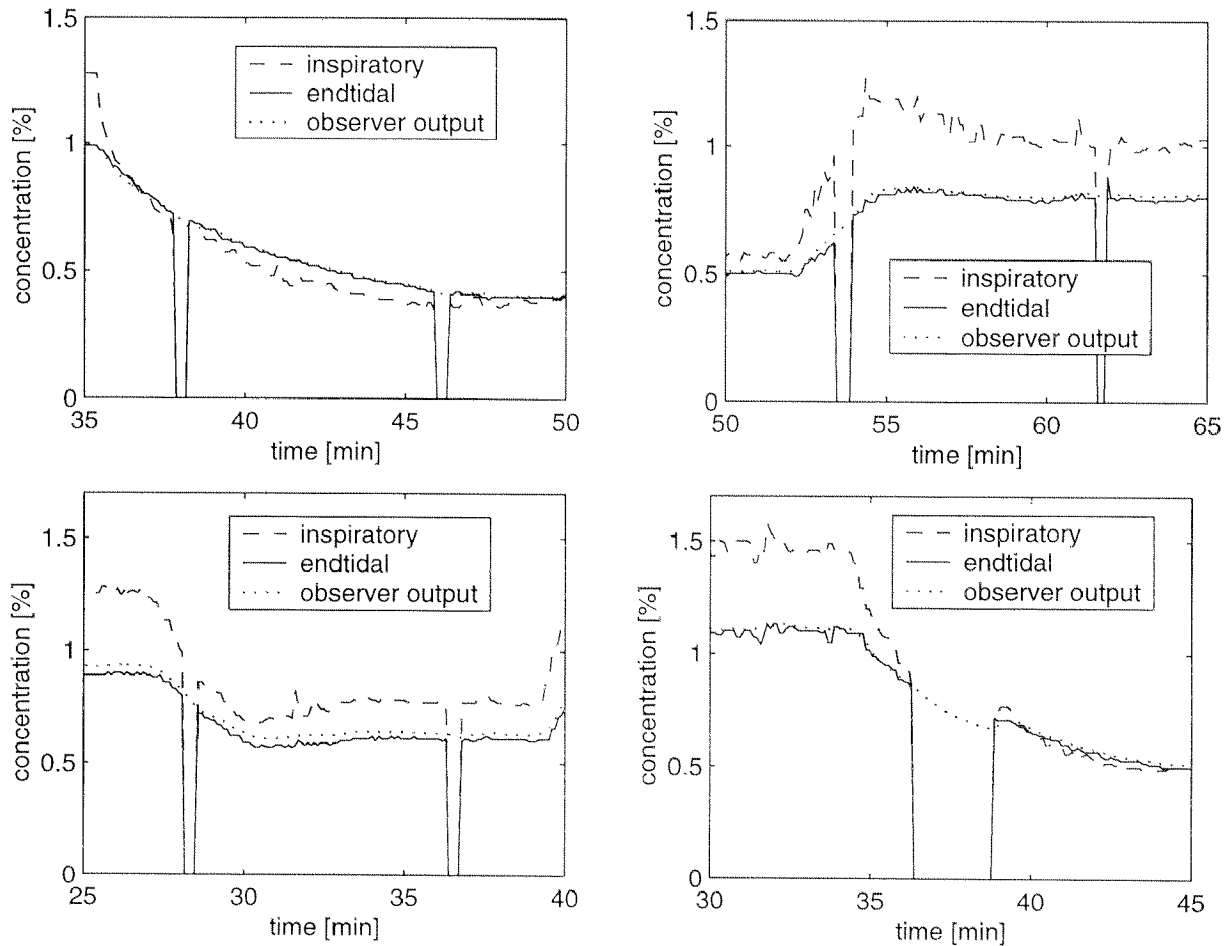
Figure 6.17: Series of plots demonstrating the successful suppression of artifacts during various control maneuvers during control of endtidal anesthetic concentration.

6.4.3 Application of the artifact tolerant control scheme to blood pressure control

Since the clinical validation of the MAP controller with endtidal override had just started when this thesis was completed fewer examples of successful artifact suppressions are available. Nevertheless, suppression results for the most severe artifacts could be recorded. They are shown in figure 6.18. The last plot in the series documents the reaction to physiological stimulations. It can be seen that the observer is following these blood pressure variations.
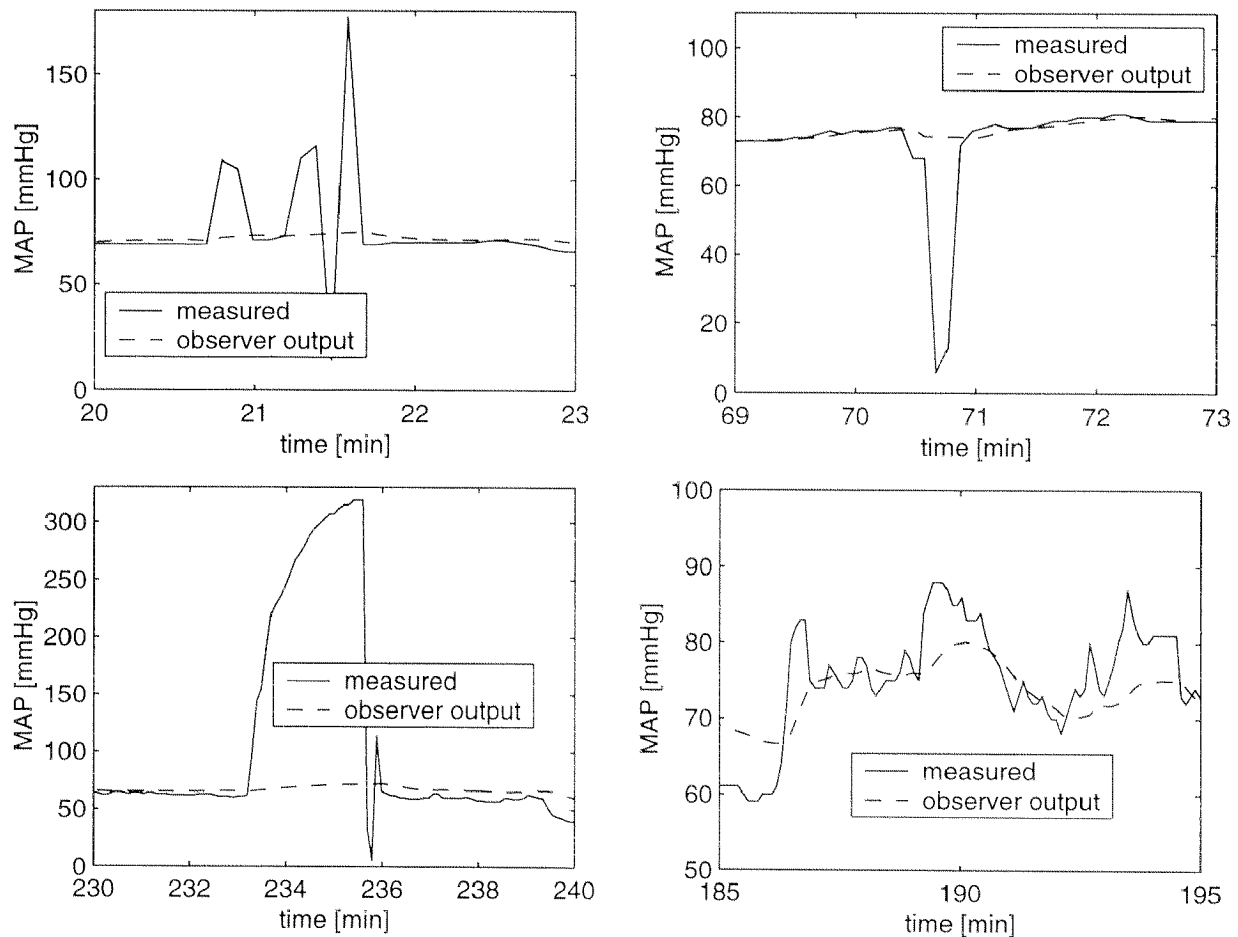
Figure 6.18: Series of plots demonstrating the successful suppression of various blood pressure artifacts during control of MAP. The upper left plot shows a flush, the upper right plot shows a central venous pressure measurement, the lower left plot shows a blood sample, and the lower right plot shows physiological blood pressure variations caused by stimulations.

6.5 Conclusions

With a nonlinear modification to the classical linear state observer a novel and elegant means is obtained to solve the detection and prediction problem underlying the artifact suppression

problem. The method was extensively tested during a clinical evaluation of the endtidal controller and during pilot studies for the MAP controllers. All artifacts that occurred were successfully suppressed.

An important question concerns the ability to resume normal operation after termination of an artifact. In view of the modeling errors it is possible that the observer output diverges enough so that the output injection remains inactive also after termination to the artifact. Consider for example the case shown the last plot of figure 6.17 where the observer error at the end of the artifact is larger than at the beginning. Such cases would be treated like sensor faults (see chapter 7). However, during all studies such a case never occurred.

Although we have been dealing with asymptotically stable linear systems here the method is in principle also applicable to unstable linear systems. There the condition $\psi_i(\pm\infty) = 0$ will have to be changed to $\psi_i(\pm\infty) = k_{i,0}$ for some stabilizing $k_{i,0}$. Note, however, that with $\psi_i(\pm\infty) = k_{i,0}$ a considerable portion of the suppression capability might be lost. That is in case of an unstable system one might re-consider signal based approaches. A promising method is described in [322].

Chapter 7

Fault tolerant control

7.1 Introduction

In this chapter the main contribution of this work is presented. Since fault tolerant control (FTC) is a relatively new research area first an introduction to FTC will be given first in section 7.2. The definitions given are taken from [45]. Although not an international standard the publication gives consistent definitions for the different terms usually used in FTC. Their relation to international standards will be pointed out where applicable. Then the design procedure for FTC systems as proposed by Blanke et al. [46, 56, 45] is introduce in section 7.3. In sections 7.4 to 7.10 the individual design steps are carried out for the Isoflurane-MAP control problem. Finally, some concluding remarks will be given in section 7.11. This section will include some comments on the experiences made with applying the formalized design procedure. Last but not least a theoretical contribution to FTC is provided in appendix C. For definitions distinguishing faults and artifacts see chapter 5.

7.2 Introduction to FTC

Automated systems are vulnerable to faults. Defects in sensors, actuators, in the process itself, or within the controller, can be amplified by the closed-loop control systems, and faults can develop into malfunction of the loop. The closed-loop may alternatively hide a fault from being observed until a situation is reached in which a failure is inevitable. A control-loop failure will easily cause production to stop or system malfunction at a plant level and thus cause costs or even casualties [455].

For safety critical systems different requirements may be imposed. [45] distinguishes *fail-operational* or *fail-safe* systems which are defined as follows:

Definition 7.2.1 *fail-operational: A system is able to operate with no change in objectives or performance despite of any single failure [187, 45]. Note that [219] refers to this property as "fehlertolerant".*

Definition 7.2.2 *fail-safe: In case of faults the system fails to a state that is considered safe in the particular context [219, 45]. Note that protection systems are of this type. If protection systems shut down a system part it must of course be assumed that this results in a safe system state. A typical example is the occurrence of a "SCRAM" in a nuclear reactor.*

Traditionally these requirements are fulfilled by means of redundant hardware. For example to detect a sensor fault a "2 out of 3" decision of equivalent sensors is made. But hardware redundancy increases cost and on the other hand fail safety is not a mandatory requirement for all systems. In fact there are applications where it is acceptable to run the system with reduced performance or functionality in case of a fault as long as minimal performance requirements (such as stability) are met. The idea of renouncing redundant hardware and of designing the control system for nominal operation and to alter the control law and possibly the control objectives if faults occur is an essential ingredient of FTC. By renouncing hardware redundancy FTC is a cost-effective way to obtain increased dependability in automated systems. In fact [455] shows that FTC has economic benefits. It has gained considerable attention in recent years [134, 55, 42, 46, 367, 442, 455, 45, 43, 291]. Areas of application include flight control [217, 475, 228], satellite control [55], ship engines [44, 240], as well as laboratory experimental systems [300]. It might be defined as follows

Definition 7.2.3 *fault-tolerant-control (FTC): The ability of a controlled system to maintain (some) control objectives, despite the occurrence of faults. A degradation of control performance may be accepted. [45]. Note that [219] calls this "abgestufte Fehlertoleranz".*

A abstract representation of a fault tolerant control system is shown in figure 7.1. A fault is a discrete event (σ_f) that acts on a system and by that changes some of the properties of the system (q_p). The goal of fault tolerant control is in turn to detect the occurrence of the fault and respond to it such that the faulty system still is well behaved [46]. This is achieved by reconfiguration (with a control event σ_a) of the system (e.g. shut down of a part of the system) and/or by changing the control law (q_c). The new control law can either be pre-determined for each type of critical fault or obtained from real-time analysis and optimization. Due to these discrete events of fault occurrence and reconfiguration FTC systems are hybrid in nature. A related area is thus control of discrete-event (DEDS) [384, 385, 250] and hybrid dynamical systems [135, 8, 340, 266, 458].

One possible strategy of handling faults is to design the controller such that it is stable for a set of possible fault scenarios. In this passive case FTC is a robust control problem. However, since robust controllers tend to be conservative FTC approaches the problem actively.
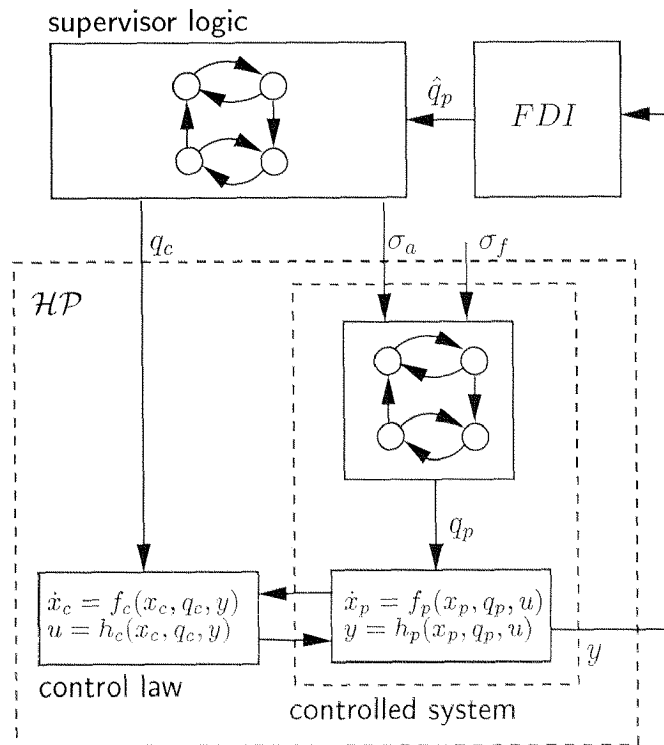
Figure 7.1: Fault tolerant control systems are hybrid in nature.

7.2.1 Accommodation, reconfiguration, supervision, and recoverability

Two ways have been mentioned how faults are handled in FTC that is by either accommodation or by reconfiguration. In [45] very formal definitions for these different approaches are given. Less formal definitions shall be used here. Let Σ_f denote the system after occurance of a fault event and Σ_a denote the system after occurance of a control event. A faulty system altered by an FTC control event is then denoted by $\Sigma_{f,a}$.

Definition 7.2.4 *Fault accommodation solves the problem of finding an admissible control law for the faulty system Σ_f to achieve the original control objective.*

Consider for example a case where the characteristics of a sensor change due to pollution. Accommodation aims at altering the controller such that it operates "optimally" under the new conditions.

Definition 7.2.5 *Reconfiguration solves the problem of finding an admissible control law and an admissible control event (σ_a) to achieve the original control objective for the system $\Sigma_{f,a}$.*

Consider for this case a plane with four engines where one engine catches fire. Reconfiguration means to shut do the engine and fly with three of them. Note that this also implies an change of the "control law".

The case where the original control objective can neither be achieved by accommodation nor by reconfiguration is treated by supervision which is defined as [45]

Definition 7.2.6 *Supervision solves the problem of finding an admissible control law, an admissible control event σ_a and an admissible control objective for the system $\Sigma_{f,a}$. Often this involves human operators. In this case the operator might for example be given a selection of possible procedures to chose from.*

Such a case will be encountered later in this chapter for blood pressure control. It will be shown that in case of an MAP sensor fault it must be switched to endtidal control which represents a change of the control objective.

Definition 7.2.7 *A system is recoverable from a fault σ_f if either the accommodation or the reconfiguration problem can be solved.*

Definition 7.2.8 *A system is called weakly recoverable if only the supervision problem can be solved.*

Since recoverability and weak recoverability only depend on the existence of a solution to the control problem and not on the control law it becomes obvious that both are system properties as suggested in [154].

7.3 Design Procedure for FTC Systems

Up to now we have described features of FTC systems. In this section a systematic 7-step procedure to build FTC systems is presented. The procedure was suggested by Blanke et al. [46, 56, 45].

S-1 *Fault listing and fault propagation:* The fault listing scans all the lowest level components like sensor and actuators of the system and identifies the different faults that may occur in each component. The subsequent fault propagation analysis (FPA) aggregates the fault effects at the top level of the system. If necessary this step can also include multiple fault scenarios. There are different means to perform the FPA. A fairly old method is the failure mode effect analysis (FMEA) [233, 42, 56, 43, 45] originating from reliability theory [18, 263, 208]. The FMEA method, however, has some limitations [42, 56]. One limitation is the inability to analyze closed loops consistently [42, 56]. And another limitation concerns the treatment of "XOR" conditions. To overcome the later difficulty [42, 56] suggest to use BEOLOGIC which is able to analyze logic networks. The treatment of feedback systems still leads to problems [56]. For small scale feedback control systems like our application the end effects of faults at system level are readily deduced without these formal methods. This first step in the design of an FTC systems represents a special form of risk analysis [42].

S-2 *Severity assessment*: The top level end-effects are judged for severity. The ones with significant influence on control performance, safety or availability are selected for treatment. A reverse deduction of the fault propagation is performed to locate the faults that cause severe end-effects. This gives a short-list of faults that should be detected.

S-3 *Assessing possibilities for FTC*: For each fault (or multiple faults) hardware and analytical redundancy are evaluated to determine possible means of fault detection, isolation, and identification (FDI) as well as the remedial actions (fault accommodation or system reconfiguration) possibilities. Typically this step is first performed qualitatively as described in e.g. [442, 441]. To rank different FTC strategies, however, quantitative measures of recoverability as suggested in [154] might be utilized. During this step as much understanding about the system as possible should be gained. Since different applications generally provide very different combinations of hardware and analytical redundancy this step is usually very application specific. In fact Patton [367] points out that this is true for FTC systems in general.

S-4 *Select remedial actions*: Among the different remedial actions identified during the previous step those are selected which agree best with the overall control objectives. The selected remedial actions determine the requirements for FDI and are the basis for the supervisor logic design.

S-5 *Fault detectors and isolators design*: While step 3 checked whether the different faults are detectable and isolable this step actually designs the detectors. For this design there is a large number of FDI design strategies under various conditions. Overview papers are [491, 221, 27, 147, 366, 148, 222, 7], textbooks covering the topic in more detail are [168, 79].

S-6 *Supervisor logic control design*: The supervisor logic maps FDI results into configuration events for controller and plant (recall also figure 7.1). In the logic design also ambiguous situations (e.g. due to multiple faults) have to be considered. Supervisor logic control encompasses more than "supervision" according to definition 7.2.6. It rather handles accommodation, reconfiguration, and supervision.

S-7 *Testing*: Testing should be as complete as possible. Three main problems have to be dealt with

   (a) limitations in the number of fault scenarios that can be tested

   (b) restrictions on the introduction of faults into running systems for test purposes

   (c) the complexity of the resulting hybrid system consisting of controller and plant. Transient conditions should be carefully tested.

   For our application testing includes two stages first off-line simulation testing and after successful completion of the first stage the in-vivo testing.

In the following sections the different steps of FTC design are applied to the combined Isoflurane-MAP control problem.

7.4   Fault listing and fault propagation

In scanning the anesthesia environment for possible faults we apply one major restriction. That is only faults affecting the safety of either blood pressure or endtidal control loop directly are considered. This is particularly true with respect to "faults" in the patient which would provide in itself an enormous field for research [30, 469, 232, 12, 352]. Here hypotensive situations e.g. due to the mesenteric traction syndrome [73] are considered. However, hypercapnia due to inadequate ventilation is not considered. Similarly a failure of the electrically driven vaporizer must be considered while a loose pulse-oximeter is not. Note also that according to [2] only single fault scenarios must be considered.

The set of devices representing potential fault sources are shown in figure 7.2 with their interconnections. The anesthetic gas is added to the carrier gas by the electrically driven vaporizer. It is controlled via an analog output of the target computer system. The gas stream then enters the ventilator which pumps the gas into and out of the patient's lung. This gas stream to and from the patient is continuously analyzed by the patient monitor. For this purpose a small portion of the gas stream is continuously sampled via a sampling line. Blood pressure is invasively measured with a catheter system as described in section 6.2.1. The data from the monitor is read periodically by the target computer. The faults in the different elements and their effect with respect to the patient in a control loop will be discussed next. A summary of faults and their effects is provided in table 7.1.

7.4.1   Faults of the vaporizer

We consider three potential fault scenarios for the modified electrically driven vaporizer. These are:

- empty vaporizer

- no electric power at the driving motor

- error (e.g. wire disconnected) in the local positioning loop

- no connection to the target computer.

In case of an empty vaporizer no anesthetics are mixed to the fresh gas stream. The effect is that the anesthetic concentrations decay asymptotically to zero as if the vaporizer was closed. For the patient this will lead to light anesthesia.

In case of a power loss the the vaporizer remains at the latest position before the loss. This scenario thus also includes situations where the vaporizer is stuck for mechanical reasons. We will refer to this scenario as "stuck". The concentrations of anesthetics asymptotically reach the value at which the vaporizer position has been "frozen". Depending on the actual value at which this happens the patient might get too light, still adequate, or too deep anesthesia.
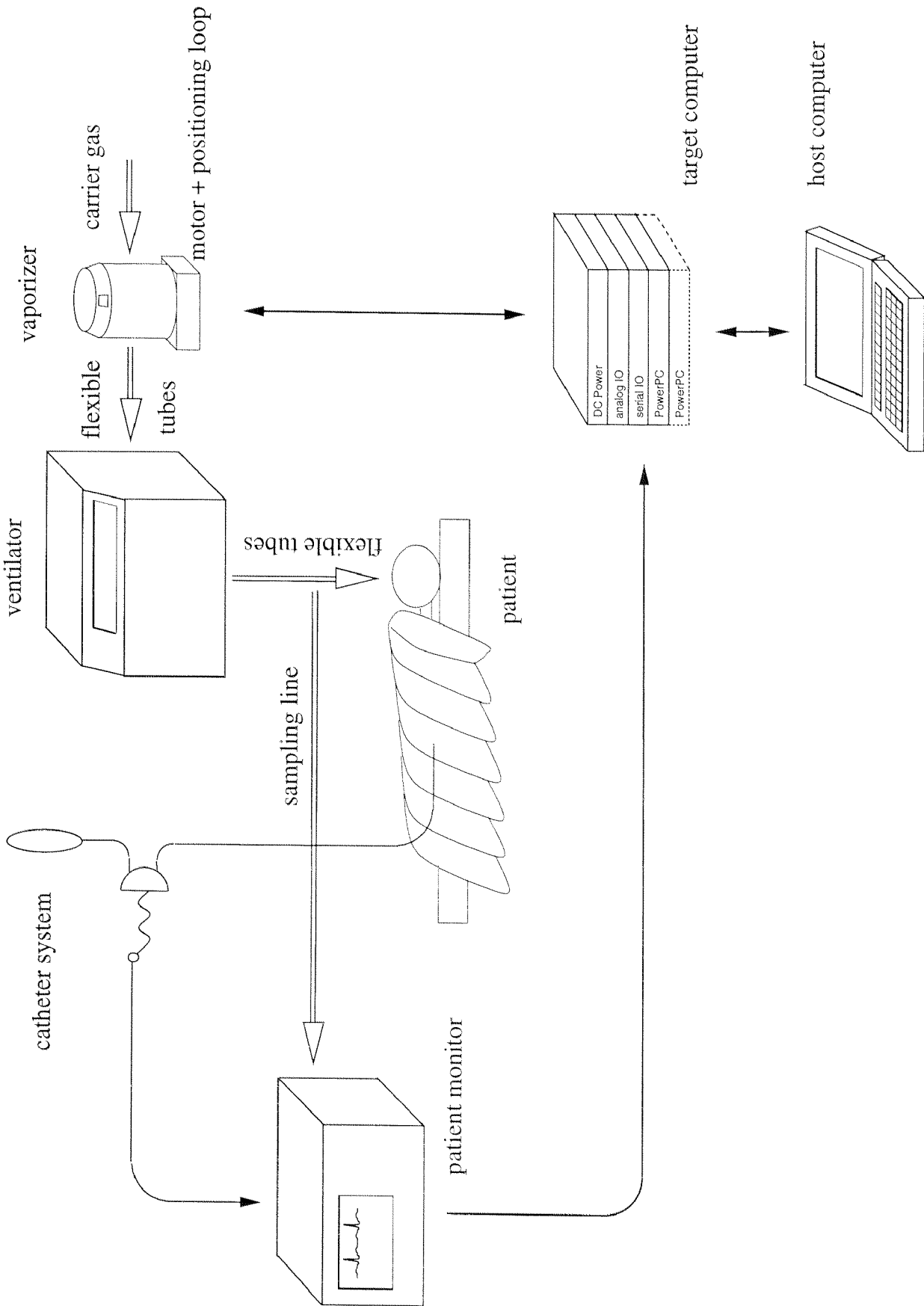
Figure 7.2: Candidate elements for starting points of fault modeling.

If the connection to the target computer is lost the local positioning loop receives a zero reference value. It will close the vaporizer which has the same consequences as an empty vaporizer.

An error in the local position control loop (e.g. due to a disconnected wire in the feedback path) leads - in the worst case - to a fully opened or a closed vaporizer. Which potentially leads to light or too deep anesthesia.

7.4.2   Faults in the flexible tubes connecting vaporizer and ventilator

The hose connecting vaporizer and ventilator is mounted rigidly. Nevertheless, it might partially disconnected, or leak e.g. due to the vibrations caused by the regular dislocation of the research platform between the lab and the OR. In case of a leak only part of the fresh gas flow enters the ventilator. Considering the respirator system equation (3.35) it may be seen that a reduced value for FF leads to larger time constants and therefore a slower response of the system. In case of an aggressively tuned controller this in turn might lead to badly damped or even unstable closed loop behavior. This effect is more pronounced the larger the leak is.

7.4.3   Faults in the ventilator

The ventilator is a mechanically very sophisticated device which may fail in a number of ways. However, the manufacturer has built in a number of diagnostic and self test functions which indicate such faults. We will therefore not deal with problems like detecting the malfunction of a valve or other faults in the ventilator. They are assumed to have been adequately addressed by the equipment manufacturer already.

7.4.4   Faults in the flexible tubes connecting ventilator and patient

The tubes connecting ventilator and patient are even more likely to disconnect partially or completely. In case of a complete disconnection the respirator partial pressure p_R is measured during inspiration and the anesthetic partial pressure of the environmental air i.e. zero is measured during exspiration. This sudden drop in the endtidal measurement signal will be handled like artifacts by the artifact tolerant control algorithm. That is the control starts to run as if in open loop. After two minutes the situation will not be treated as an artifact anymore but as a fault (see section 5.3). In addition the patient monitor detects the missing CO_2 signal and will issue an apnea alarm to the anesthetist. If the tubes are disconnected only partially the same problems as in section 7.4.2 are encountered.

7.4.5 Faults in the gas sampling line

Several faults may be envisioned that are basically of the same type. That is instead of sampling from the gas supplied to the patient environmental air is sampled and analyzed. Causes for this can be a mispositioned valve at the Y-piece, a not properly connected line (after a temporary removal for example), a leak, or a disrupted line (e.g. after entangling a wheel of the research platform). In all cases the inspiratory and the exspiratory concentration measurement drop to zero. Due to the artifact suppression mechanisms developed in chapter 6 the control algorithm starts to run open loop. This guarantees that the patient still receives adequate anesthesia for at least two minutes (see section 6.4.2). However, since the control algorithms were not designed for open loop control it is necessary to detect the situation. Since these fault affect the gas measurement only it will be treated as a sensor fault subsequently.

7.4.6 Faults in the catheter system

The detailed setup of the invasive blood pressure monitoring system was discussed in section 6.2.1. There air bubbles and the clogging of the catheter were mentioned as possible faults. In addition the transducer might break or the electric wire connecting the to monitor might be disconnected. Air bubbles lead to changed transfer characteristics of the catheter system. More precisely both the bandwidth and the damping are reduced [163, 174]. This mainly affects the transmission of the pressure waveform and leads to over estimation of the systolic pressure, under estimation of the diastolic pressure and an amplification of artifacts [163]. The mean which varies slowly compared to the pulse wave is almost not affected. A clogging of the catheter affects the transmission of the waveform as well as the mean. Since clogging leads to increased damping the waveform is smoothed [174, 259]. Due to the increased flow resistance of the catheter and the constant flush at low rate the pressure drop increases (see figure 6.2 for reference). Thus, as the catheter starts to clog the MAP signal starts to drift. The control algorithm attempts to compensate for this MAP drift which eventually leads to too deep anesthesia and low blood pressure. If the transducer breaks the MAP signal abruptly changes. Assuming that the change is small so that the artifact suppression does not become active then the controller will treat this change as if it was a physiological MAP change. Depending on the value provided and the reference set the controller will either open or close the vaporizer. Which leads to too deep or light anesthesia. If the abrupt change is large enough to activate artifact suppression the control system starts to run open loop.

7.4.7 Faults in the connection form the target computer to the monitor

If the connection from the monitor to the target computer is broken no new values are received by the monitor software I/O driver objects (see figure 2.10 for reference). The software object keeps providing the latest value. Both concentration and blood pressure measurements are affected by this fault. Depending on that value and the reference the control algorithm will eventually fully open or closed the vaporizer with the earlier described consequences. This situation is already

detectable in the software since every measurement values has a time tag attached to it which indicates when the value was received from the monitor.

7.4.8   Faults in the monitor

The critical part of the monitor with respect to measurements of anesthetics is the measuring cell for anesthetics. But also faults in the electronics or the software for processing the signal may be envisioned. In any case the controller will attempt to compensate for these errors. It may eventually lead to too deep or to light anesthesia depending on the actual evolution of the fault.

7.4.9   Faults in the target computer

On the target computer the software is structured in different processes as discussed in section 2.7.2. Each of these processes might trap due to run time errors like timing violations or floating point overflows. Now if for example the task of the I/O object for the patient monitor traps then the main application is still able to read data from the object but no new data is read from serial connection. The application will get the last valid values whenever data from the object is requested. A trapping of the monitor I/O object leads to the same problems like an abrupt sensor fault with the same effects for the patient. Similarly if the IfAGADOS object traps no further adjustment of the vaporizer occurs. This has the same consequences as a loss of power in the motor driving the vaporizer. Although exhibiting similar effects like sensor or actuator faults trapped I/O processes are easier to detect. It is done by the XOberon operating system and treated by means of exception handling routines.

During pilot studies situations occurred where controllers were switched on before they were properly initialized or before the observer errors had converged sufficiently. In some cases this resulted in heavy transients. Since the introduction of the supervisor logic control as described in section 4.3 such situations have successfully been avoided.

7.4.10   Faults in the connection for the target computer to the host computer

If the connection between target and host is lost the measurements on the display are not updated anymore and it is not possible to change the setpoints of the controllers. It does not affect the functioning of the control loops directly. They will continue to work with their latest setpoint. Assuming that these setpoints are set correctly there is no immediate threat to the patient. The fault must nevertheless be treated. This is done in the model control object. The regular update request from the host elements (see section 2.7.4) are registered on the target computer. If no regular host request occurs the system falls back to manual control.

subsystem	fault	worst case effect	severity
vaporizer	empty	light anesthesia	critical
	power loss, "stuck"	light or too deep anesthesia	critical
	target connection loss	light anesthesia	critical
	error in positioning loop	light or too deep anesthesia	critical
tube vaporizer-ventilator	leak	unstable control loop	critical
	disconnect	lack of fresh gas	detected by standard ventilator)
ventilator	not considered here	–	treated by manufacturer)
tube ventilator-patient	leak	unstable control loop	critical
	disconnect	apnea	detected by standard monitor)
gas sampling line	off, disrupted	open loop control	critical
	leak	too deep anesthesia	critical
catheter-transducer system	clogging	low blood pressure, deep anesthesia	critical
	air bubble	slower response	minor
	failure in transducer	light or too deep anesthesia	critical
patient monitor	serial line disconnect	light or too deep anesthesia	detected by I/O software objects
	Agas cell defect	light or too deep anesthesia	critical
target computer	controller not initialized	heavy transients	treated with SLC
	monitor I/O process trapped	light or too deep anesthesia	treated with exception handler
	gas dosing I/O process trapped	light or too deep anesthesia	treated with exception handler
	"crash" of operating system	light or too deep anesthesia	treated with fall back to manual
target-host	connection lost	autonomous control	treated by mode control object
patient	hypotension	light anesthesia	treated with lower override
	hypertension	too deep anesthesia	treated with upper override

Table 7.1: List of faults and there top level effects and their severity. This list is the result of steps 1 and 2 of the design procedure.

actuator faults	vaporizer "stuck", "empty"
component faults	leaks and disconnections of tubes
sensor faults	faulty gas measurements faulty blood pressure measurements

Table 7.2: Critical faults to be handled in the FTC procedure.

7.4.11   Special patient situations

There are special patient conditions that need to be addressed also in this analysis. Of concern are hypotensive and hypertensive situations. Hypotensive situations might arise as a result of e.g. the mesenteric traction syndrome or blood loss. In this case the patient's blood pressure potentially falls far below the setpoint. In attempting to rise blood pressure the controller will stop the application of anesthetics which leads to light anesthesia. Hypertensive situations might occur e.g. due to pheochromocytoma [98]. This potentially leads to an excessive high endtidal concentrations and to a hypotonic crisis, cardiac arrhythmias, or even cardiac arrest. Remedy for these situations was provided by introducing upper and lower endtidal override controllers as described in section 4.2.3. No such patient conditions were encountered affecting the endtidal control loop.

7.5   Severity assessment

The faults listed in table 7.1 are readily assigned to severity classes. This represents step 2 of the design procedure. Any fault representing a potential threat to the patient is critical and must be handled. These are the cases of potentially light or too deep anesthesia as well as unstable controllers. Light anesthesia may lead to awareness. That is the patient is conscious but due to relaxation is not able to communicate his/her awareness. This situation is experience as very unpleasant. Too deep anesthesia may lead to a hypotonic crisis, cardiac arrhythmias, or even cardiac arrest. Both are critical situations. The cases where faults lead to open loop control are non-critical only in the first couple of minutes. Due to modeling errors open loop control might in the long run also lead to light or too deep anesthesia and must therefore also be viewed as critical. Faults already taken care of during controller or software design are labeled "treated" and will not be considered further.

Faults are often classified according to actuator faults, component faults, and sensor faults [147, 78, 148, 79]. Table 7.2 lists the critical faults for further treatment according to this classification.

7.6 Assessing the possibilities for FTC

This represents step 3 of the design procedure. Before discussing the FTC possibilities for the different faults some general comments shall be made.

Note that there is no direct hardware redundancy built into the system. It would of course be simpler to use a redundant gas sensor or blood pressure monitoring system to detect malfunctions [136]. However, it has been designated a deliberate goal of the work to explore the FTC possibilities without additional hardware. In other words analytical redundancy must be utilized. Analytical redundancy is provided by models. We will distinguish two levels of redundancy according to the description fidelity of the underlying model.

Definition 7.6.1 *High and low fidelity analytical redundancy are distinguished. High fidelity redundancy is provided in terms of differential equations and system parameters. Low fidelity analytical redundancy is provided by qualitative relations.*
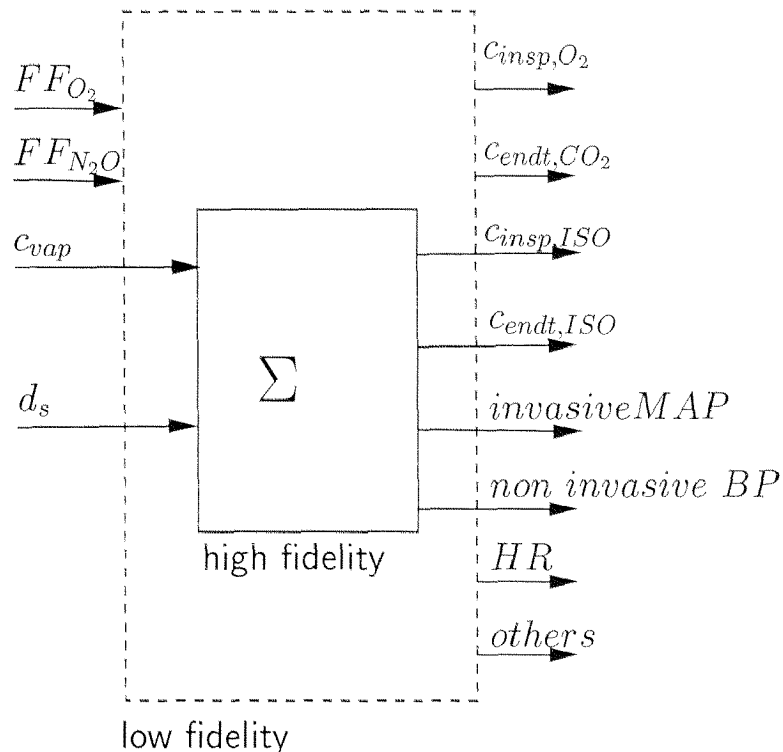
Figure 7.3: Analytical redundancy is generally available at different fidelity levels.

A typical example for low fidelity redundancy is a mental model of a human operator. Note also that for high fidelity redundancy no specification about the accuracy of the model is made. This is not necessary at this point since fidelity refers to the representation of the redundancy and not to the accuracy of the underlying model.

A similar discussion along this line is found in [149] where model requirements for FDI are discussed. It is pointed out that FDI does not always require high fidelity redundancy. For

our situation the separation of high and low fidelity redundancy is illustrated by figure 7.3. That is the mathematical model derived in chapter 3 provides the high fidelity redundancy. This high fidelity redundancy is a direct yield of a large modeling effort and it allows to detect even small inconsistencies among the input and output signals. But a standard patient monitor provides much more information than is captured by the high fidelity model. Often such additional measurements might support FDI in qualitative manner. For example consider a case where FDI finds inconsistencies in the anesthetics gas concentration measurements. Based on the model it is not possible to determine whether the fault is due to a problem in the cell measuring the anesthetic gas concentration or a disconnected sampling line. If a check reveals a valid CO_2 signal then the disconnected sampling line may be ruled out as possible fault source.

7.6.1 Component faults and actuator faults

To address the FDI problem the standard FDI literature [79, 168] considers LTI systems of the form

$$
\begin{aligned}
\dot{\mathbf{x}}(t) &= \mathbf{A}\mathbf{x}(t) + \mathbf{B}\mathbf{u}(t) + \mathbf{E}\mathbf{f}(t) \\
\mathbf{y}(t) &= \mathbf{C}\mathbf{x}(t) + \mathbf{D}\mathbf{u}(t) + \mathbf{F}\mathbf{f}(t)
\end{aligned}
\tag{7.1}
$$

where $\mathbf{x}(t) \in \mathbb{R}^n$ denotes the state vector of the system, $\mathbf{u} \in \mathbb{R}^m$ is a vector of system inputs which might be known or unknown, $\mathbf{y}(t) \in \mathbb{R}^p$ is the vector of system outputs, $\mathbf{f}(t)$ denotes the additive fault vector, and $\mathbf{A}, \mathbf{B}, \mathbf{C}, \mathbf{D}, \mathbf{E}$, and $\mathbf{F}$ are matrices of appropriate dimensions. In this formulation $\mathbf{f}(t)$ only contains actuator and sensor faults. To comply with this formulation the component faults therefore have to be recast in terms of additive sensor or actuator faults (see e.g. [79]). For our application this must be done for the leaks in the respiratory circuit (any of the flexible tubes). For the leak in the respiratory circuit consider the respiratory equation 3.35. Replacing $FF \rightarrow FF - FF_\Delta$ where FF_Δ represents the leak flow the equation may be written

$$
\dot{p}_R = \frac{FF}{V_R}p_{vap} + \frac{f_R(V_T - V_D - V_{AD})}{V_R}[p_L - p_R]
$$
$$
- \frac{(FF - Q_\Delta)}{V_R}\left[\frac{V_{AD}}{V_T - V_D}p_R + (1 - \frac{V_{AD}}{V_T - V_D})p_L\right] + \frac{FF}{V_R}f_c(t) \tag{7.2}
$$

where

$$
f_c(t) = \left[\frac{V_{AD}}{V_T - V_D}p_R + (1 - \frac{V_{AD}}{V_T - V_D})p_L - p_{vap}\right]\frac{FF_\Delta}{FF} \tag{7.3}
$$

now represents the additive component fault signal that enters the system dynamics like an actuator fault. In our case thus $\mathbf{f}(t)$ has three components, i.e.

$$
\mathbf{f}(t) = \begin{bmatrix} f_{actuator,leak}(t) \\ f_{gasmeasurement}(t) \\ f_{MAPmeasurement}(t) \end{bmatrix}. \tag{7.4}
$$

That is one component combining the vaporizer faults and the component faults into one actuator fault, one component corresponding to faults in the concentration measurement and one

component corresponding to faults in the MAP measurement system. This implies

$$\mathbf{E} = \begin{bmatrix} \mathbf{B} & 0 & 0 \end{bmatrix}, \text{ and } \mathbf{F} = \begin{bmatrix} 0 & 1 & 0 \\ 0 & 1 & 0 \\ 0 & 0 & 1 \end{bmatrix}.$$

Expressed in words this means that component and actuator faults affect the system like an additive input and have no direct effect on the system outputs. Faults in the gas sensor affect both the inspiratory and the endtidal concentration measurement. And faults in the blood pressure measuring system only affect the MAP output (see also figure 7.9).

As a consequence of combining component and actuator faults it will not be possible to distinguish between the two unless additional (low fidelity) redundancy is utilized. Nevertheless, the formulation given by equations (7.1) is in appropriate form for the discussion of general FDI aspects in the next section.

7.6.2 Fault detectability

The first ingredient in FTC is FDI. It encompasses the detection, isolation and in some case identification of faults [167]. If the identification problem is also addressed the abbreviation FDII or FDI^2 could be used instead. Whether these problems are solvable may be determined without actually designing the detectors [78, 79].

The detectability condition follows directly from the structure of the general residual generator [78, 168, 79] shown in figure 7.4. The blocks $G_u(s)$ and $G_f(s)$ are given by

$$\begin{aligned} \mathbf{G}_u(s) &= \mathbf{C}(s\mathbf{I} - \mathbf{A})^{-1}\mathbf{B} + \mathbf{D} \\ \mathbf{G}_f(s) &= \mathbf{C}(s\mathbf{I} - \mathbf{A})^{-1}\mathbf{E} + \mathbf{F}. \end{aligned}$$

The second equation yields a fault transfer matrix $\mathbf{G}_f(s)$ for our problem of the form

$$\mathbf{G}_f(s) = \begin{bmatrix} G_f^{1,1} & 1 & 0 \\ G_f^{2,1} & 1 & 0 \\ G_f^{3,1} & 0 & 1 \end{bmatrix}. \tag{7.5}$$

Equation wise figure 7.4 is

$$R(s) = \mathbf{H}_u(s)U(s) + \mathbf{H}_y(s)Y(s). \tag{7.6}$$

For FDI we require that the residuals are non-zero iff a fault has occurred, i.e.

$$\mathbf{r}(t) \neq 0 \quad \Longleftrightarrow \quad \mathbf{f}(t) \neq 0 \tag{7.7}$$

to achieve this we have to impose

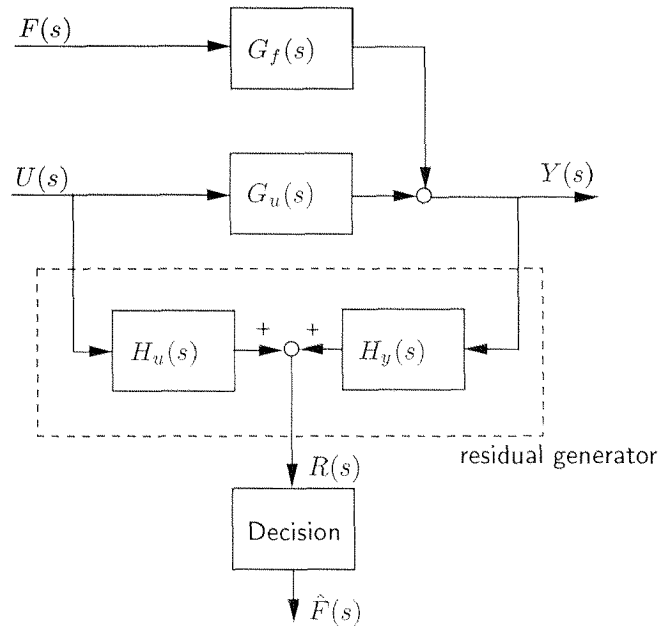$$\mathbf{H}_u(s) + \mathbf{H}_y(s)\mathbf{G}_u(s) = 0 \tag{7.8}$$

Figure 7.4: Obviously a residual generator must rely on system signals that are known. These are either control signals, measured disturbances or measured outputs. The most general (linear) residual generator thus consists of (linear) operators acting on input and output signals [168] as shown in the figure.

which results in the desired fault response given by

$$R(s) = \mathbf{H}_y(s)\mathbf{G}_f(s)F(s). \tag{7.9}$$

The ith fault of the fault vector $\mathbf{f}(t)$ is detectable iff there is at least one residual j that responds to the fault. That is at least one component of the ith row of $\mathbf{H}_y(s)\mathbf{G}_f(s)$ has to be non-zero, i.e.

$$[\mathbf{H}_y(s)\mathbf{G}_f(s)]_i \neq 0 \tag{7.10}$$

which is trivially achieved for any i in view of equation (7.5).

Detecting faults is the first step. Then for remedial action selection it must also be determined what fault had occurred. This problem is addressed by fault isolation. A sufficient condition for isolability in the deterministic case is [167] that the incidence matrix form of $G_f(s)$ given by

$$\tilde{\mathbf{G}}_f(s) = \begin{bmatrix} 1 & 1 & 0 \\ 1 & 1 & 0 \\ 1 & 0 & 1 \end{bmatrix}. \tag{7.11}$$

has full column rank. This is clearly satisfied for our FDI problem. The analysis provides the assurance that the FDI problem may be solved. Note that at this point still no distinction between vaporizer faults and leaks is possible.
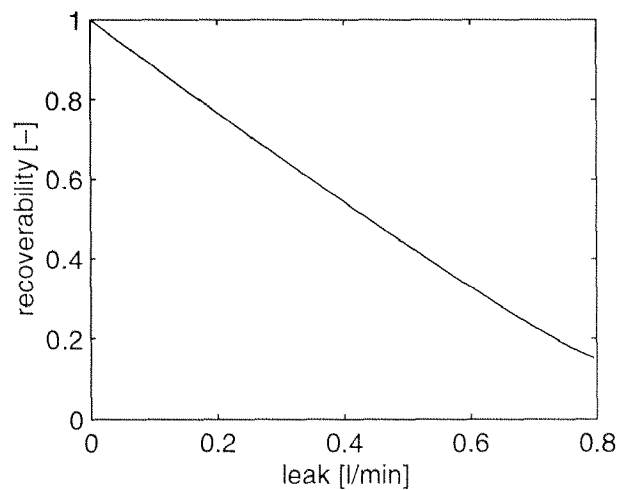
Figure 7.5: Recoveratility measure ρ_c for different leak flows and a fresh gas flow of $1\ell/min$.

7.6.3 FTC possibilities for the actuator (vaporizer) faults

Appendix D shows that eventually all partial pressure values in the system asymptotically approach the partial pressure at which the vaporizer is "stuck" or they asymptotically decay to zero if the vaporizer is "empty". There is no other remedial action than to switch to manual dosing and put the human anesthetist back in charge. In other words the system does not provide any redundancy that would allow to accommodate or reconfigure without the help of a human operator. An alternative dosing design providing more FTC possibilities is also discussed in appendix D. Since the function of the control system can not be recovered after this actuator fault it is not recoverable from the fault.

7.6.4 FTC possibilities for the component faults

In case of a leak the system does not lose the controllability property as long as the leak flow $FF_\Delta < FF - Q_\Delta$. I.e. it is recoverable from the leak. With decreasing net fresh gas flow $(FF - Q_\Delta - FF_\Delta)$, however, it will become more difficult to achieve the control objective. This is clearly indicated by figure 7.5 where the recoverability measure ρ_c elaborated in appendix C is computed as a function of the leak.

For remedial actions the redundancy relation provided by the respirator circuit equation allows to estimate the actual total fresh gas flow entering the respiratory circuit. It may then be switched to a predefined controller parameter set that was designed for a fresh gas flow closest to the one estimated. The controller implementation as described in section 4.2.6 already allows for this run time switching of controller parameter sets.

fault	ρ_o
blood pressure measurement	0.0
inspiratory measurement	0.3397
endtidal measurement	0.3929
both concentration measurements	0.0074

Table 7.3: Recoverability measures for the different sensor fault scenarios.

7.6.5 FTC possibilities for the sensor faults

Sensor faults provide an even more interesting object to study with respect to FTC possibilities. As a first step the recoverability measures according to appendix C for the different sensor fault scenarios will be computed to get an impression on how much of the observability is lost in each case. To obtain meaningful values the system states and outputs have to be put into a per unit representation such that the dynamic range of the states all lie in the same range. [177] suggests to set

$$\left| \frac{x(t)}{x_{Ref}} \right| \lesssim 1$$

$$\left| \frac{y(t)}{y_{Ref}} \right| \lesssim 1.$$

To achieve this we set

$$T = \text{diag} \begin{bmatrix} \frac{1.5}{[\%]} & \frac{1.2}{[\%]} & \frac{1.2}{[\%]} & \frac{1.2}{[\%]} & \frac{1.2}{[\%]} & \frac{0.5}{[\%]} & \frac{1.2}{[\%]} & \frac{0.5}{[\%]} & \frac{0.01}{[\%]} & \frac{1.2}{[\%]} & \frac{1.2}{[\%]} & \frac{1.2}{[\%]} & \frac{1.2}{[\%]} & \cdots \\ & & & & & & & & \cdots & \frac{20}{[mmHg]} & \frac{0.5}{[-]} & \frac{25}{[\frac{pg}{ml}]} & \frac{2.5}{[\frac{pg}{ml}]} \end{bmatrix}$$

$$T_y = \text{diag} \begin{bmatrix} \frac{1.5}{[\%]} & \frac{1.2}{[\%]} & \frac{20}{[mmHg]} \end{bmatrix}.$$

To obtain the reference values for the concentration of anesthetics we were relying on experience gained during the endtidal study. From there reference values for inspired and endtidal concentrations of 1.5% and 1.2% appear meaningful. For the fast body compartments the same reference value as for the endtidal measurement is used. The medium fast compartments (muscles, poorly perfused organs) reach partial pressures of about 0.5% during the experiments. And the slowest compartment (fat) reaches only about 0.01%.

The system matrices in the new coordinates are

$$\bar{A} = T^{-1}AT \qquad \bar{B} = T^{-1}B \qquad \bar{C} = T_y^{-1}CT.$$

With this coordinate transformation the recoverability measures listed in table 7.3 are obtained. The values indicate the following. First, there is only weak recoverability from a failure of the

fault	possible remedial actions
vaporizer fault	- fallback to manual dosing
leaks	- switch to predefined controller for lower freh gas flow
	- fallback to manual dosing
blood pressure measurement	- switch to a non invasive blood pressure measurement
	- switch to endtidal concentration controller
concentration measurements	- switch to blood pressure control
	- switch to open loop electronic dosing

Table 7.4: Remedial action possibilities for the different fault scenarios.

MAP measurement. This is a result of the missing coupling of disturbance related states to the anesthetic related states (see equation 3.110). Further, if either the endtidal or the inspiratory measurement failed the recoverability measure indicates that state estimation and a possible reconstruction of the faulty output is possible. However, as was discussed it must be assumed that inspiratory and endtidal measurement are equally affected by faults. Therefore, although, the structural representation (3.110) and a check of the observability matrix suggest that the system is still observable the recoverability measure indicates that most of the observability is lost. This means that an observer using the MAP measurement only would basically result in an "open loop" observer for the states for the partial pressures of volatile anesthetics.

7.7   Selecting the remedial actions

Since the control system is not recoverable from a blood pressure measurement failure the blood pressure control objective can not be achieved as originally desired. There are predominantly two remedial action possibilities. One possibility is to use a non-invasive blood pressure measurement instead of the invasive one. The second remedial action would be to switch back to endtidal control. This requires that a meaningful fallback endtidal reference value has been specified by the anesthetist.

In case of a failure of the concentration measurement also mainly two remedial actions are possible. One action would be to change to MAP control the other action would be to switch to open loop electronic dosing. Note that, switching back from endtidal control to inspiratory control is not a valid alternative since both concentration measurements are affected by the fault.

The different remedial action possibilities are listed in table 7.4. From these a final selection for the implementation must be made. The reasons for selection are discussed in the following sections.

7.7.1 Faults in concentration measurements

The recoverability measure for the concentration measurement faults (see table 7.3) reveal that endtidal control can not be continued with the MAP measurement only. The value of $\rho_o = 0.0074$ indicates that the control would be almost open loop.

In principle one could switch to an MAP controller. However, in section 4.2.3 we have stated that blood pressure control requires constraints on the endtidal concentration to be satisfied. Thus, without concentrations measurements safe MAP control is not guaranteed. This leaves switching to manual electronic dosing as the only acceptable remedial action.

7.7.2 Faults in the blood pressure measurement

Using a non invasive blood pressure measurement at first glance seems to lead to a total recovery of functionality. However, the invasive monitoring system provides a low pass filtered MAP value every $2\ s$. The non invasive cuff measurement values are provided at most every $2\ min$.

To judge whether this low sampling rate causes problems two aspects need to be considered: The closed loop bandwidth of the controller and the frequency content in the disturbance signal. The closed loop bandwidth of the MAP control loop is about $0.2\frac{rad}{min}$ (see figure 4.4). A rule of thumb states that the sampling frequency should be a factor of ten larger. The sampling frequency of non-invasive MAP measurements is $3.1\frac{rad}{min}$. Thus, from the bandwidth point of view there is no problem. The problem lies with the frequency content of the disturbances. The fact is illustrated in figure 7.6. From the parameter estimation in section 3.6 the bandwidth of the neural reaction of approximately $37\frac{rad}{min}$ was obtained. With $3.1\frac{rad}{min}$ the sampling frequency of non invasive blood pressure measurements lies a decade below this bandwidth. This represents a violation of the sampling theorem and leads to aliasing of high frequencies into the low frequency band where good disturbance rejection is required. Loosely speaking it will become impossible for the control algorithm to distinguish between fast transient disturbances and slow or permanent disturbances. Note that the problem can not just be resolved by low pass pre-filtering because of the cuff measurement. MAP control can therefore not simply be continued by replacing the invasive measurement with a non-invasive measurement. We therefore view switching back to endtidal control as the appropriate remedial action. The anesthetist will then change the endtidal reference based on occasional non-invasive MAP measurements. He/she takes care for the "low pass pre-filtering" in that case.

7.7.3 Leaks

Switching to predefined controller parameters for lower fresh gas flows in case of a leak is a "safe" remedial action. However, this will no longer work if the leak flow (FF_Δ) is close to ($FF - Q_\Delta$). To avoid these problems leaks up to $0.5\ \frac{l}{min}$ are treated by changing the controller. For larger leaks a fall back to manual dosing is performed.
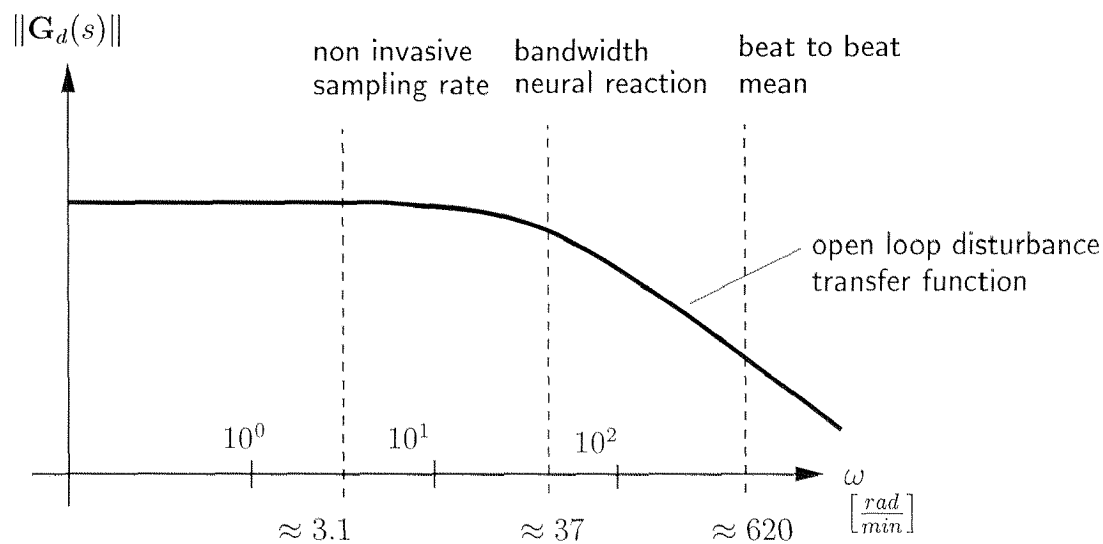
Figure 7.6: The non invasive sampling rate (≈ 3.1) violates the sampling theorem which leads to problems when attempting to use the non invasive measurement for control purpose.

7.7.4 Fault of the vaporizer

The only alternative is to fall back to manual dosing.

7.8 Fault detection and isolation (FDI)

The amount of literature published on the FDI problem which is step 5 in the design process is very large and to get a good overview is not easy. The main reason for this is that the FDI design very much depends on the conditions under which the problem is to be solved. The next section and figure 7.7 give a brief overview on different FDI designs. Rather than providing details these design methods will be classified according to their "problem domain". It will enable to select the appropriate approach for our problem.

7.8.1 Short overview on FDI designs

Classifications of different FDI schemes can be found in most survey papers [491, 221, 27, 147, 366, 148, 222]. Depending on where the focus of the survey lies this classification is slightly different. Our classification shown in figure 7.7 is a fusion of these and tailored to our case.

Similarly to the different levels for artifact treatment a first classification may be made based on the type of information used. We distinguish between knowledge based, signal based, and model based approaches. Knowledge based approaches subsume all methods utilizing only low fidelity redundancy. Signal based are all approaches that rely on a single signal to generate a residual. Approaches working with auto regressive (AR) signal models still fall into the category

FDI
[491, 27, 147, 366, 148, 222]

knowledge based
(low fidelity)
- qualitative models [289, 521]
- structural models [75]

model based
(high fidelity)

signal based
- changes in distribution [362, 287, 376]
- extensions like GLR [29]
- others [195]

nonlinear models
- observers [7, 424]
- bilinear systems [511, 314]
- descriptor systems [427]
- neural networks [123, 300]
- hybrid systems [324]

linear models

data based
[127, 325]

parameter estimation
[221]

observer based
[492, 89, 501, 122]
[251, 146, 148, 480]

parity space
[500, 244, 349, 28, 169, 168]

geometric
[312]

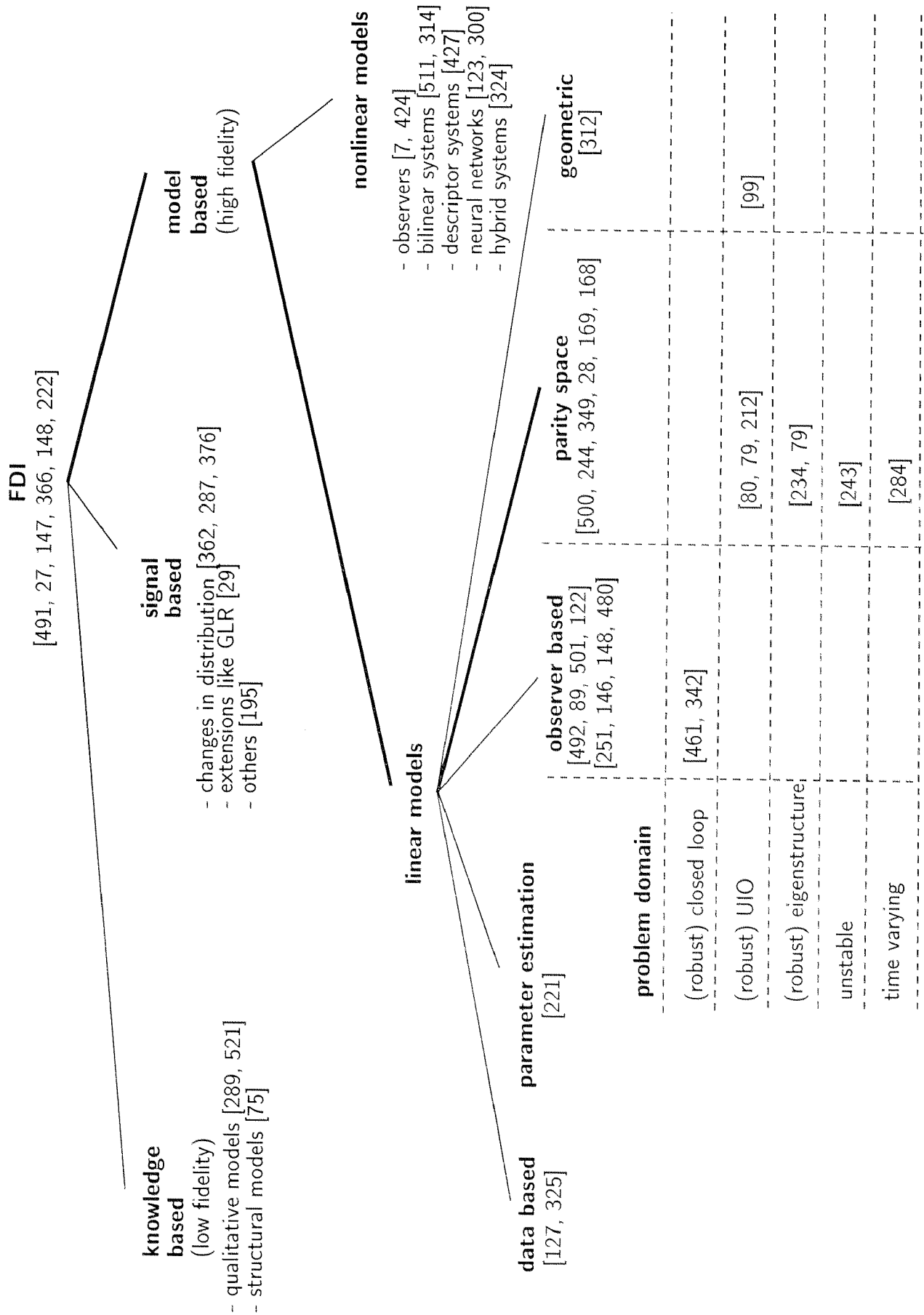| problem domain	observer based	parity space	geometric
(robust) closed loop	[461, 342]		
(robust) UIO		[80, 79, 212]	[99]
(robust) eigenstructure		[234, 79]	
unstable		[243]	
time varying		[284]	

Figure 7.7: Overview over the most common FDI designs.

of signal based methods. We only speak of model based FDI if the information of more than one signal is utilized. Among the model based FDI methods nonlinear model based FDI has only recently got considerable attention while linear FDI methods are already well established. The linear methods may further be divided into data based, parameter estimation, parity space, observer based, and geometric methods. Parity space and observer based methods are structurally equivalent [368, 168]. Parity space design can be done in the time domain or the frequency domain. Depending on further problem constraints and system properties additional special design procedures may be distinguished.

For our purpose we are interested in the methods that allow to use the state space linear model derived in chapter 3. This model is not explicitly time varying nor unstable. The robustness question in FDI does not only address the problem of model uncertainty but also of unknown disturbance inputs. In fact for unknown input observer (UIO) and eigenstructure (eigenvectors + eigenvalues) assignment [439], plant uncertainties have to be cast into unknown inputs for treatment [80, 79]. The ability of either approach to decouple the state estimation error from unknown inputs makes both methods also suitable for actuator fault detection. While the UIO and the eigenstructure design solve an open loop FDI problem, the problem of uncertainties may also be addressed for closed loop. This is done by jointly designing controller and detector in the "four degree of freedom" framework [341]. A short discussion on FDI in closed loop systems will be given next.

7.8.2 FDI in closed loop systems

FDI usually is discussed in a open loop setup. This section explains how the open loop formulation transfers to the closed loop case and what problems are encountered. The issues shall be analyzed for a general SISO control loop with a residual generated with the parity space approach as shown in figure 7.8. If there are no model/plan uncertainties, i.e. $\Delta_G = 0$ the residual response is given by

$$E(\Delta_G = 0) = F_y + GF_u. \tag{7.12}$$

This is equivalent to the residual response for the open loop formulation. In "real life" Δ_G will always be non-zero. This lead to a residual response of the form

$$E = \left(1 + \frac{\Delta_G C}{1 + C(G + \Delta_G)}\right) F_y + (\Delta_G + G)\left(1 + \frac{\Delta_G}{1 + C(G + \Delta_G)}\right) F_u$$
$$+ \frac{\Delta_G C}{1 + C(G + \Delta_G)} Y_{ref}. \tag{7.13}$$

The response sill contains contributions from the fault signals $f_u(t)$ and $f_y(t)$. They are just modified dynamically. But it also contains a contribution from the reference signal $y_{ref}(t)$. This contribution is multiplied by Δ_G. That is the contribution of the reference signal is directly proportional to the modeling errors. If disturbances were considered in this analysis they would contribute similarly.

This has consequences for FDI. First, since for any practical scenario $\Delta_G \neq 0$ the problem requires treatment. Second, it indicates the high model quality requirements for model based FDI. There
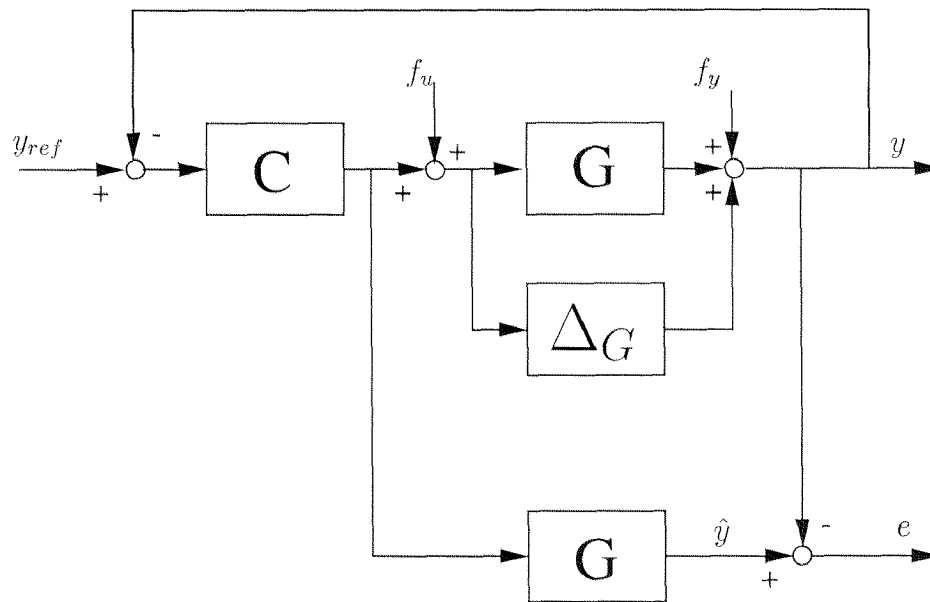
Figure 7.8: FDI in closed loop systems.

are predominantly two ways to address the problem. Either controller and detector are designed simultaneously [461] or the effects of reference changes and possibly disturbances on the residuals are taken into account in the decision process. This is done through adaptation of the detection thresholds (see e.g. [148]).

The controller/detector co-design approach [341, 461] is cogent mainly for its consistent mathematical formulation as an H_∞ problem. But it has also disadvantages. First, controller and detector always build a pair that have to be modified simultaneously. Second, the controller and detector are always obtained in form of linear transfer functions. For our experimental environment, however, it might very well be desired to only change the controller. For example it was desired to use the fuzzy controller of Derighetti [111] or new concepts such as high gain adaptive control [67] without redesigning the FDI modules. We will therefore prefer to design the detector independently of the controller by a high quality model (i.e. Δ_G as small as possible) and by compensating for the remaining modeling errors through adaptation of the threshold.

7.8.3   Existence conditions for robust FDI

Recalling the MIMO representation of the Isoflurane-MAP control system given in figure 3.1 it is seen that the FDI problem is indeed a robust FDI problem. And this mainly due to the unknown disturbances introduced by surgical stimulations. [79] provides necessary and sufficient conditions for the existence of robust observer designs. Neither for the UIO nor for the eigenstructure assignment, however, the design conditions are satisfied in our case. This fact may also be shown

using an input- output representation of the system given by

$$
\begin{aligned}
a_1(s)C_{insp}(s) &= b_{11}(s)C_{vap}(s) \\
a_2(s)C_{endt}(s) &= b_{21}(s)C_{vap}(s) \\
a_3(s)MAP(s) &= b_{31}(s)C_{vap}(s) + b_{32}(s)D_s(s).
\end{aligned}
$$

There is now way to combine above equations to derive a redundancy relation containing MAP and which is independent of d_s. For this an additional output affected by d_s would be needed. Assume for example that the beat-to-beat heart rate was given by

$$
a_4(s)HR(s) = b_{41}(s)C_{vap}(s) + b_{42}(s)D_s(s). \tag{7.14}
$$

In this case

$$
b_{42}(s)a_3(s)MAP(s) - b_{32}(s)a_4(s)HR(s) = (b_{42}(s)b_{31}(s) - b_{32}(s)b_{41}(s)) \, c_{vap}(s) \tag{7.15}
$$

would provide such a redundancy relation.

The non existence of a robust observer design may also be understood from the structural representation of the system equations (3.110) given as a block diagram in figure 7.9. Since the disturbance has no effect on the volatile anesthetics part of the system (respiratory circuit + patient) the corresponding states may be estimated independent of the disturbance influence. The problem lies with the estimation of the disturbance related states. Since MAP is the only output affected by the disturbance no redundancy is available that allows to remove the disturbance influence in the MAP measurement.

7.8.4 Structural equivalence of parity space and observer based residual generators

For detector design this equivalence will be utilized and it will therefore briefly be re-established in this section. Consider a full order state observer

$$
\begin{aligned}
\dot{\hat{\mathbf{x}}}(t) &= \mathbf{A}\hat{\mathbf{x}}(t) + \mathbf{B}u(t) + \mathbf{L}(o(t)) \tag{7.16} \\
o(t) &= y(t) - \mathbf{C}\hat{\mathbf{x}}(t) - \mathbf{D}u(t) \tag{7.17}
\end{aligned}
$$

where $\mathbf{K}$ is the output injection matrix and $o(t) = y(t) - \hat{y}(t)$. After a few manipulations one obtains

$$
O(s) = \left[\mathbf{I} + \mathbf{C}(s\mathbf{I} - \mathbf{A})^{-1}\mathbf{L}\right]^{-1} \left[Y(s) - \left\{\mathbf{C}(s\mathbf{I} - \mathbf{A})^{-1}\mathbf{B} + \mathbf{D}\right\}U(s)\right] \tag{7.18}
$$

or

$$
O(s) = H_y(s)\left[Y(s) - G_u(s)U(s)\right] \tag{7.19}
$$

which is now in parity space form with

$$
H_y(s) = \left[\mathbf{I} + \mathbf{C}(s\mathbf{I} - \mathbf{A})^{-1}\mathbf{L}\right]^{-1}. \tag{7.20}
$$

This residual filter $H_y(s)$ allows to favor certain frequencies in the residual $r(t)$. Often it is a low pass filter like a "cum sum" algorithm.
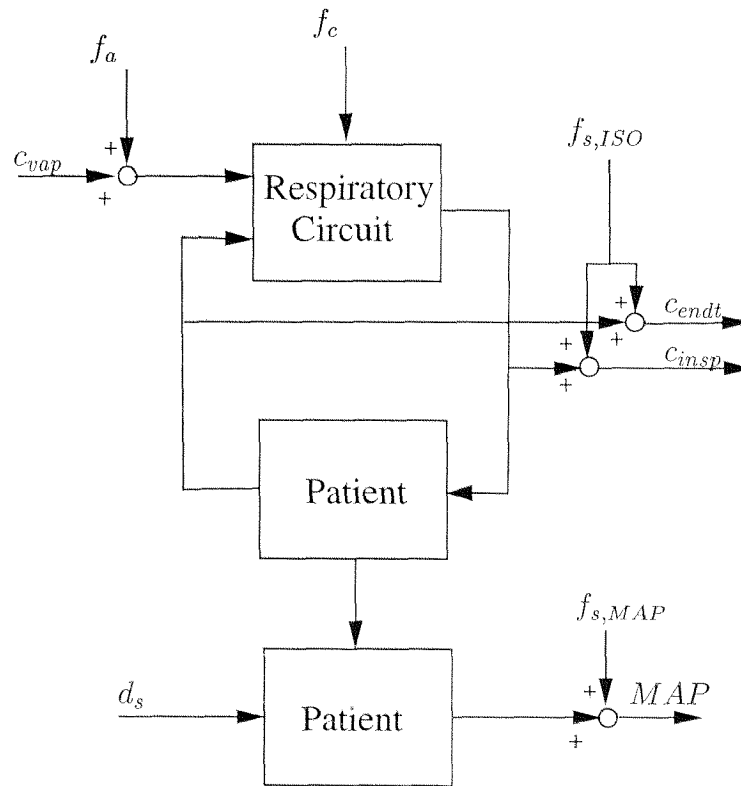
Figure 7.9: Block structure representation of the linearized system given by equation 3.110.

7.8.5 FDI design

As the couplings in the system are not rich enough for robust detector design and since the particular structure is composed of three MISO subsystems, we propose an engineering approach to the FDI problem. That is the redundancy relations provided by the different subblocks will be utilized individually rather than in a MIMO setup.

7.8.6 FDI for concentration measurement faults

To detect and isolate faults in the concentration measurements the redundancy provided by the pharmacokinetics of the anesthetic is used. From equation (3.110) we get

$$\frac{C_{endt}(s)}{C_{insp}(s)} = G_{Gas}(s) = \mathbf{C}_{endt,Gas}(s\mathbf{I} - \mathbf{A}_{Gas})^{-1}\mathbf{A}_{Gas,R} + \mathbf{C}_{endt,R}. \tag{7.21}$$

Since for this system input (c_{insp}) and output (c_{endt}) are equally affected by faults it is not obvious that this relation provides useful redundancy. But consider the general residual generator for this subsystem in parity space formulation as shown in figure 7.10. The response of the residual is given by

$$
\begin{aligned}
R(s) &= C_{endt}(s) - \hat{C}_{endt}(s) = H_{Gas}(s)\left[G_{Gas}(s) - 1\right]F_{s,ISO}(s) \\
&= H_{Gas}(s)\left[\mathbf{C}_{endt,Gas}(s\mathbf{I} - \mathbf{A}_{Gas})^{-1}\mathbf{A}_{Gas,R} + \mathbf{C}_{endt,R} - 1\right]F_{s,ISO}(s). \tag{7.22}
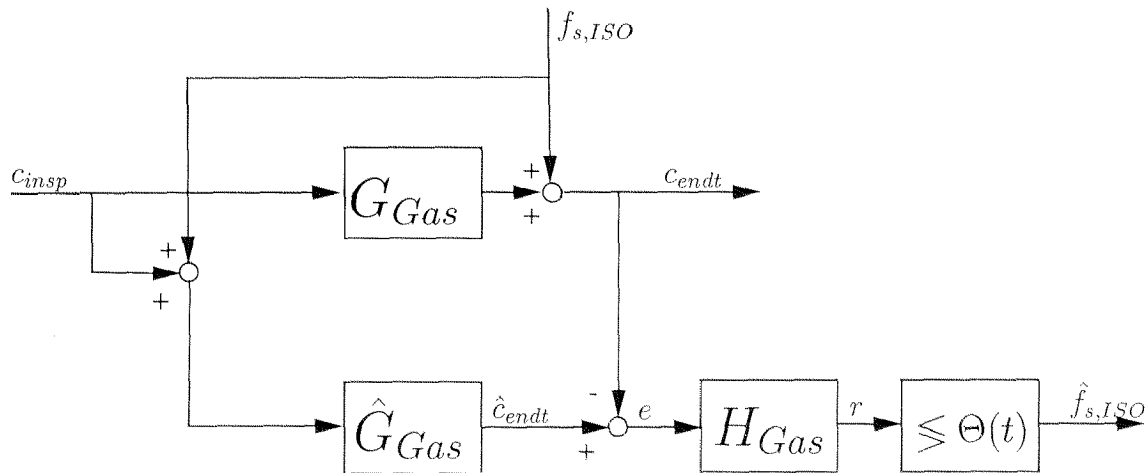\end{aligned}
$$

Figure 7.10: Residual generation for concentration measurement faults. It is given in parity space form. The residual filter H_{Gas} is obtained through proper selection an output injection matrix (see equation (7.20)). The detection itself is done by comparing the residual to a threshold.

Obviously the fault appears in the residual but the term $[G_{Gas} - 1]$ causes the response to decay quite rapidly. The residual filter $H_{Gas}(s)$ has to make sure that $r(t)$ persists long enough for a unique detection. The observer-parity-space-equivalence property allows a straight forward design for $H_{Gas}(s)$. Set

$$\mathbf{K} = -\frac{1}{1 - \mathbf{C}_{endt,R}}\mathbf{A}_{Gas,R}. \tag{7.23}$$

Note that since the respirator model of reduced order has dimension one $\mathbf{C}_{endt,R}$ is a scalar. After some manipulations we get

$$R(s) = (1 - \mathbf{C}_{endt,R})F_{s,ISO}(s) = \left(1 - \frac{V_{AD}}{V_A}\right)F_{s,ISO}(s). \tag{7.24}$$

That is with this choice of observer the residual is equal to the actual fault signal reduced by the alveolar dead space fraction. In fact, the alveolar dead space is a fundamentally limiting factor for the detectability of concentration measurement faults. To get an intuitive understanding for this phenomenon perform a thought experiment. Assume that $G_{Gas} = 1$ i.e. the alveolar dead space is equal to the total alveolar space. In this case no uptake of anesthetics occur and the endtidal concentration equals the inspired concentration. Clearly, in this limiting case it can not be distinguished between abrupt changes due to faults and changes in the input signal. Since both affect c_{insp} and c_{endt} in exactly the same manner.

A typical fault free residual response for this detector is shown in figure 7.11. The data is taken from a clinical evaluation of an endtidal controller. Two observations can be made:

- the residual is noisy

- large deviations are occurring whenever the set point for endtidal control changes.
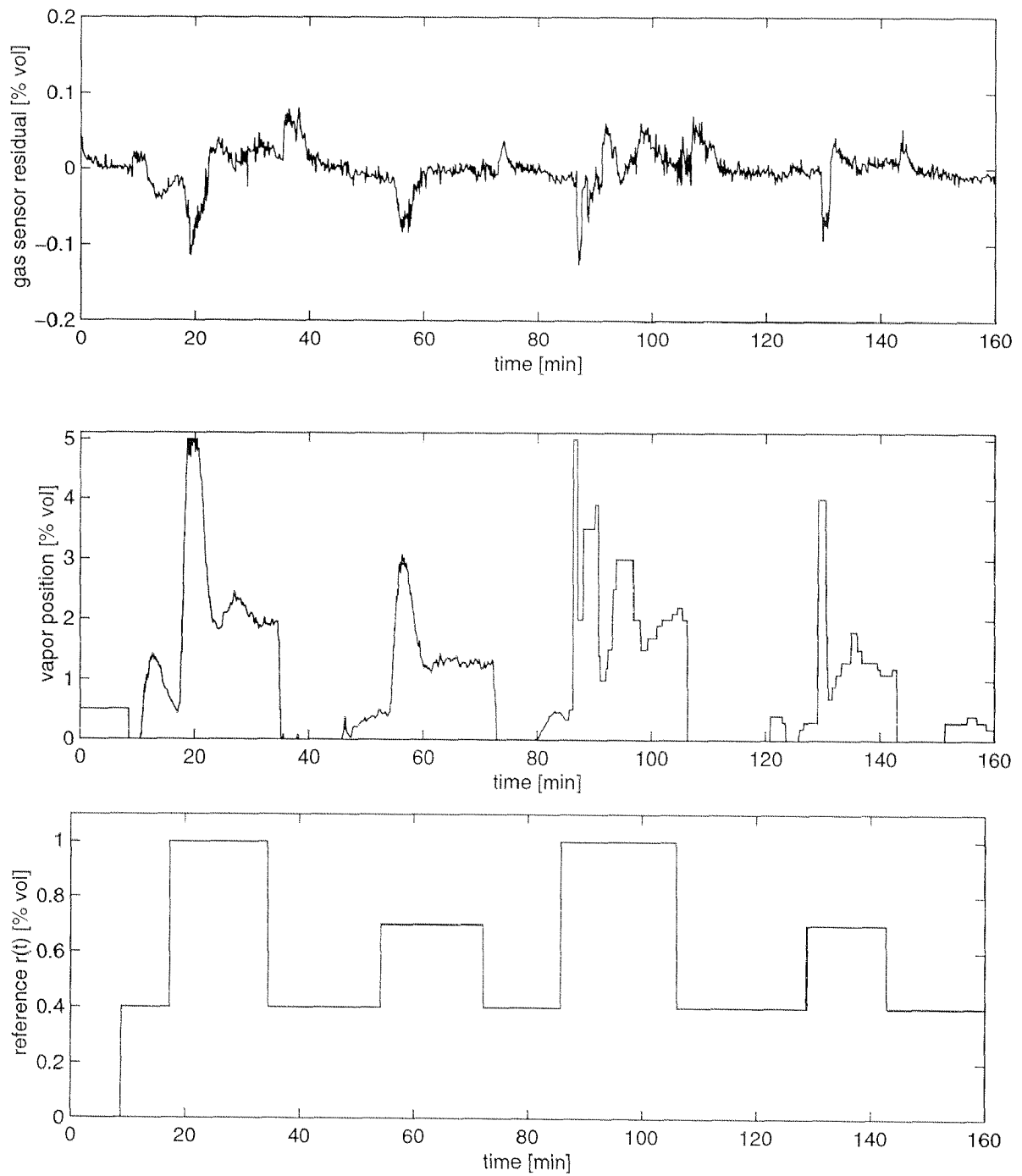
Figure 7.11: Fault free residual response for the detector of concentration measurement faults.
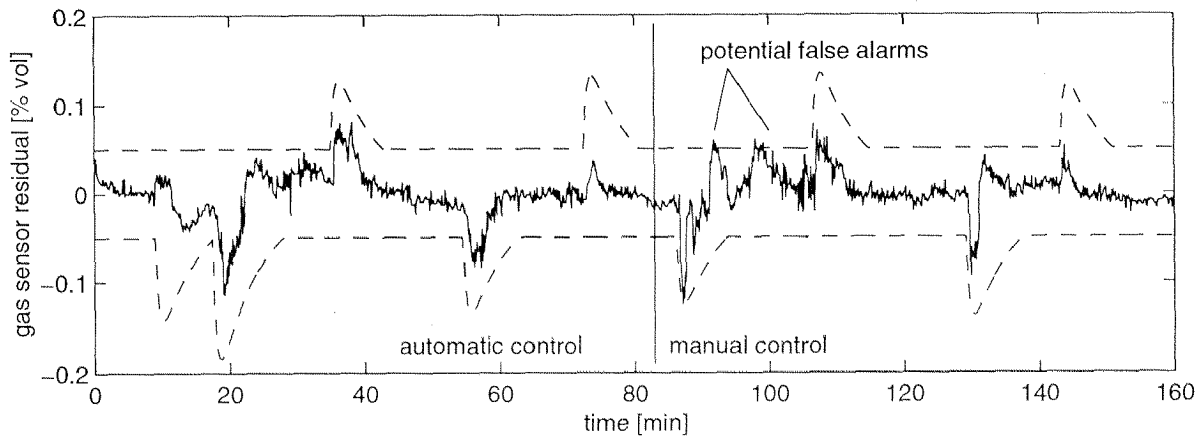
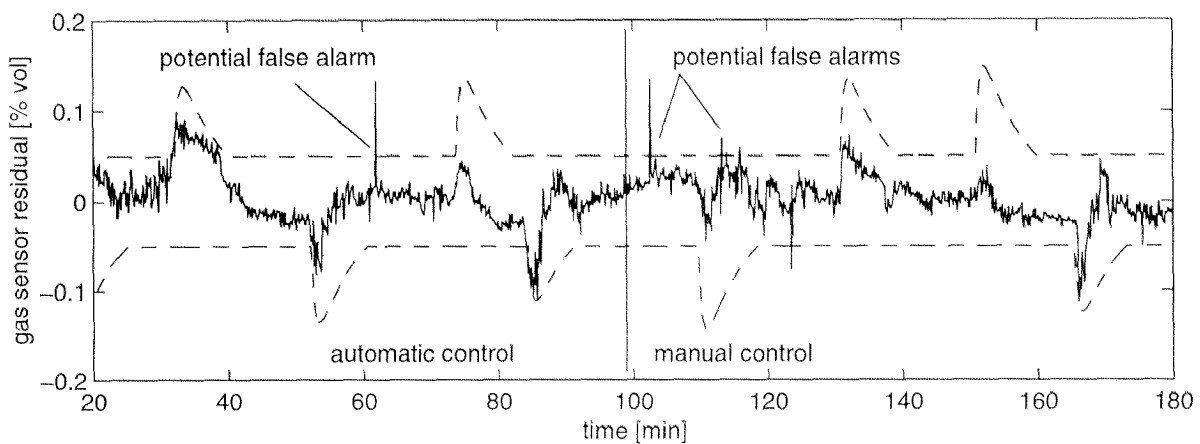Figure 7.12: Time varying fault detection thresholds for a recording of an endtidal controller applications.

Figure 7.13: Time varying fault detection thresholds for a recording of an endtidal controller applications.

The noise stems from the normal sources, it is process and measurement noise. The large deviations are a result of the model uncertainty as discussed in section 7.8.2. If FDI would be based on a fixed detection threshold (Θ_0) either the detection quality is poor if a large threshold is selected or a high false alarm rate would result for a small threshold. The observation from figure 7.11 that deviations excursions of the residual correlate with setpoint changes, however, allows to select a narrow threshold which is widened whenever the set point for control changes. This procedure is also referred to as adaptive threshold selection or threshold adaptation [148].

The upper and lower threshold are computed according to

$$\Theta^{\uparrow} = \max\{\Theta(r(t)), \Theta_0\} \tag{7.25}$$

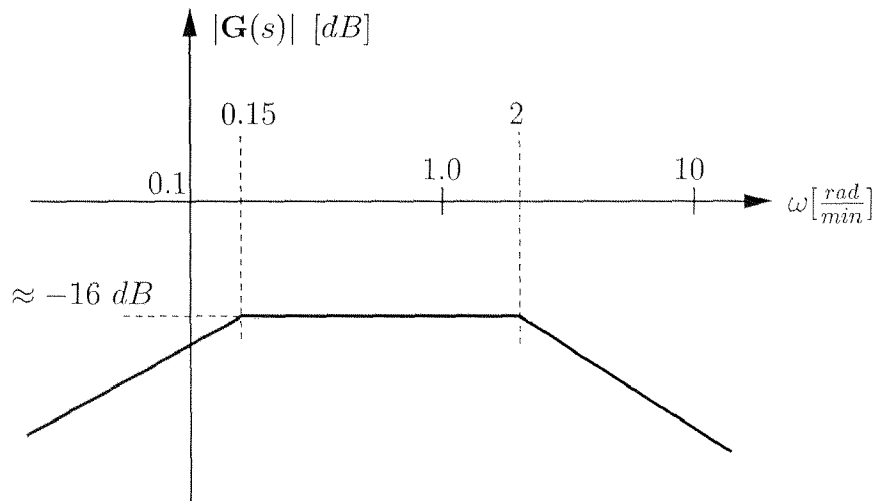$$\Theta_{\downarrow} = \min\{\Theta(r(t)), -\Theta_0\} \tag{7.26}$$

Figure 7.14: Approximation of the bode diagram for the threshold adaptation filter given by equation (7.28).

with

$$\Theta_0 \quad = \quad 0.05 \ [\% \ vol] \tag{7.27}$$

$$\Theta(R(s)) \quad = \quad \frac{-0.35s}{(s+2)(s+0.15)}\tilde{R}(s) \ [\% \ vol]. \tag{7.28}$$

In this equation $\tilde{R}(s)$ denotes the transform of a signal $\tilde{r}(t)$ where every step in $r(t)$ has been changed to a unit step. For small steps the threshold could as well be adapted proportionally to the step height. But for large steps this "normalization" of the step height accounts for the saturation of the control signal. The linear filter in equation (7.28) is implemented in discrete time using a Tustin approximation for s [150]. The filter constants were found empirically in off-line simulations. This experimental approach is necessary since the modeling uncertainties were not a priori known. In a "reverse engineering" approach the adaptation law provides information about the modeling uncertainties. For this consider figure 7.14 which shows an approximation of the bode diagram for the threshold adaptation filter. From this it is concluded that the dominant modeling uncertainties are between 0.15 and $2 \ \frac{rad}{min}$.

These time varying threshold values are shown for residuals generated for two different recordings of endtidal control applications in figure 7.12 and 7.13. It can be seen that during phases of automatic control the adaptation of the thresholds well envelopes the residual excursions. Only isolated crossings of the threshold occur that lead to potential false alarms. During phases of manual control several cases of potential false alarms are encountered. This is due to the nonlinear non-predictable character of manual control. If the FDI is supposed to work properly during manual control also the adaptation policy has to be altered. Alternatively the adaptation of the threshold could be done based on the vaporizer control signal rather than the reference signal. This strategy will be shown to work equally well in the next section.

To reduce the number of false alarms a minimum duration for the threshold violation of two minutes is introduced before an alarm is generated. Note that this also necessary since artifacts of up to two minutes are not to be treated as faults.

7.8.7   FDI for actuator faults

According to figure 7.9 the respiratory circuit equation (3.35) provides a redundancy relation which allows to detect the vaporizer faults f_a and component faults f_c. Note, however, that since both have been combined into actuator faults they can not be isolated with this relation. From the detector for concentration measurement faults described in the previous section it is known whether the signals c_{insp} and c_{endt} are correct. This allows to isolate the actuator faults via this relation. A detector in the parity space set up according to figure 7.15 is used.
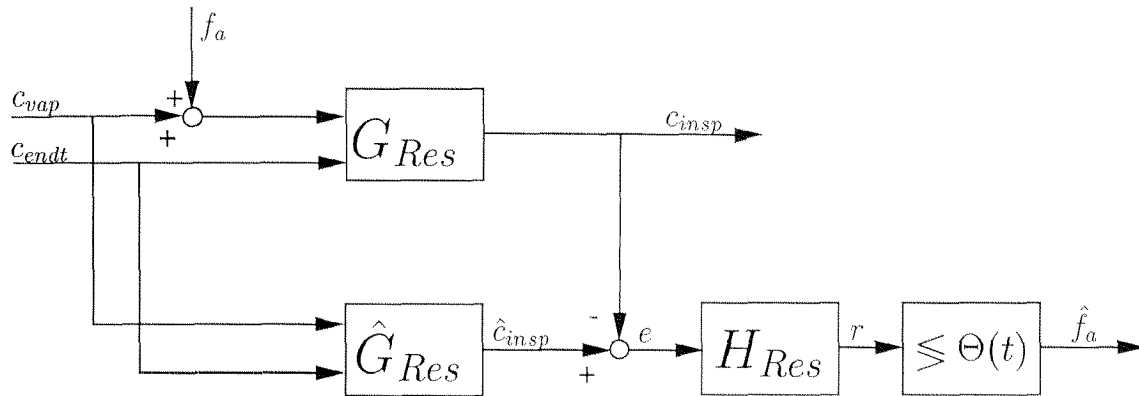

Figure 7.15: Residual generation for actuator faults.

A typical fault free residual signal is shown in figure 7.16. This residual also shows noise contamination and systematic large excursions which are correlated with reference signal changes and the vaporizer control signal. Compared to the residual of the concentration measurement fault detector the systematic excursions are much larger. This is due to larger model uncertainties for the respiratory circuit model. To optimize the power of detection and the false alarm rate an adaptation of the detection threshold is also required in this case. Since the previous section showed that the adaptation based on the reference signal only provides satisfactory results for automatic control but not for manual control an alternative approach will be used here. Since for manual control the residual is stronger correlated with the vapor signal than with the reference signal the vapor signal will be used as basis for the adaptation. The adaptation law becomes

$$\Theta^\uparrow = \max\left\{\Theta(c_{vap}(t)), \Theta_0\right\} \tag{7.29}$$

$$\Theta_\downarrow = \min\left\{\Theta(c_{vap}(t)), -\Theta_0\right\} \tag{7.30}$$

where

$$\Theta_0 = 0.1 \ [\% \ vol] \tag{7.31}$$

$$\Theta(s) = \frac{-0.6s(s+9)}{(40s+1)(s+1)}C_{vap}(s) \ [\% \ vol]. \tag{7.32}$$

The bode diagram for this threshold adaptation filter is shown in figure 7.17. It clearly shows the lower quality of the respirator model compared to the patient model. The dominant modeling uncertainties lie between 0.025 and 1 $\frac{rad}{min}$. Again the filter constants in equation (7.32) were found empirically off-line from experimental recordings.
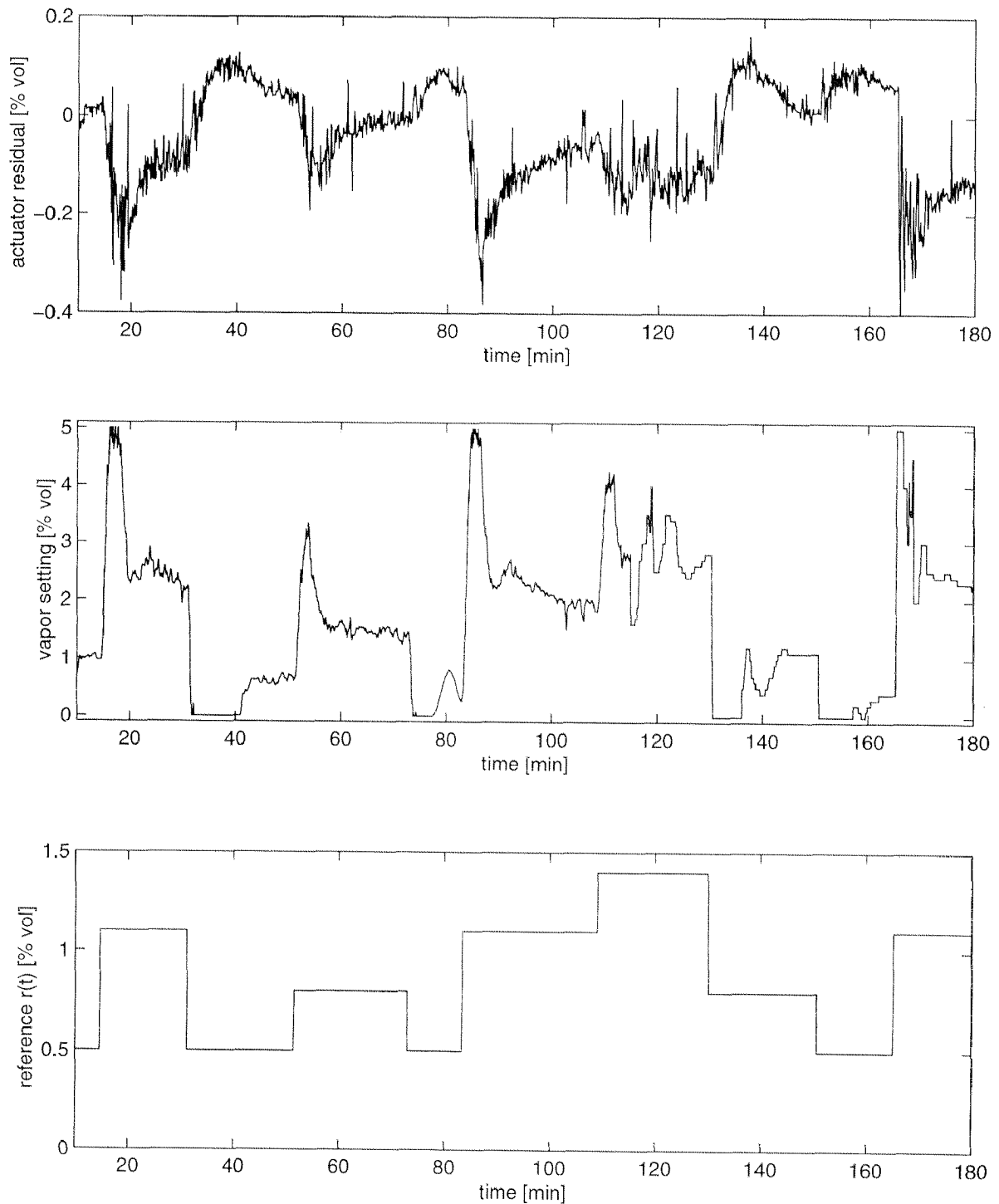
Figure 7.16: Fault free residual response for the detector of actuator faults. The data originates form an application of the endtidal controller where automatic control was active in the first part. Manual control starts at minute 116.

Figure 7.17: Approximation of the bode diagram for the threshold adaptation filter given by equation (7.32).

Two typical trajectories of residuals and thresholds are shown in figures 7.18 and 7.19. The upper plot was generated from data recorded during an endtidal controller study. The data for the lower plot originates from an MAP controller pilot study. Note that there are only single outliers that violate the threshold.

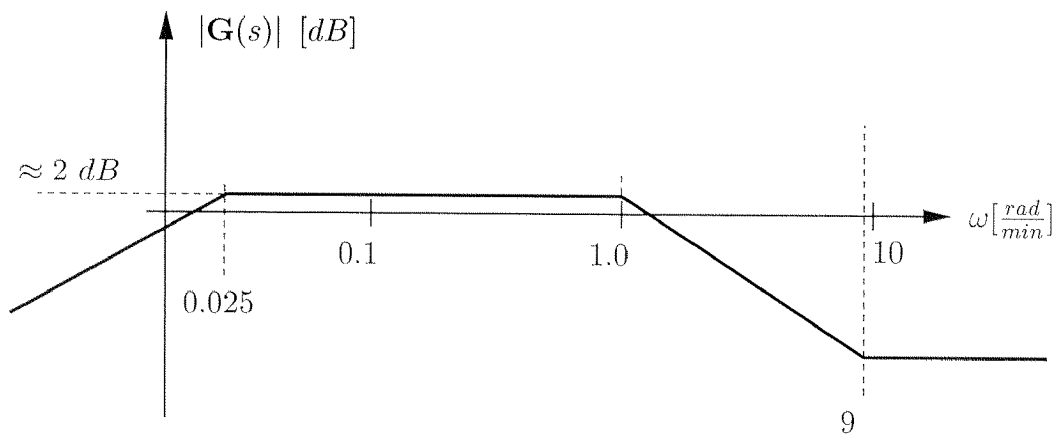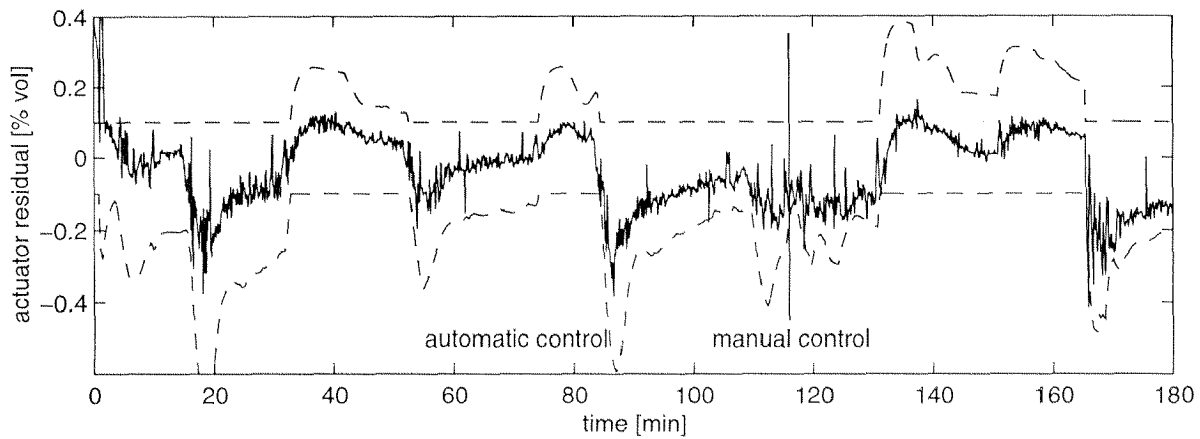Figure 7.18: Time varying fault detection threshold for a recording of an endtidal controller application. There is a potential false alarm occurring at minute 166. Since the duration is less than 2 minutes it will be suppressed.
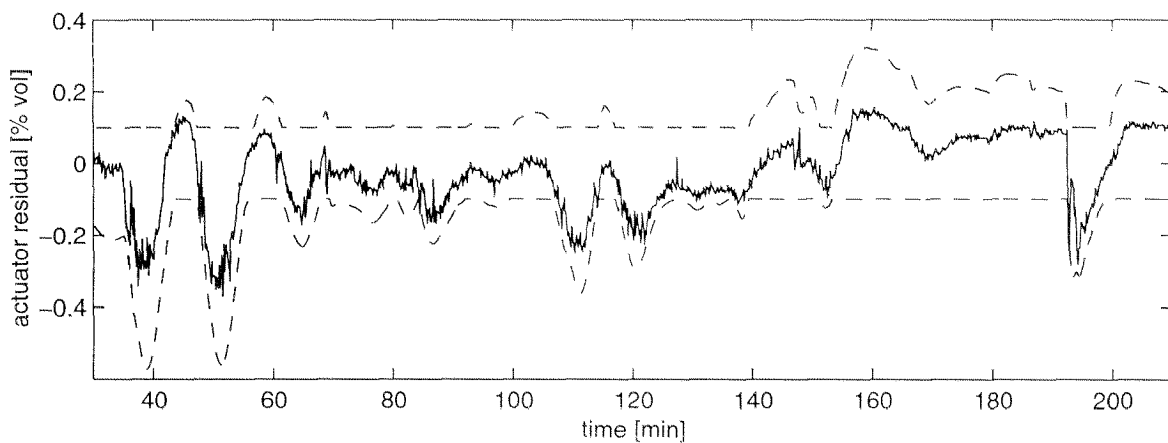
Figure 7.19: Time varying fault detection threshold for a recording of an MAP controller application.

7.8.8 Isolating component and vaporizer faults

For the design of the supervisor logic it is desirable to isolate component faults (leaks and disconnects) and vaporizer faults. The reason is simply that while the vaporizer faults require the fallback to manual dosing not all sizes of leaks require the same.

The detector design in section 7.8.7 is not able to isolate the two different type of faults. The isolation requires additional (low fidelity) redundancy. This redundancy is provided by the fact that not only volatile anesthetics follow the respiratory circuit dynamics. All components of the carrier gas do. The way to isolate component and vaporizer faults is thus to build an identical detector using the oxygen concentration measurements. Leaks will affect the residual of both detectors while vaporizer faults only affect the residual of the anesthetic detector. Assuming that no multiple faults occur, the O_2 based residual can discriminate vaporizer and component faults.

7.8.9 FDI for the blood pressure measurements

In section 7.8.3 it was shown that a classical residual generator can not be designed for validation of the MAP measurement. A straight forward but nonetheless very efficient validation can be obtained from the non-invasive cuff measurement. While less suited for closed loop control it serves very well to check the invasive measurement.

Figure 7.20 shows a blood pressure episode recorded during a routine operation. The non-invasive MAP values are marked with "o" in the upper plot. It is apparent that the slow sampling rate resulting from the cuff measurements is not able to capture most of the fast MAP variations. It is the consequence of the violation of the sampling theorem [522]. The plot shows that the non-invasive measurement is not always reliable, here in particular towards the end of the record. In addition the sampling time can occasionally differ from the nominal value (e.g. at minute 43).

In the lower plot of figure 7.20 the residuals are plotted versus time. The dashed line indicates the mean of the residuals. It shows that the non-invasive measurement on the average lies below the invasive measurement. Further, it seems that there is some correlation between residuals and disturbances, although larger errors also occur during moderately disturbed phases.

Despite these short comings of the non-invasive MAP measurement the regular comparison at the sampling instances should nevertheless allow to detect persistent measurement errors. Rather than a signal the residual may be viewed as a sequence of random values. In this environment the detector is preferably designed purely from statistical considerations.

Statistical detector design

A straight forward way to design such a detector is to compare each residual to a threshold. This threshold has to be chosen such that a acceptable false alarm rate is obtained. Figure 7.20 shows that the threshold would have to be set fairly high ($\approx 16mmHg$) to avoid frequent false alarms. But this would also lead to poor detection quality. An intuitive solution is to base the test not on a single value but on the average of m residuals. That is new "observations" o_i are generated and compared to a new threshold Θ_0 for detection. Formally this is may be written [490] as

$$o_i = \frac{1}{m} \sum_{j=1}^{m} e_{i-m+j} \geq \Theta_0. \tag{7.33}$$

where

$$e_i = MAP_i(t_i) - MAP_{ni}(t_i) \tag{7.34}$$

is the difference between the ith invasive and the ith non-invasive MAP measurement.

This intuitive detector can also be motivated by using detection theory [490] which also allows to compute detection threshold. For a detector usually two characteristic values are of interest. That is the probability of false alarms usually denoted by α and the probability of detection usually denoted by β [490]. If no assumption for the a priori probability of faults and no meaningful cost
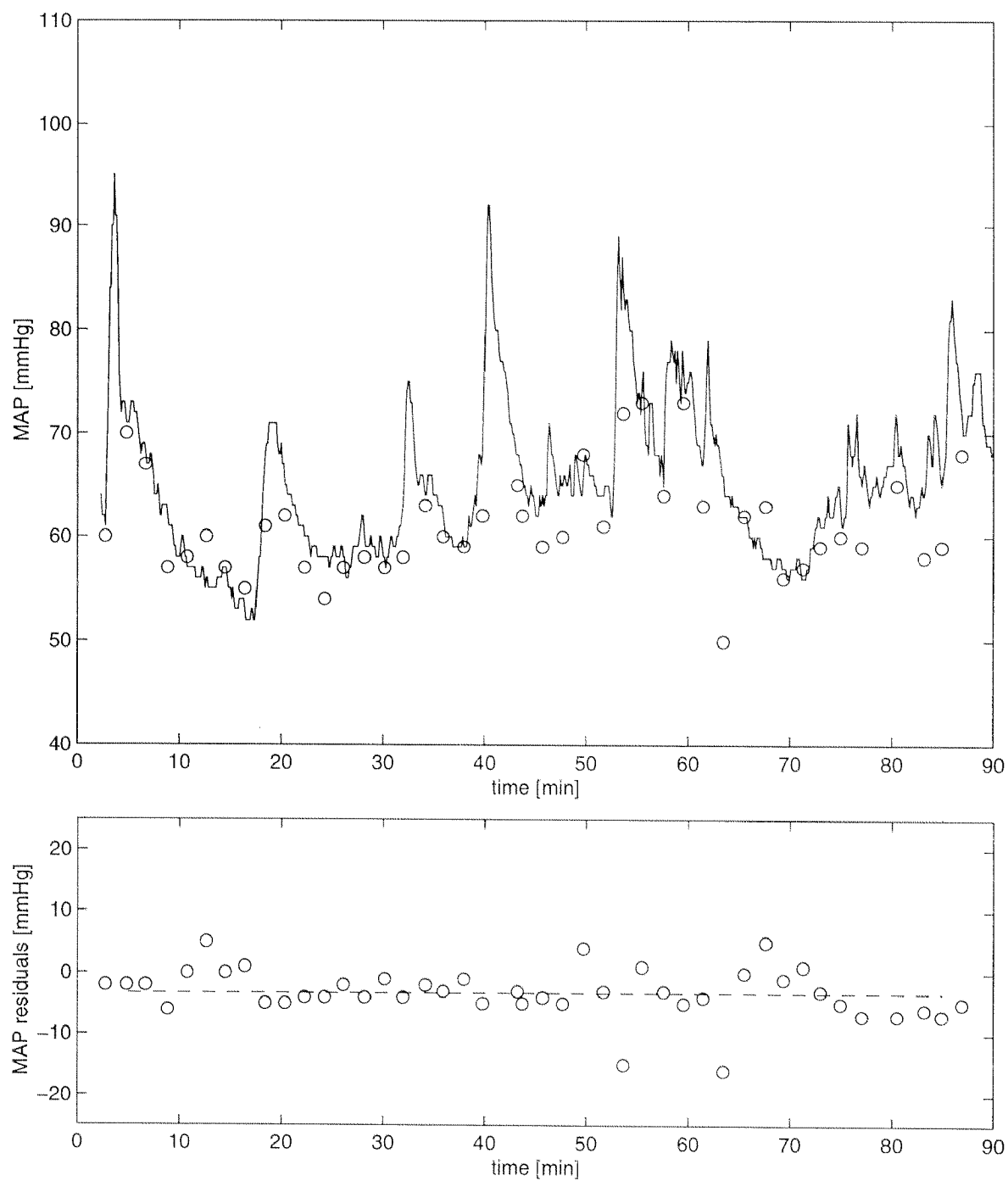
Figure 7.20: Residuals of the noninvasive blood pressure measurement.

assignment for false alarms and missed faults can be made, then detectors are often designed based on the Neyman-Pearson criterion [490]. This criterion maximizes the probability of detection for a given (specified) false alarm rate. The decision for this type of detector is performed based on the likelihood ratio $\Theta(\tilde{o})$ of an observation $\tilde{o}$ under the fault hypothesis (p_{fault}) and the no-fault hypothesis $(p_{nofault})$. A fault is declared if this ratio is larger than a fixed detection threshold $\tilde{\Theta}_0$ which is computed to satisfy the false alarm requirement specification [490]. Formally we write

$$\Theta(\tilde{o}) = \frac{p_{fault}(\tilde{o})}{p_{nofault}(\tilde{o})} \geq \tilde{\Theta}_0. \tag{7.35}$$

In the case of the MAP residual sequence an observation $\tilde{o}$ may in consist of several residuals. I.e.

$$\tilde{o}_i = \{e_{i-m}, e_{i-m+1}, \cdots, e_i\}. \tag{7.36}$$

Assume that the residuals e_i are independent and normally distributed with

$$p_{\Delta niBP}(e) = \mathcal{N}(\mu, \sigma) = \frac{1}{\sqrt{2\pi}\sigma} e^{-\frac{(e-\mu)^2}{2\sigma^2}}. \tag{7.37}$$

From clinical data $\sigma \approx 3.73\ mmHg$ and $\mu \approx -2.9\ mmHg$ may be estimated. Then the sufficient statistic [490] for the decision (7.35) is the sample mean of the individual residuals e_{i-m} to e_i [490]. So that the decision alternatively becomes

$$o_i = \left\{ \frac{1}{m} \sum_{j=1}^{m} e_{i-m+j} \right\} - \mu \geq \Theta_0. \tag{7.38}$$

The new decision threshold Θ_0 has to be chosen such that the false alarm specifications are satisfied. This leaves two parameters which have to be determined: The length of an observation m and the threshold Θ_0. To determine these parameters from false alarm specifications the probability of a false alarm during a surgical operation of average length is computed. Let N denote the number of residuals for an average operation. Normally a non-invasive measurement is obtained every $2\ min$. From table 4.1 an average duration for surgical operations of $218\ min$ is estimated. Which corresponds to $N \approx 109$. Let e denote the vector of MAP residuals and let o denote the vector of observations given by equation (7.38). e and o are related by

$$o = \mathcal{P}e \tag{7.39}$$

where $\mathcal{P} \in \mathbb{R}^{N-m+1 \times N}$

$$\mathcal{P} = \frac{1}{m} \begin{bmatrix} 1 & \cdots & 1 & 0 & 0 & 0 & \cdots & 0 \\ 0 & 1 & \cdots & 1 & 0 & 0 & \cdots & 0 \\ & & & & \ddots & & & \\ 0 & 0 & 0 & \cdots & 0 & 1 & \cdots & 1 \end{bmatrix}. \tag{7.40}$$

The probability density function for o under the no fault hypothesis is then

$$p_{nofault}(o) = \mathcal{N}(0, \mathcal{P}\Sigma\mathcal{P}^T). \tag{7.41}$$

The probability of a false alarm during an operation is the probability that any $o_i > \Theta_0$ computed as

$$\alpha(m, \Theta_0) = 1 - \int_{\boxdot(N-m+1,\Theta_0)} \mathcal{N}(0, \mathcal{P}\Sigma\mathcal{P}^T) d\mathbf{o} \qquad (7.42)$$

where $\boxdot(N - m + 1, \Theta_0)$ denotes the $N - m + 1$- dimensional hyper cube centered at the origin and length $2\Theta_0$.

The false alarm probabilities for different observation lengths as a function of the detection threshold are shown in figure 7.21. Selecting

$$m = 2 \quad \text{and} \quad \Theta_0 = 2.15 \; \sigma. \qquad (7.43)$$

we obtain a probability of false alarm of 10%. This corresponds roughly to one false alarm every 10 operations.

Figure 7.22 shows the performance (probability of detection) of this detector. The probability of detecting faults of different sizes is plotted versus the different fault sizes.
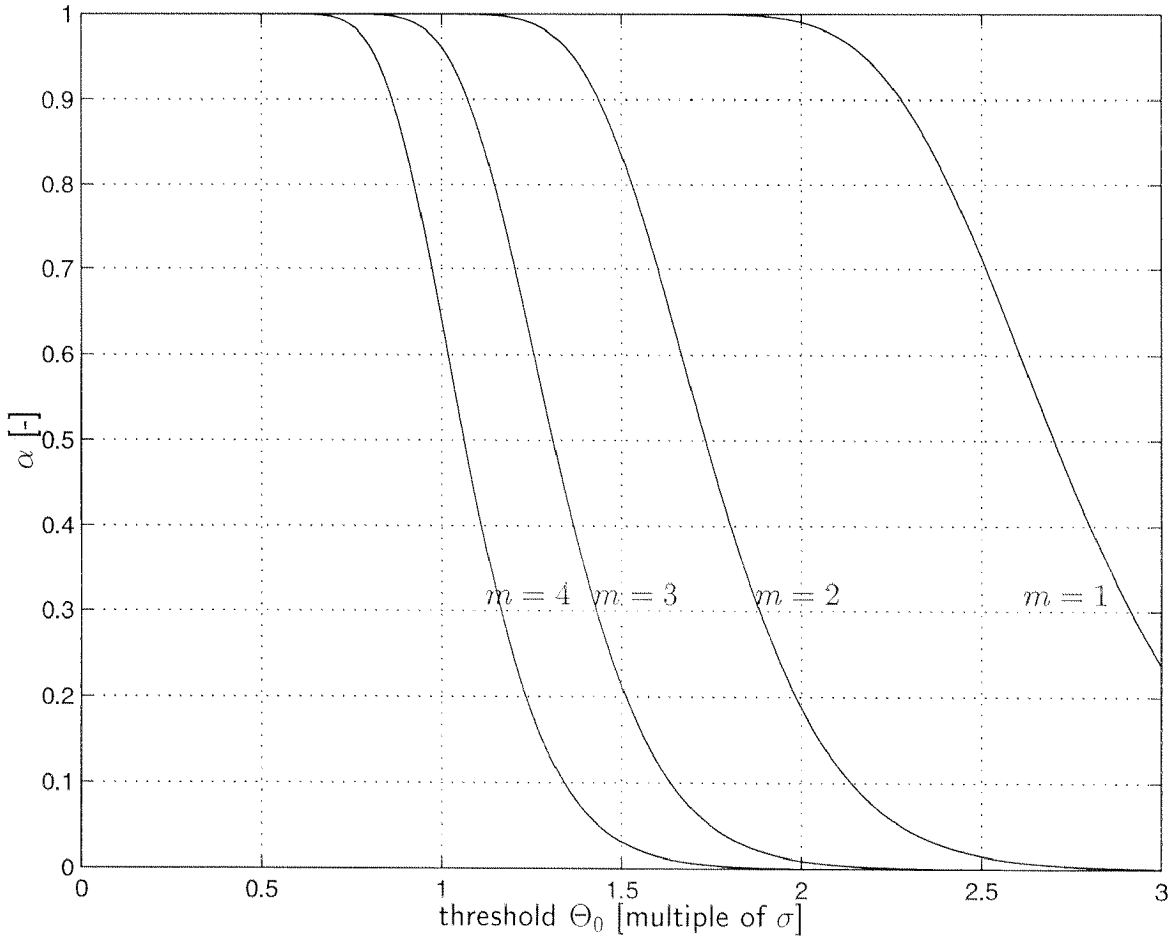
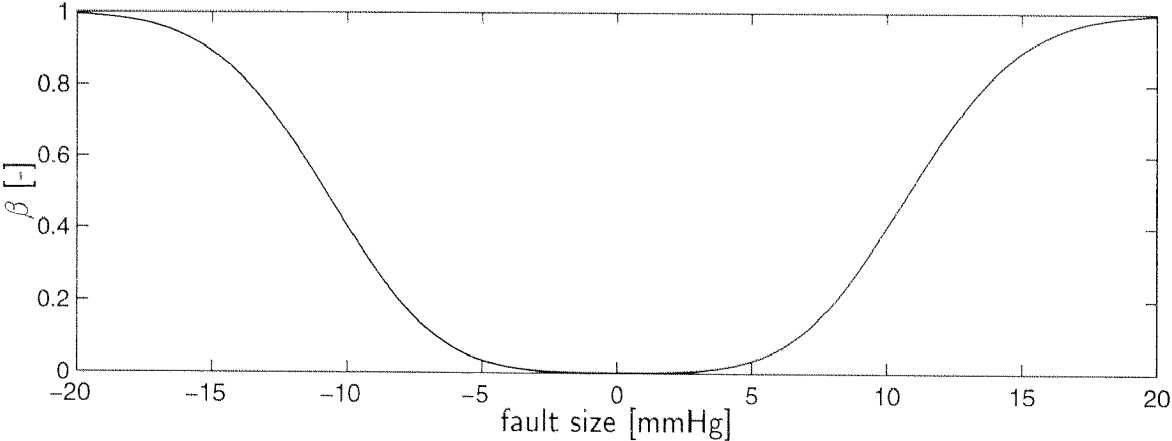Figure 7.21: Probability of a false alarm during an operation.

Figure 7.22: Probability of detection β for different constant faults in the MAP measurement.

7.8.10 Supervisor logic control design

With the design of the supervisor logic control we have reached step 6 of the design procedure. There are basically two tasks to be performed in this step. First, for any possible residual combination an appropriate remedial action must be assigned. And second, the SLC for mode control from section 4.3 must be extended to incorporate the resulting transitions.

The assignment of residual responses and remedial actions are summarized in table 7.5. The table assigns for every SLC state and residual combination a transition event σ_i. SLC states to which a certain event applies are marked with "+" the others are marked with "-". For the residual combinations a "1" denotes a residual indicating a fault, a "0" denotes a residual indicating no fault, and "x" denotes a residual which is not relevant for the transition.

Translation of table 7.5 into the extended state automaton is shown in figure 7.23. The notation for the transitions is the same as introduced in section 4.3. I.e.

$$\textbf{fault event}[condition] : action. \tag{7.44}$$

State transitions that are already implemented to occur autonomously are drawn with solid lines. Dashed lines indicate state transitions which are up to now only suggested by means of a warning and where the actual transition has to be invoked by the anesthetist.

transition event	$f_{s,MAP}$	$f_{s,ISO}$	$f_{a,vap}$	f_{a,O_2}	"PASSIVE"	"DOSING"	"ENDTCTRL"	"MAPCTRL"	action
σ_A	0	0	0	1	-	+	+	+	give leak warning
σ_B	x	x	1	0	-	+	+	+	fallback to manual control
σ_C	x	x	1	1	-	+	+	+	adapt controller parameters for leak
σ_D	0	1	0	0	-	-	+	+	switch to electronic dosing
σ_E	0	1	0	x	+	+	-	-	disable controllers
σ_F	1	0	0	0	-	-	-	+	switch to endtidal control
σ_G	1	0	0	0	+	+	+	-	disable MAP controller
σ_H	1	0	0	1	-	-	-	+	switch to endtidal control, give leak warning
σ_I	1	0	0	1	+	+	+	-	disabel MAP controller, give leak warning

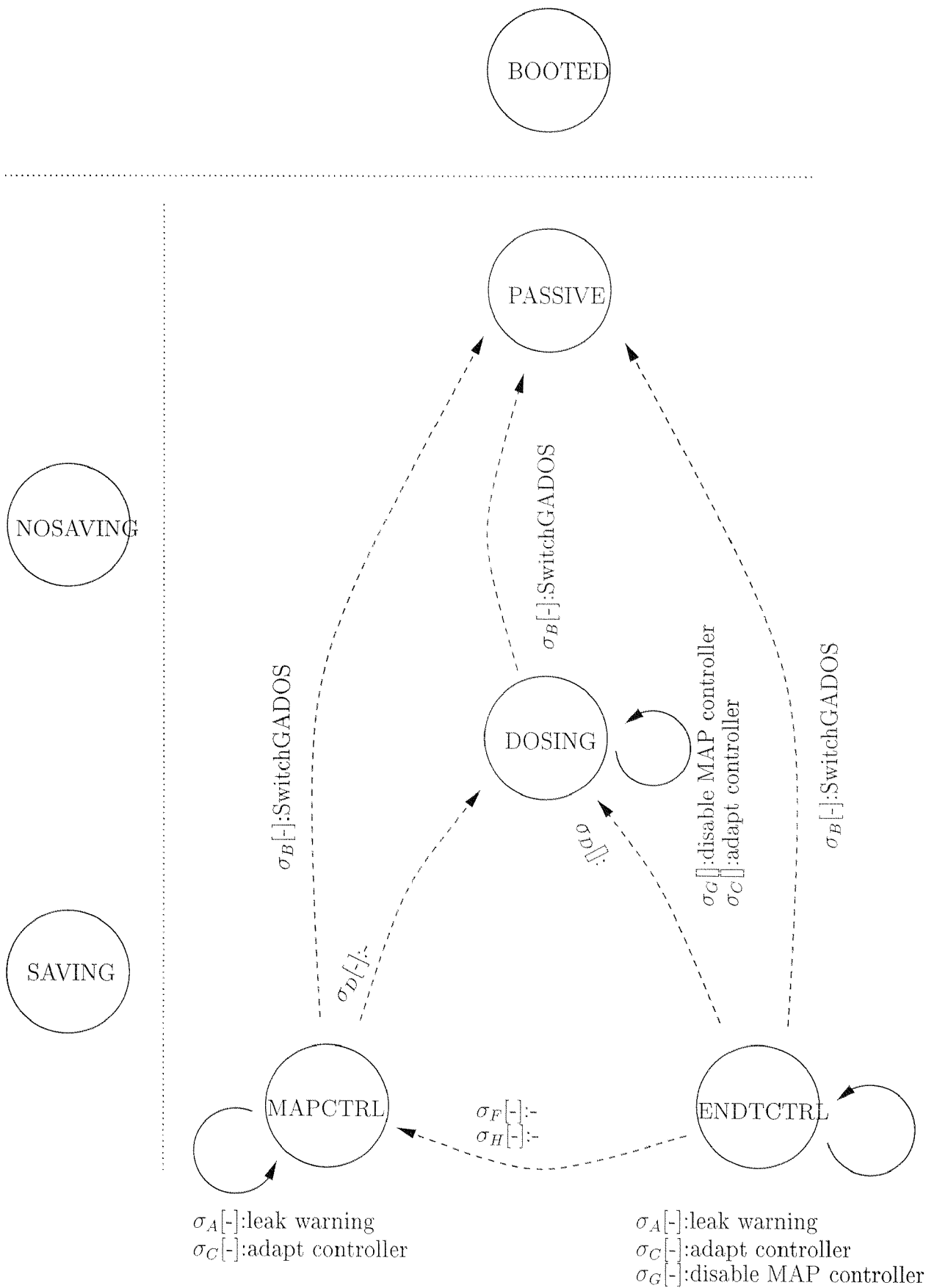Table 7.5: State transitions for supervisor logic.

Figure 7.23: Extensions of the FAS to include the FTC possibilities.

7.9   Off line testing

We have finally reached step 7 of the design procedure. The step will be divided in an off line testing and an in vivo testing.

Before performing in vivo tests confidence about the proper detection of faults must be gained through extensive off line simulations. The fact that in the nominal (uncertainty free) case open loop and closed loop FDI are identical allows to test the FDI performance in an open loop frame work (see also section 7.8.2 for reference). These open loop evaluations are documented in this section.

To analyze FDI performance for any possible fault signal would be very tedious. Usually representative fault models are used for this purpose instead. [168] suggests three classes of fault signals. That is

- drift faults

- jump faults

- intermittent faults.

They are representative in the sense that drift faults stand for slow varying and incipient faults, jump faults stand for fast and abrupt faults, and intermittent faults stand for what we defined as artifacts. As artifacts have already been dealt with in chapter 6 only drift or jump faults will be analyzed in the sequel.

7.9.1   Simulation evaluation of sensor fault detection performance

For the concentration measurements slow and abrupt faults may be envisioned. The detection of jump as well as drift faults has thus to be tested. Besides the fault types also their sizes have to be specified. Since there is no clinical or manufacturer data available giving a realistic size for these faults we decided to specify a rather hard detection problem. For the jump fault detection test a fault size of 0.1 $[\% \ vol]$ is chosen. In our opinion this is reasonable since 0.1 $[\% \ vol]$ is usually the displayed resolution of concentration measurements by monitors. For the drift fault detection test a slope of 0.01 $[\% \ vol/min]$ is chosen. A slope which is even difficult to detect for an anesthetist.

Figure 7.24 shows representative detection scenarios. In the upper plot the detection of a jump fault is shown and in the lower plot the detection of a drift fault is shown. It can be seen that the jump fault of size 0.1 $[\% \ vol]$ produces a residual response which is large enough and persists long enough to be detected. In case of the drift fault it is important to note that after about $10min$ the residual is large enough to be uniquely detected. After this time the fault has only reached the size of 0.1 $[\% \ vol]$.
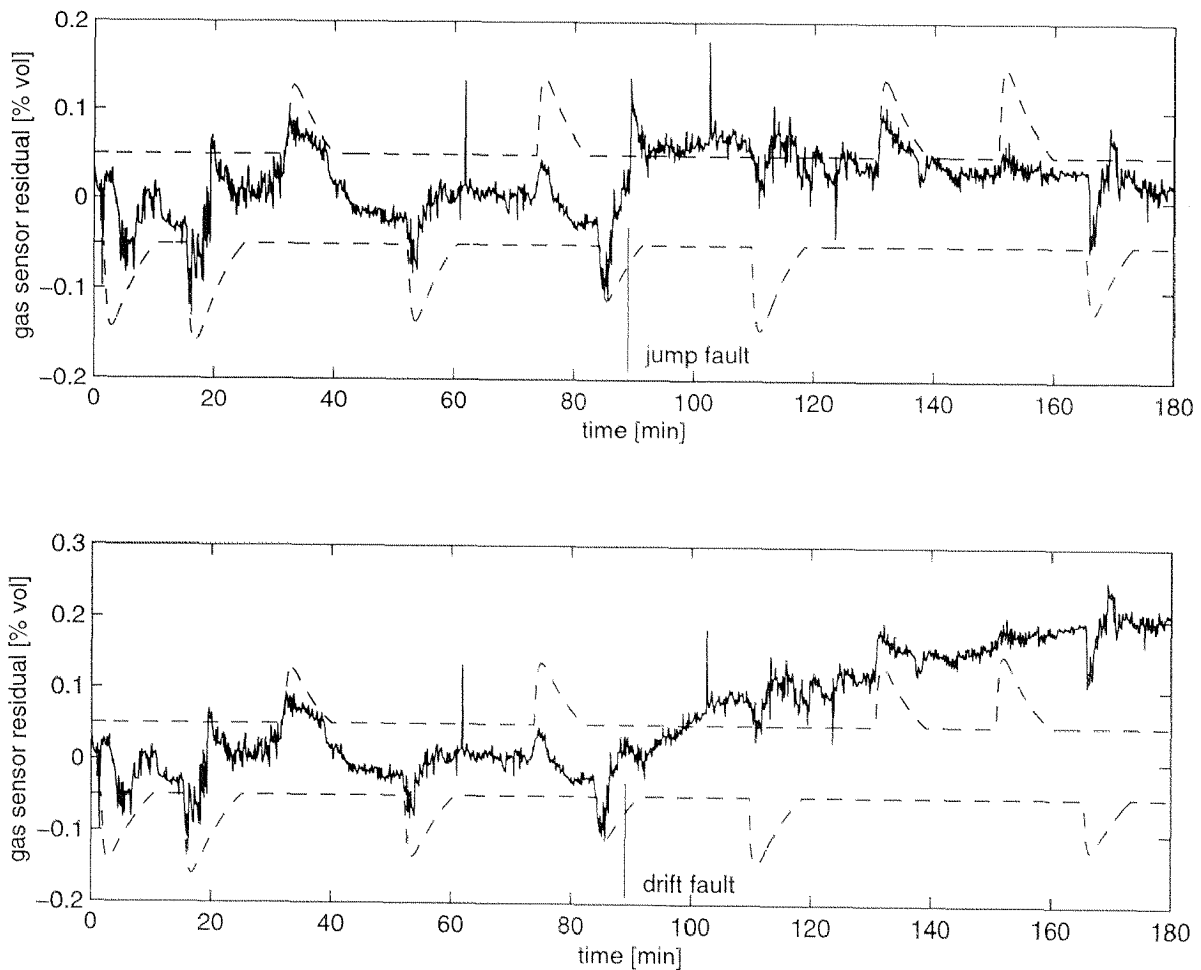
Figure 7.24: Detection performance of jump and drift faults in concentration measurements. The height of the jump fault in the upper plot is 0.1 $[\%vol]$ occuring at $t_f = 89$ min. The slope of the drift fault in the lower plot is 0.01 $[\%vol/min]$ starting at $t_f = 89$ min also.

7.9.2 Testing vaporizer fault FDI

For testing the vaporizer fault detector it is not necessary to rely on hypothetic fault signals like jumps of drifts. For simulation testing the fault signals for an empty or stuck vaporizer are easily obtained from the recorded vaporizer control signal. Let the vaporizer signal be denoted by $c_{vap}(t)$ then the fault signal for a "stuck vaporizer" is

$$f_{a,stuck} = f_0 - c_{vap}(t) \tag{7.45}$$

and the fault signal for an empty vaporizer is

$$f_{a,empty} = -c_{vap}(t). \tag{7.46}$$

The typical detection results for these two faults are shown in figure 7.25.

It should be noted that the detection performance for these two faults types may depend on the maneuver performed. Consider a maneuver for an endtidal controller where the endtidal setpoint changes from 1 % to 0.5 %. To track this setpoint the controller will close the vaporizer for some time. If the vaporizer becomes empty during this period the fault can not be detected, simply because the fault signal vanishes according to equation (7.46). It is only after reputed reopening of the vaporizer that the non zero fault signal may be detected. This delay in detection is not critical, however, since the vaporizer delivers what is actually required. Similar reasoning can be applied for the case where the vaporizer is stuck during steady state phases.

7.9.3 Testing MAP sensor FDI

For testing MAP sensor FDI again the hypothetical signals drift and jump are utilized. There is again the problem of missing experimental data that would allow to chose the size of the fault signals. We therefore also decided to specify a rather hard detection problem. The size of the jump fault was taken as 5 $mmHg$. This value represents MAP errors which are not yet critical for the patient. For the drift fault a slope of 0.5 $mmHg/min$ is chosen. That is the total error after 10 min will be 5 $[mmHg]$.

Typical detection results are shown in figure 7.26. It can be seen that both faults are detected in reasonable time.
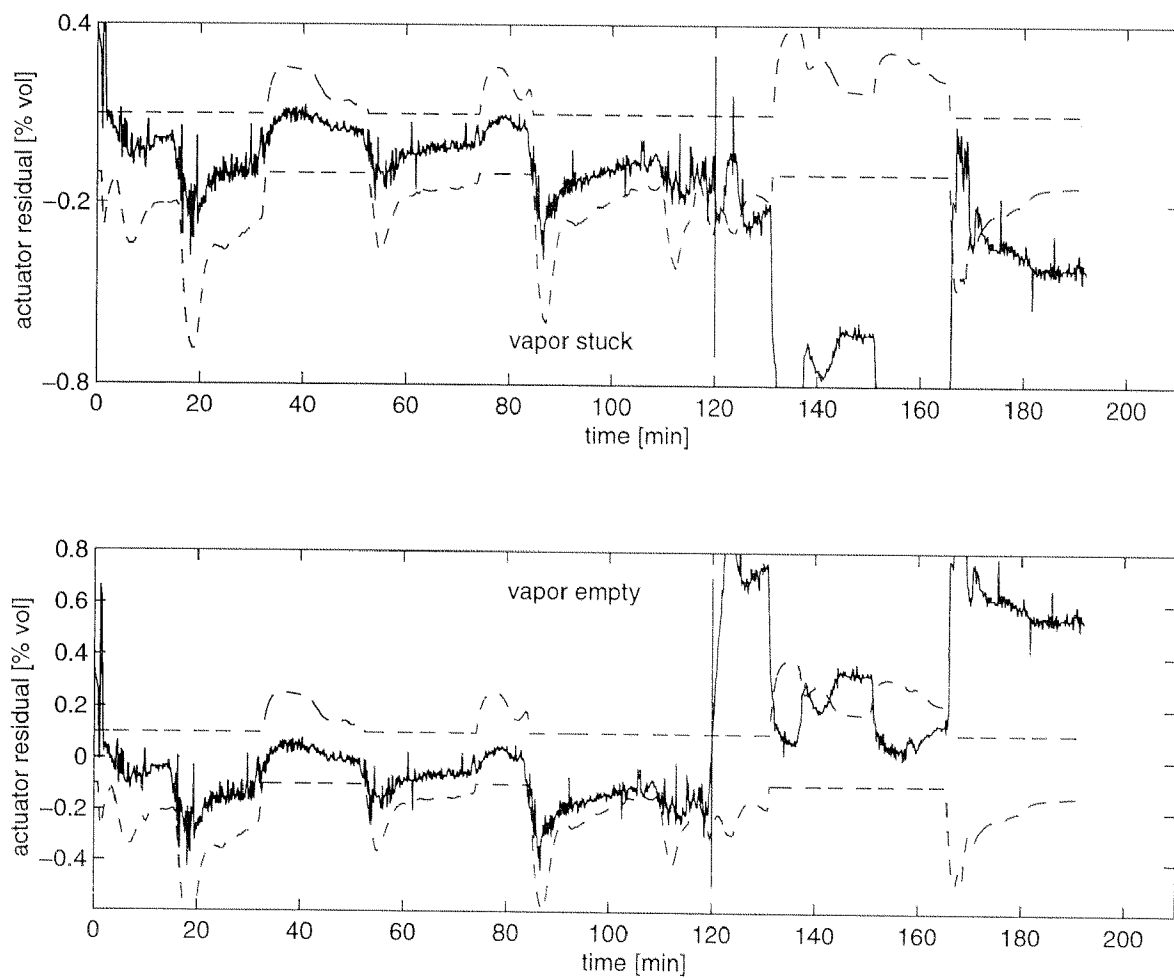
Figure 7.25: Detection results of the actuator fault detector. The upper plot shows a "vaporizer stuck" scenario and the lower plot shows and "vaporizer empty" scenario.
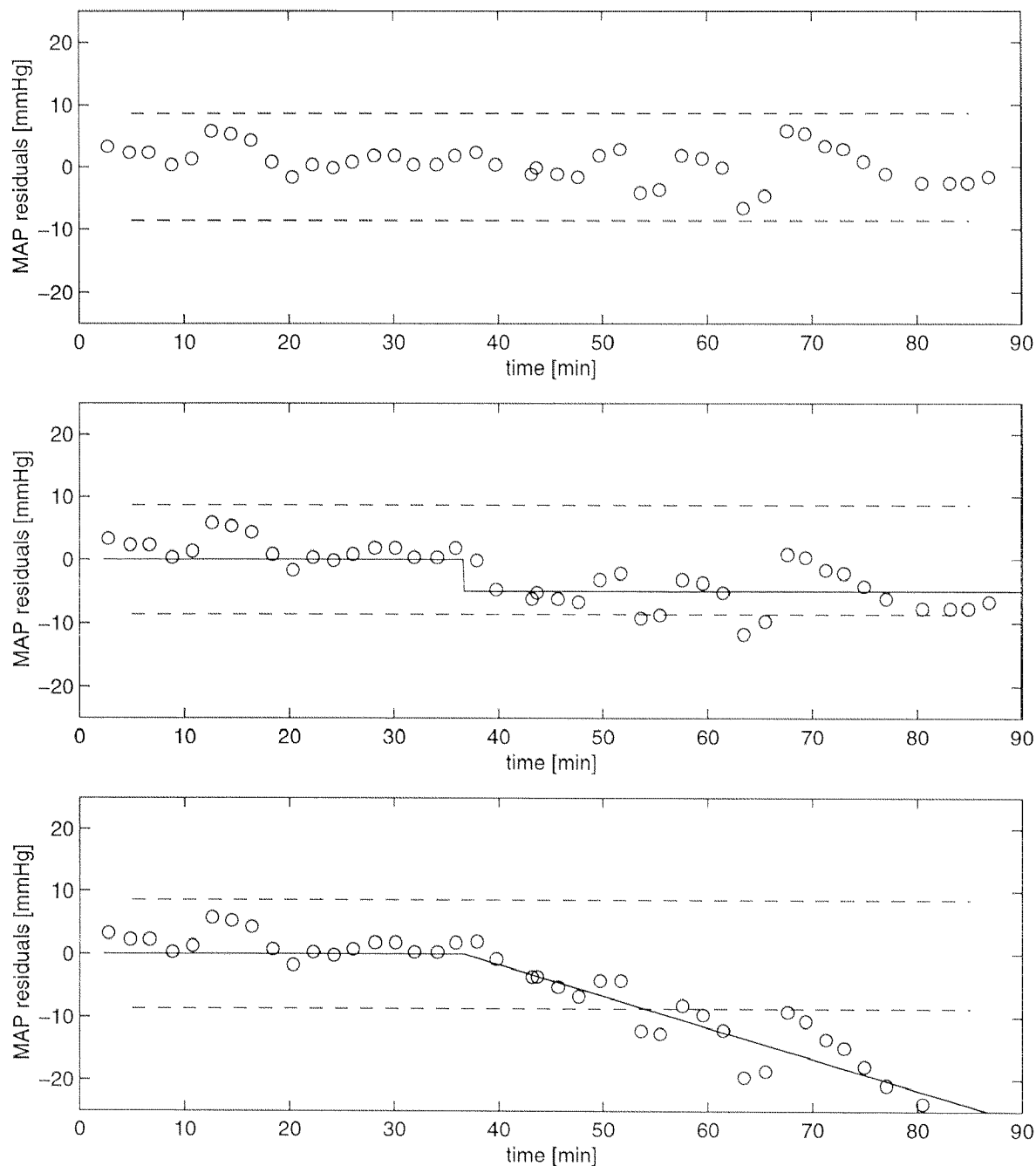
Figure 7.26: Example of detection performance for the detector based on non-invasive blood pressure measurements. Each "o" corresponds to an observation o_i given by equation (7.38). The detection thresholds are shown with dashed lines.

7.10 In vivo testing

This section presents three successful in vivo test of the FDI algorithms. The section may be viewed as step 7b of the design procedure.

The test cases included a fault for every sensor and actuator. In the first example the detection of a drift fault is demonstrated. In the second example an empty vaporizer is mimicked. And the last example shows the detection of a jump fault in the invasive blood pressure measurement. All experiments occurred under closed loop conditions.

To mimic the drift fault a ramp signal has been added to the inspiratory and exspiratory concentration measurements in the PM8060 device driver (see figure 2.10 for reference). The result of this fault scenario is shown in figure 7.27. The fault starts at minute 246 and it ends immediately after the detector has registered a clear crossing of the threshold. The drift signal is $0.01\ \%vol/min$. This corresponds to an error of 0.15% at the time of detection.
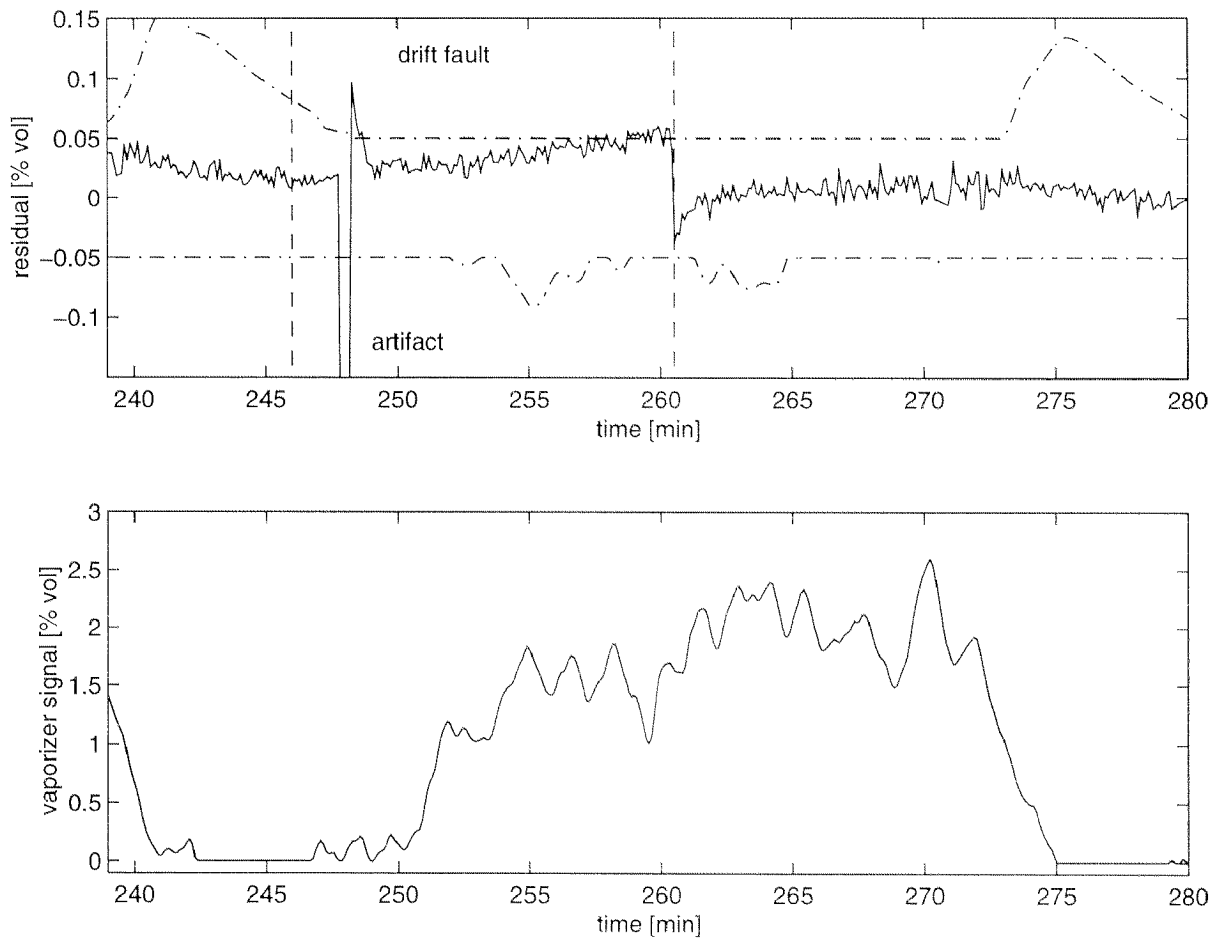
Figure 7.27: Detection example for a drift fault on the gas sensor. The drift is stopped after successful detection. Note how easily an artifact is detected compared to the slow drift fault.

The empty vaporizer was mimicked by switching off the power supply for the electro mechanic vaporizer and then closing it manually. The result of this fault scenario is documented in figure 7.28. The vaporizer is closed at minute 125 and power is switched on again after the detector had given clear indication for an actuator fault.
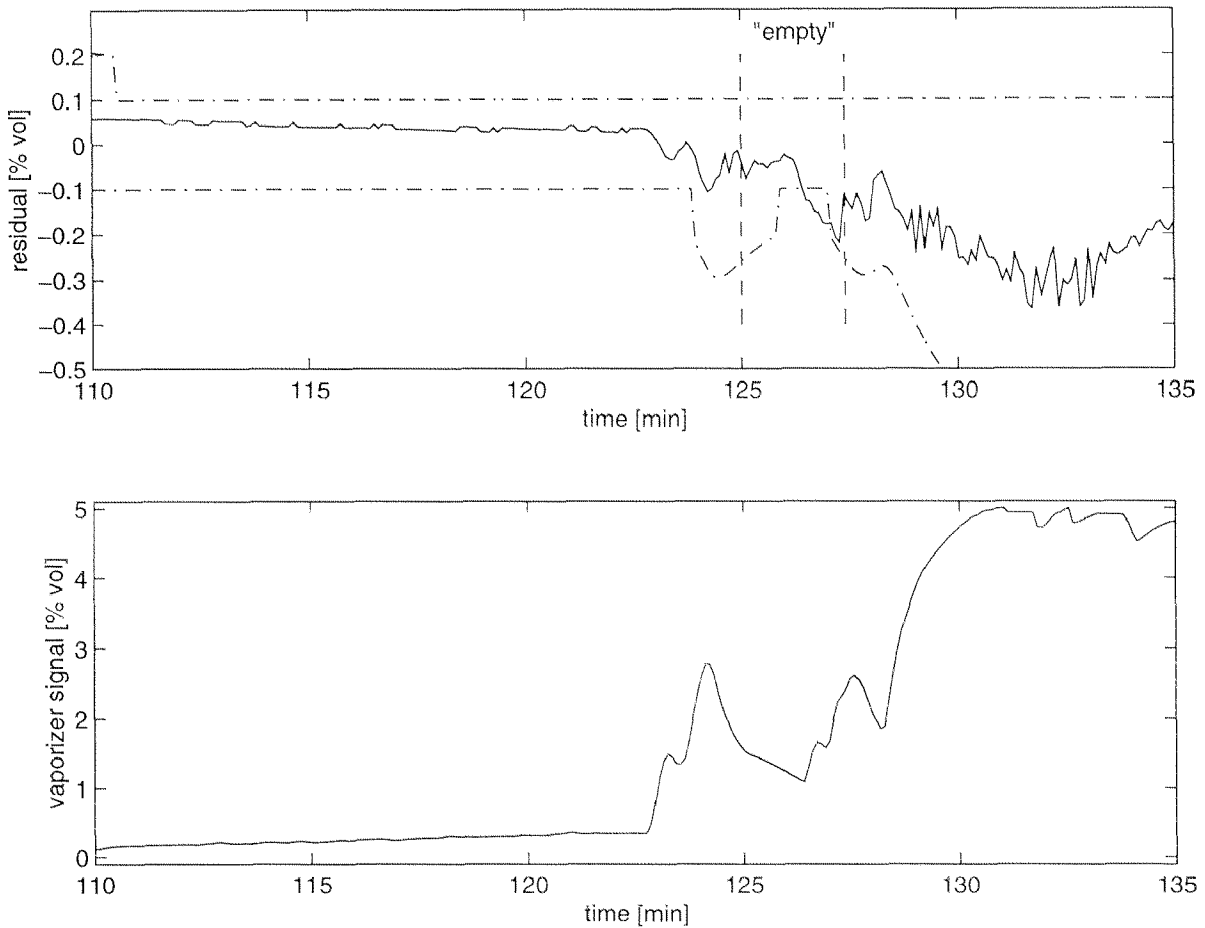
Figure 7.28: Detection result of the actuator fault detector. The duration of the "empty" fault is indicated by the vertical dashed lines.

Finally, the blood pressure measurement fault was mimicked by shifting the level at which the transducer was mounted. It is shifted by $25\ cm$ at minute 238 and it is re-established after several consistent positive detection results. The detection result is shown in figure 7.29.
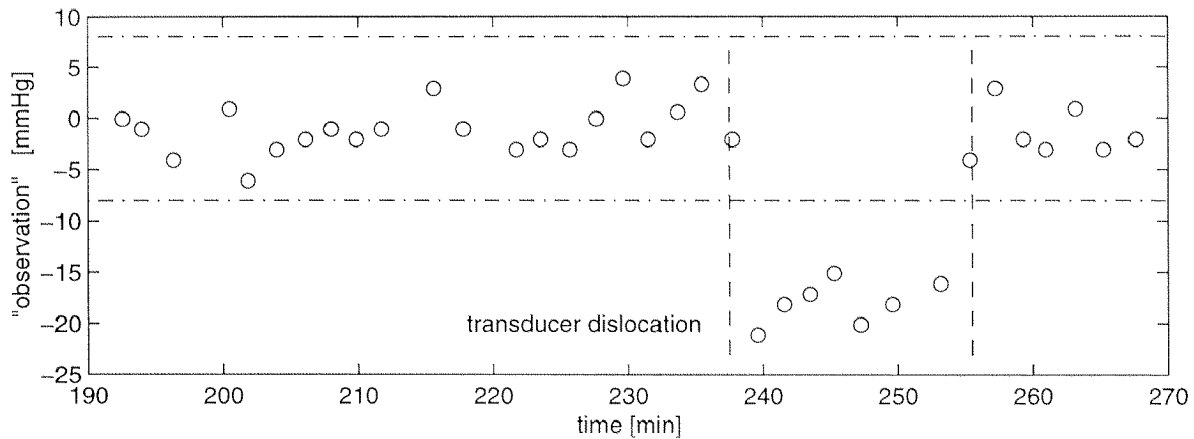
Figure 7.29: Detection example of a fault in the blood pressure measurement system. To mimic the fault the transducer was shifted up $25\ cm$.

7.11   Conclusions

In this chapter we have followed the design procedure by Blanke et al. for the design of FTC systems. The procedure has shown to be very useful in ensuring that "nothing is forgotten". However, we feel that there is a certain overlap among the different steps. For example some aspects of step 1 (fault listing and propagation) are mentioned again in step 2 (severity assessment). The same is felt for step 3 (FTC possibilities) and step 4 (remedial action selection). Similarly this is the case for step 3 and step 5 (FDI design). From this experience we suggest to merge step 1 and step 2. Step 3 could be split into FTC possibilities for detection and FTC possibilities for remedial actions and then could be integrated into step 5 and step 4, respectively.

The chapter shows that model based detection of faults in a clinical environment is possible. The application reveals that there are still considerable unmodeled phenomena in these models. The problems arising form these model uncertainties were solved by means of threshold adaptation. The applicability finally was demonstrated in three pilot examples. To "prove" the general clinical applicability an extensive clinical study will be required. A task that must be left to future projects. There are still a number of open questions that will have to be addressed then. First, the O_2-based detector allowing the isolation of vaporizer faults and leaks could not be implemented due to time limitations. Second, at the current stage the decision signal is "chattering" when crossing a threshold due to the noise on the residual. A possible remedy for this will be to introduce a decision hysteresis.

Chapter 8

Human Machine Interface

8.1 Introduction

In figure 5.1 the HMI was identified as the part of the supervisor which is responsible for the communication with the operator. But we have not gone into the realization aspects for this HMI. This is subject of this chapter. The aspects are particularly important for two reasons

HMI-1 The design of an HMI is a key factor in how well the system is accepted by the end user [186, 206].

HMI-2 A well designed user interface increases operational safety [269]. That is if it allows the anesthetist to grasp a critical situation faster then corrective actions will be more effective [419].

However, to design the perfect HMI would go far beyond the scope of this work. What we will present here is a usable solution knowing that the development of a "perfect" solution would require a thesis of its own. The general guidelines for designing user interfaces shall nonetheless be followed.

For the further discussion it must often be referred to earlier versions of the user interface. For convenience these versions will be labeled. Version A refers to the MS-DOS text oriented interface shown in figure 8.1. Version B refers to the Oberon based graphical user interface shown in figure 8.2 which was used during the endtidal controller study. And Version C refers to the interface to be described in this chapter.

Note at this point that graphical user interfaces (GUI) are a subset of human machine interfaces (HMI) since HMI may also include e.g. acoustic or haptic elements. That is

$$GUI \subset HMI. \tag{8.1}$$

Figure 8.1: Screen for the Human Machine Interaction used to operate the first prototype system. Number and arrow keys on the keyboard were used to browse through the menus and to input data.

In absence of other than graphical elements we will use the terms GUI and HMI interchangeably.

8.2 Ergonomic dialogue design criteria

The design of adequate user interfaces is one aspect of software ergonomy [462, 261, 15, 246, 358, 203]. These publications in particular discuss ergonomic dialogue design criteria. Such criteria are also covered by the international standards [1, 3]. We will utilize the guidelines given in [1] which are

DC-1 **Suitability for task:** Suitability for task essentially requires that the system should support the user in performing his task and not hinder him. This includes [15, 358, 261]:

- that the different steps required to achieve a certain goal should be in a natural order
- the system must provide a clear set of services that have a corresponding meaning in the user environment
- icons and keywords should be borrowed from the users environment
- no special computer knowledge should be required to operate the system

For our case this means that all Oberon specific features should be hidden from the user by the interface. And only commands must be provided that are intuitively understood.

DC-2 **Self-descriptiveness:** Self-descriptiveness requires [1]: *"A dialogue is said to be self-descriptive if each dialogue step is either immediately comprehensible or may be explained to the user on his/her requesting the relevant information. After any user action the system should have the capability to provide feedback or explanations on request or initiate feedback if severe consequences may result"*. In particular for the immediate understanding it is useful to use consistent terminology drawn from the task environment [15, 358] and intuitively understandable pictograms [261]. For example, it is nonsense to inform the anesthetist about pharmacokinetic parameters used in the infusion pump. What he is interested in are the actual patient parameters for which the infusion has been computed like weight, age, sex, etc.

The following test questions that can help to decide about self-descriptiveness are (adapted from [15, 358])

- what state is my system in?
- what are the possible actions in this state ?
- how did the system get into this state ?
- into what other states can it be transfered ?
- how can it be transfered into these other states ?

DC-3 **Controllability:** The demand for "controllability" is based on the observation that the more control one has over a system the less afraid one is to use it [261]. Please note, that

controllability here refers to something different from what is normally used in control engineering. The fallback concept in our case for example gives the anesthetist the assurance that whatever goes wrong he will always be able to inactivate the system completely.

Controllability includes that the user determines the speed at which things (e.g. mode transitions) happen [15, 358]. Restrictions to controllability of course apply if mis-manipulations must be prevented.

DC-4 **Conformity with user expectations:** *"In order to achieve conformity with user expectations it is important that the dialogue system of the application incorporates as precisely as possible a model of the task the application is required to perform under both procedural and structural aspects. Hence, the user should have easy access to the task and simple navigation mechanisms."* This includes [261, 246]:

- similar commands should lead to similar reactions

- feedback must be given whether a command is being executed or whether additional inputs are required

- the application should "employ the user's vocabulary which is used for the task and commit to polite formulations" [1]

- any information given to the user should be limited to the absolute minimum

DC-5 **Learnability:** *"Dialogue systems are said to support learnability if they guide the user through the learning stages minimizing the learning time. Reducing complexity and maintaining consistency are the prerequisite goal for this principle. .... All kinds of dialogue elements supporting "getting used to" behavior should be applied (e.g. standard locations for same type of messages, similar layout of screen elements for similar task objects)."*

DC-6 **Individualization:** *" Dialogue systems are said to support individualization if the system is constructed to allow for adaptation to the user's individual needs and skills for a given task. Parts of the dialogue which are developed with certain user characteristics in mind (such as normal color vision) support individualization if they can be modified to support users who differ in these characteristics (such as color-blindness).*

Examples of individualization might include allowing the user to use different command names incorporating his/her own vocabulary, providing different techniques for condensing input and representing output, and providing the capability of adding individualized functions within the semantics of the application or even expanding the semantics."

DC-7 **Error tolerance:** A dialogue is error tolerant if despite an erroneous input the system does not end up in an undefined state. In some cases it might be appropriate to automatically correct obvious input errors. In other cases it might be better to ignore the input and inform the user. The user interface should indicate what the allowed inputs are [261].

The attentive reader has realized that there is a certain overlap between these criteria (see also [246]). It is therefore not surprising that different sources give slightly different criteria [462, 3].
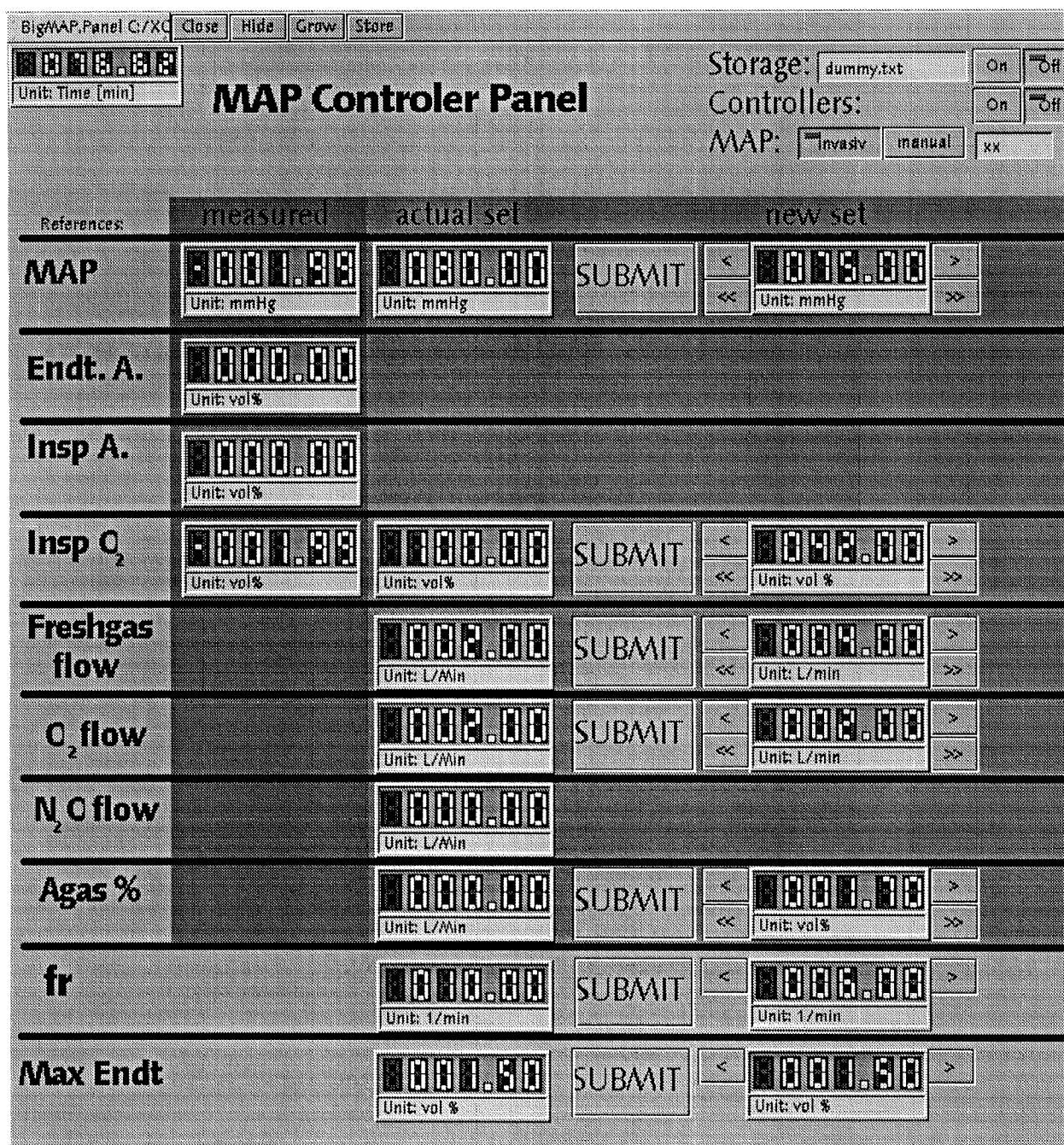
Figure 8.2: Prototype HMI used during the clinical evaluation of the endtidal controller. It is on a touch screen which is operated by means of a pen especially designed for touch screen interaction.

8.3   Applying the design criteria

If we analyze Version A of the HMI it complies with many of the above guidelines DC-1 to DC-7. But there are also points that violate these guidelines: The use of a keyboard in the OR violates DC-1. The text-only mode violated DC-4. The user was expecting a "Windows-like" GUI. A later - Oberon/touch-screen-based - prototype designed by Derighetti for evaluation of his endtidal and MAP controllers was much better received. However, during the clinical evaluation of the endtidal controller the interface proved to have a series of considerable drawbacks. For example the interface suggests that the vaporizer concentration (line $Agas\%$ in HMI Version B) can always be overwritten manually. But this was not the case during automatic control. This violates DC-3. Parts of the HMI that can not be used must not be displayed. The display did also not indicate whether the controller was initialized properly but it still allowed to switch the controller on - a violation of DC-7. A new solution therefore had to be sought based on the experience gained during the different studies conducted so far.

While the design criteria DC-1 to DC-7 serve well to separate good from bad designs they don't provide a direct help in the sense of a design recipe. For more specific design suggestions others sources were consulted. These are

- Publications discussing HMI design elements for industrial applications [107, 523, 229]. There it is common practice to use so called mimics ("Fliessbilder") [107] on which the different control and display elements are positioned according to their location in reality [523, 229]. It is also common to have trend data available on demand [229]. And there exist rules concerning the use of colors [107]. Finally, there is an tendency towards the use of touch screens [523].

- Existing medical devices with a similar purpose like patient monitors

- Publications presenting new prototype user interfaces for patient monitors [37, 245, 414, 389, 454].

- A series of publications presenting visionary ideas for future monitors and anesthesia workplaces [19, 50, 83, 133, 137, 151, 188, 190, 231, 372, 375, 410, 411, 487].

- Interviews with users [446]. In these interviews the shortcomings of the HMI version A and B were discussed. It was during these interviews that the poor "controllability" of version B became apparent. The users also unisonously were in favor of the "single knob" concept of the Draeger devices. This motivated our concept with the "common adjustment element".

Numerous ideas from above sources were picked up to get to Version C for the HMI that will be described in the next section.

Overview Screen (Mimic)　　　Histories Screen (Trends)

mode control

common adjustment element

error + status messages

empty
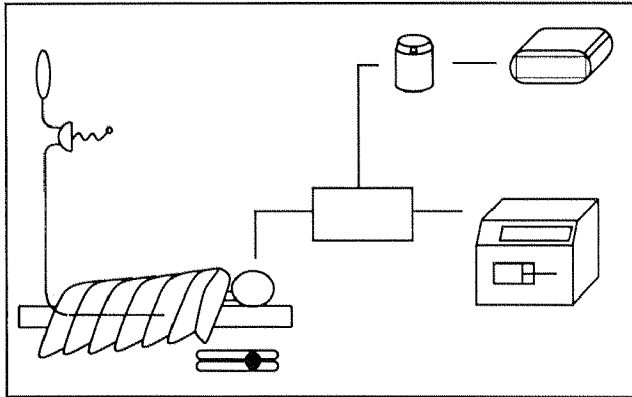
dosing
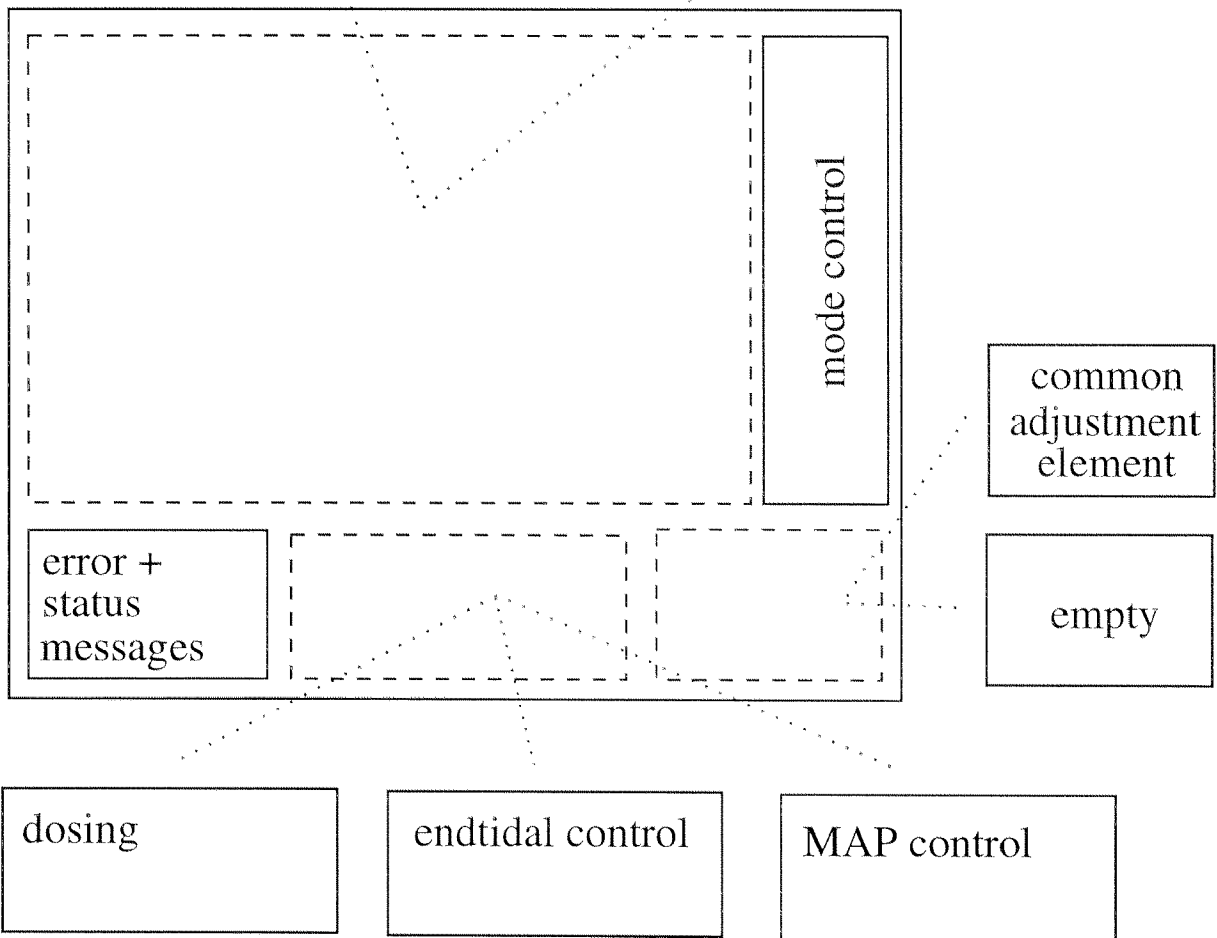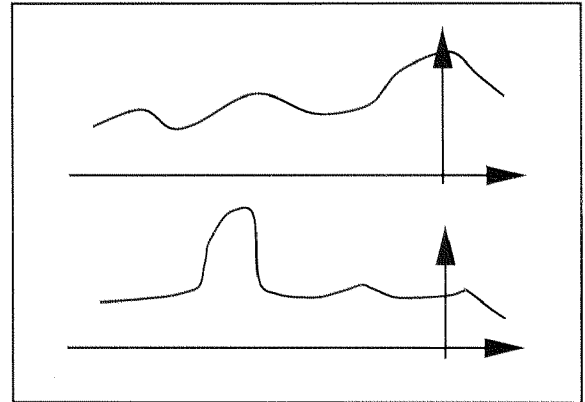
endtidal control

MAP control

Figure 8.3: Partitioning of screen into different fixed and variable segments. The different panels "dosing", "endtidal control", and "MAP control" are displayed based on the selected mode of the control system (see figure 4.8). "Overview" and "Histories" screen are shown depending on the corresponding user selection in the mode control panel (see figure 8.4).

8.4   Description of HMI Version C

Figure 8.3 shows the partitioning of the HNI screen into different segments. It has fixed areas and variable areas. The variable areas are filled according to user selections. They are drawn with dashed lines. The fixed areas are drawn with solid lines.

The fixed areas are those required for navigation. They must be displayed always since from them the state of the control system is inferred (DC-3). The mode control area is shown in figure 8.4. The upper three buttons are for handling overview and trend screen. The lowest two buttons are for controlling the storage. The rest of the buttons are for selecting the control modes. The active mode is marked by a green status indicator "light".

The messages are handled by a designated gadget. It is able to handle a variable number of messages (1 − 10) provided by the target application. The color of a displayed message depend on the message type. Complying with [474] we use green, yellow, and red for no fault, warning, and critical messages, respectively (see also [470]).

With the upper most buttons in the mode control section the user can choose between an overview and an a trend screen (or several trend screens in the future). The overview screen (figure 8.5) allows to get a rapid overview over the state of the control system. It displays the application relevant parameters and measurements. For every value to be displayed a so called "Value Item" is placed on the screen and connected with a datum of an object model on the target screen. For details see section 2.7.4. Adding and removing Value Items can be done through "drag and drop" and does not require any programming. Up do date the Value Items are all off the same shape and are only discriminated by their name. In principle these Value Items should be replaced by pictograms. A suggestion made by several authors [414, 389, 372, 83, 133]. Each Value Item is placed on the screen atop of a schematic drawing of the anesthesia environment. A technique common for industrial applications [229, 107] but also suggested for medical applications by several authors [188, 487].

The trend screen (figure 8.6) allows to view the time course of (control) relevant variables. The selection of the variables to be displayed can be done through button clicks and may be altered online.

Another variable area is the space where the control panels are displayed. The space is occupied by a controller panel which corresponds with the selected mode. This principle allows to hide system inputs that do not apply in certain modes.

The last variable screen area is the "common adjustment element" (figure 8.7). It allows to change values of Value Items. Since potentially every Value Item needs occasionally to be changed every Value Item needs an adjustment mechanism. In order not to waste screen area with numerous scroll bars the idea was to have only one adjustable element that can be used with any Value Item. Note that this concept is similar to the "One-Button-Handling" common in Dräger devices. By clicking on the name button of a Value Item the common adjustment element panel pops up. The scroll bar allows to adjust the item's value. And when clicking on the "OK" button the new value is accepted and the common adjustment element disappears.
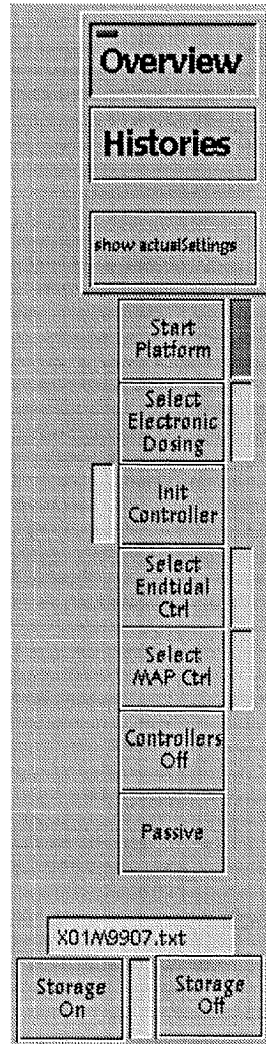
Figure 8.4: Mode control segment of the HMI (fixed object). The upper two buttons allow to switch between the "Overview" (mimic) and the "Histories" (trend) screen (figure 8.3). The button "show actual settings" allows to display the currently set values of the *Value Items*. The next seven buttons allow to navigate through the SLC (see section 4.3). And finally, the lower buttons allow to switch storage on and off. The "LED" between the buttons indicates whether storage is on or off.
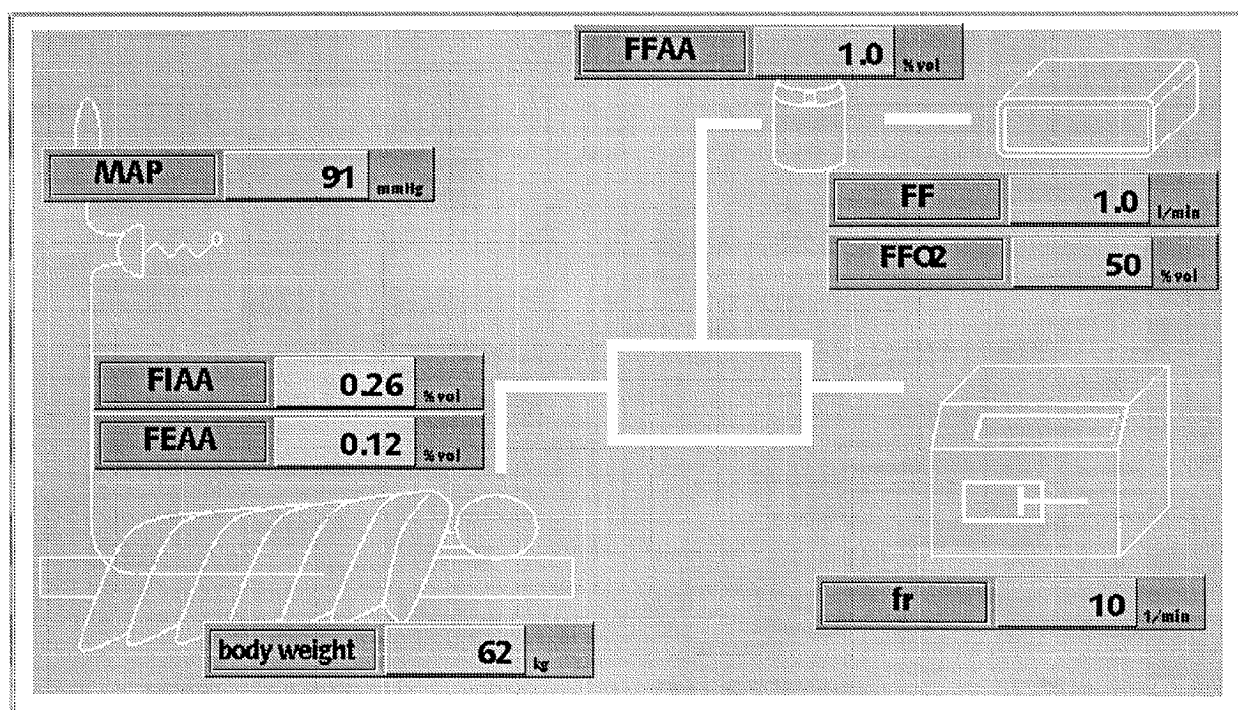
Figure 8.5: Overview screen (mimic) segment. *Value Items* are placed on this screen by "drag and drop". For the different items name, resolution, color, alarm limits, etc. can be specified individually. Note that the naming complies with the abbreviations commonly used in anesthesia.
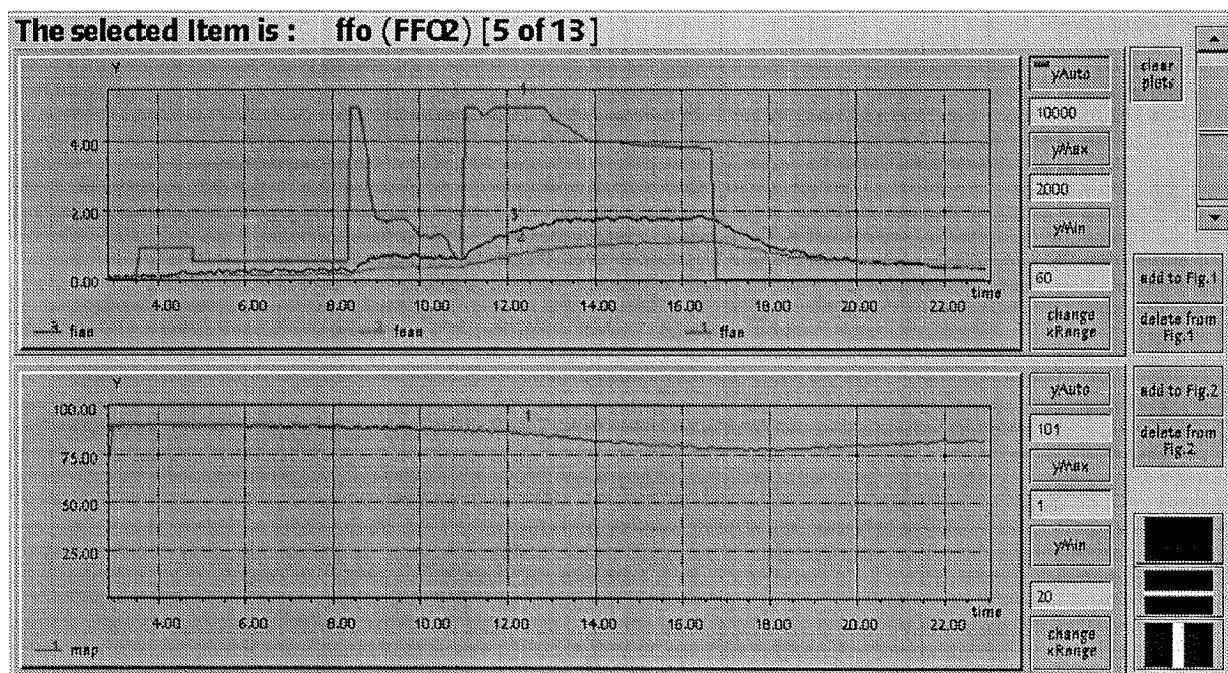
Figure 8.6: Histories screen (trends) segment for the HMI. In this example the upper plot shows concentration variables. That is vaporizer signal, inspiratory concentration, and exspiratory concentration. The actual screen will show the different graphs with different colors. The lower plot the MAP signal. At the bottom of each plot a legend is provided. Signals may be added or removed from a graph at run time. To do so the upper right scroll bar allows to browse through the available items. The selected item is indicated in the title bar of the panel (FFO2 is Nr. 5 out of 13 items). Using the "add to" or "delete from" button the item may be added or removed from the plot.
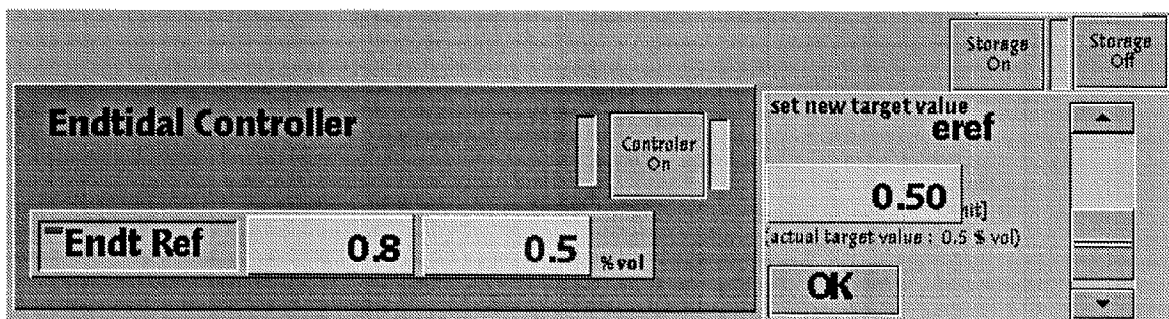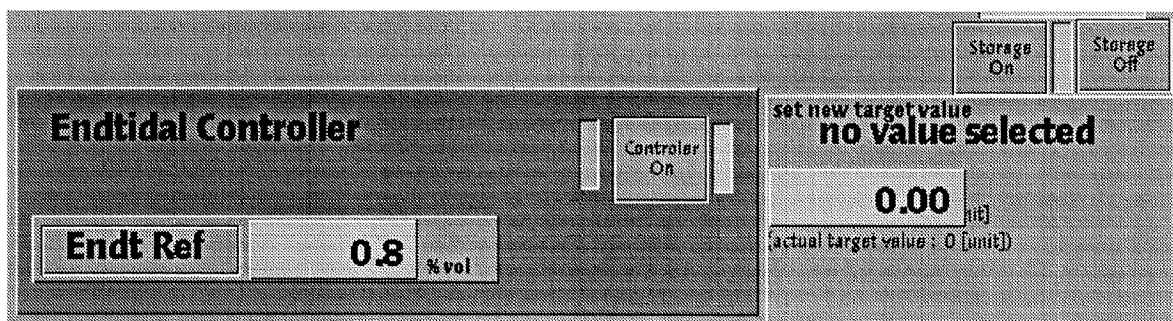
Figure 8.7: The "common adjustment element" allows to adjust values of Value Items.
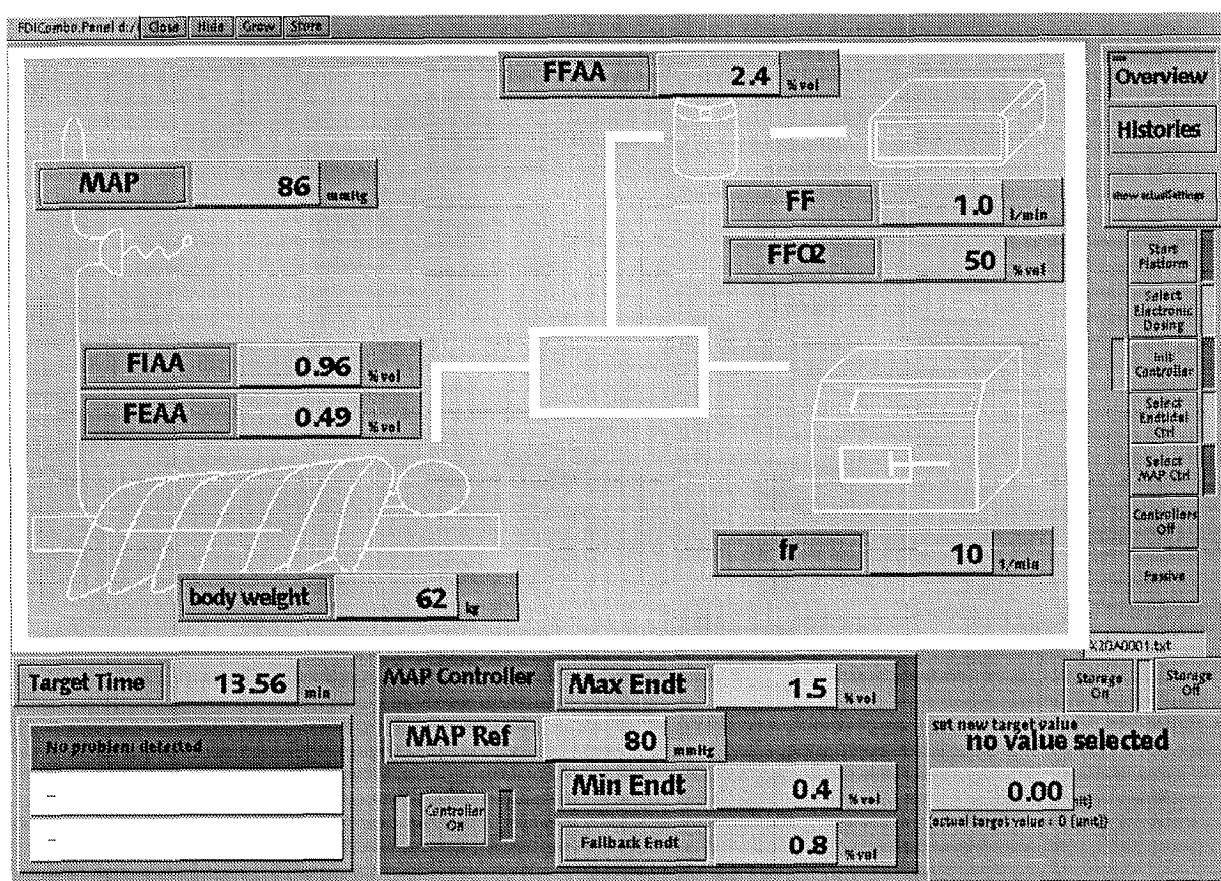
Figure 8.8: Screen for MAP controller with endtidal override.

Finally, a complete panel as it is used for the MAP controller study is shown in figure 8.8. Note that the interaction with the touch screen also occurs with a pen typically used for this purpose.

8.5   Conclusions

At the beginning of the design of HMI Version C, design guidelines available in software ergonomy literature were consulted. These guidelines were found to be very helpful in identifying short comings of a certain HMI solution or to compare different solutions. But they were of little help for finding "the design". For this purpose other sources had to be consulted.

The current solution (Version 3) removes a number of drawbacks of the earlier Versions A and B. It is much better received due to the graphical components (DC-4) and because of the touch screen (DC-1). It complies much better with DC-3 (controllability) since only elements are shown that really can be manipulated. The interface now also allows to always see in what mode the control system is (DC-2).

Some short comings have been detected already during the first pilot studies with the MAP controller. First, the *Value Items* are still only distinguishable through their name. It might

be better to use intuitive pictograms in the future. Also the items are fairly large. This will make it difficult to arrange them appropriately on the overview screen as more control loops are integrated. Final conclusions must, however, be drawn after completion of the study. An interesting question will be to evaluate how often the "Histories" screen is used compared to the "Overview" screen.

Chapter 9

Conclusions

9.1 What has been achieved

The scope of the presented thesis is to solve a number of problems that arise when intending to bring feedback controllers from a clinical study environment to clinical practice. The introductory discussion in chapter 1 shows that this mainly requires the development of what we call supervisor functions. In a first part of the thesis (chapters 2 to 3) the necessary foundations are elaborated and in a second part (chapters 4 to 8) selected supervisor aspects are developed (see also figure 1.6).

The foundations are first a hard- and software platform which allows to implement and use controllers as well as supervisor functions in the clinical environment. Second there is a mathematical model that is required for controller development as well as supervisor function design.

Considerable effort was dedicated to the development of the hard- and software research platform. The design specifications may be summarized with: "developing an extensible, easy to use experimental platform that allows the "safe" application of feedback controllers in the OR". With Oberon-2 an object oriented programming language has been used for software development. However, not all concepts of object orientation were needed for the software design. In fact it seems that for our type of problem it is sufficient to have a modular programming language at disposition. The evaluation of three different controllers (i.e. an observer based state feedback controller, an override controller, and a high gain adaptive controller [67]) each having an appropriate graphical user interface confirm that these specifications have been met. The strictly modular design and the skeleton mode control object (see section 2.7.3 for details) reduced the implementation effort considerably. The same is true for the design of the graphical user interface. The system is now in a development state where it may routinely be used by an instructed anesthetist without engineer's support.

In chapter 3 we presented a model which describes the dynamic relationship between vaporizer

concentrations and surgical stimulations on the input side and the inspiratory and endtidal Isoflurane concentration as well as MAP on the output side. The model is a refined version of a model introduced by Derighetti [111]. The refinements concern the pharmacokinetic and pharmacodynamic parameters of the model for Isoflurane, the model structure and the model parameters for the model of the surgical stimulations, and the model of the respiratory circuit. Some parameter changes in the Isoflurane model are minor in the sense that they do not affect the design of controllers much. They are necessary to improve the residual quality for FDI. One change of parameters, however, has a great influence also on the controller design. It was found that the pharmacodynamic parameters describing the dependence of the cardiac output form Isoflurane are such that the model becomes non-minimum phase. A phenomenon which is not described by Derighetti. For an early model for the influence of surgical stimulations [112] it was hypothesized that there is a neural and a humoral component involved. This assumption has also been used by Derighetti. In this thesis experiments are shown which for the first time clearly support this hypothesis and which allow to separate the two components. The model has been modified to comply with this observed response. Finally, for the respiratory circuit a physically motivated order reduction of the model by Derighetti is presented.

In chapter 4 the observer based control algorithms for endtidal Isoflurane concentration and MAP developed by Derighetti are brought to the point where they are applicable in a clinical study. This means the following. The computation of the controller parameters is done online. The MAP controller has been redesigned to account for the non-minimum phase characteristic of the plant and it has been extended with an additional endtidal override controller which guarantees a minimum endtidal Isoflurane concentration. For the endtidal controller the results of an extensive clinical study comparing manual and automatic control performance are presented. The evaluation reveals a statistically significant superior performance of automatic control. For the MAP controller a similar study was still in progress when the thesis was completed. From the few trials it must be expected that the difference between manual and automatic control will be less significant. The reason for this lies in the limited range of available control signal which applies to both manual as well as automatic control.

In chapter 5 a possible structure for a supervisor is developed. It is suggested to distinguish input/output conditioning, supervisor logic control, fault detection/isolation, decision support, and man machine interface. The structure allows to allocate supervisor functions generally postulated for automatic control applications during anesthesia.

Chapter 6 develops a novel and elegant solution to the artifact problem. It is based on a nonlinear modification of the generic observer based state feedback controller. The stability of this modified controller is checked using standard methods. Several examples of successfully suppressed artifacts in the concentration as well as in the MAP signals are presented.

In chapter 7 a design procedure for fault tolerant control (FTC) systems proposed by Blanke et al. is applied to the Isoflurane-MAP control problem. A key step in this procedure is to determine the FTC possibilities provided by a system. To support this analysis the concept of recoverability is developed (appendix C). Recoverability is supposed to answer the question of how well the function of a control system may be recovered after a fault (and possibly a system reconfiguration). The concept proposes a measure for the degree of recoverability of linear systems subject to faults. These measures are used in the design procedure to rank the different

FTC possibilities. An important ingredient of FTC is fault detection and isolation (FDI). The FDI problem is solved by using the models developed in chapter 3. The analysis of the different detectors revealed that despite the large modeling effort still considerable unmodeled dynamics are affecting the residuals. The problem is resolved by means of threshold adaptation. The final FTC system is able to handle faults in measurements and actuators. Three clinical experiments of successfully detected faults are shown. This lets us conclude that FTC based on analytical redundancy provided by dynamic system models is possible in this clinical environment. The general clinical validation, however, must be done in a future project. The supervisor logic is not yet enabled to perform mode transitions autonomously. At the current state of development the FDI findings are communicated to the anesthetist along with a suggestion for mode transition. It is still him/her who is responsible for mode transitions. Autonomous transitions will only be introduced once the clinical validation of this "assistance" mode has been completed.

Finally, in chapter 8 a prototype human machine interface (HMI) is presented. For the layout of this prototype guidelines from software ergonomy, examples of HMIs existing in other medical devices, and inputs form potential users were combined. The current prototype is generally accepted in terms of its appearance. But the evaluation of the practical suitability must also be left to future clinical studies.

9.2 Where are still open points

Some potential for future research has been outlined in the introduction. The aim of this section is not to elaborate those aspects further but to point out research directions that start from where this thesis ends. There are mainly three areas where we think additional research is necessary. This includes aspects of the model, the recoverability measure, and the user interface. More precisely they are:

Unmodeled dynamics: The analysis of the fault detectors showed that there must be still considerable unmodeled dynamics. To further improve the detector quality these unmodeled dynamics must be localized and included in the model. For the pharmacokinetics of Isoflurane unmodeled dynamics are likely to be introduced by the simplification concerning the respiratory tract. For the respiratory circuit unmodeled dynamics may be associated with the manual ventilation bag or the CO_2 absorber.

Non ideal gas exchange: To comply with experimental data we had to introduce a fairly large alveolar dead space. Although there is evidence for this in the literature it is not clear whether it is due to incomplete mixing of Isoflurane in the alveoli or to a limited ability of Isoflurane to cross the alveolar membrane.

Inverse MAP response: The pharmacodynamic parameters for cardiac output have been obtained from a single experiment. At this point is it not clear whether there are individuals that do perhaps not show this behavior, whether it is truly due to the sympathomimetic effect of the Isoflurane or rather due to auto regulation mechanisms, or whether it is a nonlinear phenomenon.

Pain Model: The model for the hemodynamic stress response was developed in absence of analgesics. Analgesics change the response of MAP [105], the neural activity [105] and the catecholamines [101] to stimuli. And since analgesics are generally used during normal anesthesia the model should be modified to account for these effects. We think that this could be done by introducing a modulation of the neural stimulation with the plasma level of analgesics.

Catecholamines: Unfortunately we were not able to confirm the humoral component in the stress response model through measurements.

Disturbance anticipation: The potential improvements in blood pressure regulation through disturbance anticipation was studied in simulations with promising results. However, the clinical applicability can only be demonstrated with a clinical experiment. Before this will be possible, the handling of the output constraints on the endtidal concentration must be solved.

Recoverability: The recoverability measure proposed in appendix C and [154] must not be taken as a "gold standard". Perhaps there are more useful measures of recoverability. Also the consequences for FTC should further be elaborated. And finally, it is not clear how to define recoverability analogously for nonlinear systems.

FTC: For FTC we have only been able to present a few successful detection results and the "FTC loop" is still closed manually. Here a broad clinical evaluation will be required so that the FTC loop eventually can be closed automatically.

HMI: Most information is still displayed very text oriented. The cited visions of "the" future anesthesia system [19, 50, 83, 133, 137, 151, 188, 190, 231, 372, 375, 410, 411, 487] unisonously postulate the use of pictograms, barplots, etc. It is therefore likely that the clinical evaluation of the MMI will uncover shortcomings in exactly this direction.

Appendix A

The linear model

This appendix provides the coeffecents for the liearized model dynamics according to (3.106).

$$\partial \mathbf{f}_{R,R}^1 = \left.\frac{\partial f_R}{\partial p_R}\right|_{\bar{\mathbf{x}},\bar{\mathbf{u}}} = -\frac{f_R(V_T - V_{AD} - V_D)}{V_R} - \frac{FF - Q_\Delta}{V_R}\frac{V_{AD}}{V_T - V_D}$$

$$\partial \mathbf{f}_{R,L}^2 = \left.\frac{\partial f_R}{\partial p_L}\right|_{\bar{\mathbf{x}},\bar{\mathbf{u}}} = \frac{f_R(V_T - V_{AD} - V_D)}{V_R} - \frac{FF - Q_\Delta}{V_R}\left(1 - \frac{V_{AD}}{V_T - V_D}\right)$$

$$\partial \mathbf{f}_{i,i}^3 = \left.\frac{\partial f_i}{\partial p_i}\right|_{\bar{\mathbf{x}},\bar{\mathbf{u}}} = -\frac{k_i g_{i,0}(1 + \beta_i \bar{p} + \gamma_i \bar{c}_P + \kappa_i \bar{n})CO_0(1 + \alpha_1 \bar{p} + \alpha_3 \bar{p} + \alpha_4 \bar{c}_P + \alpha_6 \bar{n})}{(1 + k_{BR}HR_0 \bar{r}_b)\sum\limits_{j=1}^{9} g_{j,0}(1 + \beta_i \bar{p} + \gamma_i \bar{c}_P + \kappa_i \bar{n})}$$

$$\partial \mathbf{f}_{R,L}^4 = \left.\frac{\partial f_R}{\partial p_L}\right|_{\bar{\mathbf{x}},\bar{\mathbf{u}}} = k_L f_R(V_T - V_{AD} - V_D)$$

$$\partial \mathbf{f}_{L,L}^5 = \left.\frac{\partial f_L}{\partial p_L}\right|_{\bar{p},\bar{\mathbf{u}}} = -k_L\left\{\frac{\lambda_b(1 - ls)CO_0(1 + \alpha_1 \bar{p} + \alpha_3 \bar{p} + \alpha_4 \bar{c}_P + \alpha_6 \bar{n})}{(1 + k_{BR}HR_0 \bar{r}_b)} + f_R(V_T - V_{AD} - V_D)\right\}$$

$$\partial \mathbf{f}_{L,V}^6 = \left.\frac{\partial f_L}{\partial p_V}\right|_{\bar{\mathbf{x}},\bar{\mathbf{u}}} = \frac{k_L \lambda_b(1 - ls)CO_0(1 + \alpha_1 \bar{p} + \alpha_3 \bar{p} + \alpha_4 \bar{c}_P + \alpha_6 \bar{n})}{(1 + k_{BR}HR_0 \bar{r}_b)}$$

$$\partial \mathbf{f}_{A,L}^7 = \left.\frac{\partial f_A}{\partial p_L}\right|_{\bar{\mathbf{x}},\bar{\mathbf{u}}} = \frac{k_A(1 - ls)CO_0(1 + \alpha_1 \bar{p} + \alpha_3 \bar{p} + \alpha_4 \bar{c}_P + \alpha_6 \bar{n})}{(1 + k_{BR}HR_0 \bar{r}_b)}$$

$$\partial \mathbf{f}_{A,A}^8 = \left.\frac{\partial f_A}{\partial p_A}\right|_{\bar{\mathbf{x}},\bar{\mathbf{u}}} = -\frac{k_A CO_0(1 + \alpha_1 \bar{p} + \alpha_3 \bar{p} + \alpha_4 \bar{c}_P + \alpha_6 \bar{n})}{(1 + k_{BR}HR_0 \bar{r}_b)}$$

$$\partial \mathbf{f}_{A,V}^9 = \left.\frac{\partial f_A}{\partial p_V}\right|_{\bar{\mathbf{x}},\bar{\mathbf{u}}} = \frac{k_A ls CO_0(1 + \alpha_1 \bar{p} + \alpha_3 \bar{p} + \alpha_4 \bar{c}_P + \alpha_6 \bar{n})}{(1 + k_{BR}HR_0 \bar{r}_b)}$$

$$\partial \mathbf{f}_{V,k}^{10} = \left.\frac{\partial f_V}{\partial p_k}\right|_{\bar{\mathbf{x}},\bar{\mathbf{u}}} = \frac{k_V CO_0(1 + \alpha_1 \bar{p} + \alpha_3 \bar{p} + \alpha_4 \bar{c}_P + \alpha_6 \bar{n})g_{k,0}(1 + \beta_k \bar{p} + \gamma_k \bar{c}_P + \kappa_k \bar{n})}{(1 + k_{BR}HR_0 \bar{r}_b)\sum\limits_{j=1}^{9} g_{j,0}(1 + \beta_j \bar{p} + \gamma_j \bar{c}_P + \kappa_j \bar{n})}$$

$$\partial \mathbf{f}_{V,V}^{11} = \left.\frac{\partial f_V}{\partial p_V}\right|_{\bar{\mathbf{x}},\bar{\mathbf{u}}} = -\frac{k_V CO_0(1 + \alpha_1 \bar{p} + \alpha_3 \bar{p} + \alpha_4 \bar{c}_P + \alpha_6 \bar{n})}{(1 + k_{BR} H R_0 \bar{r}_b)}$$

$$\partial \mathbf{f}_{b,1}^{12} = \left.\frac{\partial f_b}{\partial p_1}\right|_{\bar{\mathbf{x}},\bar{\mathbf{u}}} = \frac{CO_O}{\tau_{BR}(1 + k_{BR} H R_0 \bar{r}_b) \sum\limits_{j=1}^{9} g_{j,0}(1 + \beta_j \bar{p} + \gamma_j \bar{c}_P + \kappa_j \bar{n})}$$

$$\left\{ \alpha_1 - \frac{(1 + \alpha_1 \bar{p} + \alpha_3 \bar{p} + \alpha_4 \bar{c}_P + \alpha_6 \bar{n})\beta_1 g_{1,0}}{\sum\limits_{j=1}^{9} g_{j,0}(1 + \beta_j \bar{p} + \gamma_j \bar{c}_P + \kappa_j \bar{n})} \right\}$$

$$\partial \mathbf{f}_{b,i}^{13} = \left.\frac{\partial f_b}{\partial p_i}\right|_{\bar{\mathbf{x}},\bar{\mathbf{u}}} = -\frac{CO_0(1 + \alpha_1 \bar{p} + \alpha_3 \bar{p} + \alpha_4 \bar{c}_P + \alpha_6 \bar{n})g_{i,0}\beta_i}{\tau_{BR}(1 + k_{BR} H R_0 \bar{r}_b)\left[\sum\limits_{j=1}^{9} g_{j,0}(1 + \beta_j \bar{p} + \gamma_j \bar{c}_P + \kappa_j \bar{n})\right]^2}$$

$$\partial \mathbf{f}_{b,A}^{14} = \left.\frac{\partial f_b}{\partial p_A}\right|_{\bar{\mathbf{x}},\bar{\mathbf{u}}} = \frac{CO_0 \alpha_3}{\tau_{BR}(1 + k_{BR} H R_0 \bar{r}_b) \sum\limits_{j=1}^{9} g_{j,0}(1 + \beta_j \bar{p} + \gamma_j \bar{c}_P + \kappa_j \bar{n})}$$

$$\partial \mathbf{f}_{b,b}^{15} = \left.\frac{\partial f_b}{\partial r_b}\right|_{\bar{\mathbf{x}},\bar{\mathbf{u}}} = -\frac{CO_0(1 + \alpha_1 \bar{p} + \alpha_3 \bar{p} + \alpha_4 \bar{c}_P + \alpha_6 \bar{n})k_{BR} H R_0}{\tau_{BR}(1 + k_{BR} H R_0 \bar{r}_b)^2 \sum\limits_{j=1}^{9} g_{j,0}(1 + \beta_j \bar{p} + \gamma_j \bar{c}_P + \kappa_j \bar{n})}$$

$$\partial \mathbf{f}_{b,n}^{16} = \left.\frac{\partial f_b}{\partial n}\right|_{\bar{\mathbf{x}},\bar{\mathbf{u}}} = \frac{CO_O}{\tau_{BR}(1 + k_{BR} H R_0 \bar{r}_b) \sum\limits_{j=1}^{9} g_{j,0}(1 + \beta_j \bar{p} + \gamma_j \bar{c}_P + \kappa_j \bar{n})}$$

$$\left\{ \alpha_6 - \frac{(1 + \alpha_1 \bar{p} + \alpha_3 \bar{p} + \alpha_4 \bar{c}_P + \alpha_6 \bar{n}) \sum\limits_{j=1}^{9} g_{j,0}\kappa_j}{\sum\limits_{j=1}^{9} g_{j,0}(1 + \beta_j \bar{p} + \gamma_j \bar{c}_P + \kappa_j \bar{n})} \right\}$$

$$\partial \mathbf{f}_{b,P}^{17} = \left.\frac{\partial f_b}{\partial c_P}\right|_{\bar{\mathbf{x}},\bar{\mathbf{u}}} = \frac{CO_O}{\tau_{BR}(1 + k_{BR} H R_0 \bar{r}_b) \sum\limits_{j=1}^{9} g_{j,0}(1 + \beta_j \bar{p} + \gamma_j \bar{c}_P + \kappa_j \bar{n})}$$

$$\left\{ \alpha_4 - \frac{(1 + \alpha_1 \bar{p} + \alpha_3 \bar{p} + \alpha_4 \bar{c}_P + \alpha_6 \bar{n}) \sum\limits_{j=1}^{9} g_{j,0}\gamma_j}{\sum\limits_{j=1}^{9} g_{j,0}(1 + \beta_j \bar{p} + \gamma_j \bar{c}_P + \kappa_j \bar{n})} \right\}$$

$$\partial \mathbf{f}_{n,2}^{18} = \left.\frac{\partial f_n}{\partial p_2}\right|_{\bar{\mathbf{x}},\bar{\mathbf{u}}} = \frac{\tilde{\alpha}_2}{\tau_n}$$

$$\partial \mathbf{f}_{n,n}^{19} = \left.\frac{\partial f_n}{\partial n}\right|_{\bar{\mathbf{x}},\bar{\mathbf{u}}} = -\frac{1}{\tau_n}$$

$$\partial \mathbf{f}_{L,1}^{20} = \left.\frac{\partial f_L}{\partial p_2}\right|_{\bar{\mathbf{x}},\bar{\mathbf{u}}} = -\frac{\alpha_1}{\tilde{V}_L}\frac{k_{AM}\bar{n}}{(1 + k_{BR} H R_0 \bar{r}_b)(1 + \alpha_1 \bar{p} + \alpha_3 \bar{p} + \alpha_4 \bar{c}_P + \alpha_6 \bar{n})}$$

$$\partial \mathbf{f}_{L,A}^{21} = \left.\frac{\partial f_L}{\partial p_A}\right|_{\bar{\mathbf{x}},\bar{\mathbf{u}}} = -\frac{\alpha_3}{\tilde{V}_L}\frac{k_{AM}\bar{n}}{(1 + k_{BR} H R_0 \bar{r}_b)(1 + \alpha_1 \bar{p} + \alpha_3 \bar{p} + \alpha_4 \bar{c}_P + \alpha_6 \bar{n})}$$

$$\partial \mathbf{f}_{L,r}^{22} = \left.\frac{\partial f_L}{\partial r_b}\right|_{\bar{\mathbf{x}},\bar{\mathbf{u}}} = \frac{k_{BR} H R_0 k_{AM}\bar{n}}{(1 + k_{BR} H R_0 \bar{r}_b)^2 \tilde{V}_L}$$

$$\partial \mathbf{f}_{L,n}^{23} = \frac{\partial f_L}{\partial n}\bigg|_{\bar{\mathbf{x}},\bar{\mathbf{u}}} = \frac{k_{AM}}{\tilde{V}_L}\left(1 - \frac{\alpha_6 \bar{n}}{(1 + \alpha_1 \bar{p} + \alpha_3 \bar{p} + \alpha_4 \bar{c}_P + \alpha_6 \bar{n})}\right)$$

$$\partial \mathbf{f}_{L,L}^{24} = \frac{\partial f_L}{\partial c_L}\bigg|_{\bar{\mathbf{x}},\bar{\mathbf{u}}} = -\frac{CO_0(1 + \alpha_1 \bar{p} + \alpha_3 \bar{p} + \alpha_4 \bar{c}_P + \alpha_6 \bar{n})}{(1 + k_{BR} HR_0 \bar{r}_b)\tilde{V}_L}$$

$$\partial \mathbf{f}_{L,P}^{25} = \frac{\partial f_L}{\partial c_P}\bigg|_{\bar{\mathbf{x}},\bar{\mathbf{u}}} = \frac{CO_0(1 + \alpha_1 \bar{p} + \alpha_3 \bar{p} + \alpha_4 \bar{c}_P + \alpha_6 \bar{n})}{(1 + k_{BR} HR_0 \bar{r}_b)\tilde{V}_L}$$
$$- \frac{\alpha_4 k_{AM} \bar{n}}{\tilde{V}_L (1 + k_{BR} HR_0 \bar{r}_b)(1 + \alpha_1 \bar{p} + \alpha_3 \bar{p} + \alpha_4 \bar{c}_P + \alpha_6 \bar{n})}$$

$$\partial \mathbf{f}_{P,1}^{26} = \frac{\partial f_P}{\partial p_1}\bigg|_{\bar{\mathbf{x}},\bar{\mathbf{u}}} = \frac{\alpha_1 k_{AM} \bar{n}}{\tilde{V}_P (1 + k_{BR} HR_0 \bar{r}_b)(1 + \alpha_1 \bar{p} + \alpha_3 \bar{p} + \alpha_4 \bar{c}_P + \alpha_6 \bar{n})}$$

$$\partial \mathbf{f}_{P,A}^{27} = \frac{\partial f_P}{\partial p_A}\bigg|_{\bar{\mathbf{x}},\bar{\mathbf{u}}} = \frac{\alpha_3 k_{AM} \bar{n}}{\tilde{V}_P (1 + k_{BR} HR_0 \bar{r}_b)(1 + \alpha_1 \bar{p} + \alpha_3 \bar{p} + \alpha_4 \bar{c}_P + \alpha_6 \bar{n})}$$

$$\partial \mathbf{f}_{P,r}^{28} = \frac{\partial f_P}{\partial r_b}\bigg|_{\bar{\mathbf{x}},\bar{\mathbf{u}}} = -\frac{k_{BR} HR_0 k_{AM} \bar{n}}{(1 + k_{BR} HR_0 \bar{r}_b)^2 \tilde{V}_P}$$

$$\partial \mathbf{f}_{P,n}^{29} = \frac{\partial f_P}{\partial n}\bigg|_{\bar{\mathbf{x}},\bar{\mathbf{u}}} = \frac{\alpha_6 k_{AM} \bar{n}}{(1 + \alpha_1 \bar{p} + \alpha_3 \bar{p} + \alpha_4 \bar{c}_P + \alpha_6 \bar{n})\tilde{V}_P (1 + k_{BR} HR_0 \bar{r}_b)}$$

$$\partial \mathbf{f}_{P,L}^{30} = \frac{\partial f_P}{\partial c_L}\bigg|_{\bar{\mathbf{x}},\bar{\mathbf{u}}} = \frac{CO_0(1 + \alpha_1 \bar{p} + \alpha_3 \bar{p} + \alpha_4 \bar{c}_P + \alpha_6 \bar{n})}{(1 + k_{BR} HR_0 \bar{r}_b)\tilde{V}_P}$$

$$\partial \mathbf{f}_{P,P}^{31} = \frac{\partial f_P}{\partial c_P}\bigg|_{\bar{\mathbf{x}},\bar{\mathbf{u}}} = \frac{\alpha_4 k_{AM} \bar{n}}{(1 + k_{BR} HR_0 \bar{r}_b)(1 + \alpha_1 \bar{p} + \alpha_3 \bar{p} + \alpha_4 \bar{c}_P + \alpha_6 \bar{n})\tilde{V}_P}$$
$$- \frac{CO_0(1 + \alpha_1 \bar{p} + \alpha_3 \bar{p} + \alpha_4 \bar{c}_P + \alpha_6 \bar{n})}{(1 + k_{BR} HR_0 \bar{r}_b)\tilde{V}_P} - k_E$$

$$\partial \mathbf{f}_{R,V}^{32} = \frac{\partial f_R}{\partial p_{vap}}\bigg|_{\bar{\mathbf{x}},\bar{\mathbf{u}}} = \frac{FF}{V_R}$$

$$\partial \mathbf{f}_{n,d}^{33} = \frac{\partial f_n}{\partial d_s}\bigg|_{\bar{\mathbf{x}},\bar{\mathbf{u}}} = \frac{1}{\tau_n}$$

$$\partial\mathbf{h}_{i,R}^1 = \frac{\partial h_{insp}}{\partial p_R}\bigg|_{\bar{\mathbf{x}},\bar{\mathbf{u}}} = 1$$

$$\partial\mathbf{h}_{e,R}^2 = \frac{\partial h_{endt}}{\partial p_R}\bigg|_{\bar{\mathbf{x}},\bar{\mathbf{u}}} = \frac{V_{AD}}{V_T - V_D}$$

$$\partial\mathbf{h}_{i,R}^3 = \frac{\partial h_{endt}}{\partial p_L}\bigg|_{\bar{\mathbf{x}},\bar{\mathbf{u}}} = 1 - \frac{V_{AD}}{V_T - V_D}$$

$$\partial\mathbf{h}_{m,1}^4 = \frac{\partial h_{map}}{\partial p_1}\bigg|_{\bar{\mathbf{x}},\bar{\mathbf{u}}} = \frac{CO_O}{(1 + k_{BR}HR_0\bar{r}_b)\sum\limits_{j=1}^{9} g_{j,0}(1 + \beta_j\bar{p} + \gamma_j\bar{c}_P + \kappa_j\bar{n})}$$

$$\left\{\alpha_1 - \frac{(1 + \alpha_1\bar{p} + \alpha_3\bar{p} + \alpha_4\bar{c}_P + \alpha_6\bar{n})\beta_1 g_{1,0}}{\sum\limits_{j=1}^{9} g_{j,0}(1 + \beta_j\bar{p} + \gamma_j\bar{c}_P + \kappa_j\bar{n})}\right\}$$

$$\partial\mathbf{h}_{m,i}^5 = \frac{\partial h_{map}}{\partial p_i}\bigg|_{\bar{\mathbf{x}},\bar{\mathbf{u}}} = -\frac{CO_0(1 + \alpha_1\bar{p} + \alpha_3\bar{p} + \alpha_4\bar{c}_P + \alpha_6\bar{n})g_{i,0}\beta_i}{(1 + k_{BR}HR_0\bar{r}_b)\left[\sum\limits_{j=1}^{9} g_{j,0}(1 + \beta_j\bar{p} + \gamma_j\bar{c}_P + \kappa_j\bar{n})\right]^2}$$

$$\partial\mathbf{h}_{m,A}^6 = \frac{\partial h_{map}}{\partial p_A}\bigg|_{\bar{\mathbf{x}},\bar{\mathbf{u}}} = \frac{CO_0\alpha_3}{(1 + k_{BR}HR_0\bar{r}_b)\sum\limits_{j=1}^{9} g_{j,0}(1 + \beta_j\bar{p} + \gamma_j\bar{c}_P + \kappa_j\bar{n})}$$

$$\partial\mathbf{h}_{m,b}^7 = \frac{\partial h_{map}}{\partial r_b}\bigg|_{\bar{\mathbf{x}},\bar{\mathbf{u}}} = -\frac{CO_0(1 + \alpha_1\bar{p} + \alpha_3\bar{p} + \alpha_4\bar{c}_P + \alpha_6\bar{n})k_{BR}HR_0}{(1 + k_{BR}HR_0\bar{r}_b)^2\sum\limits_{j=1}^{9} g_{j,0}(1 + \beta_j\bar{p} + \gamma_j\bar{c}_P + \kappa_j\bar{n})}$$

$$\partial\mathbf{h}_{m,n}^8 = \frac{\partial h_{map}}{\partial n}\bigg|_{\bar{\mathbf{x}},\bar{\mathbf{u}}} = \frac{CO_O}{(1 + k_{BR}HR_0\bar{r}_b)\sum\limits_{j=1}^{9} g_{j,0}(1 + \beta_j\bar{p} + \gamma_j\bar{c}_P + \kappa_j\bar{n})}$$

$$\left\{\alpha_6 - \frac{(1 + \alpha_1\bar{p} + \alpha_3\bar{p} + \alpha_4\bar{c}_P + \alpha_6\bar{n})\sum\limits_{j=1}^{9} g_{j,0}\kappa_j}{\sum\limits_{j=1}^{9} g_{j,0}(1 + \beta_j\bar{p} + \gamma_j\bar{c}_P + \kappa_j\bar{n})}\right\}$$

$$\partial\mathbf{h}_{m,P}^9 = \frac{\partial h_{map}}{\partial c_P}\bigg|_{\bar{\mathbf{x}},\bar{\mathbf{u}}} = \frac{CO_O}{(1 + k_{BR}HR_0\bar{r}_b)\sum\limits_{j=1}^{9} g_{j,0}(1 + \beta_j\bar{p} + \gamma_j\bar{c}_P + \kappa_j\bar{n})}$$

$$\left\{\alpha_4 - \frac{(1 + \alpha_1\bar{p} + \alpha_3\bar{p} + \alpha_4\bar{c}_P + \alpha_6\bar{n})\sum\limits_{j=1}^{9} g_{j,0}\gamma_j}{\sum\limits_{j=1}^{9} g_{j,0}(1 + \beta_j\bar{p} + \gamma_j\bar{c}_P + \kappa_j\bar{n})}\right\}$$

Improving Regulation of Mean Arterial Blood Pressure During Anesthesia Through Estimates of Surgery Effects

The clinical evaluation of the MAP controller with endtidal override has shown limitations in the ability to reject disturbances caused by surgical stimulations. One approach to further improve MAP regulation is to utilize any available knowledge about the progress of surgery in the control algorithm. In this appendix we propose to provide a model predictive controller (MPC) with rough estimates of the effects of surgical events and to use it to improve blood pressure regulation during anesthesia. Since it is merely a feasibility study without a clinical validation it is placed in this appendix instead of chapter 4.

Predictive control schemes have already successfully been applied for drug application. Linkens and Mahfouf [279] have applied Generalized Predictive Control (GPC) to control blood pressure during anesthesia. However, the scheme was only used to obtain a linear controller, constraints on the control variables were not taken into account and no use was made of any knowledge about future surgical events. Rao et al. [388] applied MPC to control MAP, cardiac output (CO) and mean pulmonary arterial pressure (MPAP). In this study input constraints were taken into account but still no use was made of knowledge about future disturbances. Derighetti applied MPC to blood pressure regulation with Isoflurane but he also did not include the possibility to use knowledge about future disturbances. Wada and Ward [478] used open loop MPC for optimal application of alfentanil. The potential of incorporating knowledge about future surgical events is mentioned but not explored.
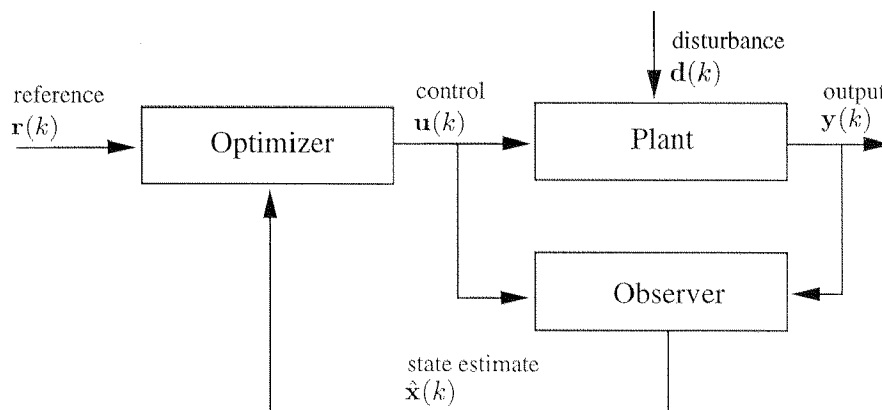
Figure B.1: Structure of the generic MPC controller with the elements plant, observer, and optimizer.

B.1 Model Predictive Control (MPC)

MPC is a control scheme which has gained popularity in recent years. Originating in process control, MPC has been successfully applied to numerous other areas. To discuss MPC in depth is beyond the scope of this section, therefore we only provide minimal information about the algorithm used for this study. A more detailed treatment can be found in [72] and [262]. The key motivation for using MPC in our application is that knowledge about the future (e.g. future reference values or future disturbances) can be used by the algorithm. There are other features of MPC that we benefit from for blood pressure regulation with Isoflurane. First, the input (actuator) constraints which must be imposed for physical and safety reasons can be handled explicitly. Further, the strategy can be extended naturally to multiple input multiple output (MIMO) systems and time delays caused by actuators or sensors can be handled easily. MPC has one drawback which makes it impractical for some on line applications: it is computationally complex. This is not a problem here since physiological processes are relatively slow, thus allowing enough time for computations between sampling intervals as Derighetti has demonstrated in [111].

The generic structure of MPC is shown in figure B.1 and its functioning is best understood together with figure B.2. At every time k an optimization is performed to compute the sequence of optimal control values $\mathcal{U}(k)$ over the control horizon m such that a certain performance criterion is optimized over the prediction horizon p. Of the computed control move sequence $\mathcal{U}(k)$ only the first control move $u(k)$ is then implemented, measurements of the outputs $y(k)$ are taken, updates of the estimated system states $\hat{x}(k)$ are computed and a next series of optimal control values is determined based on the estimated state, the system dynamics, and the reference signal $r(k)$. In most applications a quadratic objective function of the form

$$J = \sum_{i=1}^{p} e(k+i|k)^{T} R e(k+i|k) + \sum_{i=0}^{m-1} \Delta u(k+i|k)^{T} S \Delta u(k+i|k) \qquad (B.1)$$

is used, where $e(k+1|k)$ denotes the predicted error between desired and future predicted states $x(k+i|k)$ of the system. Very often a linear plant model is used for MPC. This has
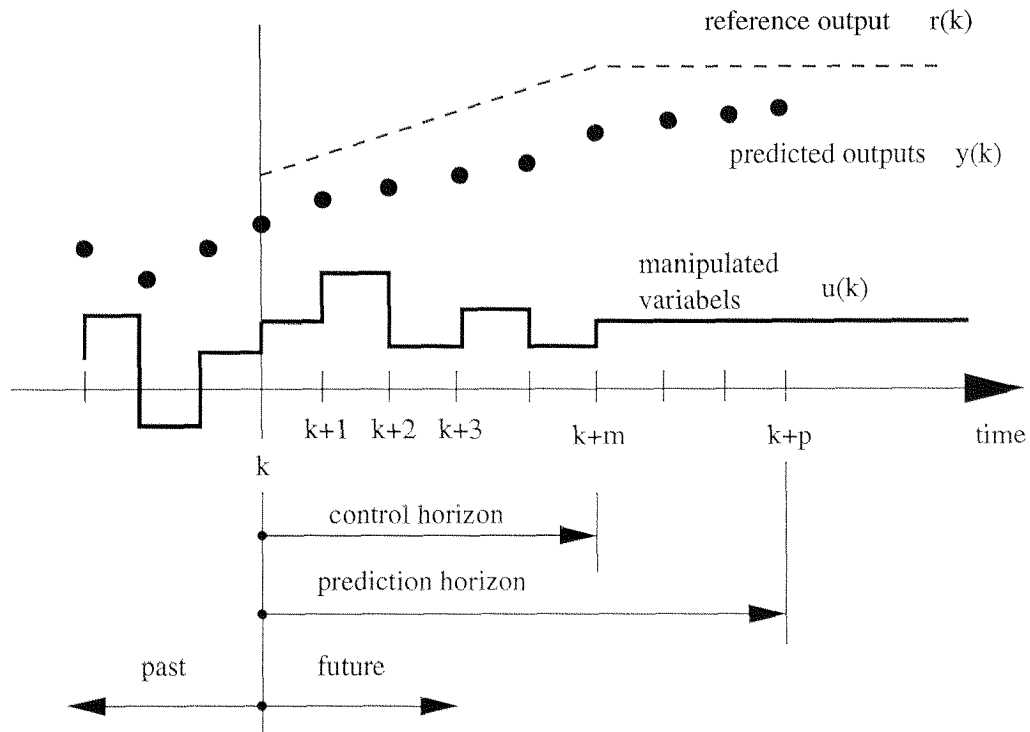
Figure B.2: Illustration of the MPC scheme for a SISO system.

the advantage that if no constraints are imposed on $x(k)$ and $u(k)$ the optimization problem can be solved explicitly and leads to a linear dynamic output feedback control law. If, however, constraints on $x(k)$ and $u(k)$ exist, a quadratic program (QP) has to be solved at every time step. In this case (linear plant model) convergence to the global optimum is assured since the resulting optimization problem is convex. If the plant model is nonlinear the problem is not necessarily convex and finding the global optimum is not trivial. In that case it might become difficult to meet timing specifications for real time applications. This is the reason why quadratic cost functions and linear plant models are most commonly used.

The MPC algorithm has essentially four tuning parameters. These are the matrices $\mathbf{R}$ and $\mathbf{S}$ in equation (B.1) and the prediction horizon p and the control horizon m indicated in figure B.2. $\mathbf{R}$ and $\mathbf{S}$ determine how much errors in the states are weighted against control effort. Putting the main weight on the state errors results in an aggressive controller whereas we get conservative controllers by putting most weight on the control action. The prediction horizon p determines how far into the future predictions are made and future reference values (or disturbance predictions) are taken into account. The control horizon m determines how many future control moves are computed. For infinite p stability results for the closed loop system are available. For computational reasons, however, the horizons p and m are often chosen to be finite.

B.2 Anticipating Model Predictive Control

The detailed MPC setup with disturbance estimates for our scenario is shown in figure B.3. The plant is now represented by the patient and the ventilator (see also figure 3.1 for reference). The control input $u(k)$ corresponds to the concentration of anesthetic gas in the fresh gas $c_{vap}(k)$, the output $y(k)$ corresponds to the change in mean arterial blood pressure (MAP) caused by the drug and disturbances. The major source of disturbance is assumed to be the surgical stimulation $d_s(k)$ which is not measurable. The optimal control values $\mathcal{U}(k)$ are computed on the basis of estimates of the future plant states represented by future outputs of the system $\hat{\mathbf{Y}}(k|k) = \widehat{\mathbf{MAP}}(k|k)$, estimates of future disturbances $\hat{\mathcal{D}}_s(k)$ and the knowledge about future values of the reference signal $\mathcal{R}_{MAP}(k)$. Both $\mathcal{R}_{MAP}(k)$ and $\hat{\mathcal{D}}_s(k)$ are provided by the anesthetist.

Although the trajectory of future disturbances will never be known exactly an anesthetist is able to roughly predict the instant of occurrence and the size of major surgical stimulations such as skin incision. The extensive study of the hemodynamic reaction under Isoflurane/oxygen anesthesia to different noxious stimuli by Zbinden et al. [519] gives an example of such knowledge. Their results allow to estimate average blood pressure increase and corresponding confidence intervals for different noxious stimuli at different levels of endtidal Isoflurane concentration. Table B.1 summarizes these results for an endtidal Isoflurane concentration of 1 MAC. The numbers reveal a clear correlation between the kind of stimulation and the average blood pressure increase, though, the variability is very broad. For the natural stimuli (laryngoscopy, skin incision, intubation) the individual response can deviate up to 57% from the average value. Making this rough information available to an MPC may still be advantageous compared to no information about future events, even if size and the instant of occurrence of the stimuli are not predicted precisely.

For this study we have been working with a finite step response model representation of the control input dynamics and the disturbance input dynamics. They were obtained from the linearized model equations (3.106). Note that in this linear model the disturbance d_s may be measured in $mmHg$ after scaling the steady state gain of the linear disturbance transfer function to one. For that case the state vector for the system is represented by the future output values of the system

$$\mathbf{Y}(k) = \begin{bmatrix} y(k) \\ y(k+1) \\ \vdots \\ y(k+n) \end{bmatrix} \tag{B.2}$$

where n and the sampling frequency are chosen such that the important dynamic effects resulting form disturbance input and control input are captured. The advantage of using step response models is that they can be obtained experimentally quite easily as was done by Furutani et al in [159]. The state estimate is computed in two steps, i.e. one step ahead prediction and correction after taking a measurement. Assuming an estimate of the state $\hat{\mathbf{Y}}(k|k)$ available at time k, the one step ahead prediction is

$$\hat{\mathbf{Y}}(k+1|k) = \mathbf{M}\hat{\mathbf{Y}}(k|k) + \mathbf{s}^u \Delta u(k) \tag{B.3}$$

where M is the matrix that maps the state vector at time k to the time $k+1$. That is for our
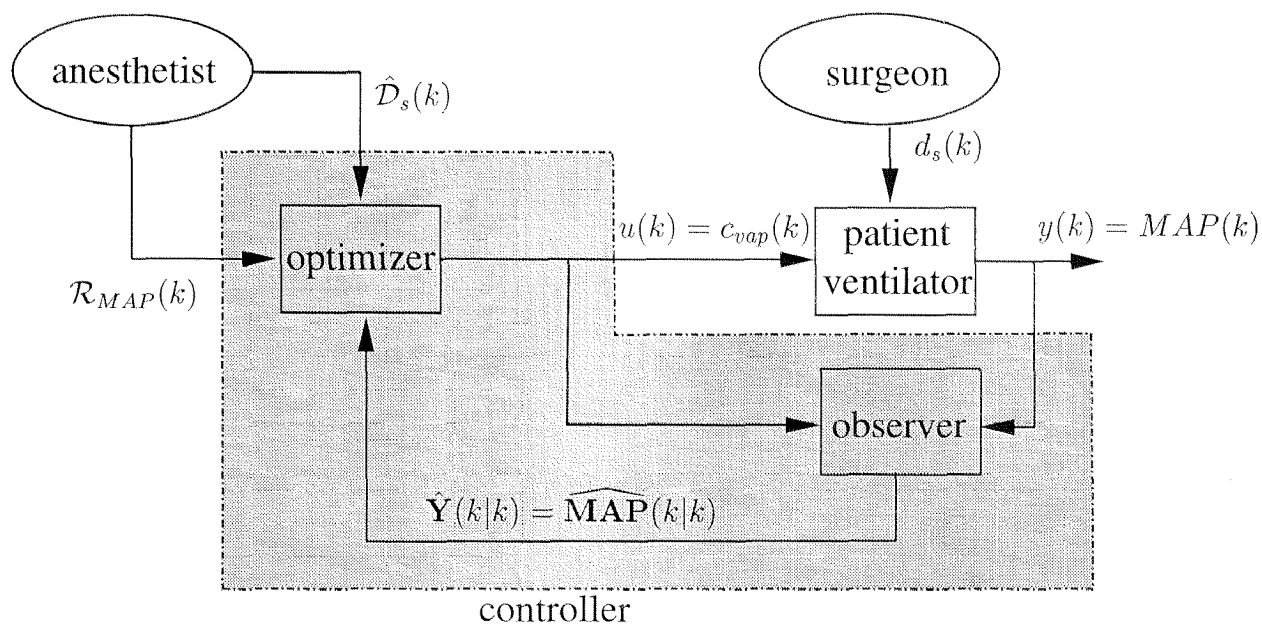
Figure B.3: Setup for MPC with disturbance estimates. The plant (patient + ventilator) is "driven" by the input $u(k)$ (anesthetics applied to the fresh gas stream c_{vap}) and the disturbance $d_s(k)$ (surgical and other stimuli), the output $y(k)$ is the change in blood pressure. The reference signal $\mathcal{R}_{MAP}(k)$ (desired blood pressure), the actual output $y(k)$ (measured blood pressure $MAP(k)$), and an estimate of the disturbance trajectory $\hat{\mathcal{D}}_s(k)$ (estimates of major stimuli) are available to the controller, based on which the optimal trajectory for the control signal $u(k)$ is computed. To compute this optimal control signal the optimizer utilizes estimates of the system states (in our case represented by future outputs of the system $\widehat{MAP}(k|k)$), they are obtained via an observer. Note that the actual disturbance $d_s(k)$ is not measurable

Stimulus	Average blood pressure increase in $mmHg$	95 % confidence interval in $mmHg$
Trapezius squeeze	9	$\pm\ 8.2$
Tetanic stimulation	15	$\pm\ 7.5$
Laryngoscopy	23	$\pm\ 13$
Skin incision	35	$\pm\ 20$
Intubation	49	$\pm\ 23$

Table B.1: Average blood pressure increase and confidence intervals for different noxious stimuli at an endtidal Isoflurane level of 1 MAC deduced form [519]. Trapezius squeeze and tetanic stimulation are well defined artificial stimuli, the other stimuli are naturally occurring during surgery. A clear correlation between the kind of stimulation and the average blood pressure increase can be observed. However, for the natural stimuli the individual response can deviate up to 57% from the average value

non-integrating single output system:

$$\mathbf{M} = \begin{bmatrix} 0 & 1 & 0 & 0 & \cdots & 0 & 0 & 0 \\ 0 & 0 & 1 & 0 & \cdots & 0 & 0 & 0 \\ \vdots & \vdots & \vdots & \vdots & & \vdots & \vdots & \vdots \\ 0 & 0 & 0 & 0 & \cdots & 0 & 1 & 0 \\ 0 & 0 & 0 & 0 & \cdots & 0 & 0 & 1 \\ 0 & 0 & 0 & 0 & \cdots & 0 & 0 & 1 \end{bmatrix} \quad \text{and} \quad \mathbf{s}^u = \begin{bmatrix} s_1^u \\ s_2^u \\ \vdots \\ s_n^u \end{bmatrix} \tag{B.4}$$

is the vector of control input step response coefficients of the system. The correction is given by

$$\hat{\mathbf{Y}}(k+1|k+1) = \hat{\mathbf{Y}}(k+1|k) + \mathbf{K}_F\{\hat{y}(k+1) - y(k+1)\} \tag{B.5}$$

where $\mathbf{K}_F$ is a filter gain matrix computed according to [262] and $y(k+1)$ is the measurement of the system output at time $k+1$.

The basis for the computation of the future control moves is the p-step ahead prediction

$$\hat{\mathcal{Y}}(k+1|k) = \mathcal{M}\hat{\mathbf{Y}}(k|k) + \mathbf{S}^d\Delta\hat{\mathcal{D}}_s(k) + \mathbf{S}^u\Delta\mathcal{U}(k) \tag{B.6}$$

where $\mathcal{M}$ is a submatrix of $\mathbf{M}$ of dimension $n \times p$ i.e.

$$\mathcal{M} = \begin{bmatrix} 0 & 1 & 0 & 0 & \cdots & 0 & 0 & 0 & \cdots & 0 \\ 0 & 0 & 1 & 0 & \cdots & 0 & 0 & 0 & \cdots & 0 \\ \vdots & \vdots & \vdots & \vdots & & \vdots & \vdots & \vdots & \vdots & \vdots \\ 0 & 0 & 0 & 0 & \cdots & 0 & 1 & 0 & \cdots & 0 \end{bmatrix} \tag{B.7}$$

$\mathbf{S}^d$ and $\mathbf{S}^u$ are the matrices with step response coefficients corresponding to the disturbance and control input respectively

$$\mathbf{S}^d = \begin{bmatrix} s_1^d & 0 & \cdots & 0 \\ s_2^d & s_1^d & \cdots & 0 \\ \vdots & \vdots & \vdots & \vdots \\ s_p^d & s_{p-1}^d & \cdots & s_{p-m+1}^d \end{bmatrix} \quad \mathbf{S}^u = \begin{bmatrix} s_1^u & 0 & \cdots & 0 \\ s_2^u & s_1^u & \cdots & 0 \\ \vdots & \vdots & \vdots & \vdots \\ s_p^u & s_{p-1}^u & \cdots & s_{p-m+1}^u \end{bmatrix} . \tag{B.8}$$

The essential point in the algorithm is the $\Delta\hat{\mathcal{D}}_s$ term in equation (B.6). Here an estimate of future disturbances can be provided to the algorithm which will be taken into account for the computation of the optimal control values. This sequence of future control moves is obtained as the result of the following constrained quadratic optimization problem

$$\min_{\Delta\mathcal{U}} \left\{ \left\| \Gamma^y \left[\mathcal{R}_{MAP}(k+1) - \hat{\mathcal{Y}}(k+1|k) \right] \right\|^2 + \left\| \Gamma^u \Delta\mathcal{U}(k) \right\|^2 \right\} \qquad (B.9)$$

$$s.t. \quad \mathcal{C}^u \Delta\mathcal{U}(k) \geq \mathcal{C}(k+1|k).$$

Γ^y and Γ^u are weighting matrices related to $\mathbf{S}$ and $\mathbf{R}$ in equation (B.1). The matrices $\mathcal{C}^u$ and $\mathcal{C}(k+1|k)$ result from the constraints on the manipulated variables, on their rate of change and on the outputs. In our study constraints were imposed on the manipulated variables only. The constraints have the form

$$\begin{bmatrix} -I_L \\ I_L \end{bmatrix} \Delta\mathcal{U}(k) \geq \left. \begin{bmatrix} u(k-1) - u_{high} \\ \vdots \\ u(k-1) - u_{high} \\ u_{low} - u(k-1) \\ \vdots \\ u_{low} - u(k-1) \end{bmatrix} \begin{array}{c} \left.\rule{0pt}{30pt}\right\} m \\ \\ \left.\rule{0pt}{30pt}\right\} m \end{array} \right.$$

where I_L is a lower triangular matrix of appropriate dimension with the nonzero elements being equal to 1.

B.3   Simulation Study

A simulation study was conducted to demonstrate the potential improvements in blood pressure regulation during anesthesia that can be achieved by using rough estimates of disturbances. To evaluate performance we applied a single disturbance step d_s of $30\ mmHg$ (figure B.4). This stimulation is large enough to justify a change in drug application even for manual control. From table B.1 it can be seen that this disturbance hight is indeed realistic. This may also be confirmed with the experimental results of section 4.5. And with figure 4.15 the step like disturbance input d_s can be justified.

It is reasonable to assume that an anesthetist is able to make predictions (or educated guesses) of the major future disturbances based on the progress of surgery. Consider for example the operation shown in figure 4.15. In this case the begin of the operation and skin incision after the break could have easily been anticipated. It is however not very likely that these guesses are correct especially if made over a large horizon. Assuming a step disturbance the estimates can be off with respect to the instant of occurrence as well as the step size (figure B.4). We will refer to a positive mismatch in time if the actual disturbance occurs later than estimated and we will refer to a positive mismatch in height if the estimated disturbance is larger than the actual disturbance. Anticipation horizons of 2 and $5\ min$ were tested. Both horizons reasonably reflect the anesthetist's ability to make predictions.
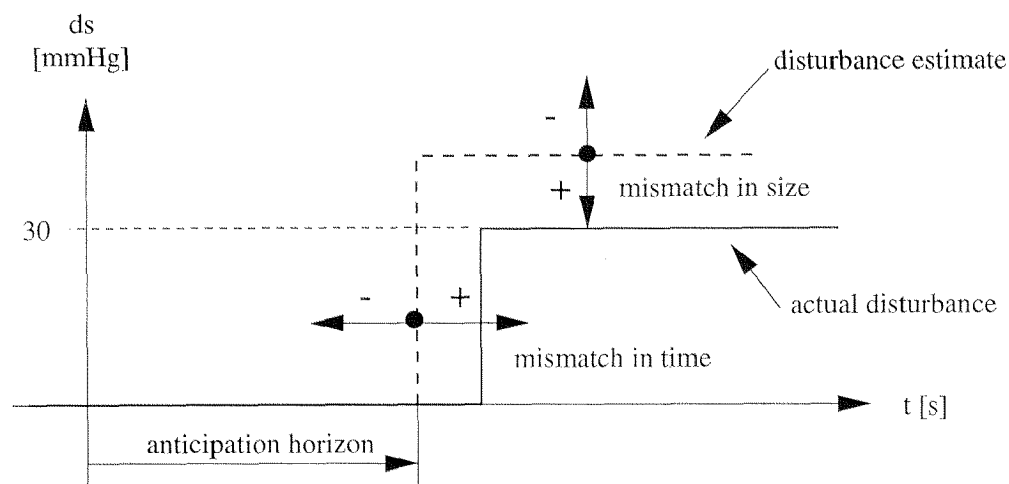
Figure B.4: Disturbances inputs (d_s) are assumed to be step like. There are two ways in which a disturbance estimate can be inaccurate: There can be a mismatch in time of occurrence and there can be a mismatch in the height of the disturbance.

Since a vaporizer equipped with a DC motor may be moved between its extreme positions in less than a second no constraints on the rate of change for the control signal need to be introduced. The main limitations are thus minimum (u_{low}) and maximum (u_{high}) of the vaporizer position. A linearized model describes the system dynamics around an operating point (u_0, MAP_0). u_0 may be viewed as the mean value of $u(k)$. Simulations with a linear model are therefore valid for the differential signals $u(k) - u_0$ and $MAP(k) - MAP_0$ and the input constraint have to be adjusted accordingly to $u_{low} - u_0$ and $u_{high} - u_0$, respectively. No weight was put on the control signal (i.e. $\Gamma^u = 0$) since this would further decrease the effectiveness of the already limited control action.

The algorithm used a prediction horizon of 102 (17 min) and a control horizon of 30 (5 min). These values were found through some trial and error. Note that the prediction horizon has nothing to do with the anticipation horizon. The prediction horizon determines how far into the future the algorithm is predicting based on the available information. The anticipation horizon determines when the disturbance estimate is made available to the algorithm.

B.4   Results

The simulation results are shown in the figures B.5 to B.8. Figure B.5 shows an example trajectory and figure B.6 shows the typical qualitative behavior of output trajectories for three typical mismatches in the estimated time of disturbance occurrence. The summarized results for different mismatches in the estimated instant of occurrence and different mismatches in estimated disturbance height are shown in figure B.7 and B.8, respectively. Since the objective for the control algorithm is formulated in terms of the integral squared error (ISE) or 2-norm the controller performance is first evaluated in terms of the ISE. The interpretation of the ISE results
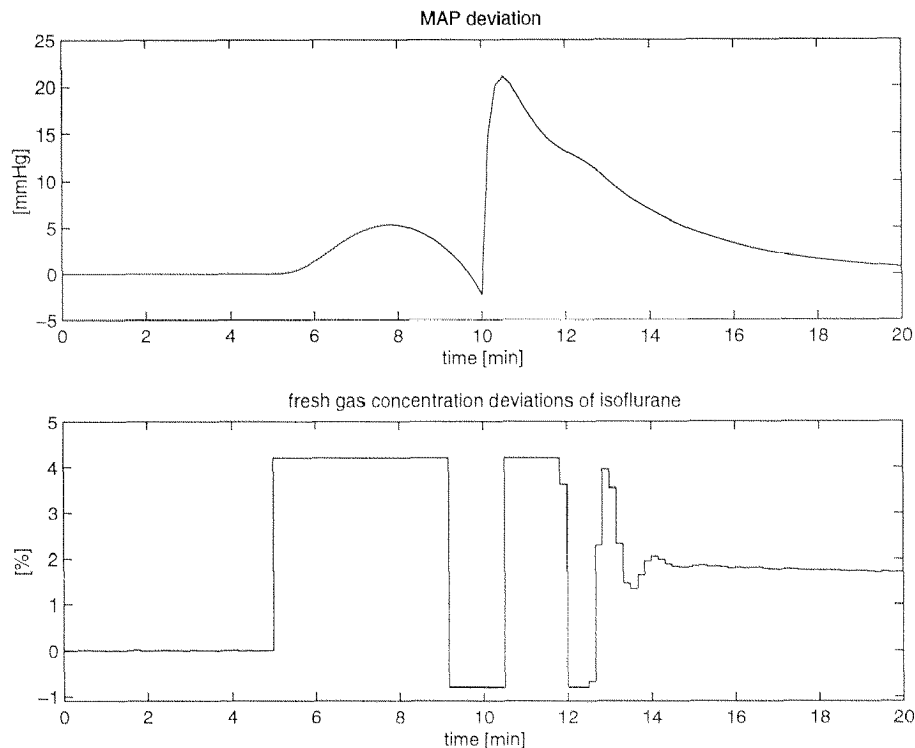
Figure B.5: A typical Trajectory that demonstrates how MPC handles disturbance estimates. The sampling time is $10s$. The upper plot shows how the deviation of MAP from a reference value evolves with time and the lower plot shows the corresponding vaporizer concentration expressed in deviations from their mean value u_0. Note, the absolute constraints on the vaporizer isoflurane concentration are $0 \ldots 5\%$, however, by using a linear model we implicitly assumed to work at an operating point. This fact has to be taken into account, when running simulations with this model, by adjusting the constraints accordingly.

are, however, not very intuitive. We therefore also look at minimum and maximum deviations of the output from the setpoint. They show a similar qualitative result and are easier to interpret. In particular, they allow to asses how the algorithm trades post-stimulation high pressure for pre-stimulation low pressure.

From the example trajectory shown in figure B.5 it can be understood how MPC uses the disturbance prediction information. In this example the disturbance occurs at 10 minutes whereas it is estimated to occur at 9 minutes. With a anticipation horizon of 4 minutes the MPC algorithm starts to react to the predicted disturbance in advance by increasing the fresh gas concentration. Due to the non-minimum phase characteristic MAP first increases but after a while decreases blow its reference value. By this the algorithm attempts to compensate post-stimulation high pressure with pre-stimulation low pressure. Because of the mismatch in the estimated instant of occurrence in this example, however, the disturbance does not occur as anticipated and the controller immediately stops drug application at 9 minutes 10 seconds. Drug application is resumed only after the disturbance has actually occurred. This phenomenon that drug application is suspended when the disturbance occurs later than anticipated guarantees that pre-stimulation MAP is not lowered arbitrarily. The graph demonstrates that it is not possible to compensate
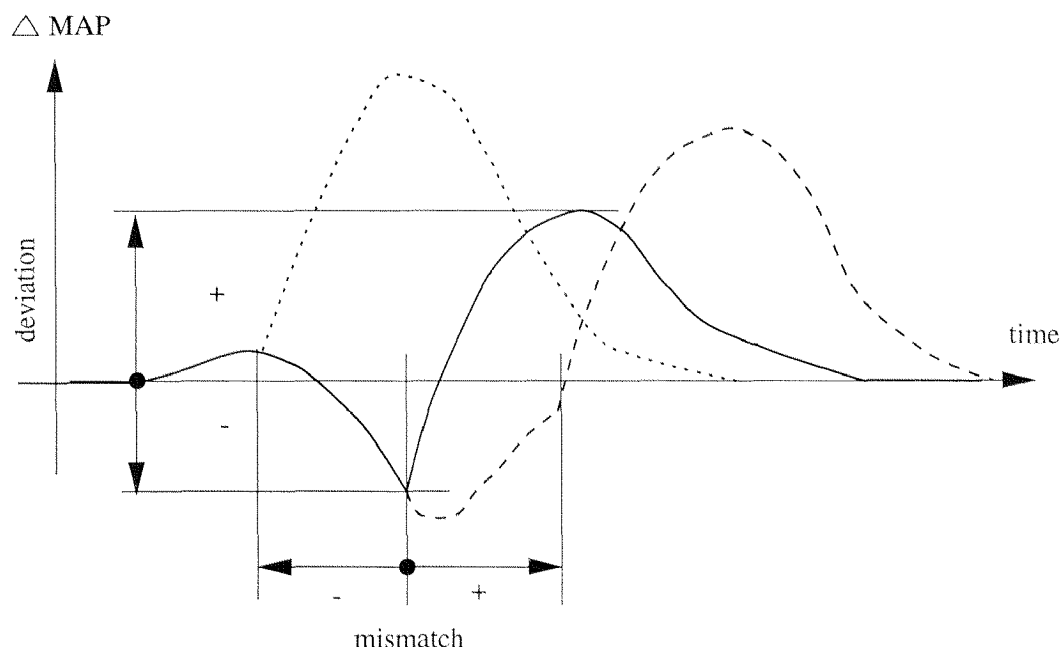
Figure B.6: Qualitative picture of typical trajectories. The solid line corresponds to a case where the instant of occurrence is estimated correctly, the dashed trajectory corresponds to a case where the actual disturbance occurs late compared to the estimate (positive mismatch in time), and the dotted trajectory denotes a case where the actual disturbance arrives early (negative mismatch in time).

for the disturbance effects totally (due to the relatively fast disturbance dynamics and the input constraints) and that the performance objective given by equation (B.1) is thus minimized by lowering MAP prior to the occurrence of the disturbance. This also reduces the maximum positive deviations from the desired reference MAP value. The graph further reveals that in order to react to large blood pressure changes the actuator signal is saturated most of the time which in particular limits pre-stimulation blood pressure reduction.

Figure B.6 shows the qualitative picture of typical trajectories for different mismatches in the estimated instant of disturbance occurrence and no mismatch in the estimated size of the disturbance. It will help to interpret the results shown in figure B.7. The solid line corresponds to a case where instant of occurrence and disturbance height are estimated correctly. The dashed trajectory corresponds to a case where the actual disturbance occurs late compared to the estimate (positive mismatch in time). The control algorithm already started to increase MAP after the estimated time of occurrence by stopping the drug application. This results in a larger maximum positive deviation of MAP from the desired value as well as a larger integral squared error. However, the maximum negative deviation is almost the same which happens because drug application is suspended. The dotted trajectory denotes a case where the actual disturbance arrives early. The algorithm is not able to decrease MAP enough prior to the occurrence of the disturbance which also results in a larger maximum positive deviation of MAP and integral squared error. Note however, that the maximum negative deviation is significantly smaller. We will see that even if the disturbance occurs while MAP could not be lowered below the reference value it is

Figure B.7: Variation of integral squared error (ISE, left column of plots), maximum positive and negative deviations of mean arterial blood pressure (MAP) from a desired reference value (right column of plots) as a function of mismatch in the estimates of the instant of occurrence of a stimulus. For reference the ISE and the maximum positive deviations resulting if no disturbance prediction is available to the MPC algorithm are shown dashed lines. The disturbance height was assumed to be exactly known and was equal to 30 mmHg for all cases.

advantageous over the case with no anticipation.

Figure B.7 summarizes the results for different mismatches in instant of occurrence. The left column of plots evaluates performance in terms of the ISE while the right column of plots evaluates the performance in terms of maximum positive and maximum negative deviations of the output from the setpoint. For the results in the upper row of plots an anticipation horizon of 2 min was used and for the plots in the lower row a prediction horizon of 5 min was used.

The ISE result reveal that a reduction of up to 80 % in ISE can be achieved over the situation where no anticipation information is used (taken as 100%). A larger reduction is obtained for longer anticipation horizons. The result of the algorithm further depends on the accuracy of the anticipation of the instant of occurrence, however, there is a broad range of mismatch for which anticipation information is advantageous. The problem with this ISE result is that it is not clear what this means for the patient. This is much more clearer when looking at maximum positive and negative deviations of MAP from the reference value.
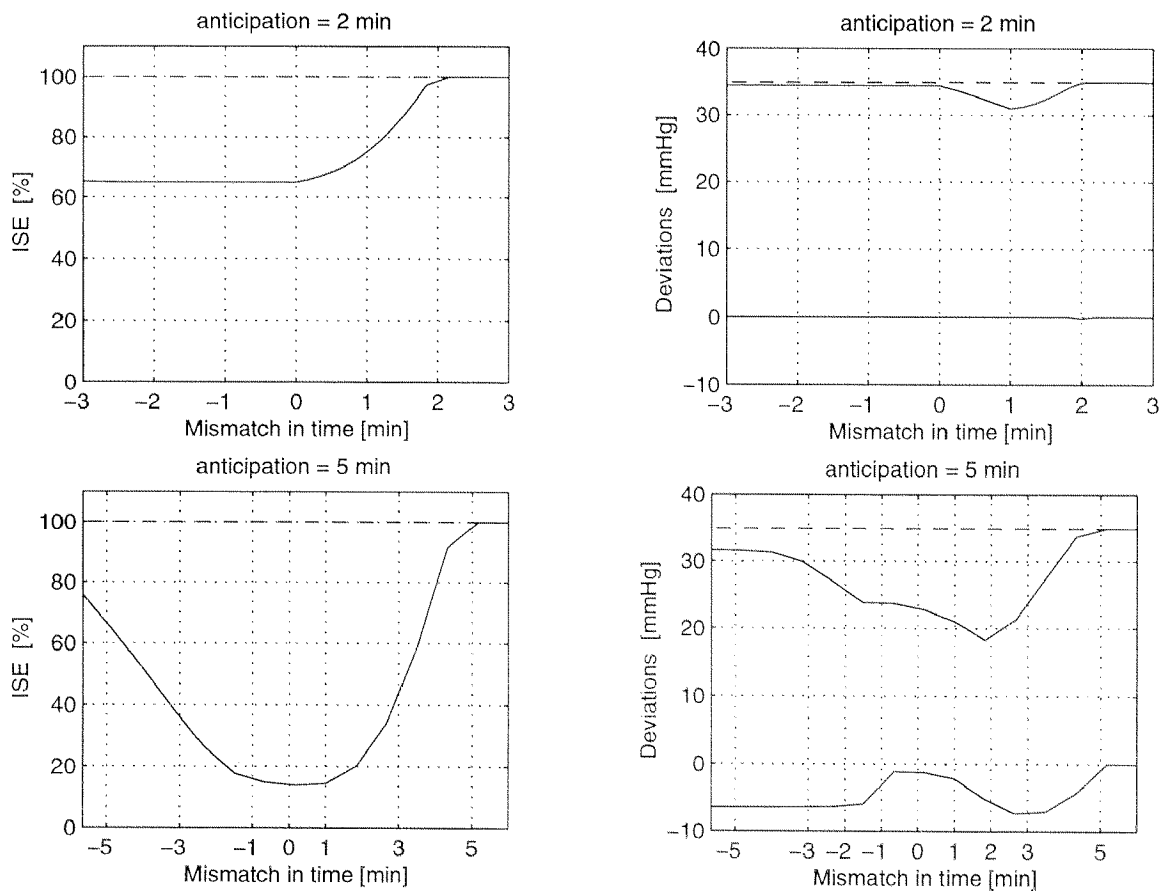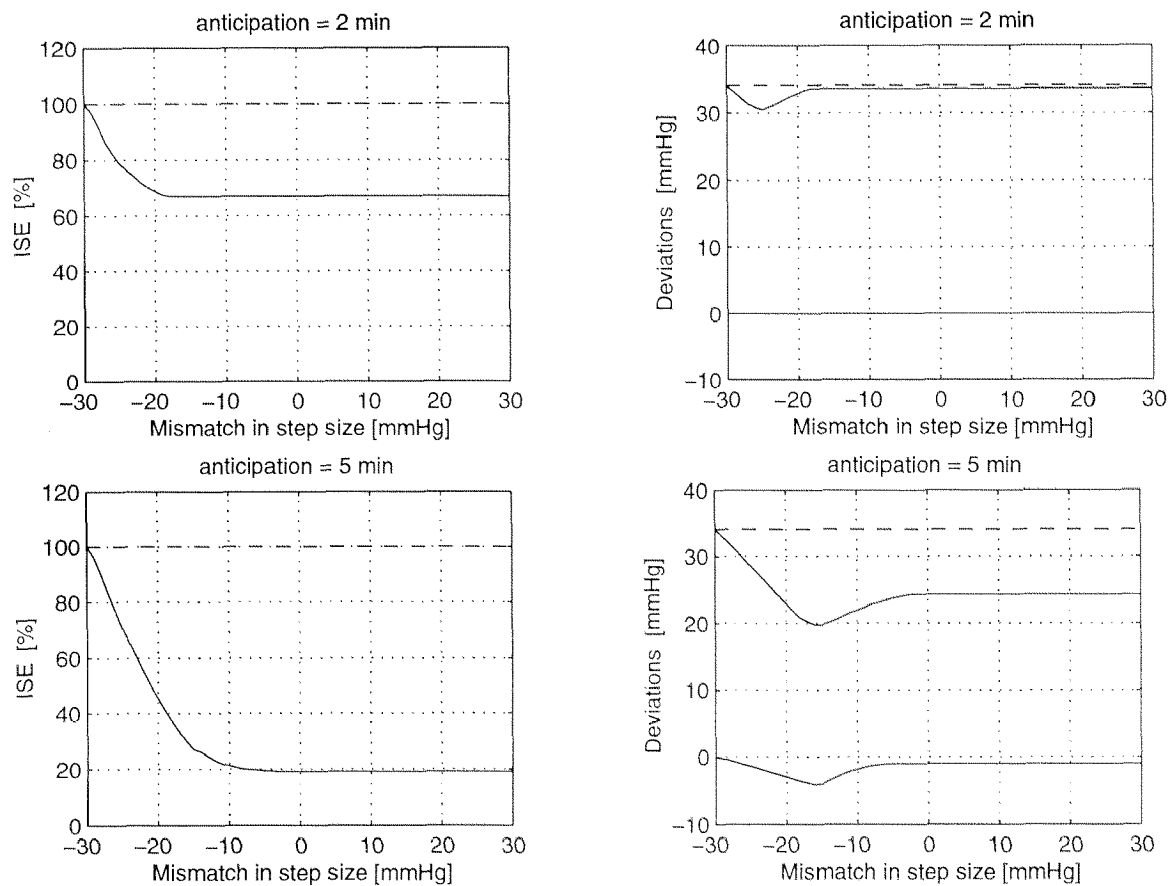
Figure B.8: Variation of integral squared error (ISE), maximum positive and negative deviations of mean arterial blood pressure (MAP) from a desired reference value as a function of mismatch in estimates of the size of the disturbance (actual hight was 30 mmHg). For reference the ISE and the maximum positive deviations resulting if no disturbance prediction is available to the MPC algorithm are shown by dashed lines. There is no mismatch in the estimate of the time of occurrence of the disturbance.

The evaluation in terms of maximum positive deviations from the setpoint (basically post-stimulation blood pressure increase) shows the qualitative similar behavior. A reduction of up to 35 % over the un-anticipated case can be achieved. The achieved decrease is minor for an anticipation horizon of 2 min. The reduction of the maximum positive deviation is partially obtained at the cost of negative deviations.

Figure B.8 summarizes the results where the instant of occurrence is assumed to be correct but a wrong disturbance height is assumed. Again evaluations in terms of ISE (left column of plots) as well as maximum positive and maximum negative deviation (right column of plots) are shown for anticipation horizons of 2 min (upper row) and 5 min (lower row).

For the ISE evaluation the case with no disturbance anticipation is taken as 100 %. It can be seen that the ISE decreases from a mismatch of -30 $mmHg$ (estimated height $= 0$) to approach a constant value for positive mismatches. Again the ISE does not allow to tell what this means for the patient.

The evaluation in terms of maximum positive deviations from the set point again is similar to the ISE result. With anticipation horizons of 2 *min* and 5 *min* there is almost no pre-stimulation lowering of blood pressure. This results in small maximum negative deviations. The results show that 2 *min* anticipation is too short for improving blood pressure regulation significantly. However, for an anticipation of 5 *min* significant improvements are possible even with very poor "guesses".

B.5 Conclusions

From the different plots in figure B.7 we conclude that when information about the effect of surgical events on MAP is utilized by the controller ISE and the maximum MAP deviations can be reduced significantly even when this information is inaccurate. The anticipation time must be on the order of 5 minutes to produce significant imporvements. This reduction is in some cases achieved through lowering of pre-stimulation MAP resulting in negative deviations from the desired reference MAP. As expected we find that the effectiveness of the disturbance anticipations depends on the accuracy of the estimated instant of occurrence. However, there is a broad range of even very poor time estimates for which an improvement can be achieved over the situation where no predictions are used. At worst (highly inaccurate information) no improvement is obtained.

The plots in figure B.8 show that the improvement is less sensitive with respect to the accuracy of estimates of the disturbance height. Obviously less improvement is obtained if the disturbance height is underestimated. However, it is important to note that there is no degradation in case of overestimation. The results of Zbinden et al. [519] suggest that the height of the blood pressure response to natural stimuli (laryngoscopy, skin incision, intubation) can deviate up to 60% from the average value. From figure B.8 we conclude that this variation cannot lead to unacceptable performance.

The disturbance step that has been applied for the simulations was positive but analogous results would be obtained for a negative step. While positive disturbance steps denote the onset of a stimulation negative steps denote the end of a stimulation. Obviously the presented algorithm can also be used to prevent low blood pressure situations after the termination of a stimulation.

These results suggest that estimates of the effects of major surgical events during anesthesia can be used to improve blood pressure regulation during anesthesia even if they are inaccurate. It has been demonstrated that model predictive control (MPC) allows to use rough disturbance estimates in a straight forward manner.

It was demonstrated that the reduction of post-stimulation blood pressure is in some cases obtained through lowering of pre-stimulation pressure. This might not be acceptable for all patients and there are two ways how low pressure can be limited. The most straight forward treatment is to introduce constraint on the output for the optimization (equation (B.9)). We have seen that pre-stimulation pressure is limited by the prediction horizon and the upper limit of the control signal. Alternatively one could choose the prediction horizon based on the allowed

pre-stimulation blood pressure. The final decision, however, of whether or not the algorithm should be invoked has to be left to the anesthetist.

In chapter 4 it was discussed that for control of MAP limits on the endtidal Isoflurane concentration must be taken into account. This has not been done in this feasibility study but can be introduced by imposing so called output constraints in the MPC optimization.

Finally, it should be pointed out that robustness (with respect to inter and intra patient variability) issues have not been addressed in this study. Studying these robustness issues will of course be a main focus for future research.

Appendix C

The Recoverability Concept

The goal of fault tolerant control is to recover as much system functionality as possible in case of a fault. In definition 7.2.4 to 7.2.8 this functionality is represented by an objective. If this objective is given as a functional the degree of recoverability may be measured based on the maximum achievable value for the objective function [45]. Often, however, the control objective is not given as a functional or the functional is not the ultimate objective and rather serves to formalize the design procedure as in the LQR method.

Alternatively one might therefore ask how much control over the system is left and how much information might be obtained about the system through measurements after a fault occurred. This view leads to a definition of recoverability based on controllability and observability of the faulty system compared to the fault free case. In [154] the hybrid formulation of FTC systems was used to derive recoverability conditions based on the controllability of hybrid systems. This analysis is not very useful in practice since no analytic solution to the problem can be derived. In addition, the definitions 7.2.7 and 7.2.8 (and the more formal definitions in [45]) address the problem only after successful detection and isolation of the fault. No attention is paid to the fact that the time between fault occurrence and its detection and isolation might be crucial for the decision whether the system is recoverable from a fault or not.

If, however, we agree to neglect the time between fault occurrence and remedial action it is natural to derive recoverability conditions that are based on system properties of the faulty and the non-faulty system. In this appendix we propose to base the recoverability conditions for LTI systems on controllability and observability measures (see also [154])..

C.1 Recoverability for parameterized LTI systems

Consider a set of systems $S(q_f, q_a)$ parameterized by the configurators q_f and q_a. That is $S(\varnothing, \varnothing)$ represents the nominal fault free system, $S(q_f, \varnothing)$ represents the system after occurrence of the

fault event and $S(q_f, q_a)$ denotes the faulty system after reconfiguration. That is for every $S(q_f, q_a)$ there is a linear time invariant system given by

$$\dot{\mathbf{x}}(t) = \mathbf{A}(q_f, q_a)\mathbf{x}(t) + \mathbf{B}(q_f, q_a)\mathbf{u}(t)$$
$$\mathbf{y}(t) = \mathbf{C}(q_f, q_a)\mathbf{x}(t) + \mathbf{D}(q_f, q_a)\mathbf{u}(t) \tag{C.1}$$

where $\mathbf{x}(t) \in \mathbb{R}^n$ denotes the state vector of the system, $\mathbf{u} \in \mathbb{R}^m$ is a vector of system inputs, $\mathbf{y}(t) \in \mathbb{R}^p$ is the vector of system outputs, and $\mathbf{A}, \mathbf{B}, \mathbf{C}$, and $\mathbf{D}$ are matrices of appropriate dimensions.

The goal is now to derive measures for recoverability based on measures for controllability and observability of the fault free system $S(\varnothing, \varnothing)$ and the reconfigured faulty system $S(q_c, q_f)$. For sensor and actuator faults this problem is related to the problem of optimally selecting inputs and outputs for control systems [331, 434, 238, 237]. While for the classical sensor/actuator selection problem the goal is to identify the most effective sensor/actuator locations the recoverability analysis uses this redundancy measures to asses what is left of the system after a fault. [335] uses controllability and observability measures to optimize adjustable system parameters. Possible measures are the observability gramian

$$\mathbf{W}_o(S) = \int_0^\infty e^{\mathbf{A}^T t}\mathbf{C}^T\mathbf{C}e^{\mathbf{A}^T t}dt \tag{C.2}$$

and similarly the controllability gramian

$$\mathbf{W}_c(S) = \int_0^\infty \mathbf{B}^T e^{\mathbf{A}^T t}e^{\mathbf{A}^T t}\mathbf{B}dt. \tag{C.3}$$

A discussion of the concept of gramians lies outside the scope of this appendix for more details the references [236, 440] should be consulted.

Gramians allow to identify directions in state space of different degree of controllability and observability. For the observability gramian this means, for some state $\mathbf{x}_0$, the quantity $\mathbf{x}_0^T W_o x_0$ represents the observation "energy" obtained from this state $\mathbf{x}_0$. To verify this just multiply equation (C.2) from both sides with $\mathbf{x}_0^T$ and $\mathbf{x}_0$, respectively. For any vector ν, which is a unit length eigenvector, the obtained observation energy is determined by the corresponding eigenvalue. An unobservable direction provides zero observation energy.

Based on these gramians scalar measures $\rho_o(q_f, q_a)$ and $\rho_c(q_f, q_a)$ for recoverability shall be derived. The following properties are desired for such a measure

$$\rho(\mathbf{W}) = 0 \Leftrightarrow \text{loss of observability or controllability} \tag{C.4}$$
$$\rho(\mathbf{W}(\varnothing, \varnothing)) = 1 \tag{C.5}$$
$$\rho(\alpha\mathbf{W}) = \alpha\rho(\mathbf{W}) \tag{C.6}$$
$$\rho(\mathbf{W}_3) \geq \rho(\mathbf{W}_1) + \rho(\mathbf{W}_2) \quad \text{for} \quad \mathbf{W}_3 = \mathbf{W}_1 + \mathbf{W}_2 \tag{C.7}$$

These requirements are satisfied by the following measures

$$\rho_o(q_f, q_a) = \sqrt[n]{\frac{|\mathbf{W}_o(S(q_f, q_a))|}{|\mathbf{W}_o(S(\varnothing, \varnothing))|}}. \tag{C.8}$$

For an intuitive understanding of the nth root recall that the determinant is equal to the product of the eigenvalues. That is it depends on the dimension (number of eigenvalues) of the system. The nth root therefore serves to make the measure independent of the system dimension n.

The measure can be interpreted as follows. Since the determinant is equal to the product of the eigenvalues, $\sqrt[n]{|\mathbf{W}_o|}$ represents an "average" observation energy that can be obtained form the system. Where the "average" is expressed in terms of the geometric mean of the observation energies obtained from the different eigen-directions. The measure $\rho_o(q_f, q_a)$ therefore defines the ratio of "average" observation energies obtained from the faulty system compared to the fault free system.

For "real world" systems the state vector $\mathbf{x}$ might combine states with different units and different ranges. For a meaningful interpretation of the measure the system's states, inputs, and outputs have to be brought into a per unit representation.

For illustration, consider a system with two equivalent sensors, i.e.

$$y_1(t) = \mathbf{C}_1 \mathbf{x}(t) = \mathbf{C}_2 \mathbf{x}(t) = y_2(t). \tag{C.9}$$

Assume that sensor two fails, and operation is continued with sensor one only. The measure $\rho_o(q_f, q_a)$ is computed for

$$\mathbf{C}(\varnothing, \varnothing) = \begin{bmatrix} \mathbf{C}_1 \\ \mathbf{C}_2 \end{bmatrix} \tag{C.10}$$

and

$$\mathbf{C}(q_f, q_a) = \begin{bmatrix} \mathbf{C}_1 \end{bmatrix} \tag{C.11}$$

which yields $\rho_o(q_f, q_a) = \frac{1}{2}$. In this deterministic framework, there is no difference between the two scenarios. But the value of $\frac{1}{2}$ indicates a harder state estimation problem in the stochastic framework.

Note that $\rho_o(q_f, q_a) = 0$ if the system is not recoverable from the sensor fault q_f by the reconfiguration q_a. The consequence of a zero measure C.8 is that an observer constructed from the corresponding measurements results in an open loop estimation of certain modes. Nevertheless, an open-loop estimate might still be used as a short-term replacement for a failed sensor [44].

Similar arguments lead to the definition

$$\rho_c(q_f, q_a) = \sqrt[n]{\frac{|\mathbf{W}_c(S(q_f, q_a))|}{|\mathbf{W}_c(S(\varnothing, \varnothing))|}} \tag{C.12}$$

as a quality indicator for control recovery after an actuator fault.

Both measures C.8 and C.12 only make sense if $S(\varnothing, \varnothing)$ is controllable and observable. If this is not the case, the measure should be applied to the observable or controllable subspaces, only.

The general condition for recoverability form an arbitrary fault can now be stated as:

$$\textbf{system recoverable} \iff \rho_c(q_f, q_a) > 0 \text{ and } \rho_o(q_f, q_a) > 0. \tag{C.13}$$

C.2   Consequences for FTC

In this section we will show that this recoverability concept is indeed a system property with immediate consequences for fault tolerant control.

C.2.1   Reconstruction of measurements

A strategy which is sometimes considered as a remedial action to a sensor fault is to reconstruct the missing measurement, using this instead of the original measurement with the existing control law [300] and [47]. However, this might not always be possible. First, it must be possible to reconstruct the missing measurement from the remaining measurements. Otherwise, the strategy leads to open loop control of certain modes, which could only be a short time remedial action.

A measurement of a faulty sensor can be reconstructed from the remaining measurements if and only if the system is recoverable from that sensor fault. To show this, consider the generalized eigenvector decomposition of the system and write:

$$y_i(t) = \mathbf{c}_i x(t) = \mathbf{c}_i \sum_{j=1}^{n} \xi_j(t) \mathbf{q}_j = \sum_{j=1}^{n} \xi_j(t) \mathbf{c}_i \mathbf{q}_j$$

where y_i is the measurement to be reconstructed, $\mathbf{q}_j$ are the eigenvector directions of the system, $\xi_j(t)$ the time evolution along these directions and n the dimension of the state space of the system.

To show that recoverability is sufficient note that all directions $\mathbf{q}_j$ for which $\mathbf{c}_i \mathbf{q}_j \neq 0$ contribute to the measurement y_i. If the system is recoverable from the failure of sensor i these directions remain observable and thus $y_i(t)$ can be reconstructed.

On the other hand: If the system is not recoverable it looses observability (sensor fault). The direction(s) $\mathbf{q}_j$ for which observability is lost was observable in combination with sensor i and thus $\mathbf{c}_i \mathbf{q}_j \neq 0$. That is the unobservable direction $\mathbf{q}_j$ would be needed to reconstruct the output y_i.

This basically means that there are directions that are only observable in combination with the output y_i and therefore y_i can not be reconstructed if y_i is missing.

C.2.2   Observer based state feedback

Consider the observer based state feedback controller shown in figure 6.11 where $\{\mathbf{A}, \mathbf{B}, \mathbf{C}\}$ define a LTI system of the form (C.1). The dynamic equation for the state estimation error $\mathbf{e}(t) = \mathbf{x}(t) - \hat{\mathbf{x}}(t)$ is given by

$$\dot{\mathbf{e}} = (\mathbf{A} - \mathbf{LC})\mathbf{e}. \tag{C.14}$$

Assume that $\{A, C\}$ is an observable pair. Then by properly choosing L the poles of the observer can be assigned arbitrarily [235]. Now consider a sensor failure. If it is assumed that a detection algorithm has detected that failure and that control is to be continued without that sensor we have $\Sigma(\varnothing, q_{f_\lambda}) = \{A, B, \tilde{C}\}$ where in $\tilde{C}$ the row of C corresponding to the faulty sensor has been removed. Clearly if $\{A, \tilde{C}\}$ is no longer observable , not all eigenvalues of the observer can be assigned, which means that the decay rate of some observer modes can not be specified. More precisely if the unobservable modes are stable the observation error still converges, however, if the unobservable modes are not stable the observer error will exponentially diverge. It is important to note, that although the eigenvalues can still be assigned arbitrarily for recoverable systems less freedom in assigning the eigen structure is available, which has consequences for FDI design [369, 79] for the faulty system. In this concept of recoverability this loss in design freedom is viewed as loss of detection performance.

C.2.3 Adaptive fault tolerant control

Another strategy in fault tolerant control is to use an adaptive control scheme (see e.g. [367, 54]). The idea here is that the dynamics of the system usually change after the fault and that an adaptive scheme is used to identify the new plant dynamics and change the control law accordingly.

It is straight forward to see that weak recoverability is a necessary condition for an adaptive scheme to work.

Seite Leer /
Blank leaf

A fault tolerant dosing strategy

For the discussion of the fault tolerant dosing strategy the respirator equation (3.35) is further abstracted. To do so the recirculation of exspired gas mixture is neglected and the respiratory circuit is modeled by a ideal stir tank model as shown figure D. That is a total gas stream of FF enters the respiratory circuit. It carries anesthetic with concentration c_{vap} corresponding to the vaporizer position. Thereby it is a characteristic property of vaporizers that the they add the desired concentration independently of the total flow FF. This is achieved through the special construction of the vaporizer [370]. In this simplified model the same amount of gas (FF) leaves the tank with concentration c_{insp}. The system has two independent input variables and it is thus intuitive to ask whether this provides redundancy that could be explored for FTC. To answer the question consider the dynamics of the system given by

$$\dot{c}_{insp} = -\frac{FF}{V_R}c_{insp} + \frac{FF}{V_R}c_{vap}.$$

Assume that the vaporizer is "stuck" at $c_{vap} = c_{fault}$ and let $\bar{c} = c_{insp} - c_{fault}$. Then the time evolution of $\bar{c}$ after occurance of the fault is given by

$$\bar{c}(t) = \bar{c}(0)e^{-\int_0^t \frac{FF(\tau)}{V_R}d\tau}. \tag{D.1}$$

From equation (D.1) it is easily seen that c_{insp} asymptotically approaches c_{fault} for any $FF > 0$. By manipulation of FF only the rate with which c_{fault} is approached can be influenced. And clearly no redundancy for FTC is provided by this second input.

Alternatively consider a dosing strategy as shown in figure D where the flow rates for carrier gas and anesthetic are the manipulated inputs. The dynamic equations for this scenario is given by

$$\dot{c}_{insp} = -\frac{FF_{carrier} + FF_{Agas}}{V_R}c_{insp} + \frac{FF_{Agas}}{V_R}.$$

To explore the FTC possibilities it is sufficient to consider the steady state of the system which

$\{FF, c_{vap}\}$

c_{insp}

V_R

$\{FF, c_{insp}\}$

$FF_{carrier}$ FF_{Agas}

c_{insp}

V_R

$\{FF_{carrier} + FF_{Agas}, c_{insp}\}$
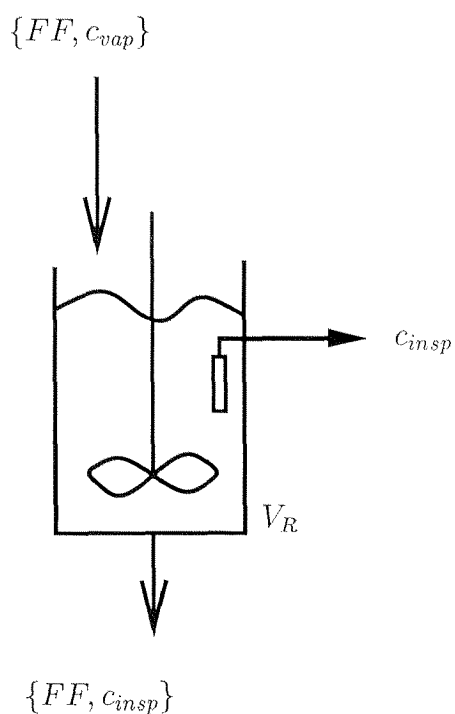
Figure D.1: Simple model representing dosing through specification of total carrier gas flow and vaporizer concentration.
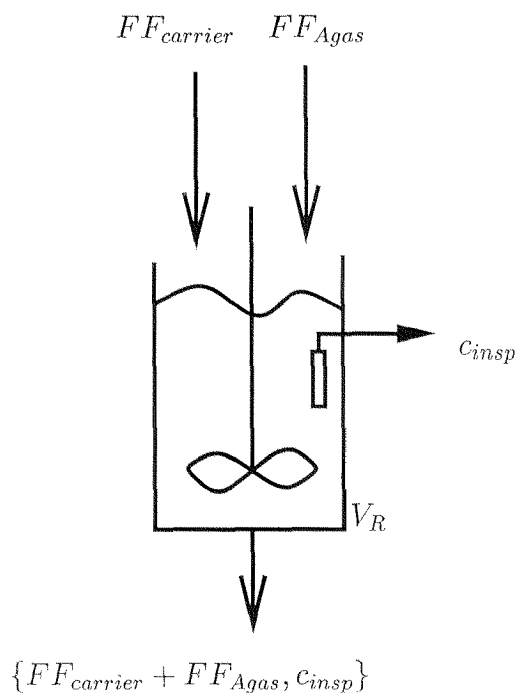
Figure D.2: Simple model representing dosing through specification of two independent flows.

is given by

$$c_{insp,ss} = \frac{FF_{Agas}}{FF_{carrier} + FF_{Agas}}.$$

This shows that even if this actuator FF_{Agas} is "stuck" at a certain $FF_{Agas,fault}$ any steady state concentration can still be achieved by manipulation of $FF_{carrier}$ only. That is this system is still controllable.

From this discussion we conclude first that whether multiple actuators indeed provide redundancy for FTC heavily depends on the nature of these actuators. And second, while dosing by means of a vaporizer is certainly appropriate for conducting anesthesia manually the example suggests that this is not true from FTC perspectives.

Your notes here

Seite Leer /
Blank leaf

Seite Leer /
Blank leaf

Bibliography

[1] ISO 9241: Part 10. Ergonomic dialogue design criteria, 1990.

[2] EN 60601-1. Medical electrical equipment - Part 1: General requirements for safety. European Norm, 1990.

[3] DIN 66234. Bildschirmarbeitsplätze. 1989.

[4] L. Aarons. Introduction to pharmacokinetic and pharmacodynamic modelling. In *Modelling and Control in Biomedical Systems, The Third IFAC Symposium, University of Warwick*. The Institute of Measurement and Control, 1997.

[5] H.A. Adams, C.S. Schmitz, and B. Baltes-Götz. Endokrine Stressreaktion, Kreislauf- und Aufwachverhalten bei totaler intravenöser und Inhalationsanästhesie. *Anaesthesist*, 43:730–737, 1994.

[6] B. Alberts, D. Bray, J. Lewis, M. Raff, K. Roberts, and J.D. Watson. *Molecular biology of the cell*. Garland Publishing, second edition, 1994.

[7] E. Alcorta García and P.M. Frank. Deterministic nonlinear observer-based approaches to fault diagnosis: A survey. *Control Engineering Practice*, 5(5):663–670, 1997.

[8] R. Alur, C. Courcoubetis, T.A. Henzinger, and P.-H. Ho. Hybrid automata: An algorithmic approach to the specification and verification of hybrid systems. In *Hybrid Systems, Lecture Notes in Computer Science*, pages 209–229. Springer-Verlag, 1993.

[9] B. D. O. Anderson and J. B. Moore. *Optimal Control: Linear Quadratic Methods*. Prentice Hall, 1990.

[10] M.L. Appel, J.P. Saul, R.D. Berger, and R. Cohen. Closed-loop identification of cardiovascular regulatory mechanisms. In *Proceedings Computers in Cardiology*, volume 16, pages 3–8, 1990.

[11] K.-E. Årzén. Grafchart: A graphical language for sequential supervisory control applications. In *Proceedings of the 1996 IFAC 13th Triennial World Congress, San Francisco*, pages 407–412. IFAC, 1996.

[12] J.K. Backory, M.F. Abbod, and D.A. Linkens. Diagnosis and decision-making for awareness during general anesthesia. In *UKACC International Conference on CONTROL '98, Conference Publication No. 455, Swansea, UK, September 1-4*, pages 73–77, 1998.

[13] J.M. Badgwell, S.E. Kleinman, and J.E. Heavner. Respiratory frequency and artifact affect the capnographic baseline in infants. *Anesthesia and Analgesia*, 77:708–712, 1993.

[14] S. Balemi. *Control of Discrete Event Systems: Theory and Application.* PhD thesis, Swiss Federal Institute of Technology (ETH), Zurich, Switzerland, 1992.

[15] H. Balzert, H.U. Hoppe, R. Oppermann, H. Peschke, G. Rohr, and N.A. Streitz, editors. *Einführung in die Software-Ergonomie.* de Gruyter, 1988.

[16] Y. Bar-Shalom and T.E. Fortmann. *Tracking and Data Association.* Academic Press, San Diego, 1988.

[17] R. Barbieri, A.M. Bianchi, J.K. Triedman, L.T. Mainardi, S. Cerutti, and J.P. Saul. Model dependency of multivariate autoregressive spectral analysis. *IEEE Engineering in Medicine and Biology Magazine*, 16(5):74–85, September 1997.

[18] G.L. Barbour. Failure modes and effects analysis by matrix method. *Proceedings of the 1977 Annual Reliability and Maintainability Symposium*, pages 114–119, 1977.

[19] S.J. Barker and Team Number 1. Anesthesia workstation for 2010. *Journal of Clinical Monitoring*, 10:304–305, 1994.

[20] T.P. Barnett, L.C. Johnson, P. Naitoh, N. Hicks, and C. Nute. Bispectrum analysis of electroencephalogram signals during waking and sleeping. *Science*, 172:401–402, Anaesthetic Pharmacology Review 1971.

[21] Harald Baron. Anesthesia - physiologischer Simulator in JAVA (3. Erweiterung). Semesterarbeit, Automatic Control Lab, Swiss Federal Institute of Technology (ETH), Zürich, October 1998. IfA 8823.

[22] M. Barr and B. Frank. Java: Too much for your system? *Embedded Systems Programming*, pages 24–32, May 1997.

[23] H. Bartels and R. Bartels. *Physiologie*, chapter "Atmung", pages 167–190. Urban & Schwarzenberg, 1983.

[24] G. Baselli, S. Cerutti, F. Badilini, L. Biancardi, A. Porta, M. Pagani, F. Lombardi, O. Rimoldi, R. Furlan, and A. Malliani. Model for the assessment of heart period and arterial pressure variability interactions and of respiration influences. *Medical & Biological Engineering & Computing*, 32(2):143–152, 1994.

[25] G. Baselli, S. Cerutti, S. Civardi, A. Malliani, and M. Pagani. Cardiovascular variability signals: Towards the identification of a closed-loop model of the neural control mechanisms. *IEEE Transactions on Biomedical Engineering*, 35(12):1033–1046, 1988.

[26] G. Baselli, S. Cerutti, M. Livraghi, C. Meneghini, M. Pagani, and O. Rimoldi. Causal relationship between heart rate and arterial blood pressure variability signals. *Medical & Biological Engineering & Computing*, 26:374–378, 1988.

[27] M. Basseville. Detecting changes in signals and systems - a survey. *Automatica*, 24(3):309–326, 1988.

[28] M. Basseville. Information criterion for FDI. *Proceedings of the 1996 IFAC World Congress, San Franciso, USA*, pages 61–66, 1996.

[29] Michèle Basseville and Igor V. Nikiforov. *Detection of abrupt changes, theory and application*. Information and System Science Series. Prentice Hall, 1993.

[30] R.H.A. Bastings. Toward the development of an intelligent alarm system in anesthesia. Masters thesis, Eindhoven University of Technology, Netherlands, October 1989.

[31] J. Baum. *Die Narkose mit niedrigem Frischgasfluss*. Bibliomed - Medizinische Verlagsgesellschaft mbH, 1993.

[32] K. Behbehani, J.S. Delapasse, and K. Klein. Accommodation of time delay variations in automatic infusion of sodium nitroprusside. In *Annual International Conference of the IEEE Engineering in Medicine and Biology Society*, volume 13, pages 2143–2144, 1991.

[33] J.E.W. Beneken. systems approach in patient monitoring. *RBM*, 13(1):41–44.

[34] J.E.W. Beneken and J.J. van der Aa. Alarms and their limits in monitoring. *Journal of Clinical Monitoring*, 5(3):205–210, July 1989.

[35] J.E.W. Beneken and J.H. van Oostrom. Modeling in anesthesia. *Journal of Clinical Monitoring and Computing*, 14:57–67, 1998.

[36] T.J. Bergin and R. G. Gibson, editors. *History of Programming Languages - II*. ACM Press, 1996.

[37] R. Bernotat and G. Rau. man-machine-interaction. *RBM*, 13(1):36–40.

[38] R.G. Bickford. Neurophysiological applications of automatic anesthetic regulator controlled by brain potentials. *The American Journal of Physiology*, 159:562–563, 1949.

[39] H.J. Bigolow. Insensibility during surgical operation produced by inhalation. *The Boston Medical and Surgical Journal*, 35(16), 1846.

[40] C.D. Bilbo, D.S. Whitehurst, and T.C. Jannett. Monte carlo simulations of open-loop and adaptive control of intravenous anesthesia. *Proceedings of the 15th Annual International Conference of the IEEE Engineering in Medicine and Bilology Society, San Diego, Oct 28-31, 1993*, pages 975–976.

[41] K. B. Bischoff and R. B. Brown. Drug distribution in mammals. *Chemical Engineering Progress Symposium Series*, 62(66):33–45, 1966.

[42] M. Blanke. Consistent design of dependable control systems. *Control Engineering Practice*, 4(9):1305–1312, 1996.

[43] M. Blanke. *Advances in Control - Highlights of ECC'99*, chapter 6, Fault-tolerant Control Systems, pages 171–196. Springer, 1999.

[44] M. Blanke, S.A. Bøgh, R.B. Jørgensen, and R.J. Patton. Fault detection for a diesel engine actuator - a benchmark for FDI. *Control Engineering Practice*, 3(12):1731–1740, 1995.

[45] M. Blanke, C.W. Frei, F.J. Kraus, R.J. Patton, and M. Staroswiecki. *Control of Complex Systems*, chapter "Fault Tolerant Control". Springer, in preparation.

[46] M. Blanke, R. Izadi-Zamanabadi, S. A. Bøgh, and C.P. Lunau. Fault-tolerant control systems - a holistic view. *Control Engineering Practice*, 5(5):693–702, 1997.

[47] M. Blanke, R. Izadi-Zamanabadi, and T.F. Loostma. Fault monitoring and re-configuration control for a ship propulsion plant. *Journal of Adaptive Control and Signal Processing*, pages 671–688, 1998.

[48] G. Blaschek, G. Pomberger, and F. Ritzinger. *Einführung in die Programmierung in Modula-2*. Springer-Verlag, 1986.

[49] E.R. Block and S.A. Stalcup. Metabolic functions of the lung. *Chest*, 81(2):215–223, 1982.

[50] F.E. Block and Team Number 2. The radical dude. *Journal of Clinical Monitoring*, 10:306–309, 1994.

[51] F.E. Block, L. Nuutinen, and B. Ballast. Optimization of alarms: A study on alarm limits, alarm sounds, and false alarms, intended to reduce annoyance. *Journal of Clinical Monitoring and Computing*, 15:75–83, 1999.

[52] A. Blyth. Issues arising from medical system's failure. *Software Engineering Notes*, 22(2):85–87, March 1997.

[53] J. Bockaert, V. Homburger, and F. Sladeczek. *Noradrenaline in the Central Nervous System*, chapter Molecular pharmacology of adrenergic receptors and their cellular localization in brain cells in culture, pages 76–117. Oxford University Press, 1990.

[54] M. Bodson and J.E. Groszkiewicz. Multivariable adaptive algorithms for reconfigurable flight control. *IEEE Transactions on Control Systems Technology*, 5(2):217–229, 1997.

[55] S. A. Bøgh, R. Izadi-Zamanabadi, and M. Blanke. Onboard supervision for the Ørsted satellite attitude control system. In *ESA/ESTEC workshop "AI and KBSs for Space", Nordwijk, Holland, Oct. 10-11*, 1995.

[56] S.A. Bøgh. *Fault Tolerant Control Systems - a Development Method and Real-Life Case Study*. PhD thesis, Department of Control Engineering, Aalboorg University, December 1997.

[57] Grady Booch. *Object-Oriented Analysis and Design with Applications*. The Benjamin/Cummings Publishing Co., Inc., second edition, 1994.

[58] S. Boyd, L. El Ghaoui, E. Feron, and V. Balakrishnan. *Linear Matrix Inequalities in System and Control Theory*. Society for Industrial and Applied Mathematics, 1994.

[59] J.M. Boyle, R.D. Resler, and V.L. Winter. Do you trust your compiler? *Computer*, pages 65–73, May 1999.

[60] Andrea Branca. Objektorientierte Modellierung der Kommunikation mit Anästhesieüberwachnugsgeräten. Diplomarbeit, Automatic Control Lab, Swiss Federal Institute of Technology (ETH), Zürich, July 1997. IfA 8805.

[61] R. Brega. A real-time operating system designed for predictability and run-time safety. In *Proceedings of The Fourth International Conference on Motion and Vibration Control (MOVIC '98), Zurich, Switzerland, August 25-28*, volume 1, pages 379–384, 1998.

[62] N. F. Britton and M. Skevington. On the mathematical modelling of pain. *Neurochemical Research*, 21(9):1133–1140, 1996.

[63] S. Brody. *Bioenergetics and Growth*. Reinhold, New York, 1945.

[64] R.W. Brower, W. Spaans, P.A.M. Rewiersma, and G.T. Meester. A fully automatic device for compensation for artifacts in conventional catheter-manometer pressure recordings. *Biomedical Engineering*, pages 305–310, August 1975.

[65] A.E. Bryson and Y.-Ch. Ho. *Applied Optimal Control - Optimization, Estimation and Control*. Taylor & Francis, 1975.

[66] H.P. Büch and U. Büch. *Pharmakologie und Toxikologie*, chapter Narkotika, pages 469–483. R.I. Wissenschaftsverlag, 7 edition, 1992.

[67] E. Bullinger, C.W. Frei, T. Sieber, A.H. Glattfelder, F. Allgöwer, and A.M. Zbinden. Adaptive λ-tracking in anesthesia. *Proceedings of the 4th IFAC/(IMEKO) Symposium Modelling and Control in Biomedical Systems - BIOMED 2000, Karlsburg, Germnay, March 30 - April 1,*, 2000.

[68] Marcel Buob. Physiologischer Simulator mit JAVA. Diplomarbeit, Automatic Control Lab, Swiss Federal Institute of Technology (ETH), Zürich, February 1997. IfA 8796.

[69] A. Burns and A.J. Wellings. A structured design method for hard real time systems. *Real Time Systems*, 6(1):73–114, 1994.

[70] G. Burnstock and M. Costa. *Adrenergic Neurons: Their organization, function and development in the peripheral nervous system*. Chapman & Hall, London, 1975.

[71] G.C. Buttazzo. *Hard Real-Time Computing Systems - Predictable Scheduling Algorithms and Applications*. Kluwer Academic Publisher, 1997.

[72] E.F. Camacho and C. Bordons. *Model Predictive Control in the Process Industry*. Springer, 1995.

[73] K.D. Candido and V.J. Collins. *Dysfuntion of the Autonomic Nervous System*, chapter 18, pages 302–315. Williams & Wilkins, 1996.

[74] E.R. Carson, C. Cobelli, and L. Finkelstein. *The Mathematical Modeling of Metabolic and Endocrine Systems, Model Fromulation, Identification, and Validation*. John Wiley & Sons, 1983.

[75] J.P. Cassar, M. Staroswiecki, and P. Declerck. Structural decomposition of large scale systems for the design of failure detection and identification procedures. *Systems Science*, 20(1):31–41, 1994.

[76] F.W. Chapman, J.C. Neweil, and R.J. Roy. A feedback controller for ventilatory therapy. *Annals of Biomedical Engineering*, 13:359–372, 1985.

[77] S. Chaudhri, J.R. Colvin, J.G. Todd, and G.N. Kenny. Evaluation of closed loop control of arterial pressure during hypotensive anaesthesia for local resection of intraocular melanoma. *British Journal of Anaesthesia*, 69:607–610, 1992.

[78] J. Chen and R.J. Patton. A re-examination of fault detectability and isolability in linear dynamic systems. In *Proceedings IFAC Symposium on Fault Detection, Supervision and Safety for Technical Processes, Espoo, Finland*, pages 567–573, 1994.

[79] J. Chen and R.J. Patton. *Robust Model-Based Fault Diagnosis for Dynamical Systems.* Kluwer Academic Publishers, 1999.

[80] J. Chen, Patton. R.J., and H.-Y. Zhang. Design of unknown input observers and robust fault detection filters. *International Journal of Control*, 63(1):85–105, 1996.

[81] G. Chiari, L. Avanzolini and M. Ursino. A comprehensive simulator of the human respiratory system: Validation with experimental and simulated data,. *Annals of Biomedical Engineering*, 25:985–999, 1997.

[82] R.T. Chilcoat. A review of the control of depth of anaesthesia. *Transactions of the Institute of Measurement and Control*, 2(1):38–45, January 1980.

[83] R.T. Chilcoat and Team Number 3. Anesthesia "R" US, Inc. *Journal of Clinical Monitoring*, 10:310–312, 1994.

[84] R.T. Chilcoat, J.N. Lunn, and W.W. Mapleson. Computer assistance in the control of depth of anaesthesia. *British Journal of Anaesthesia*, 56:1417–1431, 1984.

[85] Ch.-Ch. Chiu and S.-J. Yeh. A tentative approach based on Wiener filter for the reduction of respiratory effect in pulse signals. In *Proceedings of the 19th International Conference of the IEEE/EMBS, Oct. 30 - Nov. 2, 1997, Chicago, IL, USA*, pages 1394–1397.

[86] K.H. Chon, R. Mukkamala, K. Toska, T.J. Mullen, A.A. Armoundas, and R.J. Cohen. Linear and nonlinear system identification of autonomic heart-rate modulation. *IEEE Engineering in Medicine and Biology Magazine*, 16(5):96–105, September 1997.

[87] K.H. Chon, T.J. Mullen, and R.J. Cohen. A dual-input nonlinear system analysis of autonomic modulation of heart rate. *IEEE Transactions on Biomedical Engineering*, 43(5):530–544, 1996.

[88] M.J. Chonoles and C.C. Gilliam. Real-time object-oriented system design using the object modeling technique (OMT). *Journal of Object Oriented Programming*, pages 16–24, June 1995.

[89] R.N. Clark. Instrument fault detection. *IEEE Transactions on Aerospace and Electronic Systems*, 14(3):456–465, 1978.

[90] D.W. Clarke, C. Mohtadi, and P.S. Tuffs. Generalized predictive control - Part I. The basic algorithm. *Automatica*, 23(2):137–148, 1987.

[91] D.W. Clarke, C. Mohtadi, and P.S. Tuffs. Generalized predictive control - Part II. extensions and interpretations. *Automatica*, 23(2):149–160, 1987.

[92] D. Coates. Control of blood pressure during anesthesia. Anaesthesia Rounds by The Medical Group (Education) Ltd.

[93] C. Cobelli and M.P. Saccomani. *The Biomedical Engineering Handbook*, chapter 157, Compartmental Models of Physiologic Systems, pages 2375–2385. CRC Press / IEEE Press, 1995.

[94] D.D. Cofer and V.K. Garg. Supervisory control of real-time discrete-event systems using lattice theory. *IEEE Transactions on Automatic Control*, 41(2):199–209, February 1996.

[95] V. J. Collins. Chapter: Anatomical aspects of respiration. In *Physiologic and Pharmacologic bases of Anesthesia*, pages 1–13. Williams and Wilkins, Pennsylvania, 1996.

[96] V. J. Collins. Chapter: Autonomic nervous system. In *Physiologic and Pharmacologic bases of Anesthesia*. Williams and Wilkins, Pennsylvania, 1996.

[97] V.J. Collins. *Physiologic and Pharmacologic Bases of Anesthesia*. Williams & Wilkins, 1996.

[98] V.J. Collins and R.P. Badola. *Selected Acute and Chronic Diseases*, chapter 45, pages 762–835. Williams & Wilkins, 1996.

[99] C. Commault. On the disturbed fault detection and isolation problem. *System & Control Letters*, 38:73–78, 1999.

[100] P. Conzen and K. Peter. *Anaesthesieologie*, chapter 6.2 Pharmakodynamik, pages 157–175. Springer Verlag, Berlin, 7 th edition, 1995.

[101] D.C. Crawford, D. Fell, K. J. Achola, and G. Smith. Effects of alfentanil on the pressor response and cathecolamine responses ot tracheal intubation. *British Journal of Anaesthesia*, 59:707–712, 1987.

[102] P.E. Creyer. Physiology and pathophysiology of the human sympathoadrenal neuroendocrine system. *The New England Journal of Medicine*, August 1980.

[103] D.J. Cullen, E.I. Eger, W.C. Stevens, N.T. Smith, T.H. Cromwell, B.F. Cullen, G.A. Gregory, S.H. Bahlman, W.M. Dolan, R.K. Stoelting, and H.E. Fourcade. Clinical signs of anesthesia. *Anesthesiology*, 36(1):21–36, January 1972.

[104] M. Curatolo, M. Derighetti, S. Petersen-Felix, P. Feigenwinter, M. Fischer, and A.M. Zbinden. Fuzzy logic control of inspired isoflurane and oxygen concentrations using minimal flow anaesthesia. *British Journal of Anaesthesia*, 76:245–250, 1996.

[105] M. Daniel, R.B. Weiskopf, M. Noorani, and E.I. Eger. Fentanyl augments the blockade of the sympathetic response fo incision (MAC-BAR) produced by desflurane and isoflurane. *Anesthesiology*, 88(1):43–49, 1998.

[106] W.L. Davies. *Systems & Control Encyclopedia*, volume 1, chapter Anesthesia: Feedback Control of Depth, pages 277–281. Pergamon Press, 1987.

[107] T. de Reus. Neue Richtlinie "Prozessführung mit Bildschirmen": Fliessbilder. *Automatisierungstechnik*, 40(10):54–56, 1998.

[108] R. Deegan, H.B. He, A.J.J. Wood, and M. Wood. Effects of anesthesia on norepinephrine kinetics. *Anesthesiology*, 75(3):481–488, 1991.

[109] H. Derendorf and G. Hochhaus. Pharmacokinetic-pharmacodynamic modeling of irreversible drug effects. In H. Derendorf and G. Hochhaus, editors, *Handbook of pharmacokinetic/pharmacodynamic correlation*, chapter 4. CRC Press, 1995.

[110] M. Derighetti. Multivariable Fuzzy-Regelung in der Anästhesie. Post Graduate Thesis, Automatic Control Laboratory, Swiss Federal Institute of Technology (ETH), Zürich, 1993.

[111] M. Derighetti. *Feedback Control in Anaesthesia*. PhD thesis, Swiss Federal Institute of Technology (ETH), Zurich, Switzerland, 1999.

[112] M. Derighetti, C.W. Frei, M. Buob, A.M. Zbinden, and T.W. Schnider. Modeling the effect of surgical stimulation on mean arterial blood pressure. In *Proceedings of the 19th International Conference of the IEEE/EMBS, Oct. 30 - Nov. 2, 1997, Chicago, IL, USA*, pages 2172–2175, 1997.

[113] M. Derighetti, C.W. Frei, A.H. Glattfelder, and A.M. Zbinden. Modellbasierte Regelung in der Anästhesie. *Automatisierungstechnik*, 47(2):80–88, February 1999.

[114] M. Derighetti, A.H. Glattfelder, and A.M Zbinden. Fuzzy-control in anaesthesia: A first step to an integrated control system,. *Proceedings of the World Automation Congress (WAC '96), Montpellier, France, May 28-30, 1996*, 5:141–146, 1996.

[115] James L. Derrick, Christopher L. Thompson, and Timothy G. Short. The application of a modified proportional derivative control algorithm to arterial pressure alarms in anesthesiology. *International Journal of Clinical Monitoring and Computing*, 14(1):41–47, 1998.

[116] J. A. Di Nardo and V. J. Collins. Blood pressure, pulse, and flow. In *Physiologic and pharmacologic bases of anesthesia*. Williems and Wilkins Media, Pennsylvania, 1996.

[117] J.A. Di Nardo. *Physiologic and Pharmacologic Bases of Anesthesia*, chapter 8: Neurohumoral Control of Circulation, pages 141–154. Williams & Wilkins, 1996.

[118] M. Di Rienzo, G. Parati, G. Manica, A. Pedotti, and P. Castiglioni. Investigating baroreflex control of circulation using signal processing techniques. *IEEE Engineering in Medicine and Biology Magazine*, 16(5):86–95, September 1997.

[119] D. Diez. D'nia an object oriented real-time system. *Real-Time Magazine*, (3):51–54, 1995.

[120] D. Diez. A realtime system based on Oberon. *Informatik/Informatique*, (4):18–22, 1995.

[121] DIN (EN 1441). Risikoanalyse. Deutsche Norm.

[122] X. Ding and P.M. Frank. Comparison of observer-based fault detection approaches. In *Proceedings IFAC Symposium on Fault Detection, Supervision and Safety for Technical Processes, Espoo, Finland*, pages 533–538, 1994.

[123] J.T. Dorocicz, E. Kosmatopoulos, S. Neville, and N.J. Dimopoulos. Recurrent neural networks for fault detection. In *Proceeding WAC*, 1996.

[124] M. Dowson. The ARIANE 5 software failure. *Software Engineering Notes*, 22(2):84, 1997.

[125] Dräger. Cicero, Itegrierter Narkose-Arbeitsplatz. Gebrauchsanweisung.

[126] Geir Dullerud, Marie Csete, and John Doyle. Application of multivarable feedback mehtods to intravenous anesthetic pharmacodynamics. In *Proceeding 1995 American Control Conference*, pages 791–795, June 1995.

[127] R. Dunia, S.J. Qin, T.F. Edgar, and T.J. McAvoy. Sensor fault identification and reconstruction using principal component analysis. In *Proceeings of the 1996 IFAC 13th Triennial World Congress, San Francisco*, pages 259–264. IFAC, 1996.

[128] T.J. Ebert and M. Muzi. Sympathetic hyperactivity during Desflurane anesthesia in healthy volunteers. *Anesthesiology*, 79(3):444–453, 1993.

[129] E.I. Eger II. *Anesthetic Uptake and Action*. The Williams & Wilkins Company, 1974.

[130] C. Eintrei, W. Leszniewski, and C. Carlsson. Local application of ^{133} Xenon for measurement of regional cerebral blood flow (rCBF) during Halothane, Enflurane, and Isoflurane anesthesia in humans. *Anesthesiology*, 63:391–394, 1985.

[131] A. ElHefnawy, G.M. Saidel, and E.N. Bruce. co_2 control of the respiratory system: Plant dynamics and stability analysis. *Annals of Biomedical Engineering*, 16:445–461, 1988.

[132] S. Engell, editor. *Entwurf nichtlinearer Regelungen*. Oldenbourg, 1995.

[133] J. Erenwerth and Team Number 4. Thr FAS 2000. *Journal of Clinical Monitoring*, 10:313–316, 1994.

[134] E. Eryurek and B.R. Upadhyaya. Fault-tolerant control and diagnostics for large-scale systems. *IEEE Control Systems*, 15:34–42, October 1995.

[135] J. Ezzine and A.H. Haddad. Controllability and observability of hybrid systems. *International Journal of Control*, 49(6):2045–2055, 1989.

[136] P. Feigenwinter. Risikoanalyse Forschungs-Cicero. Technical report, Institut für Anästhesiologie und Intensivmedizin, Inselspital, Bern, 1999.

[137] J.M. Feldman and Team Number 5. Design of a workstation: A team summary. *Journal of Clinical Monitoring*, 10:317–319, 1994.

[138] A. Fischer and H. Marais. *The Oberon Companion*. vdf Hochschulverlag AG an der ETH Zürich, 1998.

[139] A.P. Fishmann and G.G. Pietra. Handling of bioactive materials by the lung (second of two parts. *New England Journal of Medicine*, 291:953–959, 1974.

[140] R. Flewelling. *The Biomedical Engineering Handbook*, chapter 88, Noninvasive Optical Monitoring, pages 1347–1356. CRC Press / IEEE Press, 1995.

[141] Y. Floderus, J. Sääf, S.B. Ross, and L. Wetterberg. Catechol-O-Methyltransferase activity in human erythrocytes: Methodological aspects. *Upsala Journal of Medical Sciences*, 86:309–318, 1981.

[142] M.L. Fors, U. Ahlquist, R. Skagerwall, L.G.A. Edwall, and G.A.T. Haegerstam. Relation between intradental nerve activity and estimated pain in man - a mathematical model. *Pain*, 18:397–408, 1984.

[143] U.G.H. Fors, M.L. Ahlquist, L.G.A. Edwall, and G.A.T. Haegerstam. Evaluation of a mathematical model analysing the relation between intradental nerve impulse activity and perceived pain in man. *International Journal of Biomedical Computing*, 19:261–277, 1986.

[144] U.G.H. Fors, LG.A. Edwall, and A.T. Haegerstam. The ability of a mathematical model to evaluate the effects of two pain modulating procedures on pulpal pain in man. *Pain*, 33:253–264, 1988.

[145] W. Forth, D. Henschler, Rummel. W., and K. Starke, editors. *Pharmakologie und Toxikologie*. R.I. Wissenschaftsverlag, 7 edition, 1992.

[146] D. Frank. Observer-based fault detection and supervision in discrete process logistics. *Proceedings of the 13th IFAC World Congress, San Francisco, USA, July, 1996*, pages 31–35, 1996.

[147] P. M. Frank. Fault diagnosis in dynamical systems using analytical and knowledge-based redundancy - a survey and some new results. *Automatica*, 26(3):459–474, 1990.

[148] P.M. Frank. Analytical and qualitative model-based fault diagnosis - a survey and some new results. *European Journal of Control*, (2):6–28, 1996.

[149] P.M. Frank, E.A. García, and B. Köppen-Seliger. Modelling for fault detection and isolation. Reprints of the 3rd Joint COSY (Control of Complex Systems) Workshop, Oct. 9-12, 1997, Budapest, Hungary.

[150] G. F. Franklin, J. D. Powell, and A. Amami-Naeini. *Feedback control of dynamic systems*. Addison Wesley, 1994.

[151] W.T. Frazier and Team Number 6. Designing the workstation for the immediate future. *Journal of Clinical Monitoring*, 10:320–322, 1994.

[152] C.W. Frei. *Fault Tolerant Control Concepts Applied to Anesthesia*. PhD thesis, Swiss Federal Institute of Technology (ETH), Zurich, Switzerland, 2000.

[153] C.W. Frei, M. Derighetti, and A.M. Zbinden. Modeling for control of mean arterial blood pressure (MAP) during anesthesia. In *Proceedings of the Second International Symposium on Mathematical Modelling (MATHMOD), Vienna, Austria (available from http://www.aut.ee.ethz.ch/ frei/publications.html)*, pages 395–400, 1997.

[154] C.W. Frei, F.J. Kraus, and M. Blanke. Recoverability viewed as a system property. In *in Proceedings of the European Control Conference (ECC'99), Aug. 31 -Sept. 3, Karlsruhe, Germany*, 1999.

[155] C.W. Frei and D. Leibundgut. Wahl einer Plattform für ein automatisiertes Anästhesie System. Technical Report Nr. AUT 97-03, Automatic Control Lab, Swiss Federal Institut of Technology (ETH), February 1997.

[156] Y. Fukui and T. Masuzawa. Knowledge-based approaches to intelligent alarms. *Journal of Clinical Monitoring*, 5(10):211–216, July 1989.

[157] Y. Fukui and N. T. Smith. Interactions among ventilation, the circulation, and the uptake and distribution of halothane - use of a hybrid computer multiple model: I. the basic model. *Anesthesiology*, 54:107–118, 1981.

[158] Y. Fukui and N. T. Smith. Interactions among ventilation, the circulation, and the uptake and distribution of Halothane - use of a hybrid computer multiple model: Ii. spontaneous vs. controlled ventilation, and the effects of CO_2. *Anesthesiology*, 54:119–124, 1981.

[159] E. Furutani, M. Araki, T. Sakamoto, and S. Maetani. Blood pressure control during surgical operations. *IEEE Transactions on Biomedical Engineering*, 42(10):999–1006, October 1995.

[160] P. Gahinet, A. Nemirovski, A.J. Laub, and M. Chilali. *LMI Control Toolbox*. The Math-Works Inc., 1995.

[161] H. Gall and K. Kemp. Einsatz und Wirksamkeit von Programmlaufüberwachungen. *Automatisierungstechnische Praxis*, 40(1):40–48, 1998.

[162] F.W. Ganong. *Review of Medical Physiology*. Appleton & Lange, 18 edition, 1997.

[163] R. M. Gardner. Direct blood pressure measurement - dynamic response requirements. *Anesthesiology*, 54:227–236, 1981.

[164] A.L. Gehin, R. Logier, M. Bayart, M. Staroswiecki, C. Cantineau, and M. Dlecroix. Application of the smart sensor concept to the anaesthesia supervision. *Proceedings of the 15th Annual International Conference of the IEEE Engineering in Medicine and Bilology Society, San Diego, Oct 28-31, 1993*, pages 616–617.

[165] S. Gelman, K. C. Fowler, and L. R. Smith. Liver circulation and function during Isoflurane and Halothane anesthesia. *Anesthesiology*, 61:726–730, 1984.

[166] S. Gelman, K. C. Fowler, and L. R. Smith. Regional blood flow during isoflurane and halothane anesthesia. *Anesthesia Analgesia*, 63:557–565, 1984.

[167] J.J. Gertler. Survey of model-based failure detection and isolation in complex plants. *IEEE Control Systems Magazine*, 8(6):3–11, December.

[168] J.J. Gertler. *Fault Detection and Diagnosis in Engineering Systems*. Marcel Dekker, Inc., 1998.

[169] J.J. Gertler and Y. Kewen. Statistical decision making for dynamic parity relations. In *Proceeings of the 1996 IFAC 13th Triennial World Congress, San Francisco*, pages 13–18. IFAC, 1996.

[170] Tobias Geyer. Modellbasierte CO_2-Regelung für die Anästhesie. Semesterarbeit, Automatic Control Laboratory, Swiss Federal Institute of Technology (ETH), Zürich, 1999. IfA 8840.

[171] M. Gibaldi and D. Perrier. *Pharmacokinetics*. Drugs and the Pharmaceutical Sciences. Marcel Dekker, Inc., 1982.

[172] M. Gibaldi and D. Perrier. *Pharmacokinetics*, volume 15 of *Drugs and the Pharmaceutical Sciences*, chapter 8: Clearance Concepts, pages 319–353. Marcel Dekker, Inc., second edition, 1982.

[173] F. A. Gibbs, E. L. Gibbs, and W. G. Lennox. Effect on the electroencephalogram of certain drugs which influence nervous activity. *Arch. Inter. Med.*, 60:154–66, 1937.

[174] H. Gilly and S. Fitzal. Prinzip und Praxis der invasiven arteriellen Blutdruckmessung. *Anaesthesist*, 44(12):931–952, 1995.

[175] K.J. Gingrich, R. Roy, R. Vishnoi, C. Yu, and G.W. Neat. Modeling the hemodynamic response to dopamine in acute heart failure. *Proceedings of the 10th International Conference of the IEEE Engineering in Medicine & Biology Society, New Orleans, LA, USA,*, 1:515–516, 1988.

[176] R. Ginn and J.R. Vane. Disappearance of catecholamines from the circulation. *Nature*, 219:740–742, August 1968.

[177] A. H. Glattfelder and W. Schaufelberger. *Lineare Regelsysteme*. vdf, Hochschulverlag AG, 1997.

[178] A.H. Glattfelder and W. Schaufelberger. Stability of discrete override and cascade-limiter single-loop control systems. *IEEE Transactions on Automatic Control*, 33(6):532–540, 1988.

[179] A.H. Glattfelder, W. Schaufelberger, and H.P. Fässler. Stability of override control systems. *International Journal of Control*, 37(5):1023–1037, 1983.

[180] Marcel Glauser. Testen von Methoden zur Artefakterkennung in Blutdruckmessungen. Semesterarbeit, Automatic Control Lab, Swiss Federal Institute of Technology (ETH), Zürich, July 1998. IfA 8820.

[181] Marcel Glauser. Artifact detection in quasi-analog blood pressure signal. Diplomarbeit, Automatic Control Laboratory, Swiss Federal Institute of Technology (ETH), Zürich, 1999. IfA 8836.

[182] J.B. Glen, H. Schwilden, and D.R. Stanski. Workshop on Safe feedback control in Anesthetic drug delivery, Schloss Rheinhartshausen, Germany, June 29, 1998. *Anesthesiology*, 91(2):600–601, 1999.

[183] G. Glöe, O. Jach, R. Mehl, and M. Müllerburg. Zuverlässigkeit komplexer Systeme aus Hardware und Software. *Automatisierungstechnische Praxis*, 40(1):32–39, 1998.

[184] H. Gomaa. *Software design methods for concurrent and real-time systems*. Addison-Wesley, 1993.

[185] J. Gosling and H. McGilton. The JAVA language environment, a white paper. Sun Mircrosystems Computer Corporation, Mountain View, CA, USA, October 1995.

[186] W. Graf. *Ergonomische Beurteilung der Mensch-Computer-Interaktion anhand von Blickbewegungen*. PhD thesis, Swiss Federal Institute of Technology (ETH), Zurich, Switzerland, 1988.

[187] T. Grams. Zuverlässigkeit und Sicherheit komplexer Systeme (Begriffe). *GMA Fachbericht, VDE Verlag, Berlin, Offenbach*, (4):17–26, 1993.

[188] J.S. Gravenstein and Team Number 7. Proposal for a less cumbersome anesthesia workstation. *Journal of Clinical Monitoring*, 10:323–325, 1994.

[189] Messer Griesheim, editor. *Gase-Handbuch*. Messer Griesheim GmbH, 1989.

[190] A.W. Grogono and Team Number 8. A new anesthesia workstation design. *Journal of Clinical Monitoring*, 10:326–331, 1994.

[191] J. Gutknecht. Oberon System 3: Vision einer Softwaretechnologie der Zukunft. *Informatique*, (3):8–15, June 1994.

[192] J. Gutknecht. Oberon System 3: Vision of a future software technology. *Software - Concepts and Tools*, 15:26–33, 1994.

[193] J. Gutknecht. Do the fish really need remote control? A proposal for self-active objects in Oberon. *Proceedings of the JMLC, Linz, Austria, 1997*, 1997.

[194] A.C. Guyton, T.G. Coleman, A.W. Cowley, J.-F. Liard, R.A. Norman, and R.D. Manning. System analysis of arterial pressure regulation and hypertension. *Annals of Biomedical Engineering*, 1:254–281, 1972.

[195] M. Häck and M. Köhne. Lokale und globale Validierung der Messsignale kontinuierlich arbeitender Prozessanalysatoren. *Automatisierungstechnik*, 46(7):315–325, 1998.

[196] W. M. Haddad and D.S. Bernstein. Explicit construction of quadratic Lypunov functions for the small gain, positivity, circle, and Popov theorems and their application to robust stability. part I: Continuous time theory. *International Journal of Robust and Nonlinear Control*, 3:313–339, 1993.

[197] M. Haese. Windows95 für den Programmierer. *Elektronik*, (9):88–93, September 1996.

[198] W. A. Halang and A.D. Stoyenko. *Constructing Predictable Real Time Systems*. Kluwer Academic Publishers, 1991.

[199] W.A. Halang and A.H. Frigeri. Methoden sicherheitsgerichteter Echtzeitprogrammierung. *Automatisierungstechnische Praxis*, 41(6):31–38, 1999.

[200] W.A. Halang, A.H. Frigeri, R. Lichtenecker, U. Steinmann, and K. Wendland. *Methoden-lehre sicherheitsgerichteter Echtzeit-programmierung.* Schriftenreihe der Bundesanstalt für Arbeitsschutz und Arbeitsmedizin, 1998.

[201] W.A. Halang and R. Konakovsky. Sicherheitsgerichtete Software. *Automatisierungstechnik,* 46(2):93–103, 1998.

[202] W.A. Halang and R. Konakovsky. *Sicherheitsgerichtete Echtzeitsysteme.* Oldenburg Verlag, 1999.

[203] W. Hampe-Neteler. *Software-ergonomische Bewertung zwischen Aarbeitsgestaltung und Softwareentwicklung.* Peter Lange, 1994.

[204] L. Hatton. Does OO sync with how we think? *IEEE Software,* 15(3):46–54, May 1998.

[205] D. Hausheer and R. Sierra. Entwicklung eines virtuellen Patienten. Semesterarbeit, Automatic Control Laboratory, Swiss Federal Institute of Technology (ETH), Zürich, 2000. IfA 8851.

[206] J. Held. *Partizipative Ergonomie, Die Prozessgestaltung zur Beteiligung Betroffener an ergonomischen Gestaltungsaufgaben.* PhD thesis, Swiss Federal Institute of Technology (ETH), Zurich, Switzerland, 1998.

[207] J.B. Henry, editor. *Clinical Diagnosis and Management by Laboratory Methods,* chapter 16, Evaluation of Endocrine Function, pages 342–347. W.B. Saunders Company, 1996.

[208] S.A. Herrin. Maintainability applications using the matrix FMEA technique. *IEEE Transactions on Reliability,* 30(3):212–217, 1981.

[209] G. Hertel, D. Olthoff, B. Vetter, O. Giessner, and S. Lange. Vergleich verschiedener Anästhesiemethoden mittels Plasma-Katecholomin-Bestimmung. *Anaesthesiologie und Reanimation,* 20(5):116–125, 1995.

[210] J. Hilsted, C. Wilken-Jensen, K. Birch, M. Damkjaer Nielsen, J.J. Holst, and H. Kehlet. Endocrine, metabolic and cardiavascular response to adrenaline after abdominal surgery. *Acta Endocrinolica,* 123:143–148, 1990.

[211] W.E. Hoffman. *Carddiovascular Actions of Anesthetics and Drugs Used in Anesthesia, Regional Blood Flow and Clinical Considerations,* chapter Influence of Anesthesia on Regional Blood Flow, pages 4–34. Karger, 1986.

[212] M. Hou and P.C. Müller. Fault detection and isolation observers. *International Journal of Control,* 60(5):827–846, 1994.

[213] J.W. Huang, Y.Y. Lu, A. Nayak, and R. J. Roy. Depth of anesthesia estimation and control. *IEEE Transactions on Biomedical Engineering,* 46(1):71–81, 1999.

[214] B. Hug. Stressantwortmodellierung von Katecholaminen und Blutdruck. Diplomarbeit, Automatic Control Lab, Swiss Federal Institute of Technology (ETH), Zürich, March 1998. IfA 8814.

[215] J. Hughes. Evaluation of mechanisms controlling the release and inactivation of the adrenergic transmitter in the rabbit protal vein and vas deferens. *British Journal of Pharmacology*, 44(3):472–491, 1972.

[216] W. Hügin. *Anesthesia: Discovery Progress Breakthroughs*. Editions Roche, Basel, Switzerland, 1989.

[217] M. Huzmezan and J.M. Maciejowski. Reconfigurable flight control of a high incidence research model using predictive control. In *UKACC International Conference on CONTROL '98, Conference Publication No. 455, Swansea, UK, September 1-4*, pages 1169–1174, 1998.

[218] Y.Z. İder, M.C. Şaki, and H.A. Güçer. Removal of power line interference in signal-averaged electrocardiography systems. *IEEE Transactions on Biomedical Engineering*, 42(7):731–735, July 1995.

[219] VDI (Verein Deutscher Ingenieure). Konzepte fehlertolerierender Automatisierungssysteme. VDI/VDE Richtlinie 3698, July 1995.

[220] S. Isaka and A.V. Sebald. Control strategies for arterial blood pressure regulation. *IEEE Transactions on Biomedical Engineering*, 40(4):353–363, 1993.

[221] R. Isermann. Process fault detection based on modeling and estimation methods - a survey. *Automatica*, 20(4):387–404, 1984.

[222] R. Isermann and P. Ballé. Trends in the application of model based fault detection and diagnosis of technical processes. *Proceedings of the 1996 IFAC World Congress, San Franciso, USA*, pages 1–12, 1996.

[223] R. Isermann and P. Ballé. Trends in the application of model-based fault detection and diagnosis of technical processes. *Control Engineering Practice*, 5(5):709–719, 1997.

[224] R. Izadi-Zamanabadi. *Fault-tolerant Supervisory Control - System Analysis and Logic Design*. PhD thesis, Department of Control Engineering, Aalborg University, July 1999.

[225] J.A. Jacquez. *Compartmental Analysis in Biology and Medicine*. The University of Michigan Press, 2 edition, 1985.

[226] G.-I. Jee and R.J. Roy. Adaptive control of multiplexed closed-circuit anesthesia. *IEEE Transactions on Biomedical Engineering*, 39(10):1071–1080, October 1992.

[227] R.W. Jellife and A. Schumitzky. Modeling, adaptive control, and optimal drug infusion. *Medical Progress through Technology*, 16:95–110, 1990.

[228] J. Jiang and Q. Zhao. Reconfigurable control based on imprecise fault identification. In *Proceedings of the American Control Conference, San Diego, California, June*, pages 114–118, 1999.

[229] G. Johannsen. *Mensch-Maschine-Systeme*. Springer-Verlag, 1993.

[230] A. T. Johnson and J. D. Bronzino. *The Biomedical Engineering Handbook*, chapter Respiratory system, pages 70–86. CRC Press / IEEE Press, 1995.

[231] W. Johnson and Team Number 9. The anesthesia workstation with autopilot design. *Journal of Clinical Monitoring*, 10:332–334, 1994.

[232] C. Jongeneel. De computer is nooit verdoofd, intelligent monitor vor de anesthesist. Delft Integraal 98.2, 1998.

[233] R.B. Jørgensen. *Development and Test of Methods for Fault Detection and Isolation*. PhD thesis, Department of Control Engineering, Aalborg University, 1995.

[234] R.B. Jørgensen, R. Patton, and J. Chen. Fault detection and isolation using eigenstructure assignment. In *Proceedings IFAC Sympmosium on Fault Detection, Supervision and Safety for Technical Processes, Espoo, Finland*, pages 463–469, 1994.

[235] T. Kailath. *Linear Systems*. Prentice Hall, 1980.

[236] R.E. Kalman, Y.O. Ho, and K.S. Narendra. Controllability of linear dynamical systems. *Contributions to Differential Equations*, 1(2):189–213, 1963.

[237] N. Karcanias. The selection of input and output schemes for a system and the model projection problems. *Kybernetika*, 30(6):585–596, 1994.

[238] J.P. Keller and D. Bonvin. Selection of input and output variables as a model reduction problem. *Automatica*, 28(1):171–177, 1992.

[239] D.A. Kendall and J.P. Robinson. *Noradrenaline in the Central Nervous System*, chapter Biochemical and functional correlates of adrenoceptor function in the central nervous system, pages 118–140. Oxford University Press, 1990.

[240] E.C. Kerrigan and J.M. Maciejowski. Fault-tolerant control of a ship propulsion system using model predictive control. *Proceedings of the 1999 European Control Conference (ECC 99), Karlsruhe, Germany, Sept.*, 1999.

[241] T. E. Keys. *The history of surgical anesthesia*. Wood Library - Museum of anesthesiology, 1996.

[242] H.K. Khalil. *Nonlinear Systems*. Prentice Hall, 1996.

[243] M. Kinnaert, R. Hanus, and Ph. Arte. Fault detection and isolation for unstable linear systems. *IEEE Transactions on Automatic Control*, 40(4):740–742, 1995.

[244] M. Kinnaert and Y. Peng. Residual generator for sensor and actuator fault detection and isolation: a frequency domain approach. *International Journal of Control*, 61(6):1423–1435, 1995.

[245] H. Klocke, S. Trispel, and G. Rau. Entwicklung einer Mensch-Rechner Schnittstelle für ein Anästhesie-Informationssystem unter Berücksichtigung ergonomischer Gesichtspunkte. *Angewandte Informatik*, 26(5):197–207, May 1984.

[246] M. Koch, H. Reiterer, and A Min Tjoa. *Software-Ergonomie, Gestaltung von EDV-Systemen - Kriterien, Methoden und Werkzeuge.* Springer-Verlag, 1991.

[247] M.V. Kothare, P.J. Campo, M. Morari, and C.N. Nett. A unified framework for the study of anti-windup designs. *Automatica*, 30(12):1869–1883, 1994.

[248] M.V. Kothare and M. Morari. Multiplier theory for stability analysis of anti-windup control systems. *Automatica*, 35(5):917–928, 1998.

[249] K.J. Kotrly, T.J. Ebert, E. Vucins, F.O. Igler, J.A. Barney, and J.P. Kampine. Baroreceptor reflex control of heart rate during isoflurane anesthesia in humans. *Anesthesiology*, 60(4):173–179, 1984.

[250] P Kozák and W.M. Wonham. Fully decentralized solutions of supervisory control problems. *IEEE Transactions on Automatic Control*, 40(12):2094–2097, December 1995.

[251] V. Krishnaswami and G. Rizzoni. A survey of observer based residual generation for FDI. In *Proceedings IFAC Sympmosium on Fault Detection, Supervision and Safety for Technical Processes, Espoo, Finland*, pages 35–40, 1994.

[252] R. Kumar and L.E. Holloway. Supervisory control of deterministic petri nets with regular specification languages. *IEEE Transactions on Automatic Control*, 41(2):245–249, February 1996.

[253] R. Kumar and M.A. Shayman. Nonblocking supervisory control of nondeterministic systems via prioritized synchronization. *IEEE Transactions on Automatic Control*, 41(8):1160–1175, 1996.

[254] K.E. Kwok, S.L. Shah, B.A. Finegan, and G.K. Kwong. An observational trial of a computerized drug delivery system on two patients. *IEEE Transactions On Control Systems Technology*, 5(4):385–393, July 1997.

[255] K.E. Kwok, S.L. Shah, B.A. Finegan, and G.K. Kwong. Experiences with experimental clinical evaluation of a computerized drug delivery system for regulation of mean arterial blood pressure. In *Proceedings of the American Control Conference, San Diego, California, June*, pages 1264–1268, 1999.

[256] G. K. Kwong, K. E. Kwok, B.A. Finegan, and S. L. Shah. Clinical evaluation fo long range adaptive control for mean arterial blood pressure regulation. In *Proceedings of the Ammerican Control Conference, Seattle, WA*, pages 786–790, June 1995.

[257] P.J.A. Lago and M.A. Gomes. Comparative study of design methods for drug dosage regimens. In *Modelling and Control in Biomedical Systems, The Third IFAC Symposium, University of Warwick.* The Institute of Measurement and Control, 1997.

[258] M.J. Landon, A.M. Matson, B.D. Royston, A.M. Hewlett, D.C. White, and J.F. Nunn. Components of the inspiratory - arterial isoflurane partial pressure difference. *British Journal of Anesthesia*, 70:605–611, 1993.

[259] R. Larsen. *Anästhesie und Intensivmedizin fuer Schwestern und Pfleger*, chapter Überwachung des Intensivpatienten, pages 599–618.

[260] T.P. Laubscher, W. Heinrichs, N. Weiler, G. Hartmann, and J.X. Brunner. An adaptive lung ventilation controller. *IEEE Transactions on Biomedical Engineering*, 41(1):51–59, January 1994.

[261] B. Lauter. *Software-Ergonomie in der Praxis*. Oldenbourg, 1987.

[262] J.H. Lee, M Morari, and C.E. Garcia. State-space interpretation of model predictive control. *Automatica*, 30(4):707–717, 1994.

[263] J.M. Legg. Computerized approach for matrix-form FMEA. *IEEE Transactions on Reliability*, 27(4):254–257, 1978.

[264] Norbert Leitgeb. *Sicherheit in der Medizintechnik*. expert verlag, 1995.

[265] L. Lemay and C.L. Perkins. *Teach yourself JAVA in 21 days*. Sams.net Publishing, 1996.

[266] B. Lennartson, M. Tittus, B. Egardt, and S. Petterson. Hybrid system in process control. *IEEE Control Systems*, 16(5):45–56, October 1996.

[267] J.G.C. Lerou, R. Dirksen, H.H. Beneken, and L.H.D. Booij. A system model for closed-circuit inhalation anesthesia, i. computer study. *Anesthesiology*, 75:345–355, 1991.

[268] J.G.C. Lerou, R. Dirksen, H.H. Beneken, L.H.D. Booij, and G.F.. Borm. A system model for closed-circuit inhalation anesthesia, ii. clinical validation. *Anesthesiology*, 75:230–237, 1991.

[269] N.G. Leveson and C.S. Turner. An investigation of the Therac-25 accidents. *Computer*, 26(7):18–41, 1993.

[270] K.-P. Lin and W.H. Chang. Adaptive noise reduction for pulmonary artery blood pressure. *Proceedings of the 10th International Conference of the IEEE Engineering in Medicine & Biology Society, New Orleans, LA, USA,*, 1:82–83, 1988.

[271] L. Lindgren, A. Yli-Hankala, T. Randell, M. Kirvelä, M. Scheinin, and P.J. Neuvonen. Haemodynamic and catecholamine responses to induction of anaesthesia and tracheal intubation comparison between propofol and thiopentone. *British Journal of Anaesthesia*, 70:306–310, 1993.

[272] D. A. Linkens and S. S. Hacisalihzade. Computer control systems and pharmacological drug administration: a survey. *Journal of Medical Engineering & Technology*, 14(2):41–51, March 1990.

[273] D.A. Linkens. Adaptive and intelligent control in anesthesia. *IEEE Control Systems*, pages 6–11, December 1992.

[274] D.A. Linkens. Intelligent control in anaesthesia. *Asia-Pacific Engineering Journal (Part A)*, 2(1):31–46, 1992.

[275] D.A. Linkens. Neuro-fuzzy modelling and control in biomedicine. In *Proceedings EUFIT '96, Aachen, Germany, 2-5 Sept, 1996*, pages 2021–2035, 1996.

[276] D.A. Linkens, M.F. Abbod, and J. Bachory. Auditory evoked response for measuring depth of anaesthesia using wavelet-fuzzy logic system. In *Modelling and Control in Biomedical Systems, The Third IFAC Symposium, University of Warwick*. The Institute of Measurement and Control, 1997.

[277] D.A. Linkens, M.F. Abbod, and J.K. Backory. Closed-loop control of depth of anaesthesia: A simulation study using auditory evoked responses. *Control Engineering Practice*, 5(12):1717–1726, 1997.

[278] D.A. Linkens and S.B. Hasnain. Self-organising fuzzy logic control and application to muscle relaxant anaesthesia. *IEE Proceedings D*, 138(3):274–284, May 1991.

[279] D.A. Linkens and M. Mahfouf. Generalized predictive control with feedforward (GPCF) for multivariable anaesthesia. *International Journal of Control*, 56(2):1039–1057, 1992.

[280] D.A. Linkens, M. Mahfouf, and M. Abbod. Self-adaptive and self-organizing control applied to nonlinear multivariable anaesthesia: a comparative model-based study. *IEE Proceedings-D*, 139(4):381–394, July 1992.

[281] D.A. Linkens, M. Mahfouf, and A.J. Asbury. Multivariable generalized predictive control for anaesthesia. In *Proceedings of the First European Control Conference (ECC 91), Grenoble, France, July 2-5,*, volume 2, pages 1630–1635, 1991.

[282] D.A. Linkens, M. Mahfouf, and J.E. Peacock. Propofol incuced anaesthesia: A comparative control study using a derived pharmacokinetic pharmacodynamic model. *Proceedings of the IFAC Symposium on Modeling and Control in Biomedical Systems, Galveston, Texas, March 27-30, 1994*, pages 196–197.

[283] L. Litz. Grundlagen der sicherheitsgerichteten Automatisierungstechnik. *Automatisierungstechnik*, 46(2):56–68, 1998.

[284] B. Liu and J. Si. Fault isolation filter design for linear time-invariant systems. *IEEE Transactions on Automatic Control*, 42(5):704–707, 1997.

[285] J. Liu, H. Singh, and P.F. White. Electroencephalographic bispectral index correlates with intraoperative recall and depth of propofol-induced sedation. *Anesthesia Analgesia*, 84:185–189, 1997.

[286] Ch. Loppacher and B. Lüthi. Regelung der endtidalen CO_2 Konzentration bei der Beatmung von Patienten. Semesterarbeit, Automatic Control Laboratory, Swiss Federal Institute of Technology (ETH), Zürich, 1993. IfA 8745.

[287] G. Lorden. Procedures for reacting to a change in distribution. *The Annals fo Mathematical Statistics*, 42(6):1897–1908, 1971.

[288] G. Lundeen, M. Manohar, and C. Parks. Systemic distribution of blood flow in swine while awake and during 1.0 and 1.5 MAC Isoflurane anesthesia with or without 50% nitrous oxide. *Anesthesia Analgesia*, 62:499–512, 1983.

[289] J. Lunze. Qualitative modelling of dynamical systems, motivation, methods, and prospective applications. In *Proceedings of the Second International Symposium on Mathematical Modelling (MATHMOD), Vienna, Austria*, pages 33–44, 1997.

[290] C. Lynch. Differential depression of myocardial contractility by Halothane and Isoflurane, In vitro. *Anesthesiology*, 64:620–631, 1986.

[291] J.M. Maciejowski. Modelling and predictive control: Enabling technologies for reconfiguration. *Annual Reviews in Control*, 23:13–23, 1999.

[292] M. Mahfouf. *Intelligent Control in Biomedicine*, chapter 3, Generalized predictive control (GPC) in the operating theater, pages 37–77. Taylor & Francis, 1994.

[293] M. Mahfouf and M.F. Abbod. *Intelligent Control in Biomedicine*, chapter 4, A comparative study of generalized predictive control (GPC) and intelligent self-organizing fuzzy logic controller (SOFLC) for multivariable anaesthesia, pages 79–132. Taylor & Francis, 1994.

[294] M. Mahfouf, M.F. Abbod, and D.A. Linkens. Generalised predicitive control (gpc) integrates with fuzzy logic control to regulate neuromuscular blockade. In *Modelling and Control in Biomedical Systems, The Third IFAC Symposium, University of Warwick*. The Institute of Measurement and Control, 1997.

[295] M. Mahfouf and D.A. Linkens. A comparative study ol flow-limited and diffusion limited physiological models for fentanyl. In *Modelling and Control in Biomedical Systems, The Third IFAC Symposium, University of Warwick*. The Institute of Measurement and Control, 1997.

[296] M. Mahfouf and D.A. Linkens. Constrained multivariable generalized predictive control (GPC) for anaesthesia: the quadratic-programming approach (QP). *International Journal of Control*, 67(4):507–527, 1997.

[297] M. Mahfouf and D.A. Linkens. A nonlinear GPC algorithm (NLGPC) for muscle relaxant anaesthesia. *Proceedings 1997 European Control Conference (ECC '97), Brussels, July 1-4, 1997*, 1997.

[298] M. Mahfouf and D.A. Linkens. Non-linear generalized predictive control (nlgpc) applied to muscle relaxant anaesthesia. *International Journal of Control*, 1998.

[299] W.W. Mapleson. Circulation-time models of the uptake of inhaled anaesthetics and data for quantifying them. *British Journal of Anaesthesia*, 45:319–333, 1973.

[300] T. Marcu, M. H. Matcovschi, and P.M. Frank. Neural approaches to observer-based fault diagnosis and reconfiguration of a three-tank system. presented at COSY Workshop, Mulhouse, France, April 3-4,, 1998.

[301] A. Mari. Determination of the single-pass impulse response of the body tissues with circulatory models. *IEEE Transactions on Biomedical Engineering*, 42(3):304–312, March 1995.

[302] A. Mari and A. Valerio. A circulatory model for the estimation of insulin sensitivity. *Control Engineering Practice*, 5(12):1747–1752, 1997.

[303] J.F. Martin. Fuzzy control in anesthesia. *Journal of Clinical Monitoring*, 10:77–80, 1994.

[304] J.F. Martin, A.M. Schneider, M.L. Quinn, and N.T. Smith. Improved safety and efficacy in adaptive control of arterial blood pressure through the use of a supervisor. *IEEE Transactions on Biomedical Engineering*, 39(4):381–388, Anaesthetic Pharmacology Review 1992.

[305] J.F. Martin, A.M. Schneider, M.L. Quinn, and N.T. Smith. Supervisory adaptive control of arterial pressure during cardiac surgery. *IEEE Transactions on Biomedical Engineering*, 39(4):389–393, Anaesthetic Pharmacology Review 1992.

[306] J.F. Martin, A.M. Schneider, and N.T. Smith. Multiple-model adaptive control of blood pressure using sodium nitroprusside. *IEEE Transactions on Automatic Control*, 34(8):603–611, August 1987.

[307] J.F. Martin, N.Ty Smith, M.L. Quinn, and A.M. Schneider. Supervisory adaptive control of arterial pressure: Performance during cardiac surgery. In *Annual International Conference of the IEEE Engineering in Medicine and Biology Society*, volume 13, pages 2141–2142, 1991.

[308] D.G. Mason, D.A. Linkens, N.D. Edwards, and C.S. Reilly. Development of a portable closed-loop atracurium infusion system: system methodology and safety issues. *International Journal of Clinical Monitoring*, 13:243–252, 1997.

[309] D.G. Mason, D.A. Linkens, N.D. Edwards, J. Ross, and C.S. Reilly. Intelligent fuzzy control of muscle relaxants in anaesthesia. In *Proceedings EUFIT '96, Aachen, Germany, 2-5 Sept, 1996*, 1996.

[310] D.G. Mason, D.A. Linkens, N.D. Edwards, J.J. Ross, and C.S. Reilly. Self-learning fuzzy control of atracurium-induced neuromuscular block during surgery. In *Modelling and Control in Biomedical Systems, The Third IFAC Symposium, University of Warwick*. The Institute of Measurement and Control, 1997.

[311] D.G. Mason, C.F. Swinhoe, D.A. Linkens, and C.S. Reilly. Letter to the editor: Development of a pharmacokinetic model-based infusion system for ketamine analgesia. *International Journal of Clinical Monitoring*, 13:139–142, 1996.

[312] M.-A. Massoumnia. A geometric approach to the synthesis of failure detection filters. *IEEE Transactions on Automatic Control*, 31(9):839–846, 1986.

[313] J.A. McEwen, G.B. Anderson, M.D. Low, and L.C. Jenkins. Monitoring the level of anesthesia by automatic analysis of spontaneous EEG activity. *IEEE Transactions on Biomedical Engineering*, 22(4):299–305, July 1975.

[314] C. Mechmeche, M. Zasadzinski, H. Rafaralahy, J.Y. Keller, and M. Darouach. A fault detection filter for bilinear systems with unknown inputs. In *Proceedings of the Second International Symposium on Mathematical Modelling (MATHMOD), Vienna, Austria*, pages 1077–1082, 1997.

[315] A. Megretski and A. Rantzer. System analysis via integral quadratic constraints. *IEEE Transactions on Automatic Control*, 42(6):819–830, 1997.

[316] R. Meier and J. Nieuwland. Fuzzy Logik für die optimale Regelung der Medikamentenver-
abreichung (1). Semesterarbeit, Automatic Control Laboratory, Swiss Federal Institute of
Technology (ETH), Zürich, March 1991. IfA 8683.

[317] R. Meier and J. Nieuwland. Multivariable Fuzzy-Regelung der Anästhesietiefe. Diplo-
marbeit, Automatic Control Laboratory, Swiss Federal Institute of Technology (ETH),
Zürich, 1992. IfA 8696.

[318] R. Meier, J. Nieuwland, S. Hacisalihzade, D. Steck, and A. Zbinden. Fuzzy control of
blood pressure during anesthesia with isoflurane. In *Proceedings IEEE Conference on Fuzzy
Systems*, pages 981–987, 1992.

[319] A.P. Meijler. *Automation in Anesthesia, A Relief?* Springer, 1987.

[320] L.J. Meline, D.R. Westenskow, N.L. Pace, and M.N. Bodily. Computer-controlled regulation
of sodium nitroprusside infusion. *Anestheisa Analgeisa*, 64:38–42, 1985.

[321] T.F. Mendonça, P.J. Lago, and I.M. Araújo. Control of neuromuscular blockade: A method
for the autocalibration of PID controllers. In *Modelling and Control in Biomedical Systems,
The Third IFAC Symposium, University of Warwick*. The Institute of Measurement and
Control, 1997.

[322] P.H. Menold, R.K. Pearson, and F. Allgöwer. Online outlier detection and removal. In *The
7th IEEE Mediteranean Conference on Control and Automation, June 28-30, Haifa, Israel*,
1999.

[323] B. Meyer. On to components. *IEEE Computer*, 32(1):139–140, 1998.

[324] D. Mignone, A. Bemporad, and M. Morari. A framework for control, fault detection, state
estimation, and verification of hybrid systems. In *Proceedings of the American Control
Conference, San Diego, California, June*, pages 134–138, 1999.

[325] J.J. Milek and H. Güttinger. The mechanometrics approach to monitoring and fault detec-
tion of a hydro-mechanical system. In *Proceedings of the Second International Symposium
on Mathematical Modelling (MATHMOD),, Vienna, Austria*, pages 389–393, 1997.

[326] R.K. Millard, P. Hutton, E. Pereira, and C. Prys-Roberts. On using a self-tuning controller
for blood pressure regulation during surgery in man. *Computers in Biology and Medicine*,
17(1):1–17, 1987.

[327] R.K. Millard, C.R. Monk, and C. Prys-Roberts. Self-tuning control of hypotension during
ENT surgery using a volatile anaesthetic. *IEE Proceedings Pt. D,*, 135(2):95–105, 1988.

[328] H. Mizuta, I. Takeuchi, O. Tsuda, and K. Yana. A feed back analysis of heart rate
fluctuations related to blood pressure change: Effect of autonomic blockade. In *Proceedings
of the 19th International Conference of the IEEE/EMBS, Oct. 30 - Nov. 2, 1997, Chicago,
IL, USA*.

[329] C.R. Monk, R.K. Millard, P. Hutton, and C. Prys-Roberts. Automatic arterial pressure reg-
ulation using isoflurane: Comparison with manual control. *British Journal of Anaesthesia*,
63:22–30, 1989.

[330] B. C. Moore. Principal component analysis in linear systems: controllability, observability, and model reduction. *IEEE transactions on automatic control*, 26:17–32, February 1981.

[331] M. Morari and G. Stephanopoulos. Studies in the synthesis of control structures for chemical processes. Part III: Optimal selection of secondary measurements within the framework of state estimation in the presence of persistent unknown disturbances. *AIChE Journal*, 40(2):247–259, 1980.

[332] G.E. Morgan and M.S. Mikhail. *Clincal Anesthesiology*. Prentice-Hall International, Inc., 1996.

[333] P. Morris, M.L. Tatnall, and F.J. Montgomery. Controlled anaesthesia: A clinical evaluation of an approach using patient characteristics identified during uptake. *British Journal of Anaesthesia*, 55:1065–1075, 1983.

[334] H. Mössenböck. *Objekt-Oriented Programming in Oberon-2*. Springer-Verlag, 1995.

[335] P.C. Müller and H.I. Weber. Analysis and optimization of certain qualities of controllability and observability for linear dynamical systems. *Automatica*, 8:237–246, 1972.

[336] Heinrich Munz. Windows: Echtzeit auf Umwegen. *Elektronik*, (18):133–137, 1994.

[337] A. Murbach. Computermodell der Aufnahme volatile Anästhetika. Informatikprojekt, Institut für Informatik und angewandte Mathematik der Universität Bern, May 1991.

[338] K.C. Mylrea, J.A. Orr, and D.R. Westenskow. Integration of monitoring for intelligent alarms in anesthesia: neural networks - can they help? *Journal of Clinical Monitoring*, 9(1):31–37, January 1993.

[339] O.A. Nedergaard and J. Abrahamsen. Modulation of noradrenaline release by activation of presynaptic β-adrenoceptors in the cardiovascular system. *Annals New York Academy Of Science*, (604):528–44, 1990.

[340] A. Nerode and W. Kohn. Models for hybrid systems: Automata, topologies, controllability, observability. In *Hybrid Systems, Lecture Notes in Computer Science*, pages 316–353. Springer-Verlag, 1993.

[341] Carl N. Nett. Algebraic aspects of linear control system stability. *IEEE Transactions on Automatic Control*, 31(10):941–949, October 1996.

[342] C.N. Nett, C.A. Jacobson, and A.T. Miller. An integrated approach to controls and diagnostics: The 4-parameter controller. In *Proceedings of the 1988 American Control Conference*, pages 824–835, 1988.

[343] S.H. Ngai. Plasma catecholamines - Their significance in anesthesia. *Anesthesiology*, 41(5):429–430, 1974.

[344] A. Nicolet. Programme de simulation de la pharmacocinétique et de la pharmacodynamique des anesthésiques par inhalation. MD thesis, University of Bern, 1995.

[345] J. Nie and D.A. Linkens. Automatic knowledege acquisition for multivariable fuzzy control using neural network approach. In *Proc. 1993 American Control Conference, San Francisco, CA,*, pages 767–771, June 1993.

[346] J. Nie and D.A. Linkens. Fcmac: a fuzzified cerebellar model articulation controller with self-oragnizing capacity. *Automatica*, 30(4):655–664, 1994.

[347] P. Niederer. Vorlesungen in Biomechanik I. Lecture Notes Swiss Federal Institute of Technology (ETH).

[348] P. Niederer. Vorlesungen in Biomechanik II. Lecture Notes Swiss Federal Institute of Technology (ETH).

[349] K. Nikiforov, M. Staroswiecki, and B. Vozel. Duality of analytical redundancy and statistical approach in fault diagnosis. *Proceedings of the 1996 IFAC World Congress, San Franciso, USA*, pages 19–24, 1996.

[350] T. Nishimura and M. Saito. A 24-hour prediction model of blood pressure employing endocrine system and autonomic nervous system. In *Computing and Monitoring in Anesthesia and Intensive Care - Recent Technological Advances*, pages 84–90. Springer, 1992.

[351] T. Nishiyama, M. Aibiki, and K. Hanaoka. Haemodynamic and catecholamine changes during rapid Sevoflurane induction with tidal volume breathing. *Canadian Journal of Anaesthesia*, 44(10):1066–1070, 1997.

[352] C. Oberli, J. Urzua, C. Saez, M. Guarini, A. Cipriano, B. Garayar, G. Lema, R. Canessa, C. Sacco, and M. Irarrazaval. An expert system for monitor alarm integration. *Journal of Clinical Monitoring and Computing*, 15:29–35, 1999.

[353] T.M. O'Carroll. Survey of alarms in an intensive therapy unit. *Anaesthesia*, 41:742–744, 1986.

[354] United States Department of Defense. Reference manual for the Ada programming language, 1980.

[355] D.A. O'Hara, D.K. Bogen, and A. Noordergraf. The use of computers for controlling the delivery of anesthesia. *Anesthesiology*, 77:563–581, 1992.

[356] K. T. Olkkola and T. Tammisto. Quantifying the interaction of rocuronium (org 9426) with etomidate, fentanyl, midazolam, propofol, thiopental, and isoflurane using closed-loop feedback control of rocuronium infusion. *Anesthesia Analgesia*, 78:691–696, 1994.

[357] K.T. Olkkola and T. Tammisto. Assessment of the interaction between atracurium and suxamethonium at 50 % neuromuscular block using closed-loop feedback control of infusion of atracurium. *British Journal of Anaesthesia*, 73:199–203, 1994.

[358] R. Oppermann, B. Murchner, H. Reiterer, and M. Koch. *Software-ergonomische Evaluation.* de Gruyter, 1992.

[359] J.A. Orr and Westenskow D.R. Evaluation of a breathing circuit alarm system based on neural networks. *Anesthesiology*, 73(3A):A444, September 1990.

[360] J.A. Orr, F.H. Simon, H.-J. Bender, and Westenskow D.R. Response time with smart alarms. *Anesthesilogy*, 73(3A):A447, September 1990.

[361] S. Ortiz Jr. The battle over real-time Java. *Computer*, 32(6):13–15, 1999.

[362] E.S. Page. Control charts for the mean of a normal population. *Journal of the Royal Statistics Society*, B-16(1):131–134, 1954.

[363] D. Palm, D. Hellenbrecht, and K. Quiring. *Pharmakologie und Toxikologie*, chapter Pharmakologie des noradrenergen und adrenergen Systems, page 124 ff. R.I. Wissenschaftsverlag, 7 edition, 1992.

[364] T. Pasch and C. Mörgeli. *150 Jahre Anästhesie - Narkose, Intensivmedizin,Schmerztherapie, Notfallmedizin.* Wissenschaftliche Verlagsabteilung Abbott GmbH, 1997.

[365] I. Paton and D. Murray. *The release of catecholamines from adrenergic neurons.* Pergamon Press Ltd., 1979.

[366] R.J. Patton. Robust model-based fault diagnosis: The state of the art. In *Proceedings IFAC Symposium on Fault Detection, Supervision and Safety for Technical Processes, Espoo, Finland*, pages 1–24, 1994.

[367] R.J. Patton. Fault-tolerant control: The 1997 situation. In *Preprints of IFAC Symposium on Fault Detection, Supervision and Safety for Technical Processes (Safeprocess '97)*, pages 1033–1055, 1997.

[368] R.J. Patton and H. Chen. A re-examination of the relationship between parity space and observer-based approaches in fault diagnosis. *Revue européenne Diagnostic et sûreté de fonctionnement (European Journal fo Diagnosis and Safety in Automation)*, 1(2):183–200, 1991.

[369] R.J. Patton and J. Chen. Robust fault detection and isolation (FDI) systems. *Control and Dynamic Systems*, 74:171–223, 1996.

[370] A.W. Paulsen. *The Biomedical Engineering Handbook*, chapter 86, Anesthesia Delivery Systems, pages 1322–1332. CRC Press / IEEE Press, 1995.

[371] J. Perkins, editor. *The Beta-adrenergic receptors.* The Humana Press Inc., 1991.

[372] T.G. Peterson and Team Number 10. Design of the four-component anesthesia workstation. *Journal of Clinical Monitoring*, 10:335–338, 1994.

[373] A. Petry. On-line Aufzeichnung von Monitordaten. *Anästhesist*, 44:818–825, 95.

[374] C.A. Pfister, A.M. Zbinden, S. Petersen-Felix, T. Schnider, M. Luginbühl, and C.W. Frei. Stressantwort auf einen normierten Schmerzreiz. Study Protocol, October 1997.

[375] J.H. Philip and Team Number 11. The gas busters anesthesia workstation. *Journal of Clinical Monitoring*, 10:339–342, 1994.

[376] M. Pollak. Optimal detection of a change in distribution. *The Annals of Statistics*, 13(1):206–227, 1985.

[377] M.M. Polycarpou and J.Y. Conway. Modeling and control of drug delivery systems using adaptive neural control methods. In *Proceedings of the American Control Conference, Seattle, Washington*, pages 781–785, June 1995.

[378] M. Pottman, M.A. Henson, B.A. Ogunnaike, and J.S. Schwaber. A parallel control strategy abstracted from the baroreceptor reflex. *Chemical Engineering Science*, 51(6):931–945, 1996.

[379] D.D. Price, J.J. Barrell, and R.H. Gracely. A psychophysical analysis of experimental factors that selectively influence the affective dimension of pain. *Pain*, 8:137–149, 1980.

[380] D.D. Price, P.A. McGrath, A. Rafii, and B. Buckingham. The validation of visual analogue scales as ratio scale measures for chronic and experimental pain. *Pain*, 17:45–56, 1983.

[381] P. Pundsnes, M. Balters, and S. Hacisalihzade. Open-loop control of therapeutic drug delivery with fuzzy logic. In *Annual International Conference of the IEEE Engineering in Medicine and Biology Society*, volume 13, pages 2166–2167, 1991.

[382] X.J. Qu and Z. Mao. Self-adaptive control for blood pressure. *Control Engineering Practice*, 2(4):659–664, 1994.

[383] J.C.A. Raison, J.O. Beaumont, J.A.G. Russell, J.J. Osborn, and F. Gerbode. Alarms in an intensive care unit: an interim compromise. *Computers and Biomedical Research*, 1:556–564, 1968.

[384] P.J. Ramadge and W.M. Wonham. Supervisory control of a class of discrete event processes. *SIAM Journal of Control and Optimization*, 25(1):206–230, 1987.

[385] P.J. Ramadge and W.M. Wonham. The control of discrete event system. *Proceedings of the IEEE*, 77(1):81–89, January 1989.

[386] I. J. Rampil. A primer for EEG signal processing analysis. *Anesthesiology*, 89:980–1002, 1998.

[387] R.R. Rao, B. Aufderheide, and B.W. Bequette. Multiple model predictive control of hemodynamic variables: An experimental study. In *Proceedings of the American Control Conference, San Diego, California, June*, pages 1253–1257, 1999.

[388] R.R. Rao, J.W. Huang, B.W. Bequette, H. Kaufmann, and R.J. Roy. Modeling and control of a nonsquare drug infusion system. In *Modelling and Control in Biomedical Systems, The Third IFAC Symposium, University of Warwick*. The Institute of Measurement and Control, 1997.

[389] G. Rau, T. Schecke, and M. Langen. Visualization and man-machine interaction in clinical monitoring tasks. In *First Conference on Visualization in Biomedical Computing, Atlanta, USA, May 22-25*, pages 268–272, 1990.

[390] H.U. Rehman, D.A. Linkens, and Asbury A.J. Neural networks and nonlinear regression modelling and control of depth of anesthesia for spontaneously breathing and ventilated patients. *Computer methods and programs in biomedicine*, 40:227–247, 1993.

[391] J.A. Reid and G.N.C. Kenny. Evaluation of closed-loop control of arterial pressure after cardiopulmonary bypass. *British Journal of Anaesthesia*, 59:247–255, 1987.

[392] D. Reinert, M. Schaefer, and T. Bömer. Regeln für den Entwurf und die Programmierung sicherheitsbezogener Software. *Automatisierungstechnische Praxis*, 41(6):21–30, 1999.

[393] M. Reiser. *The Oberon System, User Guide and Programmer's Manual*. ACM Press & Addison-Wesley, 1991.

[394] M. Reiser and N. Wirth. *Programming Oberon, Steps beyond Pascal and Modula*. Addison-Wesley, 1992.

[395] John A. Rice. *Mathematical Statistics and Data Analysis*. Duxbury Press, 1995.

[396] Vincent C. Rideout. *Mathematical computer modeling of physiological systems*. Prentice Hall, 1991.

[397] G. Ritchie, E.A. Ernst, B.L. Pate, J.D. Pearson, and L.C. Sheppard. Closed-loop control of an anesthesia delivery system: Development and animal testing. *IEEE Transactions on Biomedical Engineering*, 34(6):437, 1987.

[398] J.J. Ross, D.G. Mason, D.A. Linkens, and N.D. Edwards. Self-learning fuzzy logic control of neuromuscular block. *British Jouranl of Anaesthesia*, 78:412–415, 1997.

[399] R. Roy and G.-I. Jee. Adaptive control of multiplexed closed circuit anesthesia. In *Annual International Conference of the IEEE Engineering in Medicine and Biology Society*, volume 13, pages 2149–2151, 1991. O2 oxygen N2O Halothane, only simulation, Dog-Model, MPC, Sensitivity.

[400] R.J. Roy and J. Huang. Multiple input-multiple output hemodynamic control using fuzzy decision theory. In *Modelling and Control in Biomedical Systems, The Third IFAC Symposium, University of Warwick*. The Institute of Measurement and Control, 1997.

[401] R.J. Roy and A. Sharma. Depth of anesthesia using neural networks. *Proceedings of the IFAC Symposium on Modeling and Control in Biomedical Systems, Galveston, Texas, March 27-30, 1994*, pages 185–190.

[402] F.G. Rudo and J.C. Krantz. Anaesthetic molecules. *British Journal of Anaesthesia*, 46:181–189, 1974.

[403] R. Ruiz, D. Borches, A. González, and J. Corral. A new sodium-nitroprusside-infusion controller for the regulation of arterial blood pressure. *Biomedical Instrumentation & Technology*, pages 244–251, May 1993.

[404] J. Rumbaugh, M. Blaha, W. Premerlani, F. Eddy, and W. Lorensen. *Object-Oriented Modeling and Design*. Prentice Hall International Editions, 1991.

[405] A. Saberi, B.M. Chen, and P. Sannuti. *Loop Transfer Recovery: Analysis and Design*. Springer-Verlag, 1993.

[406] R.F. Salamonsen and K. Smith. An approach to programmed anaesthesia. *Anaesthesia*, 31:1043–1048, 1976.

[407] Y. Sanjo and K. Ikeda. Real time joint of pharmacokinetic simulation and monitoring in inhalational agents. In *Computing and Monitoring in Anesthesia and Intensive Care - Recent Technological Advances*, pages 78–83. Springer, 1992.

[408] R.M. Satava. The modern medical battlefiled: Sequitur on advanced medical technology. *IEEE Robotics & Automation Magazine*, pages 21–25, September 1994.

[409] J.H. Saunders. A survey of object-oriented programming languages. *Journal of Object Oriented Programming*, pages 5–11, March 1989.

[410] R.J. Saunders and Team Number 13. The anesthesia workstation of the future. *Journal of Clinical Monitoring*, 10:346–348, 1994.

[411] F.L. Scamman and Team Number 14. Designing the workstation: An innovative concept. *Journal of Clinical Monitoring*, 10:349–351, 1994.

[412] J. Schäublin, M. Derighetti, P. Feigenwinter, S. Petersen-Felix, and A.M. Zbinden. Fuzzy logic control of mechanical ventilation during anesthesia. *British Journal of Anaesthesia*, 77(5):636–641, 1996.

[413] W. Schaufelberger. Echtzeitprogrammierung in Modula-2 und Oberon. *SGA-Bulletin, OBERON in der Automatisierungtechnik Nr. 4*, (16):4–7, December 1996/1997.

[414] T. Schecke, M. Lange, G. Rau, H. Käsmacher, and G. Kalff. Knowledge-based decision support for monitoring in anesthesia: Problems, design and user interaction. In *Expert Systems and Decision Support in Medicine, 33rd Annual Meeting of the GMDS EFMI Special Topic Meeting, Hannover, Germany, September*, pages 256–263. Springer, 1988.

[415] Th. Schecke, G. Rau, H.-J. Popp, H. Kasmacher, G. Klaff, and H.-J. Zimmermann. A knowledge-based approach to intelligent alarms in anesthesia. *IEEE Engineering in Medicine and Biology*, pages 38–44, December 1991.

[416] G.F. Schils, F.J. Sasse, and V.C. Rideout. Automatic control of anesthesia using two feedback variables. *Annals of Biomedical Engineering*, 15:19–34, 1987.

[417] Andreas Schmid. Physiologischer Simulator mit JAVA (Erweiterung). Semesterarbeit, Automatic Control Lab, Swiss Federal Institute of Technology (ETH), Zürich, July 1997. IfA 8801.

[418] T.W. Schnider, A.H. Glattfelder, S. Petersen-Felix, M. Morari, and A.M. Zbinden. Development of an automatic feedback system for the delivery of anaesthetics during anaesthesia. Part 3: drug interaction. Forschungsgesuch Nr. 32-51028.97, Swiss National Science Foundation, 1997.

[419] P.J. Schreiber and J. Schreiber. Structured alarm systems for the operation room. *Journal of Clinical Monitoring*, 5(3):201–204, July 1989.

[420] D. Schweizer. *Verifikation von Implementationen abstrakter Datentypen für sicherheitskritische Systeme am Beispiel von Oberon.* PhD thesis, Swiss Federal Institute of Technology (ETH), Zurich, 1997.

[421] G. Schweizer. Der automatische Postbote. *Spektrum der Wissenschaft*, pages 14–16, November 1996.

[422] H. Schwilden and H. Stoeckel, editors. *Control and Automation in Anaesthesia.* Springer, 1995.

[423] G. A. F. Seber. *Multivariate Observations.* Wiley Series in Probability and Mathematical Statistics, 1984.

[424] Ralf Seliger. *Robuste beobachtergestützte Fehlerdetektion in nichtlinearen unsicheren Systemen*, volume 8 of *Mess-, Steuerungs und Regelungstechnik.* VDI, 1993.

[425] L. Sha, R. Rajkumar, and J.P. Lehoczky. Priority inheritance protocols: An approach to real-time synchronization. *IEEE Transactions on Computers*, 39(9):1175–1185, 1990.

[426] L.C. Sheppard. Computer control of the infusion of vasoactive drugs. *Annals of Biomedical Engineering*, 8:431–444, 1980.

[427] D.N. Shields. Observer design and detection for nonlinear descriptor systems. *International Journal of Control*, 67(2):153–168, 1997.

[428] L.C. Siegel and R.G. Pearl. Pressure measurement artifact with analog-to-digital conversion. *Journal of Clinical Monitoring*, 6(4):318–321, October 1990.

[429] S. Sigfried. *Understanding Object-Oriented Software Engineering.* IEEE Press, 1996.

[430] J.C. Sigl and N.G. Chamoun. An introduction to bispectral analysis for the electroencephalogram. *Journal of Clinical Monitoring*, 10(6):392–404, 1994.

[431] S. Silbernagel and A. Despopoulos. *Taschenatlas der Physiologie.* Thieme, München, 4 edition, 1991.

[432] O. Simanski, W. Drewlow, B.P. Lampe, R. Hofmockel, and B. Pohl. Ein System zur Regelung der Relaxation. In *Fortschritts-Berichte VDI, Reihe 17, Nr. 183, AUTOMED '99, Beiträge zum Workshop "Automatisierungstechnische Verfahren für die Medizin", 25./26. Februar, Darmstadt*, pages 39–40, 1999.

[433] D.F. Sittig and M. Factor. Physiologic trend detection and artifact rejection: a parallel implementation of a multi-state Kalman filtering algorithm. *Computer Methods and Programs in Biomedicine*, 31:1–10, 1990.

[434] R.E. Skelton and D. Chiu. Optimal selection of inputs and outputs in linear stochastic systems. *The Journal of the Astronautical Sciences*, XXXI(3):399–414, July 1983.

[435] D. Smiley. JAVA real time graphics library. *Medical Electronics*, pages 65–72, October 1997.

[436] N.T. Smith, J.F. Martin, M.L. Quinn, T.S. Scanlon, and G.I. Voss. Performance evaluation of a closed-loop sodium nitroprusside delivery device during hypotensive anesthesia in mongrel dogs. In *Computing and Monitoring in Anesthesia and Intensive Care - Recent Technological Advances*, pages 147–149. Springer, 1992.

[437] N.T. Smith and H.O. Schwede. The response of arterial pressure to halothane: A systems analysis. *Med. & Biol. Engng.*, 10:207–221, 1972.

[438] N.T. Smith, A. Zwart, and J.E.W. Beneken. Interaction between the circulatory effects and the uptake and distribution of halothane: Use of a multiple model. *Anesthesiology*, 37(1):47–58, July 1972.

[439] K.M. Sobel, E.Y. Shapiro, and A.N. Andry. *The Control Handbook*, chapter 38, Eigenstructure Assignment, pages 621–633. CRC Press / IEEE Press, 1996.

[440] E.D. Sontag. *Mathematical Control Theory, Deterministic Finite Dimensional Systems.* Springer, 1998.

[441] M. Staroswiecki, S. Attouche, and M.L. Assas. A graphic approach for reconfigurability analysis. *10th International Workshop on Principles of Diagnosis, Loch Awe, UK, 8-11, June,*, 1999.

[442] M. Staroswiecki and A.L. Gehin. Analysis of system reconfigurability using generic component models. In *UKACC International Conference on CONTROL '98, Conference Publication No. 455, Swansea, UK, September 1-4*, 1998.

[443] D. Steck. Regelung der Anäshesietiefe. Diplomarbeit, Automatic Control Laboratory, Swiss Federal Institute of Technology, Zürich, 1991. IfA 8661.

[444] M. Stein, R. Deegan, H. He, and A.J.J. Wood. β-adrenergic receptor-mediated release of norepinephrine in the human forearm. *Clinical Pharmacology & Therapeutics*, 54(1):58–63, 1993.

[445] L. Stryer. *Biochemistry of Physiology.* W.H. Freeman & Co. NY, 3 edition, 1988.

[446] U. A. Stucki. Benutzerschnittstellenkonzept für die Anästhesieregelung. Diplomarbeit, Automatic Control Laboratory, Swiss Federal Institute of Technology (ETH), Zürich, 1991. IfA 8834.

[447] T. Sukuvaara and E.M.J. Koski. Informative alarms in anaesthesia: from signal to patient-state monitoring. *Current Opinion in Anaesthesiology*, 8:526–531, 1995.

[448] R. Summers, H. Jansen, P.R. Weller, M.v. Gils, and K. Nieminen. Towards an optimal data set for intensive care. In *Proceedings of the 19th International Conference of the IEEE/EMBS, Oct. 30 - Nov. 2, 1997, Chicago, IL, USA*, pages 1025–1028.

[449] A.G. Targ, N. Yasuda, Eger E.I. II., G. Huang, G.G. Vernice, R.C. Ternell, and D.D. Koblin. Halogenation and anesthetic potency. *Anesthesia Analgesia*, 68:599–602, 1989.

[450] M.L. Tatnall, P. Morris, and P.G. West. Controlled anaesthesia: An approach using patient characteristics identified during uptake. *British Journal of Anesthesia*, 53:1019–1026, 1981.

[451] A. Teije and E. Rotterdam. Diagnostic reasoning with anesthesia knowledge. *Proceedings of the CESA '96 Multiconference Computational Engineering in Systems Application, Symposium on Modelling, Analysis and Simulation, Lille, France, July 9-12, 1996*, 1:564–569, 1996.

[452] R.C. Terrell. Physical and chemical properties of anaesthetic agents. *British Journal of Anaesthesia*, 56:3S–7S, 1984.

[453] G. Thews, E. Mutschler, and P. Vaupel. *Anatomie Physiologie Pathophysilogie des Menschen, Ein Lehrbuch für Pharmazeuten und Biologen*. Wissenschaftliche Verlagsgesellschaft mbH Stuttgart, 1982.

[454] B. Thull, H.-J. Popp, and G. Rau. Man-machine interaction in critical care settings. *IEEE Engineering in Medicine and Bilology*, pages 42–49, December 1993.

[455] C. Thybo and M. Blanke. Industrial cost-benefit assessment for fault tolerant control systems. In *UKACC International Conference on CONTROL '98, Conference Publication No. 455, Swansea, UK, September 1-4*, pages 1151–1156, 1998.

[456] M. Timmermann and J.-C. Monfret. Windows NT as real-time OS ? *REAL TIME MAGAZINE*, (2):6–13, 1997.

[457] W.D. Timmons. *The Biomedical Engineering Handbook*, chapter 158, Cardiovascular Models and Control, pages 2386–2403. CRC Press / IEEE Press, 1995.

[458] M. Tittus and B. Egardt. Control design for integrator hybrid systems. *IEEE Transactions on Automatic Control*, 43(4):491–500, 1998.

[459] T. Tsutsui and S. Arita. Fuzzy-logic control of blood pressure through Enflurane anesthesia. *Journal of Clinical Monitoring*, (10):110–117, 1994.

[460] G.T. Tucker. Pharmacokinetic and pharmacodynamic models. *Advances in Pain Research and Therapy*, 14:181–201, 1990.

[461] M.L. Tyler and M. Morari. Optimal and robust design of integrated control and diagnostic modules. Technical Report CIT/CDS 94-008, Caltech, 1994.

[462] E. Ulich. Aspekte der Benutzerfreundlichkeit. In *Arbeitsplätze morgen, Tagung II/1986 und Tutorial des German Chapter of the ACM, March 10-14, Marburg, Germany*, pages 103–121, 1986.

[463] Krämer Ullrich. Entwurf eines Zustandsreglers für die exspiratorische Anästhesiemittelkonzentration in einem Rückatemsystem unter Minimal-Flow-Bedingungen. Diplomarbeit, Technische Hochschule Achen, 1996.

[464] R. Vadigepalli and F.J. Doyle III. A simulation study of the nonlinear dynamic characteristics of a local cardiac reflex in the rat. In *Proceedings of the American Control Conference, San Diego, California, June*, pages 1248–1252, 1999.

[465] J. Valente de Oliveira, T.F. Mendoça, and J.M. Lemos. Long-range adaptive fuzzy control of neuromuscular blockade. In *Modelling and Control in Biomedical Systems, The Third IFAC Symposium, University of Warwick*. The Institute of Measurement and Control, 1997.

[466] K. van Ackern, H. Frankenberger, E. Konecny, and K. Steinbereithner, editors. *Quantitative Anaesthesia*. Sprinter-Verlag, 1989.

[467] G.C. van den Eijkel, J.C.A. van der Lubbe, and E. Backer. Fuzzy incremental learning of expert rules for a knowledge-based anesthesia monitor. In *Proceedings EUFIT '96, Aachen, Germany, 2-5 Sept, 1996*, pages 2056–2060, 1996.

[468] J. Van Egmond, M. Hasenbos, and J.F. Crul. Invasive v. non-invasive measurement of arterial pressure. *British Journal of Anaesthesia*, 57:434–444, 1985.

[469] J.H.M. van Oostrom. Intelligent alarms in anesthesia: An implementation. Master's thesis, Eindhoven University of Technology, 1989.

[470] J.H.M. van Oostrom. *A System for Automatic Alarm Limit Setting in Anesthesia*. PhD thesis, Technische Universiteit Eindhoven, 1993.

[471] J.R. Vane. The release and fate of vaso-active hormones in the circulation. *British Journal of Pharmacology*, 35(2):209–242, February 1969.

[472] M. Varanini, A. Taddei, R. Balocchi, M Macerata, F. Conforti, M. Emdin, C. Carpeggiani, and C. Marchesi. Adaptive modelling of biological time series for artifact detection. *Proceedings, Computers in Cardiology*, pages 695–698, 1993.

[473] O.I. Vasil'eva, I.P. Ionov, P.S. Kantor, and S.V. Ul'yanov. Dual control of the artificail ventilation process with use of a fuzzy controller in the feedback circuit. *Biomedical Engineering*, 23:7–17, 1989.

[474] VDI/VDE. Vorgestaltete Darstellung zur Prozessführung über Bildschirm in verfahrenstechnischen Anlagen. VDI/VDE-Richtline 3695, Düsseldorf: VDI-Verlag GmbH.

[475] S.M. Veres and H. Xin. Dual predictive control for fault tolerant control. In *UKACC International Conference on CONTROL '98, Conference Publication No. 455, Swansea, UK, September 1-4*, pages 1163–1167, 1998.

[476] S.J. Vestli and N. Tshichold-Gürman. Mops, a system for mail distribution in office type buildings. *Service Robots Journal*, 2(2), 1996.

[477] R. Vishnoi and R.J. Roy. Adaptive control of closed-circuit anesthesia. *IEEE Transactions on Biomedical Engineering*, 38(1):39–47, January 1991.

[478] D.R. Wada and D.S. Ward. Open loop control of multiple drug effects in anesthesia. *IEEE Transactions on Biomedical Engineering*, 42(7):666–677, July 1995.

[479] P. D. Wall and R. Melzack, editors. *Textbook of Pain*. Churchill Livingstone, 1994.

[480] H. Wang, Z.J. Huang, and S. Daley. On the use of adaptive updating rules for actuator and sensor fault diagnosis. *Automatica*, 33(2):217–225, 1997.

[481] T.W. Warren and R.K. Stoelting. *Cardiovascular Actions of Anesthetics and Drugs Used in Anesthesia, Basic Aspects*, chapter Hemodynamic Effects of General Anesthesia, pages 3–50. Karger, 1986.

[482] R.C. Watt, E.S. Maslana, and K.C. Mylrea. Alarms and anesthesia. *IEEE Engineering in Medicine and Biology*, pages 34–41, December 1993.

[483] R.B. Weiskopf, M.A. Moore, E.I. Eger II, M. Noorani, L. McKay, B. Chortkoff, P.S. Hart, and M. Damask. Rapid increase in Desflurane concentrations is associated with greater transient cardiovascular stimulation than with rapid increase in Isoflurane concentration in humans. *Anesthesiology*, 80(5):1035–1045, 1994.

[484] C. Weissmann. The metabolic response to stress: An overview and update. *Anesthesiology*, 73(2):308–327, 1990.

[485] H. Wenner. Software validation. *Medical Device Technology*, pages 22–25, Anaesthetic Pharmacology Review 1997.

[486] J.B. West. *Respiratory Physiology - the essentials*. Williams & Wilkins, 5th edition, 1995.

[487] D. Westenskow and Team Number 16. Holographic anesthesia lifeguard. *Journal of Clinical Monitoring*, 10:355–357, 1994.

[488] D.R. Westenskow, J.A. Orr, F.H. Simon, H.-J. Bender, and H. Frankenberger. Intelligent alarms reduce anesthesiologist's response time to critical faults. *Anesthesiology*, 77:1074–1079, 1992.

[489] D.R. Westenskow, A.M. Zbinden, D.A. Thomson, and B. Kohler. Control of end-tidal halothane concentration. *British Journal of Anaesthesia*, 58:555–562, 1986.

[490] D. Whalen, Anthony. *Detection of Signals in Noise*. Academic Press, 1971.

[491] A.S. Willsky. A survey of design methods for failure detection in dynamic systems. *Automatica*, 12:601–611, 1976.

[492] A.S. Willsky and H.L. Jones. A generalized likelihood ratio approach to the detection and estimation of jumps in linear systems. *IEEE Transactions on Automatic Control*, pages 108–112, February 1976.

[493] D. Wilner. Vx-Files: What really happened on mars? Keynote address at the 18th IEEE Real-Time Systems Symposium, Dec 2-5, San Francisco, CA, USA, 1997.

[494] N. Wirth. Tasks versus threads: An alternative multiprocessing paradigm. *Software - Concepts and Tools*, 17:6–12, 1996.

[495] N. Wirth and J. Gutknecht. *Project Oberon: The Design of an Operating System and Compiler*. ACM Press, New York, 1993.

[496] M. Wood and A.J.J. Wood. *Drugs and Anesthesia, Pharmacology for Anesthesiologists*. Williams & Wilkins, 1998.

[497] E. A. Woodruff. *The Biomedical Engineering Handbook*, chapter 162, Clinical Care of Patients with Closed-Loop Drug Delivery Systems, pages 2447–2457. CRC Press / IEEE Press, 1995.

[498] E.A. Woodruff, J.F. Martin, and M. Omens. A model for the design and evaluation of algorithms for closed-loop cardivascular therapy. *IEEE Transactions on Biomedical Engineering*, 44(8):694–705, August 1997.

[499] C.J. Woolf and M.-S. Chong. Preemptive analgesia - treating postoperative pain by preventing the establishment of central sensitization. *Anesthesia Analgesia*, 77:362–379, 1993.

[500] N.E. Wu. Some extensions to the generalized parity space method for FDI. In *Preprints 10th IFAC Symposium on System Identification (SYSID '94),, Copenhagen, Denmark, July 4-6,,* volume 3, pages 83–88, 1994.

[501] J. Wünnenberg. *Observer-Based Fault Detection in Dynamical Systems*, volume 8 of *Mess-, Steuerungs und Regelungstechnik*. VDI, 1990.

[502] N. Yasuda, S. H. Lockhart, E. I. Eger II, R. B. Weiskopf, J. Liu, M. Laster, S. Taheri, and N. A. Peterson. Comparison of kinetics of sevoflurane and isoflurane in humans. *Anesthesia Analgesia*, 72:316–24, 1991.

[503] N. Yasuda, S.H. Lockhart, E.I. Eger, R.B. Weiskopf, B.H. Johnson, and A. Faussolaki. Desflurane, Isoflurane, and Halothane pharmakokinetics in humans (abstract). *Anesthesia Analgesia*, 70:S444, 1999.

[504] N. Yasuda, S.H. Lockhart, E.I. Eger, R.B. Weiskopf, B.H. Johnson, B.A. Freire, and A. Faussolaki. Kinetics of Desflurane, Isoflurane, and Halothane in humans. *Anesthesiology*, 74:489–498, 1991.

[505] N. Yasuda, S.H. Lockhart, E.I. Eger, R.B. Weiskopf, J. Liu, M. Laster, S. Taheri, and N.A. Peterson. Comparison of kinetics of Sevoflurane and Isoflurane in humans. *Anesthesia Analgesia*, 72:316–324, 1991.

[506] N. Yasuda, A.G. Targ, and E.I. Eger. Solubility of I-653, sevoflurane, isoflurane, and halothane in human tissues. *Anesthesia Analgesia*, 69:370–373, 1989.

[507] H. Ying and L.C. Sheppard. Real-time expert-system-based fuzzy control of mean arterial pressure in pigs with sodium nitroprusside infusion. *Medical Progress through Technology*, 16:69–76, 1990.

[508] A. Yonker-Sell, M. Muzi, W. G. Hope, and T. J. Ebert. Alfentanil modifies the neurocirculatory responses to Desflurane. *Anesthesia Analgesia*, 82, 1996.

[509] C. Yu, R.J. Roy, and H. Kaufmann. A circulatory model for combined nitroprusside-dopamine therapy in acute heart failure. *Medical Progress through Technology*, 16:77–88, 1990.

[510] Clement Yu, Rob J. Roy, Howard Kaufmann, and B. Wayne Bequette. Multiple-model adaptive predictive control of mean arterial pressure and cardiac output. *IEEE transactions on biomedical engineering*, 39:765–778, 1992.

[511] D. Yu and D.N. Shields. Fault diagnosis in bilinear systems - a survey. In *Proceedings of the Third European Control Conference (ECC'95), Sept 5-8, Rome, Italy*, volume 1, pages 360–365, 1995.

[512] A. Zbinden and D. Thomson. *Anaesthesiologie*, chapter 6.1 Pharmakokinetik der Inhaltionsanaesthetika, pages 125–156. Springer Verlag, Berlin, auflage 7 edition, 1995.

[513] A.M. Zbinden. *Inhalationsanästhetika: Aufnahme und Verteilung: Allgemeine Grundlagen.* Wissenschaftliche Verlagsabteilung Deutsche Abbott GmbH, Wiesbaden, 1984.

[514] A.M. Zbinden. Pharmacokinetics of inhaled anaesthetics. *Baillière's Clinical Anaesthesiology*, 5:543–566, 1991.

[515] A.M. Zbinden, P. Feigenwinter, S. Petersen-Felix, and S. Hacisalihzade. Arterial pressure control with isoflurane using fuzzy logic. *British Journal of Anaesthesia*, 74:66–72, 1995.

[516] A.M. Zbinden, F. Frei, D.R. Westenskow, and D.A. Thomson. Control of end-tidal halothane concentration, Part B: Verification in dogs. *British Journal of Anaesthesia*, 58:563–571, 1986.

[517] A.M. Zbinden, A.H. Glattfelder, T. Sieber, and W. Schaufelberger. Development of an automatic feedback system for the delivery of inhaled anaesthetics and the control of ventilation during anaesthesia. Part 4: Integrated control. Forschungsgesuch Nr. 32-55479.98 , Swiss National Science Foundation, 1999.

[518] A.M. Zbinden, A.H. Glattfelder, and D.A. Thomson. Development of an automatic feedback system for the delivery of inhaled anaesthetics and the control of ventilation during anaesthesia. Part 2: development of an intelligent supervisor system. Forschungsgesuch Nr. 32-45527.95, Swiss National Science Foundation, 1995.

[519] A.M. Zbinden, S. Petersen-Felix, and D.A. Thomson. Anesthetic depth defined using multiple noxious stimuli during isoflurane/oxygen anesthesia, ii. hemodynamic responses. *Anesthesiology*, 80:261–267, February 1994.

[520] X. Zhang, J. A. Ashton-Miller, and C. Stohler. A closed-loop system for maintaining constant experimental muscule pain in man. *IEEE Transactions on Biomedical Engineering*, 40(4):344–352, Anaesthetic Pharmacology Review 1993.

[521] Z. Zhuang and P.M. Frank. FDI with qualitative models. pages 1–7, 1997.

[522] R.E. Ziemer, W.H. Tranter, and D.R. Fannin. *Signals and Systems: Continuous and Discrete.* Macmillan Publishing Company, 3rd edition, 1993.

[523] D. Zühlke. Entwicklungen in der Mensch-Maschine-Interaktion. *Automatisierungstechnik*, 40(6):50–53, 1998.

[524] A. Zwart, N.T. Smith, and E.W. Beneken. Multiple model approach to uptake and distribution of halothane: The use of an analog computer. *Computers and Biomedical Research*, 5:228–238, 1972.

Seite Leer /
Blank leaf

Curriculum vitae

July 17 1967	Born	Uster, Switzerland
1974 - 1983	Primary and Secondary School	Greifensee, San Jose, Klingnau (Switzerland, USA)
1983 - 1987	Apprenticeship as "Elektrozeichner" (incl. "Berufsmittelschule")	Brown Boveri & Cie., Baden, Switzerland
1988 - 1992	Undergraduate studies in EE	HTL Brugg-Windisch, Switzerland
1993	Practicing Control Engineer	Landis&Gyr Building Control, Zug, Switzerland
1994 - 1995	Graduate Studies (MSEE)	Northwestern University Evanston, IL, USA
1995 - 1998	Post Graduate Studies in Information Technology	EE Department, ETH Switzerland
since 1995	Research and Teaching Assistant	Automatic Control Lab., ETH Switzerland